Univerzita Karlova v Praze

Přírodovědecká fakulta

Studijní program: Organická chemie

RNDr. Martin Štícha

Využití hmotnostní spektrometrie pro analýzu biologicky aktivních a klinicky významných látek

Application of Mass Spectrometry for Analysis of Biologically Active and Clinically Significant Compounds

Dizertační práce

Vedoucí dizertační práce: Doc. RNDr. Ivan Jelínek, CSc.

Praha, 2016

Prohlášení:

Prohlašuji, že jsem závěrečnou práci zpracoval samostatně a že jsem uvedl všechny použité informační zdroje a literaturu. Tato práce, ani její podstatná část, nebyla předložena k získání jiného nebo stejného akademického titulu.

V Praze, 21. 6. 2016

Podpis

Tato dizertační práce vznikla na základě výsledků získaných v letech 2010 až 2016 během mého Ph.D. studia na Katedře organické chemie Přírodovědecké fakulty Univerzity Karlovy v Praze, Hlavova 2030, 128 43, Praha 2.

Školitel: Doc. RNDr. Ivan Jelínek, CSc.
Katedra analytické chemie
Přírodovědecká fakulta, Univerzita Karlova v Praze

….. Mému otci, který bohužel neměl možnost se toho dožít

Tato dizertační práce je založena na následujících vědeckých pracích, které byly publikovány v mezinárodních impaktovaných časopisech:

I. **Štícha, M**.; Jelínek, I.; Poláková, J.; Kaliba, D.: *Characterization of Rhenium (V) Complexes with Phenols Using Mass Spectrometry with Selected Soft Ionization Techniques*; ANALYTICAL LETTERS, 48 (2015) 2329-2342.

II. **Štícha, M**.; Kaliba, D.; Jelínek, I.; Poláková, J.: *Analytical study of rhenium complexeswith pyrogallol and catechol*; CHEMICAL PAPERS, In print (2016)

III. Fernandes, TA ; Solarova, H; Cisarova, I; Uhlik, F; **Sticha, M** ; Stepnicka, P *Synthesis of phosphinoferrocene amides and thioamides from carbamoyl chlorides and the structural chemistry of Group 11 metal complexes with these mixed-donor ligands;* DALTON TRANSACTIONS, 44 (7): 3092-3108 2015

IV. Konickova, R; Jiraskova, A ; Zelenka, J ; Leseticky, L ; **Sticha, M** ; Vitek, L *Reduction of bilirubin ditaurate by the intestinal bacterium Clostridium perfringens;* ACTA BIOCHIMICA POLONICA 59 (2) : 289-291 2012

V. Jasprova, J.; Dal Ben, M.; Vianello, E. ; Goncharova, I.; Urbanova, M.; Vyroubalova, K.; Gazzin, S.; Tiribelli, C.; **Sticha, M.**; Cerna, M. *The Biological Effects of Bilirubin Photoisomers;* PLOS ONE 11 (2) Article Number: e0148126 2016

VI. Kluckova, K.; **Sticha, M.**; Cerny, J.; et al. *Ubiquinone-binding site mutagenesis reveals the role of mitochondrial complex II in cell death initiation;* CELL DEATH & DISEASE Volume: 6 Article Number: e1749 2015

VII. Chytil,L; Cvacka,J; Maresova,V; Strauch,B; Widimsky,J; **Sticha, M**; Slanar, O *Development of a fast LC–MS/MS method for quantification of rilmenidine in human serum: elucidation of fragmentation pathways by HRMS;* JOURNAL OF MASS SPECTROMETRY, 45, 1179–1185 AUG 2010

VIII. Chytil, L; **Sticha, M**; Matouskova, O; Perlik, F; Slanar, O : *Enatiomeric determination of tramadol and O-desmethyltramadol in human urine by gas chromatography-mass spectrometry;* JOURNAL OF CHROMATOGRAPHY B-ANALYTICAL TECHNOLOGIES IN THE BIOMEDICAL AND LIFE SCIENCES, 877 (20-21): 1937-1942 JUL 1 2009

IX. Nespěšná, L; **Štícha, M**; Matoušková, O; Perlík,F; Slanař,O: Stanovení nabumetonu a kyseliny 6-methoxy-2-naftyloctové v plazmě pomocí HPLC s UV a MS detekcí; ČESKÁ A SLOVENSKÁ FARMACIE, 2011; 60, 17-24

Předmětová hesla

Analytická chemie, hmotnostní spektrometrie, HPLC, příprava organokovových sloučenin, organická analýza

Klíčová slova

Hmotnostní spektrometrie, rhenium, komplexy, vysokoúčinná kapalinová chromatografie, biomarker, žlučová barviva, bilirubin, urobilinoidy, sukcinát dehydrogenáza, apoptóza, nabumeton, farmakokinetika, kyselina 6-methoxy-2-naftyloctová, tramadol, O-Desmethyltramadol, enantiomerní separace, rilmenidin

Subject words

Analytical chemistry, mass spectrometry, high performance liquid chromatography, organometallic compounds, organic analysis,

Key words

Mass spectrometry, high performance liquid chromatography, rhenium, complexes, biomarkers, bile pigments, bilirubin, biliverdin, urobilinoids, succinate dehydrogenase, apoptosis, nabumeton, pharmacokinetics, 6-methoxy-2-naphtylacetic acid, tramadol, rilmenidine

Poděkování

Na tomto místě bych rád poděkoval svému školiteli Doc. RNDr. Ivanu Jelínkovi, CSc. za odborné vedení a RNDr. Janě Polákové za věcné připomínky, rady a podporu během mé dizertační práce. V neposlední řadě bych chtěl poděkovat své rodině za všestrannou podporu a nezměrnou trpělivost.

ABSTRAKT (CZ)

Předložená práce je komentovaným souborem devíti publikací dokumentujících možnosti využití hmotnostní spektrometrie v oblasti strukturní charakterizace vybraných organometalických komplexů, analýz léčiv a jejich metabolitů a monitorování významných biomarkerů metabolických poruch a onemocnění

V průběhu práce na tématice disertační práce byly úspěšně realizovány následné dílčí projekty:

- Návrh a realizace postupu mikropreparace vybraných rheniových komplexů s aromatickými ligandy za použití tetrabutylammonium tetrachlorooxorhenátu jako výchozí látky; příprava oxorhenium(V) komplexů s 1,2-dihydroxybenzenem, 1,2,3-trihydroxybenzenem a 2,3-dihydroxynaftalenem jako ligandy a jejich strukturní charakterizace s pomocí ESI/MS, APPI-MS a LDI-MS; ESI/MS a UV/Vis studie kinetického chování komplexů vznikajících při reakci tetrabutylamonium tetrachlorooxorhenátu s pyrogallolem a katecholem jako ligandy. Zvláštní pozornost byla věnována studiu následných chemických transformací primárně vzniklých Re(V) komplexů; strukturní charakterizace vybraných komplexů ferrocenu s mědí zlatem a stříbrem technikami ESI/MS.
- V rámci spolupráce na grantovém projektu zaměřeném na metabolismus cholesterolu byla navržena metodologie strukturní charakterizace rozkladných produktů katalytického rozkladu hemu a prostudována možnost chromatografické separace a strukturní charakterizace fotoizomerů bilirubinu s pomocí hmotnostní spektrometrie.
- Pro potřeby molekulárně biologické studie mechanizmů buněčné apoptózy byla úspěšně vyvinuta a prakticky využita metoda stanovení velmi nízkých intracelulárních koncentrací sukcinátu s pomocí LC-ESI/MS.
- Vývoj a validace metody stanovení rilmenidinu metodou LC–MS/MS , příprava a validace LC-MS metody stanovení nabumetonu a jeho metabolitu kyseliny 6-methoxy-2-naftyloctove (6-MNA) při úpravě vzorku lidského séra pomoci extrakce na pevné fázi (SPE) a eneantioselektivní stanovení tramadolu a O-desmethyltramadolu v lidské moči pomocí GC/MS. Všechny tyto postupy byly následně využity v reálných farmakokinetických studiích.

ABSTRACT (EN)

The thesis is submitted as a commented set of reviewed publications documenting and depicting the possibilities of mass spectrometry in the field of chemical, biological and pharmaceutical research; namely for the purposes of structure elucidation of selected organometallic complexes, analyses of drugs and their metabolites, monitoring of important biological markers.

In course of experimental work, the following objectives were studied and solved:

- Proposal and realization of micro-scale preparation of selected rhenium complexes with aromatic ligands, utilizing tetrabutyammonium tetrachlorooxorhenate as a starting material; preparation and structure characterization of oxorhenium(V) complexes with 1,2-dihydroxybenzene, 1,2,3-trihydroxybenzene, and 2,3-dihydroxynaphtalene as ligands by means of ESI/MS, APPI/MS and LDI-MS; ESI/MS and UV/Vis study of kinetic behavior of complexes arising from the reaction of tetrabutylamonnium tetrachlooxorhenate with pyrogallol and catechol as ligands. Special aim was devoted to the study of subsequent chemical transformation of primarily formed Re(V) complexes; structure characterization of selected ferrocene complexes with copper, gold and silver by means of ESI/MS.
- Proposal of methodology of structure characterization and quantification of the products of catalytic degradation of haem, proposal of the methodology aimed at chromatographic separation and structure elucidation of bilirubin photo isomers; both above mentioned projects utilized mass spectrometer with selected soft ionization techniques, alone or in combination with suitable separation technique.
- For the purposes of biological study of the mechanisms of cell apoptosis, LC-ESI/MS assay of trace amount of intracellular succinate was developed and practically utilized.
- Development and validation of LC–MS/MS assay of rilmenidine and nabumeton with the main metabolite 6-methoxy-2-naphtylacetic acid (6-MNA) in human serum by solid phase extraction (SPE); development and validation of enantioselective assay of tramadol and O-desmethyl tramadol in human urine by means of GC/MS. All of that assays were practically utilized in real pharmacokinetic studies.

…

OBSAH

SEZNAM POUŽITÝCH ZKRATEK A SYMBOLŮ

API	Ionizace za atmosferického tlaku
APCI	Chemická ionizace za atmosférického tlaku
APPI	Fotoionizace za atmosférického tlaku
BDT	Bilirubin ditaurát
Calc.	Vypočítaná hodnota
Cat	Katechol
CNS	Centrální nervová soustava
CZE	Kapilární zónová elektroforéza
C II	Komplex II
C 18	Oktadecyl
EDC	1-ethyl-3-(3-(dimethylamino)propyl)karbodiimid
EI	Elektronová ionizace
ESI	Ionizace elektrosprejem
Exp.	Experimentálně získaná hodnota
GC/MS	Plynová chromatografie s hmotnostní detekcí
Hb	Hemoglobin
HOBt	1- hydroxybenzotriazol
HPLC	Vysokoúčinná kapalinová chromatografie
HRMS	Hmotnostní spektrometrie s vysoký rozlišením
I	Relativní intenzita [%]
ICR	Ion cyklotronová resonance
IR	Infračervená spektroskopie
IS	Vnitřní standard
L	Ligand
LC	Kapalinová chromatografie
LDI	Laserová desorpce/ionizace
LLE	Extrakce kapalinou
[ML]	Komplex M (centrální atom) a L (ligand)
MS	Hmotnostní spektrometrie
MS/MS	Tandemová hmotnostní spektrometrie

ODT	O-desmethyl tramadol
PI	Fotoizomer
PG	Pyrogallol
QqQ	Trojitý kvadrupól
ROS	Reaktivní forma kyslíku
SDH	Sukcinát dehydrogenáza
SI	Index podobnosti
SIM	Sledování vybraných iontů
SPE	Extrakce tuhou fází
SRM	Záznam vybraných přechodů
TEA	Triethylamin
TFA	Kyselina trifluoroctová
TLC	Chromatografie na tenké vrstvě
TMSCl	Trimethylsilyl chlorid
TOF	Detektor doby letu
TTFA	Thenoyltrifluoraceton
UV-Vis	Spektrofotometrie v ultrafialové a viditelné oblasti spektra
X-ray	rentgenová difrakce
6 – MNA	6-methoxy-2-naftyloctová kyselina
λ	Vlnová délka

1. Úvod

Hmotnostní spektrometrie je fyzikálně chemická metoda určování hmotností atomů, molekul a jejich částí po převedení na kladné a záporné ionty. Je jednou z nejstarších instrumentálních technik využívaných pro charakterizaci organických a anorganických analytů. Prvotní aplikace, vycházející zcela z definice této techniky, umožnily velmi přesně určit relativní atomové hmotnosti mnoha prvků. Pozorovaná ionizace jednoduchých anorganických a organických molekul byla zprvu chápána jako doprovodný negativní efekt, daný přítomností přirozených kontaminantů z okolního prostředí uvnitř hmotnostního spektrometru. Záhy však byla rozpoznána možnost využití ionizace organických látek za vzniku molekulárního iontu a iontů fragmentových pro účely určení jejich struktury. Již Joseph J. Thomson na začátku minulého století ve svých původních pracích predikoval možnosti strukturní analýzy organických látek s použitím hmotnostního spektrometru. K rychlému rozvoji organické analýzy došlo v druhé polovině minulého století a to především v souvislosti s rozvojem chemického a farmaceutického průmyslu a též s vyhledáváním nových ropných nalezišť na základě identifikace organických markerů ropných nalezišť. Významná finanční podpora ropného průmyslu podpořila vývoj instrumentace pro hmotnostní spektrometrii, která byla již použitelná v běžné chemické laboratoři. Byla úspěšně zvládnuta metodika strukturní charakterizace malých organických molekul a podrobně rozpracována teorie fragmentace organických molekul umožňující strukturní charakterizaci analytu z hmotnostního spektra. V této souvislosti je vhodné připomenout jména Freda W. McLaffertyho, Klause Biemanna a Vladimíra Hanuše, osobností které významně přispěly k zařazení hmotnostní spektrometrie do skupiny technik organické strukturní analýzy. Po dlouhou dobu byla aplikační oblast hmotnostní spektrometrie omezena na nízkomolekulární organické látky s dostatečnou těkavostí pro elektronovou ionizaci. Tato situace se dramaticky změnila po uvedení nových ionizačních technik, umožňujících převést do ionizovaného stavu i látky netěkavé a tepelně labilní. S uvedením nových sprejových a desorpčních ionizačních technik prakticky zmizelo dosavadní omezení a otevřela se možnost studovat i vysokomolekulární látky. Za zásadní přínos v této oblasti byla v roce 2002 udělena Johnu B. Fennovi a Koichimu Tanakovi Nobelova cena. Hmotnostní spektrometrie náhle stála ve středu zájmu biochemiků a molekulárních biologů a významně se podílela na řešení úkolů genomiky, proteomiky, lipidomiky aj. S vývojem nových typů iontových zdrojů souvisel i vývoj hmotnostních analyzátorů vhodných pro dělení iontů s velkou hmotností a dosahujících vysokých hodnot rozlišení. Zde je nutno zmínit ion cyklotronovou rezonanci (ICR), driftovou trubici (TOF) a lineární a orbitální

iontovou past. Přirozenou vlastností měkkých iontových zdrojů ionizujících analyt z kondenzované fáze je nízký rozsah fragmentace primárně vzniklých molekulárních a kvazimolekulárních iontů, který znesnadňuje určení struktury analytu na základě charakteristických fragmentačních cest. V této souvislosti se jako velmi užitečný ukázal vývoj tandemových instrumentálních uspořádání, sdružujících více hmotnostních analyzátorů a kolizní celu. Za návrh a konstrukci iontové optiky na bázi kvadrupólu byla Wolfgangu Paulovi v roce 1989 udělena Nobelova cena. Tandemový přístroj s trojitým kvadrupólem, umožňující provádět kolizní disociaci primárně vzniklých iontů, patří mezi základní nástroje pro farmakokinetické, farmakogenetické a stabilitní studie léčiv. Měkké iontové zdroje jsou po primární ionizaci analytu schopny zachovat fragmentací netknutou strukturu nejen kovalentních vazeb, ale i vazeb koordinačně kovalentních a dalších vazeb vznikajících na základě slabých interakcí. Tím se pro hmotnostní spektrometrii otevírá potenciálně velmi zajímavá oblast strukturní charakterizace a kvantifikace různých typů komplexů a molekulárních asociátů. Význam těchto látek v chemii i biologii významně roste a aplikace hmotnostní spektrometrie v této oblasti je velmi přínosná. Vývoj nových typů iontových zdrojů a hmotnostních analyzátorů s rychlým skenováním významně rozšířil možnosti spojení hmotnostního spektrometru s kolonovými separačními technikami. Nejstarší kombinace plynového chromatografu s hmotnostním spektrometrem (GC/MS) byla záhy rozšířena o kapalinovou chromatografii (LC/MS), kapilární elektroforézu (CE/MS) a superkritickou fluidní chromatografii (SFC/MS). Všechny zmíněné instrumentální varianty jsou v současnosti komerčně dostupné a prakticky využívané. Vysoká selektivita kombinací hmotnostní spektrometrie s předřazenou separační metodou umožňuje analyzovat vzorky s velmi komplikovanou matricí, čehož je s výhodou využíváno především v oblasti klinických a farmakologických analýz, vyžadujících analyzovat vzorky tělních tekutin, ale i v oblasti environmentální analýzy organických polutantů ve vzorcích půdy, vod a ovzduší. V této souvislosti je vhodné zmínit i obecně vysokou citlivost hmotnostního spektrometru použitého jako strukturně selektivní detektor.

Je zcela nemožné v takto krátkém rozsahu komplexně zhodnotit význam hmotnostní spektrometrie, postihnout všechny významné etapy jejího rozvoje, nebo dokonce předvídat její další rozvoj; pokud však zůstane zachován trend vývoje posledních dvaceti let, je možno očekávat mnohé další významné objevy ve vývojové i aplikační oblasti. I v případě pouhé stagnace si hmotnostní spektrometr udrží své výsadní postaveni ve skupině instrumentálních analytických technik.

2. Cíle práce

Prostudovat možnosti strukturní charakterizace organometalických komplexů s pomocí hmotnostní spektrometrie s měkkými ionizačními technikami:

- Připravit vybrané komplexy rhenia s organickými aromatickými ligandy a systematicky prostudovat možnosti jejich strukturní charakterizace metodou ESI/MS, APPI/MS a LDI/MS;
- Charakterizovat produkty reakčních přeměn Re(V)-katecholového a Re(V)-pyrogallolového komplexu v aerobních podmínkách s pomocí UV/Vis a ESI/MS spektrometrie;
- Prostudovat možnosti strukturní charakterizace vybraných komplexů ferrocenu metodou ESI/MS, APPI/MS a LDI/MS.

Vypracovat metody sledování významných biomarkerů s pomocí hmotnostní spektrometrie:

- V rámci studie redukce bilirubin ditaurátu střevní bakterií Clostridium perfringens vypracovat metodiky strukturní charakterizace produktů katabolického rozkladu hemu;
- V rámci studie fotodegradace bilirubinu vyvinout techniky separace fotoizomerů bilirubinu a jejich strukturní charakterizace s pomocí hmotnostní spektrometrie;
- V rámci studie role mitochondriálního komplexu II v iniciaci apoptózy vyvinout metodu stanovení intracelulární koncentrace sukcinátu metodou LC-ESI/MS.

Vypracovat metody stanovení vybraných léčiv a jejich metabolitů:

- Vyvinout rychlou metodu stanovení rilmenidinu v lidském séru metodou LC–MS/MS;
- Vyvinout metodu stanovení enantiomerů tramadolu a O-desmethyltramadolu v lidské moči pomocí GC-MS;
- Vyvinout metodu stanovení nabumetonu a kyseliny 6-methoxy-2-naftyloctové v plasmě pomocí HPLC s UV a MS detekcí.

3. Využití hmotnostní spektrometrie při studiu koordinačních sloučenin

Pro charakterizaci koordinačních sloučenin je možné využít řadu analytických metod, jako je například nukleární magnetická rezonance (NMR), infračervená spektroskopie (IR), rentgenová difrakce (X-ray) a mnoho dalších. Využití těchto technik většinou vyžaduje mít k dispozici větší množství materiálu v přiměřeně čistém případně krystalickém stavu. Obrovskou výhodou hmotnostní spektrometrie je zejména její vysoká citlivost a i když se sice jedná o metodu destruktivní, není většinou pro získání relevantních dat potřeba více než několik mikrogramů látky. Další velmi výhodnou vlastností této techniky je její vysoká selektivita, což umožňuje pracovat i více či méně komplikovanou směsí látek. Pro tento obrovský potenciál je hmotnostní spektrometrie v posledních letech v oblasti koordinační chemie využívaná s enormně rychle rostoucí intenzitou [1].

3.1. Charakterizace komplexů rhenia (V) s fenoly pomocí hmotnostní spektrometrie s měkkými ionizačními technikami (publikace I)

3.1.1. Teoretický úvod

Rhenium je velmi vzácný kov vyskytující se v zemské kůře jen ve stopové koncentraci. I když je díky této jeho omezené dostupnosti velmi drahé, přes to nachází pro některé své unikátní a cenné vlastnosti uplatnění a to zejména jako katalyzátor hydrogenačních a dehydrogenačních reakcí ale i v dalších oblastech výzkumu. Rhenium náleží do VII. vedlejší skupiny periodické soustavy prvků a vyskytuje se převážně v mocenství od Re^{-I} po Re^{VII}. Nejstálejší jsou však sloučeniny rhenia v mocenství Re^{-I}, Re^{IV}, Re^{V} Re^{VI} a Re^{VII} [2].

Svými chemickými vlastnostmi se rhenium značně podobá techneciu, které je umístěno ve skupině před ním, i když při detailnějším studiu určité rozdíly chování nacházíme. Mezi nejvýraznějšími rozdíly lze jmenovat například to, že jsou sloučeniny rhenia ve vyšších oxidačních stupních zpravidla stabilnější než analogické sloučeniny technecia. [3]. Nicméně značné podobnosti chemického a biologického chování komplexů rhenia a technecia lze například s úspěchem využít při výzkumu a vývoji nových preparátů využívaných v nukleární medicíně [4]. Většina radiofarmak je dnes založena na komplexech kovů radionuklidů s organickými ligandy. Koordinační sloučeniny technecia ^{99m}Tc vykazují stále vysokou oblibu v oblasti radiodiagnostik. Důvodem jsou především příznivé jaderné charakteristiky tohoto radionuklidu. Jedná se o zářič gama; s dosti krátkým poločasem přeměny (6 h), takže radiační zátěž pacienta je minimální. Výhodou může být i možnost

přípravy přímo na klinice za použití elucí příslušného radionuklidu z $^{99}Mo/^{99m}Tc$ generátoru do sterilního „kitu“.

Rhenium, které se též používá jako součást diagnostických a především terapeutických radiofarmak je na rozdíl od technecia dostupné i ve formě stabilních izotopů, což pochopitelně výzkumníkům velmi usnadňuje práci. Navíc přirozené zastoupení izotopů ^{185}Re a ^{187}Re v poměru 37,4% ku 62.6% je možné výhodně využít při identifikaci iontů v hmotnostní spektrometrii.

Velmi důležitým krokem před aplikací konkrétního radiofarmaka je jeho charakterizace. Je nezbytná detailní znalost složení a struktury komplexu tvořícího reakční směs, a stejně tak jeho degradačních produktů, spolu s kinetickými aspekty přechodů mezi jednotlivými formami komplexů Diskutovaná práce se zabývá možností využití hmotnostní spektrometrie pro charakterizaci komplexů rhenia s některými aromatickými ligandy. Ačkoliv se zavedením měkkých ionizačních technik zejména ESI se význam hmotností spektrometrie v oblasti analýzy organokovových a koordinačních sloučenin enormně zvýšil, míra využití této znamenité analytické metody v oblasti rheniových komplexů tomu rozhodně neodpovídá. Naše práce si klade za cíl upozornit na některé výhody této techniky, jako je například enormní citlivost, která umožňuje pracovat s mikromolárními koncentracemi analytu, což je nedocenitelné zejména pro klinické a farmakokinetické studie.

3.1.2. Výsledky a diskuse – doplňkový komentář k publikaci

Byly připraveny rheniové komplexy s pyrogallolem, 2,3-dihydroxynaftalenem a katecholem a tyto látky byly následně charakterizovány pomocí hmotnostní spektrometrie s elektrosprejovou ionizaci (ESI), fotoionizací za atmosférického tlaku (APPI) a laserovou desorpcí (LDI). Navržené struktury byly dále potvrzeny pomocí dalších spektrálních metod, jako je infračervená spektroskopie (IR), nukleární magnetická resonance (NMR) nebo spektrofotometrie v ultrafialové a viditelné oblasti UV-Vis. Při všech použitých ionizačních technikách bylo pozorováno množství záporně nabitých molekulárních iontů studovaných komplexů s nízkou fragmentací. Protože použité ligandy neobsahují funkční skupiny, které by bylo možné protonizovat, neposkytují spektra v pozitivním módu žádné cenné informace o struktuře připravených komplexů. Zaznamenaná MS spektra v negativním módu se skládají především z dominantních molekulárních iontů komplexů a dalších iontů, odpovídajících přítomnosti zbytkových činidel, reakčních složek a jejich oxidačních

produktů, jak je patrno z obrázku 3.1, kde je uvedeno ESI-MS spektrum komplexu s katecholem $[Re(O)(cat)_2]^-$. Dokonce i v MS/MS spektru fragmentačních iontů na dolní polovině obrázku je dobře patrný charakteristický izotopový profil potvrzující přítomnost rhenia. ESI-MS/MS experimenty poskytují základní informace o fragmentech vznikajících z molekulárních iontů studovaných komplexů. Díky tomu je možné rozlišit mezi fragmentovými ionty a ionty vzniklými ze sloučenin přítomných v reakční směsi. Obecně lze říci, že MS/MS fragmentační cesty jsou jednoduché. Dceřiné ionty byly vytvořeny převážně štěpením aromatické části na jednom ligandu, nebo ztrátou celého ligandu. Nicméně tento zmíněný mechanismus fragmentace nebyl pozorován u bis(2,3-dihydroxynaftalen)oxorhenium(-) komplexu, který je nejstabilnější.

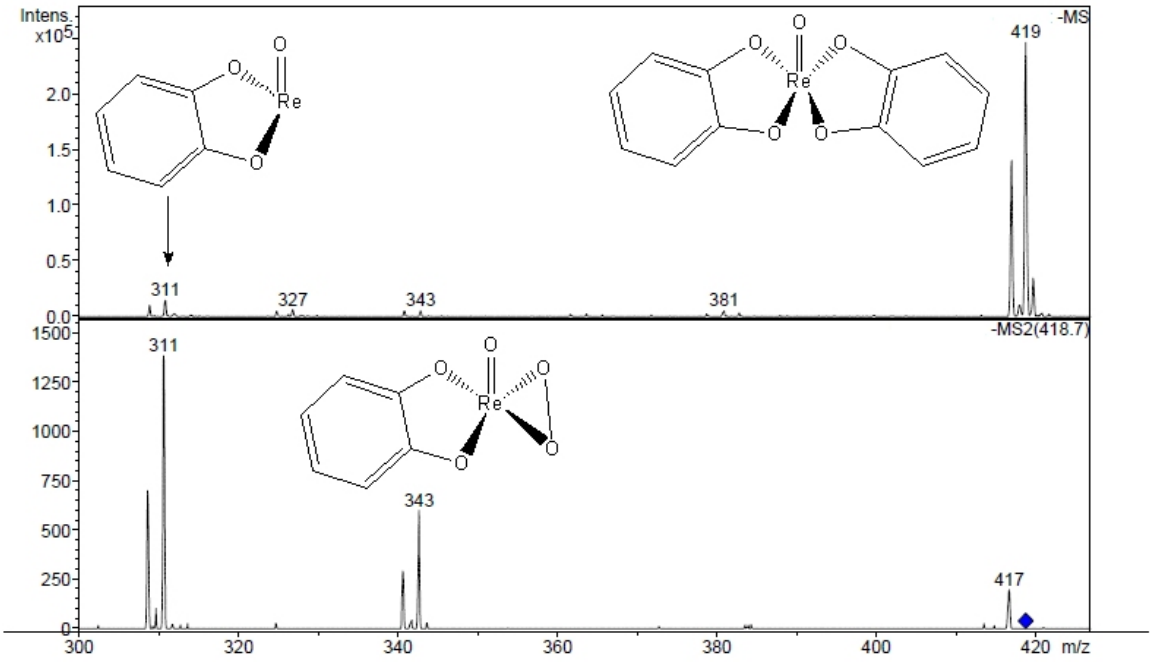

Obr. 3.1 ESI hmotnostní spektrum komplexu $[Re(O)(cat)_2]^-$ v negativním módu (horní část) ESI-MS/MS (spodní část). Přibližná koncentrace komplexu v roztoku vzorku je $5 \cdot 10^{-6}$ mol·l^{-1}.

U všech druhů komplexů byly pozorovány charakteristické izotopové klastry. Shoda mezi experimentálně získaným a teoreticky vypočítaným izotopovým zastoupením klastrů molekulárních iontů byla hodnocena na základě indexu podobnosti (*SI*) [5]. Z hodnot (1 – *SI*)*100 uvedených v tabulce 3.1 je zřejmá shoda mezi vypočítanými a experimentálně získanými daty, která tak potvrzuje správnost určení elementárního složení m/z sledovaných iontů.

			ESI		APPI		LDI	
Complex	Molecular Formula	m/z	I percent calc.	I percent exp.	I percent calc.	I percent exp.	I percent calc.	I percent exp.
bis(1,2-dihydroxybenezen) oxorhenium(-)	$C_{12}H_8O_5$ Re	417	59.1	56.9	59.1	56.9	59.1	53.4
		418	7.8	4.2	7.8	4.2	7.8	9.5
		419	100.0	100.0	100.0	100.0	100.0	100.0
		420	13.2	14.1	13.2	14.1	13.2	10.6
		421	1.8	0.4	1.8	0.4	1.8	0.7
			$(1-SI)100 = 91.9$		$(1-SI)100 = 91.9$		$(1-SI)100 = 89.0$	
bis(1,2, 3-trihydroxybenzene) oxorhenium(-)	$C_{12}H_8O_7$ Re	449	58.9	49.8	58.9	41.9	58.9	62.3
		450	7.9	20.4	7.9	8.3	7.9	15.6
		451	100.0	100.0	100.0	100.0	100.0	100.0
		452	13.3	11.9	13.3	16.5	13.3	16.5
		453	2.2	0.1	2.2	2.0	2.2	3.8
			$(1-SI)100 = 74.9$		$(1-SI)100 = 79.1$		$(1-SI)100 = 84.2$	
bis(2,3-dihydroxy-naphthalene) oxorhenium(-)	$C_{20}H_{12}O_5$Re	517	58.6	63.0	58.6	67.5	58.6	62.1
		518	12.9	11.5	12.9	13.8	12.9	13.8
		519	100.0	100.0	100.0	100.0	100.0	100.0
		520	21.8	19.0	21.8	15.4	21.8	24.5
		521	3.3	3.0	3.3	5.9	3.3	3.9
			$(1-SI)100 = 91.1$		$(1-SI)100 = 81.1$		$(1-SI)100 = 92.3$	

Tab. 3.1 Experimentální (exp.) a vypočítané (calc.) hodnoty relativních intenzit *I* [%] jednotlivých iontů v izotopovém zastoupení klastrů s vypočtenými hodnotami indexů podobnosti *SI*.

V práci bylo prokázáno, že hmotnostní spektrometrie s ESI, APPI a LDI ionizační technikou je užitečný nástroj pro charakterizaci struktury Re komplexů s aromatickými alkoholovými ligandy a pro analýzu jiných sloučenin přítomných v reakční směsi v průběhu komplexní přípravy. Získaná hmotnostní spektra poskytla jednoznačné informace o molekulových hmotnostech a struktuře studovaných sloučenin, díky dominantním molekulovým iontům komplexů a strukturně charakteristickým fragmentům přítomným ve spektrech.

3.2. Studium komplexů rhenia s pyrogallolem a katecholem (publikace II)

3.2.1. Teoretický úvod

Současná nukleární medicína často používá radiofarmaka na bázi komplexů vybraných radionuklidů s vhodnými organickými ligandy [6]. Podobně jako u jiných léčiv, tak i použití radiodiagnostický přípravků se musí řídit přísnými pravidly, která mimo jiné vyžadují

podrobné analytické údaje o složení aplikovaného přípravku. Vzhledem k tomu, že se velmi často pracuje s radionuklidy, které mají krátký poločas přeměny v řádu několika hodin, jsou tyto preparáty běžně podávány ve formě reakční směsi. Určení skutečného složení takto aplikované směsi a případně další studium struktury degradačních produktů může být extrémně obtížné. Navíc nízká koncentrační hladina sledovaných látek, se kterou se v klinické praxi běžně setkáváme, může být pro řadu metod strukturní analýzy limitující. Hmotnostní spektrometrie s měkkými ionizačními zdroji, kterou lze navíc vhodně kombinovat s výkonnými separačními technikami, jako je vysokoúčinná kapalinová chromatografie (HPLC) a kapilární zónová elektroforéza (CZE), se ukazuje jako rychlá a spolehlivá metoda pro charakterizaci a kvantifikaci komplexů. Cílem této práce bylo sledovat chování látek vzniklých reakcí tetrachlorooxorhenátu s 1,2,3-trihydroxybenzenem a 1,2-dihydroxybenzenem. Zvláštní pozornost byla věnována přeměně primárně vzniklých Re (V) komplexů spojené s přechodem kovu do vyšších oxidačních stupňů.

3.2.2. Výsledky a diskuse – doplňkový komentář k publikaci

Jak je ukázáno na obrázku 3.2 necháme-li spolu reagovat tetrachlorooxorhenát a příslušný ligand, průběh reakce je silně závislý na přítomnosti triethylaminu (TEA). S ohledem na molární poměr TEA lze získat odlišné konečné produkty reakce. Je možné konstatovat, že dominantním konečným produktem v přítomnosti čtyřikrát vyššího molárního poměru TEA je $[Re^{VII}(O)_2(PG)_2]^-$ (schéma 2), zatímco nižší koncentrace přídavku TEA vede k tvorbě komplexu $[Re^{VII}Cl(O)_2(PG)]$ (schéma 1). Z naměřených výsledků vyplývá zjevná souvislost mezi stechiometrií vznikajícího komplexu a nezbytným množstvím přídavku TEA pro kompletní neutralizaci chlorovodíku jako vedlejšího produktu reakce.

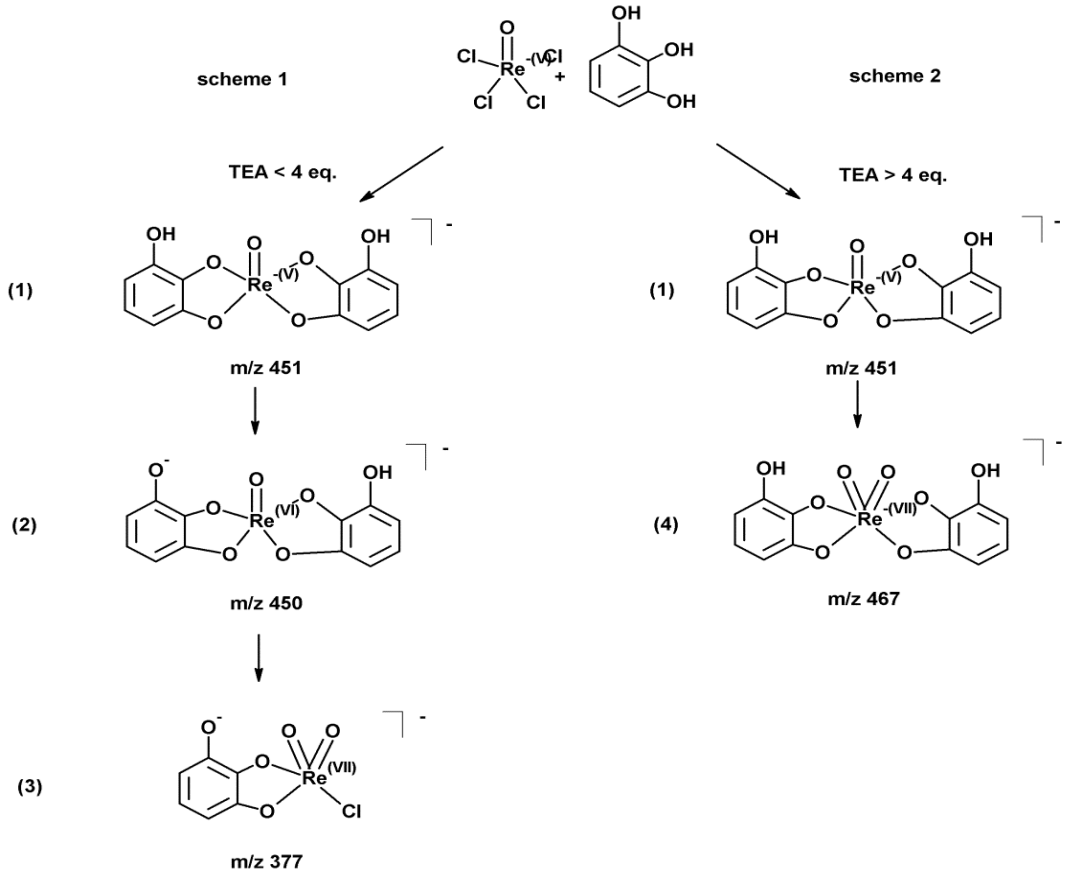

Obr.3.2 Schéma možných reakcí mezi [(*n*-Bu_4N)($ReOCl_4$)] a PG v přítomnosti různých množství TEA

Na dalším obrázku 3.3 je zdokumentován průběh pomalého samovolného přechodu $Re^{V} \rightarrow Re^{VI}$ v komplexu s pyrogallolem v přítomnosti 2 ekvivalentů TEA. V tomto případě sice nedochází ke změně elementárního složení, ale díky změně oxidačního stupně rhenia vzniká nenabitá forma komplexu, která poskytuje signál v negativním módu teprve po deprotonaci. Tento látka však není konečná a proces oxidace pokračuje až ke stabilnímu modrozelenému produktu **3**, [$Re^{VII}Cl(O)_2$(PG)] který obsahuje jen jeden ligand a rhenium zde vystupuje v nejvyšším oxidačním stupni VII.

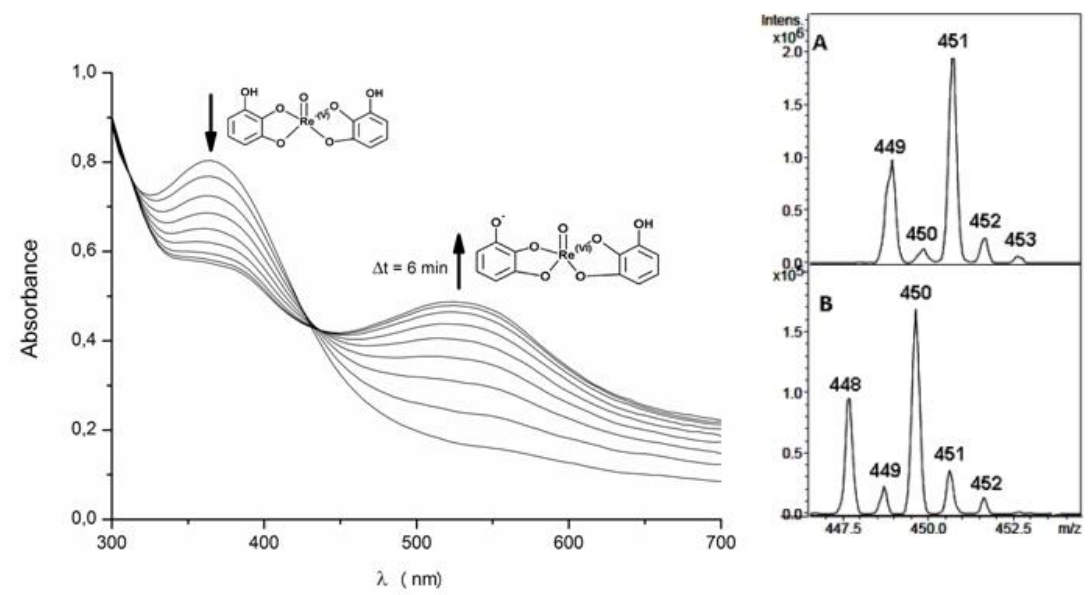

Obr. 3.3 UV-VIS absorpční spektra zobrazující konverzi světle žlutého komplexu 1 na karmínově červený komplex 2 v přítomnosti 2 ekvivalentů TEA. Šipky ukazují nárůst a/nebo pokles absorpčních maxim obou komplexů. Spektra byla shromažďována po dobu 60 minut a zobrazována v časovém intervalu 6 minut. Pravá část zobrazuje izotopické profily komplexů rhenia naměřené za použití ESI-MS v negativním módu. $[Re^{V}(O)(PG)_2]^-$ (část A) a $[[Re^{VI}(O)(PG)_2]$ - $H]^-$(část B).

Dále byla provedena srovnávací kinetická měření sledování vzniku a následné chemické transformace komplexů vzniklých v reakční směsi katecholu s $[(n\text{-}Bu_4N)(ReOCl_4)]$. Stejně jako v předchozích pokusech byla potvrzena významná role TEA při vzniku jednotlivých komplexů a jejich transformací. Byl však zaznamenán určitý rozdíl v konečném produktu v přítomnosti méně než 4 ekvivalentů TEA. V tomto případě byl získán produkt **7** $[Re^{VII}(O)Cl(Cat)_2]^0$, který bylo možné pozorovat pomocí ESI-MS až po derivatizaci s *p* - bromoanilinem za vzniku komplexu **8.** Proces derivatizace je schematicky zachycen na obrázku 3.4.

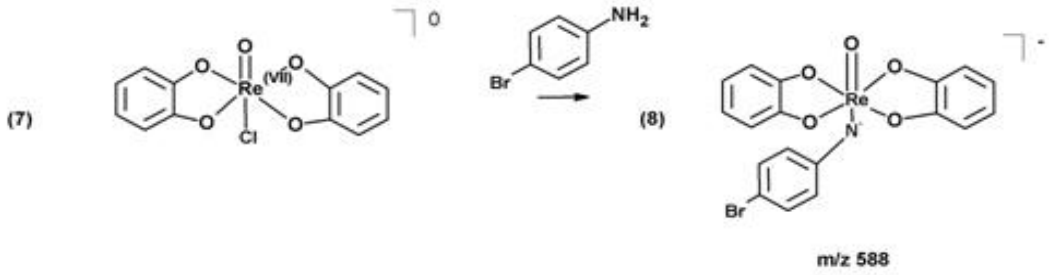

Obr.3.4 schéma derivatizace produkt **7** $[Re^{VII}(O)Cl(Cat)_2]^0$ *p*-bromoanilinem

Získané informace mohou přispět k lepšímu poznání koordinačních sloučenin rhenia s možnými dopady na oblast výzkumu a vývoje nových radiofarmaceutických preparátů.

3.3. Syntéza fosfinferrocenamidů a thioamidů z karbamoylchloridů a strukturní chemie komplexů kovů 11.skupiny s těmito logandy (publikace III)

3.3.1.Teoretický úvod

Ferroceny byly zpočátku využívány zejména pro přípravu enantioselektivních katalyzátorů, které nacházejí uplatnění například při vývoji nových materiálů [6]. Deriváty ferrocenu pro své jedinečné vlastnosti, jako jsou redoxní aktivita, elektrondonorový charakter, nebo schopnost konjugace, lákají pozornost chemiků již od samého objevení počátkem padesátých let. Není proto divu, že si výzkum těchto látek vyžádal podporu spolehlivých analytických metod poskytujících relevantní informace o struktuře a vlastnostech nově připravených preparátů. Jednou z fundamentálních technik v tomto ohledu je hmotnostní spektrometrie. Jednodušší a méně polární deriváty ferrocenu je možné díky jejich dobré tepelné stabilitě a dostatečné těkavosti analyzovat pomocí elektronové ionizace (EI), která poskytuje realitvně jednoduchá spektra s obvykle velmi intenzivními molekulárními ionty. [7-9]. Vzhledem k aromatické povaze ferrocenu není překvapivé, že je možné ve spektrech vypozorovat značnou podobnost s fragmentačními mechanizmy analogických arenů.

Hmotnostní spektrometrie s ionizací elektrosprejem (ESI/MS), případně s dalšími typy ionizací pracujícími za atmosférického tlaku (API) vyhovují analýze tepelně labilních sloučenin, jako jsou některé deriváty ferrocenu a jejich komplexy. Ukázalo se, že struktury nalezené v elektrospreji jsou velmi blízké těm formám, které se vyskytují v roztoku. Určitým usnadněním při interpretaci spekter ferrocenu a jeho derivátů, je i charakteristické zastoupení přirozených izotopů železa. Železo, jako centrální atom ferrocenu je polyizotopický element, který je v přírodě zastoupen čtyřmi stabilními izotopy ^{54}Fe (5,85%), ^{56}Fe (91,75%), ^{57}Fe (2,12%) a ^{58}Fe (0,28%) [10].

Diskutovaná práce se zabývá přípravou a charakterizací nových fosfinferrocenamidů a thioamidů, jejichž uplatnění v katalýze a koordinační chemii jako fosfin-donoru, rok od roku roste. Atraktivita těchto sloučenin spočívá zejména v jejich strukturální modularitě a jednoduché přípravě [11].

3.3.2. Výsledky a diskuse – doplňkový komentář k publikaci

Všechny připravené látky byly přečištěny sloupcovou chromatografií a následně charakterizovány spektrálními metodami (IR, NMR, ESI-MS). Hmotnostní spektra všech připravených látek společně s vypočítanými teoretickými hodnotami izotopického zastoupení jednotlivých elementů jsou přiloženy v příloze. Ve všech případech byla konstatována velmi dobrá shoda mezi naměřenými a kalkulovanými spektry.

Hmotnostní spektrometrie s elektrosprejovou ionizací byla využita pro charakterizaci fosfinferrocenamidů a thioamidů připravených podle schématu na obrázku 3.5. Reakce probíhala ve dvou krocích. Nejprve docházelo k lithiaci a následně byl přidán N,N-dimethylkarbamoyl chlorid v případě přípravy struktury **2**, nebo N,N-dimethylthiokarbamoyl chlorid pokud měl vznikat produkt **3**.

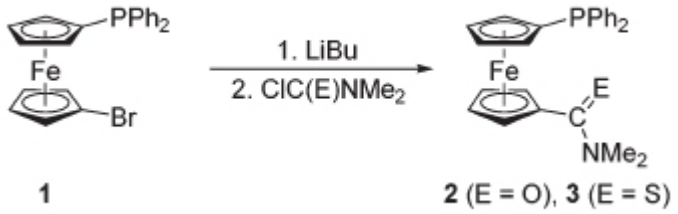

Obr. 3.5 Příprava fosfinferrocenamidu **2** a thioamidu **3** z 1'-(difenylfosfino)-1-bromoferrocenu **1** a příslušného karbamoylhalidu

Příprava fosfinoferrocenkarboxamidů byla také založena na kondenzačních reakcích za použití 1'- (difenylfosfino) ferrocen-1-karboxylové kyseliny (Hdpf), která je vhodná pro funkcionalizaci aminů. Další amidy byly syntetizovány běžnými postupy, jak je zobrazeno na obrázku 3.6. Amid **4** byl potom převeden na fosfinoxid **4O** nebo sulfid **4S** běžnou oxidací peroxidem vodíku resp. v přítomnosti elementární síry.

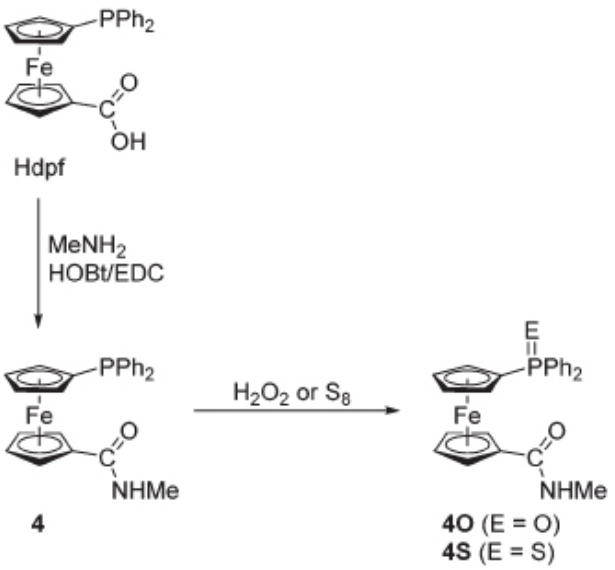

Obr.3.6 Příprava amidu 4 a příslušného P-oxidu a P-sulfidu Legenda: EDC = 1-ethyl-3-(3-(dimethylamino)propyl)karbodiimid, HOBt = 1- hydroxybenzotriazol

Ligandy připravené a popsané v předcházejících odstavcích byly potom použity pro syntézu komplexů s měďnými a stříbrnými ionty postupem schematicky znázorněném na obrázku 3.7.

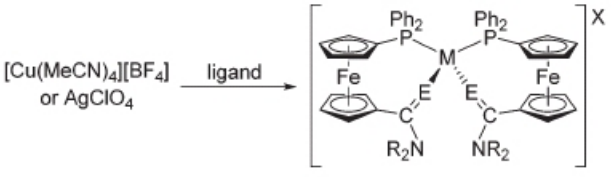

complex	M	E	NR_2	X
6a	Cu	O	NH_2	BF_4
6b	Cu	O	NHMe	BF_4
6c	Cu	O	NMe_2	BF_4
6d	Cu	S	NMe_2	BF_4
7a	Ag	O	NH_2	ClO_4
7b	Ag	O	NHMe	ClO_4
7c	Ag	O	NMe_2	ClO_4

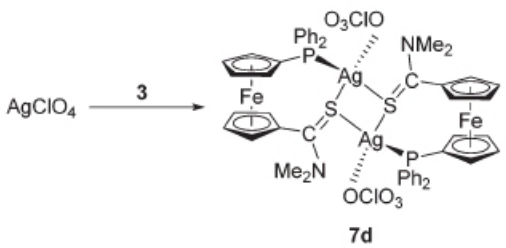

7d

Obr.3.7 Syntéza Cu(I) a Ag(I) komplexů

V ESI - MS spektrech komplexů **6a – 7c** byly v pozitivním módu nalezeny píky $[ML_2]^+$ a jejich fragmenty $[ML]^+$. Spektrum struktury **6b** je na obrázku 3.8.

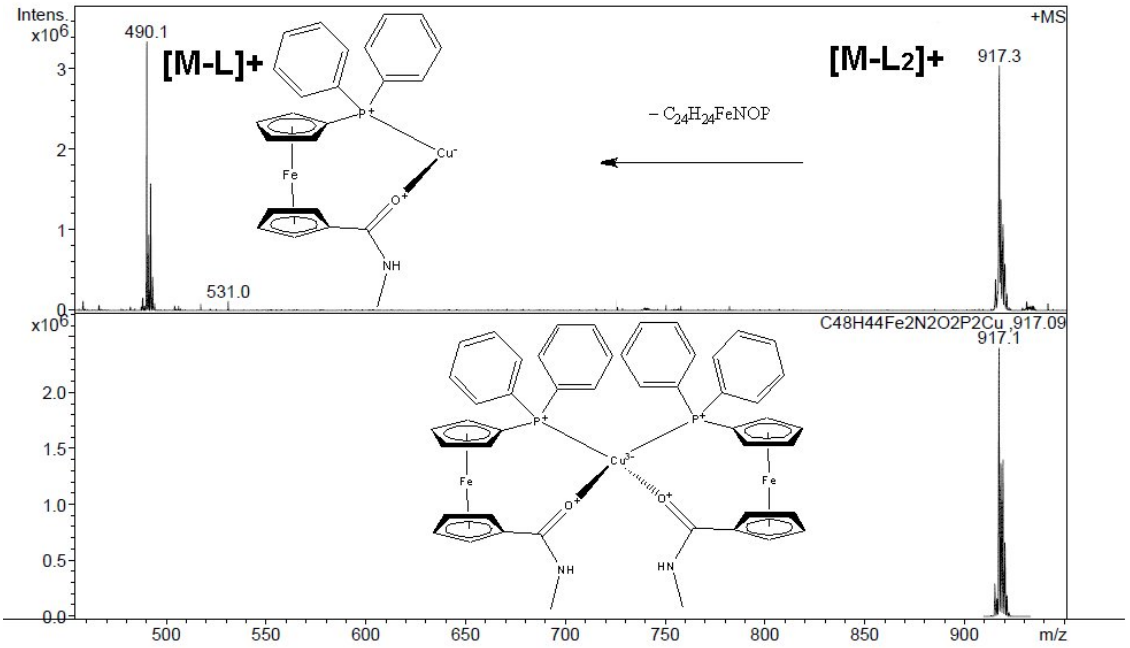

Obr.3.8 ESI – MS spektrum komplexu **6b** v pozitivním módu naměřené (horní část) a kalkulované (dolní část)

U analogického komplexu se stříbrem **7b** nebyl pík $[ML_2]^+$ patrně díky nižší stabilitě ve spektru prakticky vůbec pozorován. Na druhou stranu ion $[ML]^+$ poskytoval velmi dobrý signál s charakteristickým rozložením izotopů potvrzující přítomnost izotopů stříbra ^{107}Ag / ^{109}Ag v poměru intenzit 100:93. Naměřené hmotnostní spektrum bylo ve velmi dobré shodě s vypočítanými hodnotami pro ion $[ML]^+$ se sumárním vzorcem $C_{24}H_{22}FeNOPAg$, jak je patrno z obrázku 3.9.

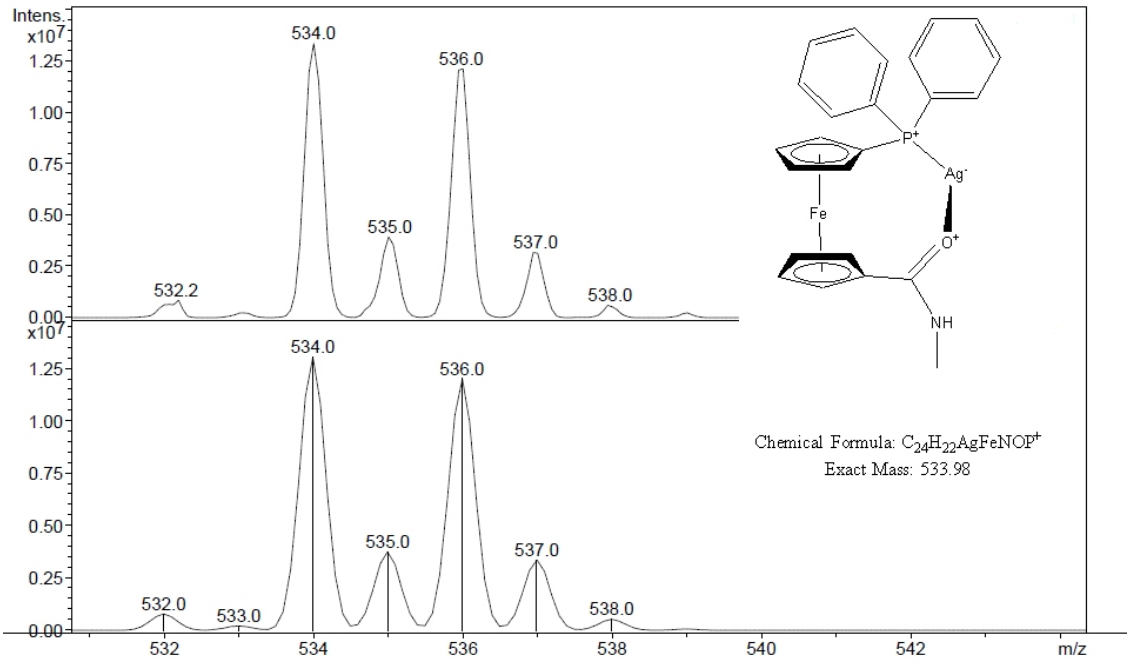

Obr.3.9 ESI – MS spektrum komplexu **7b** v pozitivním módu naměřené (horní část) a kalkulované (dolní část)

Pro doplnění byla syntetizovaná ještě série komplexů s ionty zlata, kde se u amidofosfinových ligandů účastnila koordinace pouze fosfinová skupina. Proces přípravy těchto komplexů je schematicky zachycen na obrázku 3.10.

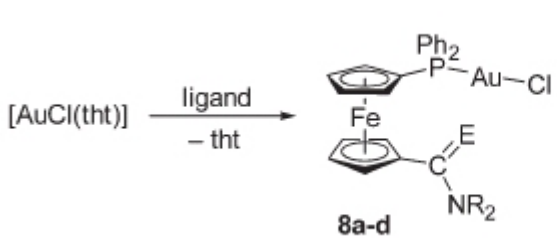

complex	E	NR_2
8a	O	NH_2
8b	O	NHMe
8c	O	NMe_2
8d	S	NMe_2

Obr.3.10 Syntéza Au(I) komplexů **8a-d** (tht = tetrahydrothiofen)

Ve spektrech ESI-MS byly v těchto případech přítomny ionty vznikající ztrátou chloridového iontu $[M - Cl]^+$ a v případě **8a** až **8c** též adukty s alkalickými kovy . $[M + Na]^+$ a $[M + K]^+$. Pro komplex **8c** je spektrum na obrázku 3.11. Ve spektru je také velmi dobře zřetelný charakteristický izotopický profil prozrazující přítomnost atomu chloru s jeho dvěma izotopy ^{35}Cl / ^{37}Cl v poměru 3:1. Ztráta atomu chloru se pak jasně projeví ve změně izotopického profilu u píku m/z 638.

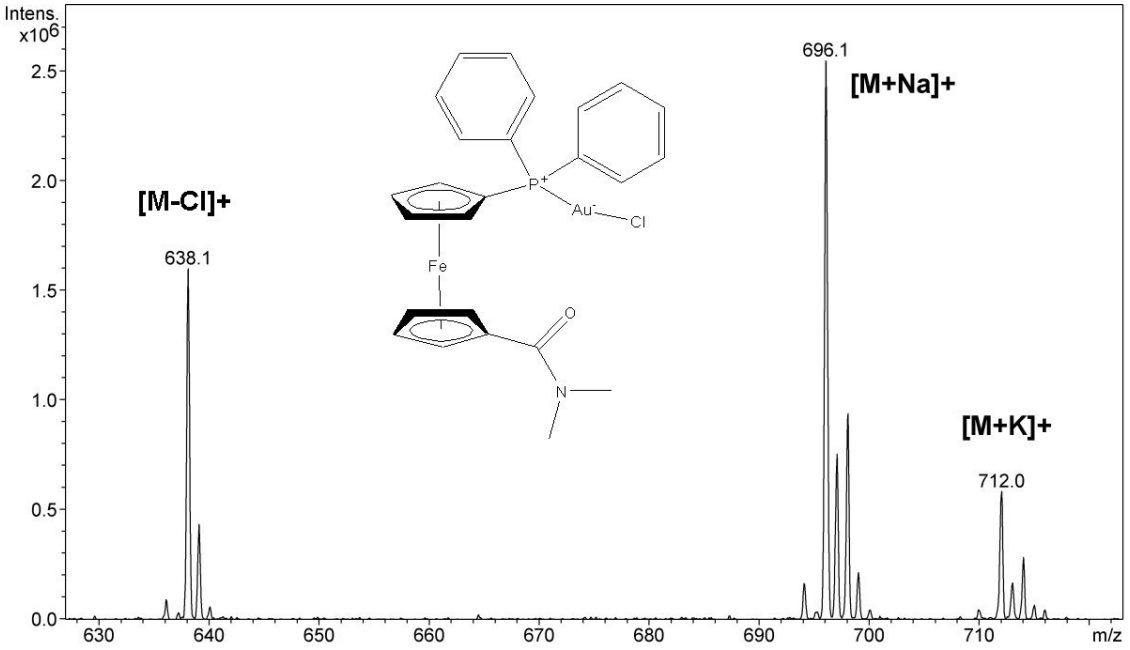

Obr.3.11 ESI – MS spektrum komplexu **8c** v pozitivním módu

U této struktury byla rovněž studována fragmentace provedením MS^2 a také MS^3 experimentu. Naměřená data jasně potvrdila navržený mechanismus fragmentace a dále doplněný o zjištění, že ion $[M - Cl]^+$ se dále rozpadá ztrátou N,N-dimethylaminu.

Výsledky prezentované práce potvrzují, že hmotnostní spektrometrie má své nezastupitelné místo v oblasti charakterizace koordinačních sloučenin. Ionizace elektosprejem je navíc schopná poskytnout velmi cenné informace o chování komplexů v roztoku, čímž je schopna vhodně doplnit údaje získané například měřením rentgenových spekter.

ESI – MS spektra všech připravených látek rozpuštěných v methanolu byla měřena na přístroji Bruker Esquire 3000.

3.4. Literatura I -III

1. R.B. Heslop, K.Jones, Anorganická chemie, Praha, SNTL 1982
2. K.Schwochau, Technetium, Wiley-VCH Verlag GmbH, Weinheim (2000)
3. Dilworth J. R., Parrott S. J.: *Chemical Society Reviews* 27: 43 - 55 (1998).
4. Wan K. X., Vidavsky I., Gross M. L.: *J. Am. Soc. Mass Spectrom.* 13: 85 – 88 (2002).
5. Abram U., Alberto R.:. *J. Braz. Chem. Soc.* 17(8): 1486 – 1500 (2006).
6. A. Togni and T. Hayashi (Eds),Ferrocenes . VCH, Weinheim (1995)
7. Polášek M., Štěpnička P., J.Mass Spectrom. 33 , 739 - 749 (1998)
8. Henderson W., McIndoe J.Scott, Mass Spectrometry of Inorganic, Coordination and Organometallic Compoound John Wiley & Sons, Ltd. 2005
9. P. Zanello, G. Opromolla, G. Giorgi, G. Sasso and A. Togni, J. Organomet. Chem. 506 , 61 (1996)
10. Vohlídal J., Julák A., Štulík K., Chemické a analytické tabulky, Grada Publishing 1999
11. P. Štěpnička, Chem. Soc. Rev., 2012, 41, 4273.

PUBLIKACE I

Characterization of Rhenium (V) Complexes with Phenols Using Mass Spectrometry with Selected Soft Ionization Techniques

Štícha, M.; Jelínek, I.; Poláková, J.; Kaliba, D.

Analytical Letters. 48 (2015) 2329-2342.

Analytical Letters, 48: 2329–2342, 2015

ISSN: 0003-2719 print/1532-236X online
DOI: 10.1080/00032719.2015.1038552

Mass Spectrometry

CHARACTERIZATION OF RHENIUM(V) COMPLEXES WITH PHENOLS USING MASS SPECTROMETRY WITH SELECTED SOFT IONIZATION TECHNIQUES

Martin Štícha,[1] Ivan Jelínek,[2] Jana Poláková,[1] and David Kaliba[2]

[1]*Faculty of Science, Department of Chemistry, Charles University in Prague, Prague, Czech Republic*

[2]*Faculty of Science, Department of Analytical Chemistry, Charles University in Prague, Prague, Czech Republic*

The synthesis, characterization, and mass spectra of oxorhenium(V) complexes with 1,2-dihydroxybenzene, 1,2,3-trihydroxybenzene, and 2,3-dihydroxynaphtalene are reported. Electrospray ionization, atmospheric pressure photoionization, and laser desorptionl ionization mass spectra of the complexes showed abundant negatively charged molecular anions and low fragmentation. Calculated similarity indexes showed significant conformity between the computed and experimental isotopic patterns of selected ions and confirmed correct assignment of elemental composition to mlz values. Electrospray tandem mass spectrometry provided essential information about fragments from molecular ions of studied complexes, making it possible to distinguish among fragment ions and the ions arising from compounds present in the reaction mixture. Based on the results, mass spectrometry utilizing soft common ionization techniques is useful for monitoring complex formation reaction kinetics and the stabilities of the complexes. Representative spectra were recorded for micromolar concentrations of the analytes.

Keywords: Complexes; Fragmentation; Mass-spectrometry; Rhenium; Structural analysis

INTRODUCTION

Nuclear medicine relies frequently on transition metal-based radiopharmaceuticals introduced to patients in form of organic ligand complexes (Abrams and Murrer 1993). The choice of radioisotopes is restricted to those fulfilling strict radiological and pharmacological requirements. Previous research has focused on technetium and rhenium (Alberto 1996; Dilworth and Parrott 1998). Both metals possess almost identical chemical properties (Colton 1965; Gerloch and Constable 1994) and their compounds possess a variety of oxidation states from -1 to $+7$ and form both cationic and anionic species with strong oxidizing to mild reducing properties. As transition metals, they are able to form coordination complexes with

Received 26 January 2015; accepted 29 March 2015.

Address correspondence to Martin Štícha, Hlavova 8, 128 43 Prague 2, Czech Republic. E-mail: sticha@natur.cuni.cz

inorganic and organic ligands whose stabilities depend on individual redox states of central metal ion and coordinated ligands. Coordination compounds of ^{99m}Tc are well established in nuclear diagnostics; among other radionuclides, there is considerable research interest in ^{186}Re and ^{188}Re for applications in bone antitumor therapy (Blower et al. 1990; Volkert and Deutsch 1993). For rhenium based radiopharmaceuticals, defined reduction of perrhenate and its stabilization via suitable complex formation remain crucial breakthroughs to be achieved. Significant effort has been spent on methods of preparation and structural characterization of rhenium complexes with aromatic organic ligands (Bandoli et al. 2002; Gerber, Luzipo, and Mayer 2004, 2006; Gerber and Mayer 2005; Booysen et al. 2007; Machura and Kusz 2008; de Souza et al. 2010; Machura, Wolff, and Gryca 2014). In these studies, it was confirmed that aromatic amines and alcohols are the most useful groups for Re to produce complexes with excellent chemical and radiochemical stability. Such promising properties warrant further investigation into their potential use in radiopharmaceutical development and practice.

The availability of analytical methods suitable for identification and quantification of metal complexes is an essential prerequisite for the chemical and pharmacological characterization of radiopharmaceuticals. Commonly used X-ray diffraction, nuclear magnetic resonance (NMR), and infrared spectroscopy (IR) usually provides detailed structural information but require higher amounts of sample. Mass spectrometry is an excellent method for quantification and structural elucidation of analytes at trace concentrations comparable to common therapeutic levels. The introduction of soft ionization techniques to mass spectrometry (MS) revealed the possibility of quantification and structure characterization of various types of complexes. Fast atom bombardment (FAB-MS) and field desorption (FD-MS) techniques were the first for the structural identification of metal complexes (Henderson and McIndoe 2005). Since the introduction of electrospray ionization (ESI), the use of mass spectrometry in the field of organometallic and metal coordination chemistry has been significantly extended (Henderson et al. 1998; Traeger 2000). Because of the soft nature of ESI, an intact molecular ion is usually observed with minor fragmentation. ESI-MS was suitable for the characterization of technetium and rhenium complexes (Hori et al. 1996, 1997; Tisato et al. 2004; Tubaro et al. 2004). Compared to other methods of analysis, the sensitivity of ESI-MS allows characterization of sample at micromolar concentrations, thus making it very useful for clinical and pharmacokinetic studies. Similar favorable characteristics are also present for recently developed ionization techniques based on electrospray, such as probe electrospray ionization (PESI) and desorption spray ionization (DESI). Recent reports have demonstrated that PESI and DESI sources are suitable for direct analysis of many kinds of samples, including organometallic compounds and metal complexes (Chen et al. 2008a, 2008b).

Similarly, laser desorption/ionization (LDI) and matrix assisted laser desorption/ionization (MALDI) are useful for metal complexes. As a consequence of LDI or MALDI ionization in the condensed phase, the majority of complexes gave simple and interpretable mass spectra (Wyatt, Stein, and Brenton 2006; Wyatt 2011). However, direct photochemical degradation and other photochemical reactions in course of LDI and MALDI ionization reduced the abundance of molecular ions in favor of fragments. The comparison of the analysis of selected rhenium(+I)

complexes (but not with phenolic ligands) by means of LDI, MALDI, and ESI ionization was reported by Petroselli et al. (2012) and Day, Payne, and Holt (2007).

Atmospheric pressure photoionization (APPI) offers a viable alternative for ionization of kinetically labile compounds and various types of complexes. Relatively low ionization energy provided by ultraviolet radiation typically generates molecular ions or protonated molecules, and relatively few adducts and fragment ions. Compared to ESI, LDI, and MALDI the extent of molecular ion fragmentation is usually negligible.

Here is reported the characterization and mass spectra of three structurally related oxorhenium(V) complexes with phenols as complex forming ligands derived from catechol. The 1,2-Dihydroxybenzene, 1,2,3-trihydroxybenzene, and 2,3-dihydroxynaphtalene were used as oxygen donor ligands with a oxorhenium(V) complex, *n*-tetrabutylamonium-tetrachlorooxorhenate (n-Bu_4N)[$ReOCl_4$]. ESI-MS, APPI-MS, and LDI-MS were compared for the identification of studied complexes and other compounds present in the reaction mixture in course of complex formation.

MATERIALS AND METHODS

Materials

All reagents were obtained commercially and were of highest purity available: the standards tetrabutylammonium tetrachlorooxorhenate(V) and 1,2-dihydroxybenzene were purchased from Sigma-Aldrich; 1,2,3-trihydroxybenzene and 2,3-dihydroxynaphthalene were purchased from Alfa Aesar; deuterated acetonitrile (ACN-d_3) for NMR (99.8 percent purity) was purchased from Euro-isotop; acetonitrile (HPLC grade) was purchased from Lach-Ner (dried and deoxygenated before use); and ESI tuning mix for the ion trap and APCI/APPI tuning mix for the ion trap were purchased from Agilent.

Instrumentation

Infrared (IR) spectra of prepared complexes were recorded on Nicolet 380 spectrometer using KBr discs. Proton nuclear magnetic resonance (^{1}H NMR) spectra were obtained in deuterated acetonitrile (ACN-d_3) and recorded using a Bruker Avance III (600 MHz) spectrometer. APPI-MS and ESI-MS were conducted on an ion trap instrument Esquire 3000; LDI-MS experiments were performed using matrix assisted laser desorption ionization with a tandem time of flight analyzer (MALDI-TOF/TOF) Ultraflex II with a 337 nanometers nitrogen laser (both Bruker Daltonics, Germany).

Synthesis of the Complexes

The structures of the ligands and prepared complexes are shown in Figure 1 and Figure 2. These complexes were prepared by modified procedure described for similar compounds by Gerber and others (Gerber, Luzipo, and Mayer 2004, 2006; Gerber and Mayer 2005; Booysen et al. 2007). The procedure was identical for all studied ligands. A mixture of 2 mg of tetrabutylamonium-tetrachlorooxorhenate

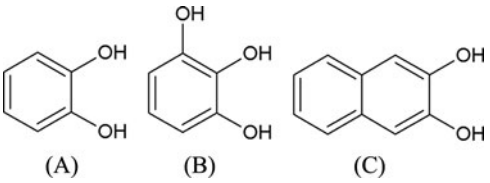

Figure 1. Structures of ligands: (A) 1,2-dihydroxybenzene, (B) 1,2,3-trihydroxybenzene, and (C) 2,3-dihydroxynaphthalene.

(3.42 millimolar) and 6.84 millimolar of appropriate ligand in 2 milliliters of acetonitrile was heated to reflux under argon with constant stirring for sixty minutes. After cooling to room temperature, the solvent was evaporated under vacuum and the resulting precipitates were stored under an inert atmosphere.

Spectroscopic Characterization

The infrared spectra of the complexes included strong absorption from 910 to 1000 per centimeter assigned to a characteristic stretch of a terminal Re=O group. The typical intense aromatic C=C stretching vibrations gave rise to absorption bands in the region from 1470 to 1520 per centimeter. Intense bands at 2962, 2932, and 1509 per centimeter corresponded to the presence of the tetrabutylammonium countercation.

The complexes in deuterated acetonitrile showed sharp, well-resolved peaks in their ^{1}H NMR spectra. The complex bis(1,2-dihydroxybenzene)oxorhenium(-) (**5**) provided shifts at (600 MHz, CDCN): δ: 6.82–6.80 (m, 6H) and 6.72–6.71 (m, 6H). Bis(1,2,3-trihydroxybenzene)rhenium(-) (**10**) had shifts at (600 MHz, CD_3CN): δ: 9.95 (bs, 2H), 6.57–6.55 (m, 2H), and 6.35–6.34 (m, 4H). Bis(2, 3-dihydroxynaphthalene) oxorhenium(-) (**14**) had peaks at (600 MHz, CD_3CN): δ: 7.61–7.59 (m, 4H) and

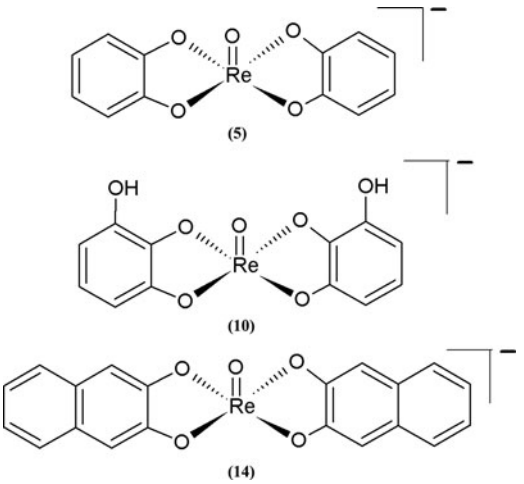

Figure 2. Structures of prepared anionic oxorhenium complexes: bis(1,2-dihydroxybenzene) oxorhenium (-) (5); bis(1,2,3-trihydroxybenzene)oxorhenium(-) (10); and bis(2,3-dihydroxynaphthalene)oxorhenium(-) (14).

7.25–7.22 (m, 8H). Characteristic shifts of terabutylammonium at 3.09–3.06 (m, 8H), 1.62–1.57 (m, 8H), 1.37–1.33 (m, 8H), and 0.97 (t, j = 7.3 Hz, 12H) ppm were present in all complexes.

Mass Spectrometry

ESI-MS and APPI-MS data were collected in negative ion mode at a scan range from *m*/*z* 260 to 1000. For APPI-MS, the source temperature was 350 degree Celsius and the nebulizer gas pressure was 20 psi. In all measurements, the flow rate of dry gas was 5 liters per minute and the temperature was 250°C. The sample was diluted in acetonitrile and delivered to the nebulizer by a syringe pump (Cole Parmer, USA) at a flow rate of 100 microliters per minute. Optimized conditions of the mass spectrometer in negative ion modes were a capillary voltage of 1500 volts, a flow rate of desolvation gas of 5 liters per minute, and a desolvation temperature of 250 degree Celsius.

In ESI-MS, the nebulizer gas pressure was 18 psi. In all measurements, the flow rate of dry gas was 5 liters per minute and the temperature was 250 degree Celsius. The sample was diluted in acetonitrile and delivered to the nebulizer by a syringe pump (Cole Parmer, USA) at a flow rate of 8 microliters per minute. Optimized conditions of the mass spectrometer in negative ion modes were a capillary voltage of 4000 volts, a flow rate of desolvation gas of 5 liters per minute, and a desolvation temperature was 250 degree Celsius. The instrument was controlled by the Esquire Control 5.3.11 software and data were processed via Data Analysis 3.3.56 from Bruker Daltonics (Germany).

LDI-MS spectra were acquired in negative ion mode at a scan range from *m*/*z* 260 to 1000. Sample solutions were spotted on an MTP 384 polished stainless steel target plate from Bruker Daltonics (Germany). The laser power was adjusted to obtain high signal-to-noise ratios and maximal resolution. Spectra were obtained and analyzed with the software FlexControl and FlexAnalysis from Bruker Daltonics (Germany).

ESI-MS/MS spectra were recorded with a fragmentation cut-off set to approximately one-third of the m/z of the parent ion. The isolation width of the parent ion was set to 4 daltons to acquire a full isotope profile of the fragments. The fragmentation amplitude was varied from 0.8 to 1.2 volts. The fragmentation time in the ion trap was 40 milliseconds. All other experimental conditions were identical to those above in conventional ESI-MS.

The similarity between the computed and experimental molecular ion isotopic clusters was evaluated on the basis of similarity indexes (SI) (Wan, Vidavsky, and Gross 2002). The corresponding formula is given in (1), where $(i - i_0)$ is a difference in signal intensities at a given mass for two peaks, divided by the smaller intensity value (i_0) and N is the number of product-ion signals that are compared:

$$SI = \sqrt{\frac{\sum_i \left\{ \frac{i - i_0}{i_0} x100 \right\}^2}{N}} \tag{1}$$

According to definition, the similarity index may have values from 0 to 1. Peak patterns with SI = 0 are identical. In order to obtain percentual expression of isotopic

patterns similarity, values of (1 – SI)100 were evaluated. Theoretical isotopic patterns were generated via Data Analysis 3.3.56 software.

RESULTS AND DISCUSSION

ESI, APPI, and LDI mass spectra of the complexes, together with supplementary ESI-MS/MS spectra, are shown in Figures 3, 4, and 5. In general, abundant negatively charged molecular ions of the complexes were observed for all ionization techniques and the extent of fragmentation was low. Recorded negative ion mass spectra primarily consisted of intact molecular ions of the complexes and other ions corresponding to the presence of residual reagents, reaction byproducts, and their oxidation products. The ligands did not contain functional groups that could be protonated; therefore, positive ion spectra did not include information about the structure of prepared complexes. In the positive mode, only the tetrabutylammonium counter cation was observed.

A survey of observed ions in prepared complexes with abundancies higher than 5 percent of corresponding base peak intensity in comparison to their mass/charge (*m*/*z*) ratio is shown in Table 1. Characteristic isotopic clusters were observed for all molecular species. The values (1 – SI)100 given in Table 2 indicate significant conformity between calculated and experimental spectra and correct assignment of elemental composition to m/z values of observed ions.

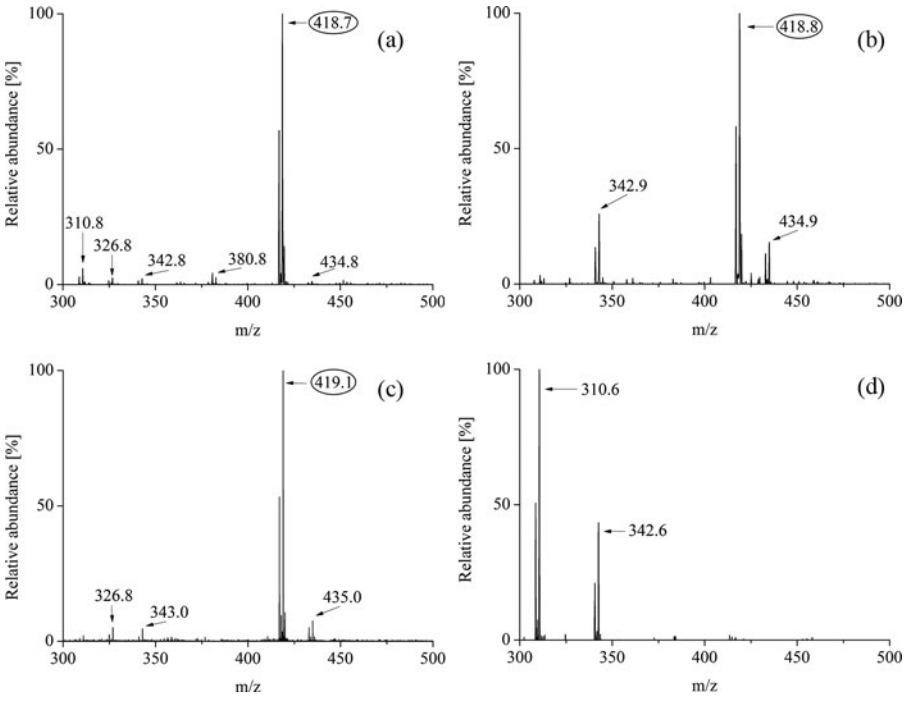

Figure 3. Negative ion mass spectra of $\sim 5 \times 10^{-6}$ molar bis(1, 2-dihydroxybenzene)oxorhenium(-): (a) ESI, (b) APPI, (c) LDI, and (d) ESI-MS/MS. Molecular ion peaks are circled.

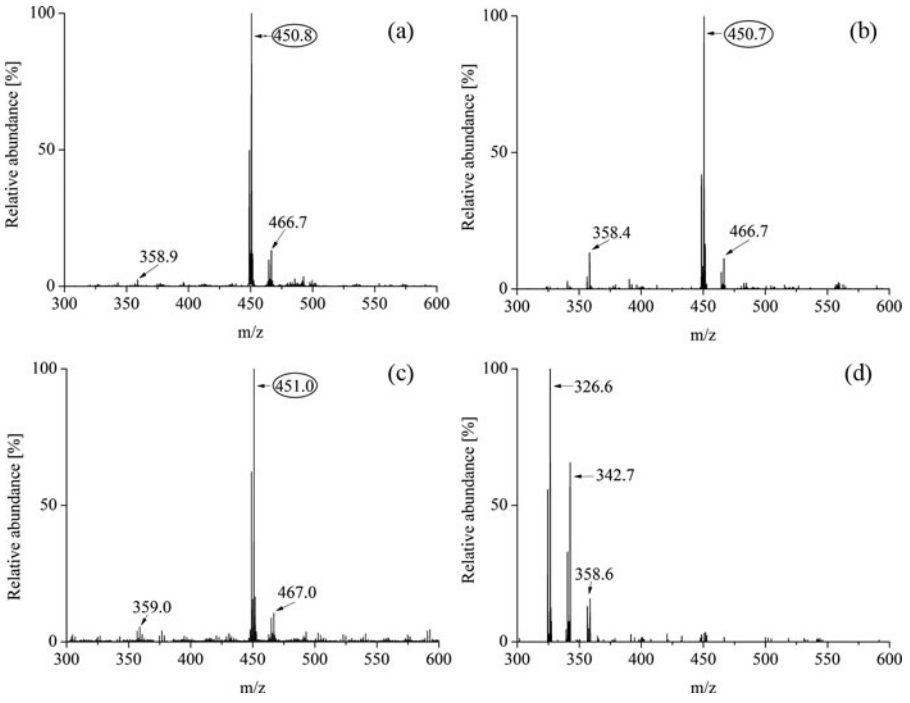

Figure 4. Negative ion mass spectra of $\sim 5 \times 10^{-6}$ molar bis(1,2,3-trihydroxybenzene)oxorhenium(-); (a) ESI, (b) APPI, (c) LDI, and (d) ESI-MS/MS. Molecular ion peaks are circled.

It is evident that all ionization techniques provide abundant molecular ions for the complexes, residual reactants, and reaction by-products in corresponding reaction mixtures. Evident isotope pattern proximity between calculated and experimental ESI spectra of bis(2,3-dihydroxynaphthalene)oxorhenium(-) complex is documented in Figure 6.

ESI-MS, APPI-MS, and LDI-MS

By ESI and APPI, it was possible to detect negatively charged intact molecular anions $[M]^-$. The complexes showed similar behavior under ESI conditions: abundant molecular anions as base peaks and minor fragment peaks. Recorded spectra were simple and provided direct information about the structure of the complexes and the presence of residual reactants and reaction by-products. No dimeric and other cluster structures were observed. The extent of possible ligand exchange with acetonitrile as a solvent was negligible. Comparison of ESI and APPI spectra showed no evidence of ions arising from electrochemical processes in the course of ESI ionization. Direct comparison of minor differences in ion intensities was difficult due to different tuning procedures used for the types of ionization. Evidently, different tuning procedures discriminated ions in a different manner and made the direct comparison of intensities impossible. Concerning the ion 343 *m/z* (fragment of Re-catechol complex), its higher relative intensity in APPI is due to a higher response

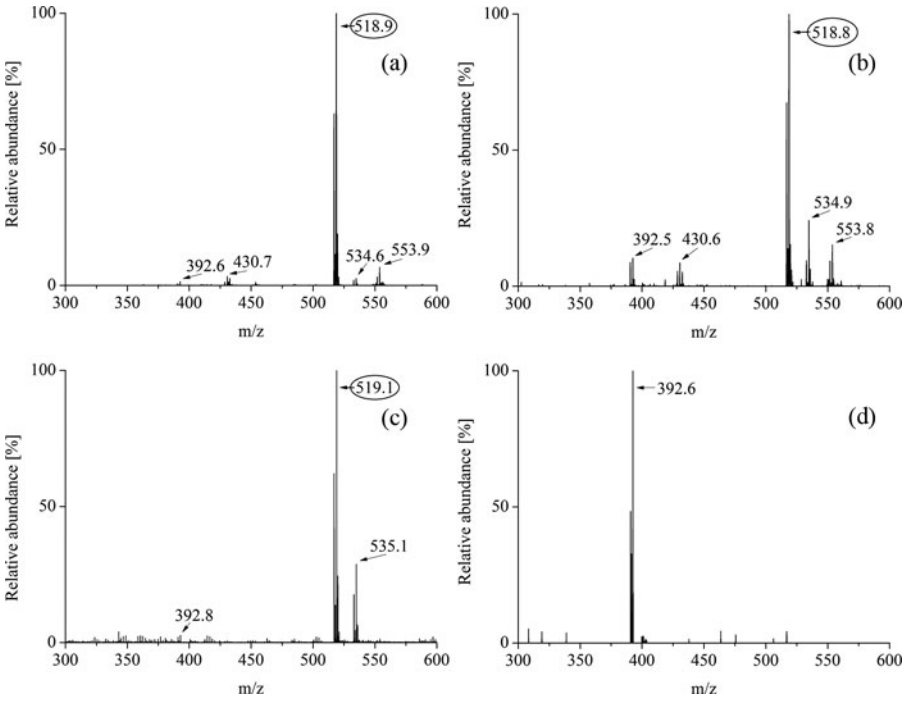

Figure 5. Negative ion mass spectra of $\sim 5 \times 10^{-6}$ M bis(2,3-dihydroxynaphthalene)oxorhenium(-); (a) ESI, (b) APPI, (c) LDI, and (d) ESI-MS/MS. Molecular ion peaks are circled.

factor or more pronounced fragmentation in course of photoionization. Moderate increases of the fragment ion intensities for APPI were also observed for the other complexes.

Due to the presence of O-substituted aromatic ligands, the complexes studied in this work showed strong absorption in the ultraviolet, particularly at 337 nanometers and, in principle, did not require the addition of a matrix. In contrast to previously reported MALDI and LDI work on rhenium complexes (Petroselli et al. 2012), we observed abundant negatively charged molecular ions as base peaks.

Table 1. Summary of observed ions in prepared complexes with abundancies higher than 5 percent of corresponding base peak intensity and listed by increasing mass to charge ratio (*m/z*)

Bis(1,2-dihydroxybenezen) oxorhenium(-)			Bis(1,2,3-trihydroxybenzene) oxorhenium (-)			Bis(2,3-dihydroxynaphthalene) oxorhenium(-)		
Entry	m/z	Formula	Entry	m/z	Formula	Entry	m/z	Formula
1*	311	$ReC_6H_4O_3$	7*	327	$ReC_6H_4O_4$	12*	393	$ReC_{10}H_6O_5$
2	327	$ReC_6H_4O_4$	8*	343	$ReC_6H_4O_5$	13	431	$ReC_{10}H_6O_3Cl_2$
3*	343	$ReC_6H_4O_5$	9*	359	$ReC_6H_4O_6$	**14**	**519**	$\mathbf{ReC_{20}H_{12}O_5}$
4	381	$ReC_6H_4O_3Cl_2$	**10**	**451**	$\mathbf{ReC_{12}H_8O_7}$	15	535	$ReC_{20}H_{12}O_6$
5	**419**	$\mathbf{ReC_{12}H_8O_5}$	11	467	$ReC_{12}H_8O_8$	16	554	$ReC_{20}H_{12}O_5Cl$
6	435	$ReC_{12}H_8O_6$						

*Identified by ESI-MS/MS as fragment ions. Desired products are highlighted in bold.

Table 2. Experimental (exp.) and calculated (calc.) relative intensities (I %) of ions in isotopic clusters and evaluated values of similarity indexes (SI) expressed as (1-SI)100

			ESI		APPI		LDI	
Complex	Molecular Formula	m/z	I percent calc.	I percent exp.	I percent calc.	I percent exp.	I percent calc.	I percent exp.
bis(1,2-dihydroxybenezen) oxorhenium(-)	$C_{12}H_8O_5$ Re	417	59.1	56.9	59.1	56.9	59.1	53.4
		418	7.8	4.2	7.8	4.2	7.8	9.5
		419	100.0	100.0	100.0	100.0	100.0	100.0
		420	13.2	14.1	13.2	14.1	13.2	10.6
		421	1.8	0.4	1.8	0.4	1.8	0.7
			$(1-SI)100 = 91.9$		$(1-SI)100 = 91.9$		$(1-SI)100 = 89.0$	
bis(1,2, 3-trihydroxybenzene) oxorhenium(-)	$C_{12}H_8O_7$ Re	449	58.9	49.8	58.9	41.9	58.9	62.3
		450	7.9	20.4	7.9	8.3	7.9	15.6
		451	100.0	100.0	100.0	100.0	100.0	100.0
		452	13.3	11.9	13.3	16.5	13.3	16.5
		453	2.2	0.1	2.2	2.0	2.2	3.8
			$(1-SI)100 = 74.9$		$(1-SI)100 = 79.1$		$(1-SI)100 = 84.2$	
bis(2,3-dihydroxy-naphthalene) oxorhenium(-)	$C_{20}H_{12}O_5$Re	517	58.6	63.0	58.6	67.5	58.6	62.1
		518	12.9	11.5	12.9	13.8	12.9	13.8
		519	100.0	100.0	100.0	100.0	100.0	100.0
		520	21.8	19.0	21.8	15.4	21.8	24.5
		521	3.3	3.0	3.3	5.9	3.3	3.9
			$(1-SI)100 = 91.1$		$(1-SI)100 = 81.1$		$(1-SI)100 = 92.3$	

This is probably due to high stability of these studied complexes, together with the absence of matrix promoting photochemically induced dissociation reactions.

ESI-MS/MS

ESI-MS/MS provided essential information about fragments arising from molecular ions of studied complexes, making it possible to distinguish among fragment ions and the ions arising from compounds present in reaction mixture.

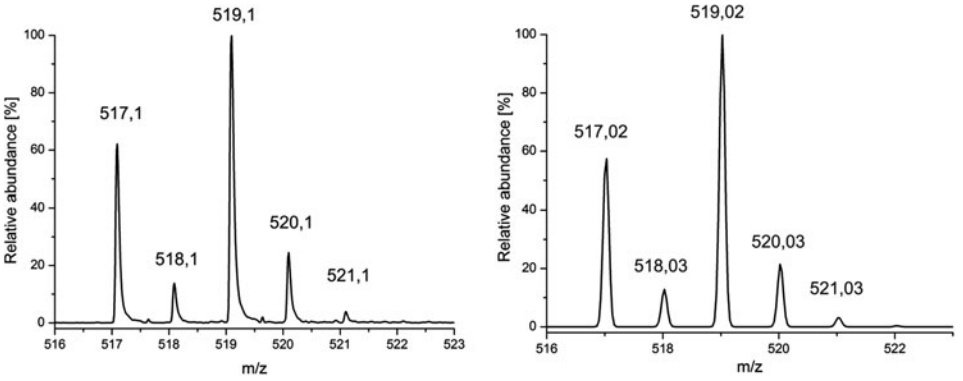

Figure 6. Experimentally (left) and theoretical (right) isotopic patterns of the bis(2,3-dihydroxynaphthalene) oxorhenium(-) molecular ion cluster.

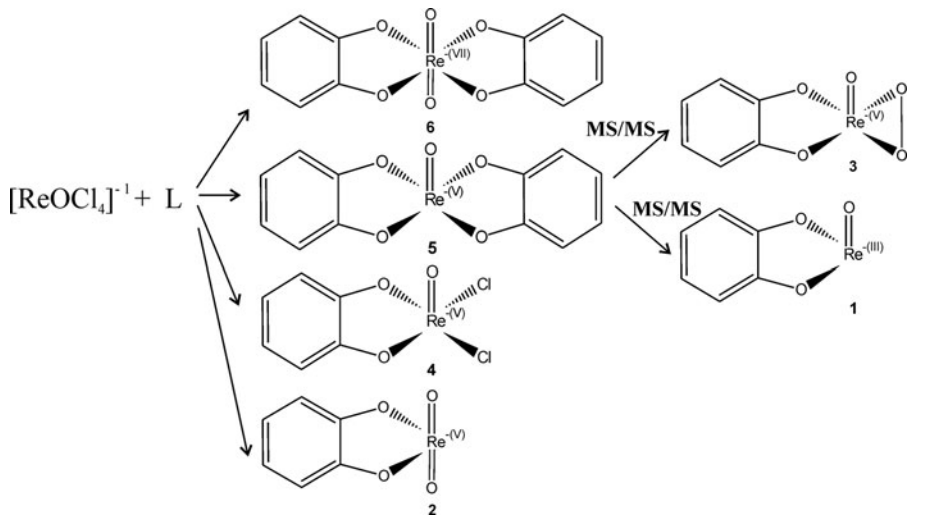

Figure 7. Molecular and fragment ions in the bis(1,2-dihydroxybenzene)oxorhenium(-) reaction by ESI-MS and ESI-MS/MS.

In some cases, chemical reactions and fragmentation processes yielded the same ionic structures. The spectra of ions arising from ESI-MS/MS fragmentation of complex molecular ion as a parent ion are shown in Figures 3, 4, and 5. Ionic structures in bis(1,2-dihydroxybenzene)oxorhenium(-) (**5**) reaction mixture are summarized in Figure 7. It may be concluded that (**1**) and (**3**) are fragments, (**4**) is a molecular

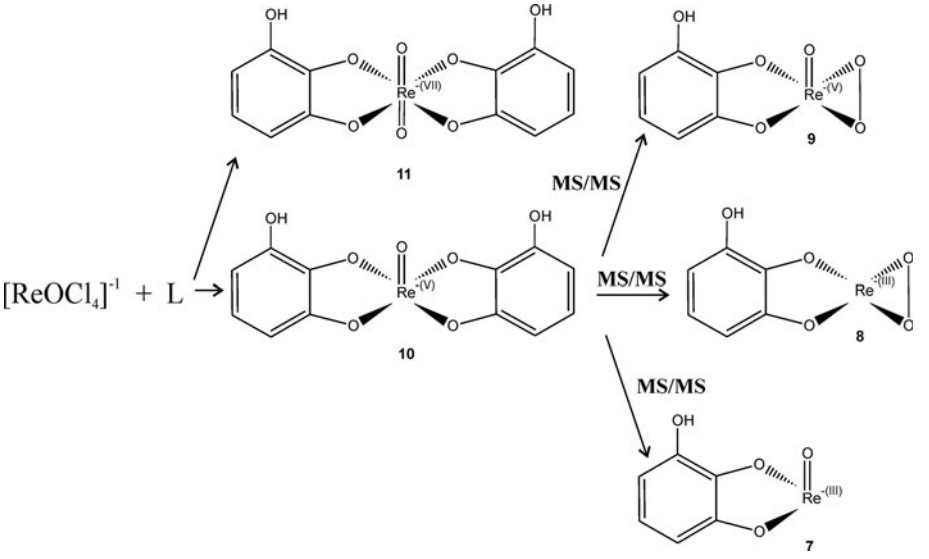

Figure 8. List of molecular and fragment ions in the bis(1,2,3-trihydroxybenzene)oxorhenium(-) reaction by ESI-MS and ESI-MS/MS.

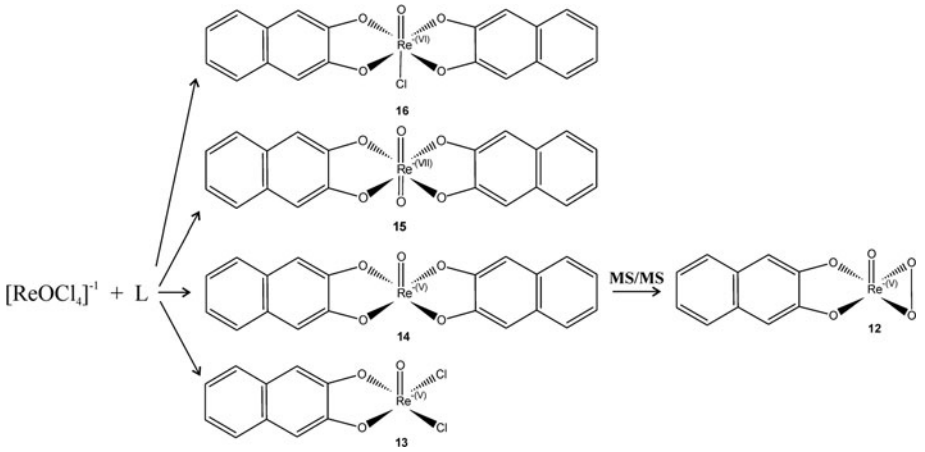

Figure 9. List of molecular and fragment ions in the bis(2,3-dihydroxynaphthalene)oxorhenium(-) reaction by ESI-MS and ESI-MS/MS.

ion of an intermediate of complex forming reaction, and (**2**) and (**6**) correspond to di-oxo derivatives of a complex and its intermediate. The ionic structures detected in bis (1,2,3-trihydroxybenzene)oxorhenium(-) (**10**) reaction mixture are shown in Figure 8. Ions (**7**), (**8**), and (**9**) are fragments and (**11**) corresponds to di-oxo derivative. Ions detected in the bis(2,3-dihydroxynaphthalene)oxorhenium(-) reaction mixture are shown in Figure 9. Here the spectrum of ions corresponding to species accompanying the complex is quite rich and involves complex intermediates [(**13**) and (**16**)] and molecular ion of di-oxo derivative [(**15**)]. Ion (**12**) was the only MS/MS fragment observed.

In general, MS/MS fragmentation pathways are straightforward. Daughter ions were formed predominantly by a cleavage of the aromatic part on a single ligand [(**3**), (**9**), and (**12**)] or by a loss of entire ligand [ML] [(**1**) and (**7**)]. However, the latter mentioned fragmentation mechanism was not observed for the bis(2,3-dihydroxynaphthalene)oxorhenium(-) complex as the most stable. For bis(1,2,3-trihydroxybenzene)oxorhenium(-), the ion at *m*/*z* 327 may be rationalized by a loss of oxygen from (**9**). Complementary APPI-MS/MS experiments did not reveal differences in fragmentation pathways; the spectra of daughter ions were nearly identical.

CONCLUSIONS

Mass spectrometry using electrospray ionization, atmospheric pressure photoionization, and laser desorption/ionization was shown to be useful for structural characterization of rhenium complexes with phenolic ligands and for other compounds present in reaction mixtures in course of complex preparation. The mass spectra obtained gave unambiguous information about molecular weights and the structures of the compounds because intact molecular ions and structurally characteristic fragments were observed. Direct information about the composition of the reaction mixture was accessible without, in principle, problematic and laborious

chromatographic separation. The uncertainty of correct structural characterization of observed ions, based on low-resolution MS data, was greatly reduced by the complementary evaluation of characteristic isotopic patterns and comparison with theoretical profiles.

The synthesis of three structurally similar rhenium complexes prepared by the reaction of rhenium precursor tetrabutylamonium-tetrachlorooxorhenate with aromatic alcohol ligands; 1,2-dihydroxybenzene, 1,2,3-trihydroxybenzene, and 2,3-dihydroxynaphtalene was performed in acetonitrile. In addition, complexes of bis (1,2-dihydroxybenzene)oxorhenium(-), bis(1,2,3-trihydroxybenzene)oxorhenium(-), and bis(2,3-dihydroxynaphthalene)oxorhenium(-) were characterized by ^{1}H NMR and infrared spectroscopy. Comparisons of data available from these methods clearly demonstrated the reliability and information obtained by mass spectrometry.

One may conclude that mass spectrometry utilizing soft ionization techniques is powerful for monitoring complex formation reaction kinetics and their stabilities. Representative spectra were recorded for micromolar concentrations of the analytes. Though it is less suitable for characterization of closely related structures, such as *cis* and *trans* isomers, its sensitivity is superior to commonly used NMR making it unique for real clinical and pharmacokinetic studies. The ESI-MS/MS results provide an initial understanding of the mechanism of rhenium oxo-complex fragmentation.

FUNDING

This work was supported by Charles University project SVV 260205.

REFERENCES

Abrams, M. J., and B. A. Murrer. 1993. Metal compounds in therapy and diagnosis. *Science* 261: 725–30. doi:10.1126/science.8102010

Alberto, R. 1996. Technetium and rhenium. *Topics in Current Chemistry* 176: 150–84.

Bandoli, G., A. Dolmella, T. I. A. Gerber, D. Mpinda, J. Perils, and J. G. H. du Preez. 2002. Complexes of oxorhenium (V) with aromatic 2-amino-alcohols. *Journal of Coordination Chemistry* 55(7): 823–33. doi:10.1080/0095897022000001575

Blower, P. J., J. Singh, S. E. M. Clarke, M. M. Bisundan, and M. J. Went. 1990. Preparation and characterisation of pentavalent Rh-186 DMSA. A possible tumour therapy agent. *Journal of Nuclear Medicine* 31: 212–13.

Booysen, I., T. I. A. Gerber, E. Hostem, and P. Mayer. 2007. Monodentate imido coordination of 2-aminodiphenylamine to rhenium(V). *Journal of Coordination Chemistry* 60: 1749–53. doi:10.1080/00958970601151273

Chen, L. C., K. Nishidate, Y. Saito, K. Mori, D. Asakawa, S. Takeda, T. Kubota, N. Terada, Y. Hashimoto, H. Hori, and K. Hiraoka. 2008a. Application of probe electrospray to direct ambient analysis of biological samples. *Rapid Communications in Mass Spectrometry* 22: 2366–74. doi:10.1002/rcm.3626

Chen, L. C., K. Nishidate, Y. Saito, K. Mori, D. Asakawa, S. Takeda, T. Kubota, N. Terada, Y. Hashimoto, H. Hori, and K Hiraoka. 2008b. Characteristics of probe electrospray generated from a solid needle. *The Journal of Physical Chemistry B* 112: 11164–70. doi:10.1021/jp803730x

Colton, R. 1965. *The chemistry of rhenium and technetium*. London. UK: Interscience.

Day, E. F., T. A. Payne, and C. A. Holt. 2007. Mass spectrometric study of dirhenium biscarboxylate: Purine dinucleotide complexes. *Rapid Communications in Mass Spectrometry* 21: 903–10. doi:10.1002/rcm.2910

de Souza, E. J., A. G. A. Fernandes, P. I. S. Maia, S. S. Lemos, J. Ellena, U. Abram, and V. M. Deflon. 2010. Oxorhenium(V) complexes with 2,3-dihydroxynaphthalene. *Zeitschrift für anorganische und allgemeine Chemie* 636: 2467–70. doi:10.1002/zaac.201000156

Dilworth, J. R., and S. J. Parrott. 1998. The biomedical chemistry of technetium and rhenium. *Chemical Society Reviews* 27: 43–55. doi:10.1039/a827043z

Gerber, T. I. A., D. G. Luzipo, and P. Mayer. 2004. Formation of an oxo-free rhenium(v) complex with 2-aminophenol. *Journal of Coordination Chemistry* 57: 1393–98. doi:10.1080/00958970412331300069

Gerber, T. I. A., D. G. Luzipo, and P. Mayer. 2006. Monodentate imido and bidentate aminophenolate coordination of 2-aminophenol in rhenium(V) complexes. *Journal of Coordination Chemistry* 59: 1055–62. doi:10.1080/00958970500410432

Gerber, T. I. A., and P. Mayer. 2005 Versatility of bidentate aniline derivatives as ligands for rhenium (V) and technetium (V). *Journal of Nuclear and Radiochemical Sciences* 6: 165–68. doi:10.14494/jnrs2000.6.3_165

Gerloch, M., and E. G. Constable. 1994. *Transition metal chemistry*. Weinheim, Germany: VCH Verlagsgesellschaft mbH.

Henderson, W., and J. S. McIndoe. 2005. *Mass spectrometry of inorganic, coordination and organometallic compounds: Tools – Techniques – Tips*. Wiltshire, UK: Wiley.

Henderson, W., B. K. Nicholson, and L. J. McCaffrey. 1998. Applications of electrospray mass spectrometry inorganometallic chemistry. *Polyhedron* 17: 4291–13. doi:10.1016/s0277-5387(98)00246-0

Hori, H., J. Ishihara, K. Koike, K Takeuchi, T. Ibusuki, and O. Ishitani. 1997. Electrospray mass-spectrometric detection of neutral rhenium bipyridine complexes using $NaNO_3$ as an ionization agent. *Chemistry Letters* 3: 273–74. doi:10.1246/cl.1997.273

Hori, H., O. Ishitani, K. Koike, K. Takeuchi, and T. Ibusuki. 1996. Electrospray mass spectrometric detection of unstable rhenium complexes as reaction intermediates of photochemical CO_2-fixation. *Analytical Sciences* 12: 587–90. doi:10.2116/analsci.12.587

Machura, B., and J. Kusz. 2008. Synthesis, spectroscopic characterisation, crystal and molecular structure of [ReOBr(quin-2-c)2] and [ReOCl(quin-2-c)2] complexes: DFT and TD-DFT calculations for [ReOBr(quin-2-c)2]. *Polyhedron* 27: 187–95. doi:10.1016/j.poly.2007.09.010

Machura, B., M. Wolff, and I. Gryca. 2014. Rhenium(V) oxocomplexes [ReOX(N–O)2] and $[ReOL(N - O)2]^+$ – Synthesis, structure, spectroscopy and catalytic properties. *Coordination Chemistry Reviews* 275: 154–64. doi:10.1016/j.ccr.2014.05.012

Petroselli, G., M. K. Mandal, L. C. Chen, G. T. Ruiz, E. Wolcan, K. Hiraoka, H. Nonami, and R. Erra-Balsells. 2012. Mass spectrometry of rhenium complexes: A comparative study by using LDI-MS, MALDI-MS, PESI-MS and ESI-MS. *Journal of Mass Spectrometry* 47: 313–21. doi:10.1002/jms.2965

Tisato, F., C. Bolzati, M. Porchia, and F. Refosco. 2004. Contribution of electrospray mass spectrometry for the characterization, design, and development of nitrido technetium and rhenium heterocomplexes as potential radiopharmaceuticals. *Mass Spectrometry Reviews* 23: 309–32. doi:10.1002/mas.20000

Traeger, J. C. 2000. Electrospray mass spectrometry of organometallic compounds. *International Journal of Mass Spectrometry* 200: 387–401. doi:10.1016/s1387-3806(00)00346-8

Tubaro, M., E. Marotta, P. Traldi, C. Bolzati, M. Porchia, F. Refosco, and F. Tisato. 2004. ESI/MSn in the structural characterisation of some nitrido-Re heterocomplexes. *International Journal of Mass Spectrometry* 232: 239–47. doi:10.1016/j.ijms.2003.11.005

Volkert, W. A., and E. A. Deutsch. 1993. *Advances in metals in medicine*. State College, PA: JAI Press.

Wan, K. X., I. Vidavsky, and M. L. Gross. 2002. Comparing similar spectra: From similarity index to spectral contrast angle. *Journal of the American Society for Mass Spectrometry* 13: 85–88. doi:10.1016/s1044-0305(01)00327-0

Wyatt, M. F. 2011. MALDI-TOFMS analysis of coordination and organometallic complexes: A nic(h)e area to work in. *Journal of Mass Spectrometry* 46: 712–19. doi:10.1002/jms.1957

Wyatt, M. F., B. K. Stein, and A. G. Brenton. 2006. Characterization of various analytes using matrix-assisted laser desorption/ionization time-of-flight mass spectrometry and 2-[(2E)-3-(4-tert-butylphenyl)-2-methylprop-2-enylidene]malononitrile matrix. *Analytical Chemistry* 78: 199–206. doi:10.1021/ac050732f

PUBLIKACE II

Analytical study of rhenium complexes with pyrogallol and catechol

Štícha, M.; Kaliba, D.; Jelínek, I.; Poláková, J.

CHEMICAL PAPERS, In print (2016)

Analytical study of rhenium complexes with pyrogallol and catechol

[a]Martin Štícha, [b]David Kaliba, [b]Ivan Jelínek, [a]Jana Poláková

[a]*Charles University in Prague, Faculty of Science, Department of Chemistry, Hlavova 8, 128 43, Prague 2, Czech Republic*

[b]*Charles University in Prague, Faculty of Science, Department of Analytical Chemistry, Hlavova 8, 128 43, Prague 2, Czech Republic*

Corresponding author: RNDr. Martin Štícha; sticha@natur.cuni.cz; Hlavova 8, 128 43, Prague 2, Czech Republic

Received

Rhenium complexes composed of β-emitting ^{186}Re and ^{188}Re isotopes coordinated with suitable organic ligand gain increased interest in radiopharmaceutical medicine. Besides suitable radiological properties given by a metal ion itself, detailed knowledge of overall chemical properties of formed complexes, namely their exact structures, chemical stabilities and possible degradation pathways are essential pre-requisites for their clinical application. It should be noted that substantial information is accessible from experiments with non-radioactive analogues. Selected rhenium complexes with pyrogallol (1,2,3-trihydroxybenzene) and catechol (1,2-dihydroxybenzene) as strongly bound ligands were prepared by a reaction of rhenium precursor tetrabutylammonium-tetrachlorooxorhenate with twofold molar excess of ligand in presence of various amounts of triethylamine. The structures of formed complexes and their consequent reaction products were estimated by means of mass spectrometry with electrospray ionization. The rate of reactions in course of complex formation and consequent decomposition were primarily followed by UV-VIS absorption spectra measurement, complemented by single or continuous electrospray mass spectrometry analyses.

Keywords: rhenium complexes, mass spectrometry, ESI-MS, structural analysis, UV-VIS absorption spectrometry, reaction kinetics

Introduction

Present nuclear medicine frequently uses transition metal based radiopharmaceuticals injected to patient's body in a form of short half-life radionuclide ion coordinated with suitable organic ligand (Abrams & Murrer, 1993; Schrotterova & Nekovar, 2006). Much alike other human drugs, radio diagnostic agents must obey strict rules requesting detailed analytical information about the composition of applied formulation. As they are commonly administered in forms of reaction mixtures, the determination of their actual composition, depicting the structures of individual complexes and their degradation products, might be extremely difficult.

Rhenium complexes composed of β-emitting ^{186}Re and ^{188}Re isotopes coordinated with a suitable ligand start to play important role in radiopharmaceutical medicine, as targeted radio diagnostics and palliative agents in bone antitumor therapy. Both metals possess close chemical properties (Gerloch & Constable, 1994; Colton, 1965). They show in their compounds a wide variety of oxidation states ranging from (−I) to (+VII) and form both cationic and anionic species with strong oxidizing to mild reducing properties. As other transition metals, they form stable coordination complexes with numerous inorganic and organic ligands, the stability of whose depend on actual redox states and properties of central metal ion and coordinated ligands. Perrhenate and pertechnetate are common starting material for the preparation of coordination complexes with organic ligands. Their ability to coordinate organic ligands and form stable complexes is insufficient, they have to be selectively reduced prior to complex formation. Reliable and reproducible procedure, yielding rhenium coordination complex with favorable chemical and pharmacological properties as a dominant reaction product still remains crucial breakthrough waiting to be achieved. Successful attempt to eliminate reduction step and bind perrhenate ion in porphyrine inclusion complex has been described (Konirova et al., 2003), however, it's clinical prospective have not been studied yet.

The spectrum of suitable analytical methods allowing to cover individual complexes arising and else decomposing in reaction mixture is rather restricted. As a consequence, there is a lack of exact analytical data describing individual chemical reactions between Re(V) species with various ligands and other components present in a reaction mixture. Accordingly, relevant data about the stabilities of the complexes and their possible decomposition routes are missing. Evidently, standard methods of structure analysis, such as X-ray diffractrometry, nuclear magnetic resonance (NMR) and infrared spectrometry (IR), are of limited use (Nicholson et al., 2001; Valliant et al., 2001; Shaker et al., 2010; Kowalczyk & Szynkowska, 2012), as they are not suitable for analyses in mixtures. Clinical practice often relies on thin layer chromatography with radiochemical detection as a technique making it possible to distinguish between initial perrhenate and formed complex,

additional details remain hidden. The use of more selective analytical techniques, such as high performance liquid chromatography and capillary zone electrophoresis revealed more detailed information about intricacy of processes proceeding in a reaction mixture within time span of its clinical applicability (Koudelkova & Jedinakova-Krizova, 2003; Kohlickova et al., 1999; Kohlickova et al., 2002).

Mass spectrometry with soft ionization techniques proved to be fast and reliable method for the structure characterization and quantification of various complexes. Electrospray ionization (ESI) usually provides mass spectra with dominant molecular ion and minor fragment ions (Hederson et al., 1998). As compared with NMR and IR techniques, ESI-MS makes it possible to achieve substantially lower detection limits and is applicable to analytes in aqueous solutions (Hori et al., 1996; Hori et al., 1997; Fedorova et al., 2014; Tisato et al., 2004). Similarly, laser induced photo desorption (LDI) and matrix assisted photo desorption (MALDI) proved to ionize effectively the complexes providing mass spectra with dominant molecular ions and low extent of fragmentation (Wyatt, 2011; Wyatt et al., 2006). Atmospheric pressure photoionization (APPI) is, at present, the softest commercially available ionization technique that was successfully utilized for structure characterization of complexes (Van Berkel, 2003). Low energy UV lamp excitation light enables to generate intact molecular ions for kinetically labile analytes with negligible extent of fragmentation. The structure analysis of selected Re(+I) complexes by means of LDI, MALDI and ESI ionization can be found in ref. (Petroselli et al., 2012; Day et al., 2007).

In our previous contribution (Stichal et al., 2015), we pointed out on suitability of low resolution ESI-MS for fast and reliable structural identification of selected Re complexes in a mixture. We proved the existence of various complex species arising from reaction of Re(V) precursor with phenolic complex forming ligands. The aim of this study is to investigate the kinetic behavior major complex compounds arising from the reaction of tetrabutylamonnium-tetrachlooxorhenate with pyrogallol (1,2,3-trihydroxybenzene) and catechol (1,2-dihydroxybenzene) as strongly bound ligands. Special aim is devoted to the study of subsequent chemical transformation of primarily formed Re(V) complexes leading to the variety of complex structures. ESI-MS kinetic data are compared to those obtained by conventional UV-VIS kinetic measurements. We believe that acquired information on chemical structure of formed complexes and corresponding reaction rates will contribute to better knowledge of chemistry of Re coordination compounds with possible impact on proposal of diagnostic kits with improved properties.

Experimental

Materials and measurements

Tetrabutylammonium-tetrachlorooxorhenate [(n-Bu_4N)($ReOCl_4$)] was purchased from Sigma-Aldrich (Gillingham, Dorset, UK). Pyrogallol (1,2,3-trihydroxybenzene) (99%) and catechol (1,2-dihydroxybenzene) (99%) ligands were purchased from Alfa Aesar (Karlsruhe, Germany). Acetonitrile HPLC grade was purchased from Lach-Ner (Neratovice, Czech Republic). Triethylamine (TEA) and p-bromoaniline were purchased from Sigma-Aldrich (Gillingham, Dorset, UK) and used as a 10% (w/w) stock solution in acetonitrile. Electrospray tuning mix for ion trap was purchased from Agilent (Santa Clara, USA). Nitrogen used as a drying and nebulizing gas was delivered by LC-MS-NGM 11 nitrogen generator (Bruker Daltonics, Germany). Helium 4.6 was purchased from Linde Gas a.s. (Prague, Czech Republic).

Solid substances were weighted using Sartorius 7085011 micro balances (Sartorius Gmbh, Gottingen, Germany).

Electrospray mass spectrometry (ESI-MS) experiments were conducted on an ion trap instrument Esquire 3000 (Bruker Daltonics, Germany) and controlled by the Esquire Control 5.3.11 software and data were processed via Data Analysis 3.3.56 software (Bruker Daltonics, Germany). ESI-MS data were collected in negative ion mode at a scan range from m/z 300 to 650. In all ESI-MS measurements the nebulizer gas pressure was 124,1 kPa at a flow rate 5 L min^{-1}, the desolvation temperature was 300°C and capillary voltage was adjusted to 4000 V. The sample solutions were delivered to nebulizer by a syringe pump (Cole Parmer, USA) at a flow rate 8 μL min^{-1}.

UV-VIS absorption spectra were measured by Thermo Evolution 60 spectrometer (Thermo Scientific, USA), using 3 mL quartz cuvettes with 1 cm optical length and processed by means of Vision Lite Scan 5 software (Thermo Scientific, USA). The spectra were sequentially collected at selected time intervals in a range 300 - 700 nm, with increment step 5 nm. The scheme, molecular formula and theoretical mass for each compound was collected by ChemSketch ACD labs (Canada) and IsotopePattern (Bruker Daltonics, Germany).

Preparation of complexes (*I – IV*) with pyrogallol ligand

Mixture of rhenium precursor tetrabutylammonium-tetrachlorooxorhenate [(n-Bu_4N)($ReOCl_4$)] (1.76 mg, 1.0 μmol) and pyrogallol (0.76 mg, 2.0 μmol) was dissolved in acetonitrile (3 mL) at room temperature. After complete dissolution, 2 to 16 equivalents of TEA (8.4 μL to 52.5 μL of

10% TEA solution in acetonitrile) were added. Alternatively, for the purposes of long-term kinetic measurements, the reaction mixture without added TEA was prepared.

Preparation of complexes (*V – IX*) with catechol ligand

Reaction compounds [(n-Bu_4N)($ReOCl_4$)] (1.76 mg, 1.0 μmol) and catechol (0.66 mg, 2.0 μmol) were dissolved in acetonitrile (3 mL) at room temperature. After complete dissolution, 2 to 16 equivalents of TEA (8.4 μL to 52.5 μL of 10% TEA solution in acetonitrile) were added. For ESI-MS determination of uncharged complex *IX*, p-bromoaniline (1.72 mg, 1.0 μmol) was added to reaction mixture.

All prepared complexes are closer described in Table 1.

Table 1. Chemical names, labels and formulas of studied rhenium complexes

Entry	Complex	Label	Formula
I	Bis(1,2,3-trihydroxybenzene)oxorhenium	$[Re^{V}(O)(PG)_2]^-$	$C_{12}H_8O_7Re$
II	Bis(1,2,3-trihydroxybenzene)oxorhenium	$[Re^{VI}(O)(PG)_2]^-$	$C_{12}H_7O_7Re$
III	1,2,3-trihydroxybenzen-chloro-dioxorhenium	$[Re^{VII}Cl(O)_2(PG)]^-$	$C_6H_4ClO_5Re$
IV	Bis(1,2,3-trihydroxybenzene)dioxorhenium	$[Re^{VII}(O)_2(PG)_2]^-$	$C_{12}H_8O_8Re$
V	Bis(1,2-dihydroxybenzen)oxorhenium	$[Re^{V}(O)(Cat)_2]^-$	$C_{12}H_8O_5Re$
VI	Bis(1,2-dihydroxybenzen)oxorhenium	$[Re^{VI}(O)(Cat)_2]^0$	$C_{12}H_8O_5Re$
VII	Bis(1,2-dihydroxybenzene)-chloro-oxorhenium	$[Re^{VII}(O)Cl(Cat)_2]^0$	$C_{12}H_8ClO_5Re$
VIII	N-(bis(1,2-dihydroxybenzene)oxorhenium)-parabromoaniline	*N*-[Re(O)(Cat)$_2$]-*p*-bromaniline	$C_{18}H_{12}BrNO_5Re$
IX	Bis(1,2-dihydroxybenzene)dioxorhenium	$[Re^{VII}(O)_2(Cat)_2]^-$	$C_{12}H_8O_6Re$

The similarity between the computed and experimental molecular ion isotopic clusters was evaluated on the basis of similarity indexes (SI) (Wan et al., 2002). The corresponding formula is given in (1), where ($i - i_0$) is a difference in signal intensities at a given mass for two peaks, divided by the smaller intensity value (i_0) and *N* is the number of product-ion signals that are compared:

$$SI = \sqrt{\frac{\sum_i \left\{\frac{i-i_0}{i_0} x100\right\}^2}{N}} \qquad (1)$$

According to definition, the similarity index may have values from 0 to 1. Peak patterns with SI=0 are identical. In order to obtain percentual expression of isotopic patterns similarity, values of (1-SI)·100 were evaluated. Theoretical isotopic patterns were generated via Data Analysis 3.3.56 software.

Results and discussion

Rhenium - pyrogallol complexes

As it is depicted in reaction scheme (Fig. 1), actual molar ratio of triethylamine (TEA) to rhenium precursor tetrabutylammonium-tetrachlorooxorhenate [(*n*-Bu_4N)($ReOCl_4$)] decisively alters the rate and course of chemical reactions (running at room temperature) yielding single complexes.

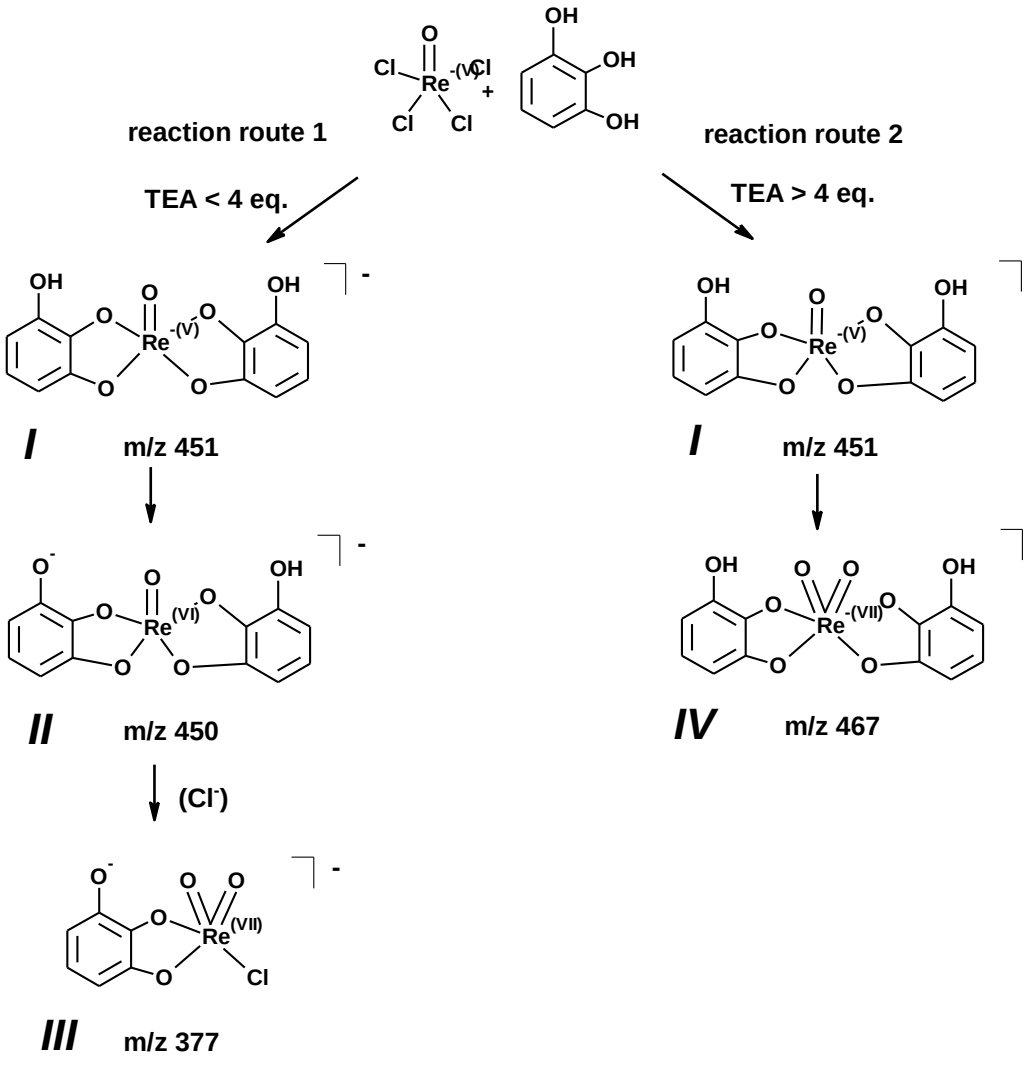

Fig. 1 Scheme of possible reactions between precursor [(n-Bu_4N)($ReOCl_4$)] and pyrogallol in presence of various amounts of TEA.

Based on the series of proved experiments it was possible to conclude, that molar ratio of TEA higher than 4 led to yields $[Re^{VII}(O)_2(PG)_2]^-$ (compound *IV*) as a dominant final reaction product synthetized in reaction of [(*n*-Bu_4N)($ReOCl_4$)] and pyrogallol (PG), while lower TEA concentration leads to the formation of $[Re^{VII}Cl(O)_2(PG)]^-$ complex (*III*). Such observation is evidently related to the stoichiometry of complex forming reaction and necessary amount of TEA for complete neutralization of hydrogen chloride as a reaction by-product. Electrospray mass spectrometry (ESI-MS) monitoring of the reaction of [(*n*-Bu_4N)($ReOCl_4$)] with twofold excess of PG in presence of 2 equivalents of TEA is shown in Fig. 2.

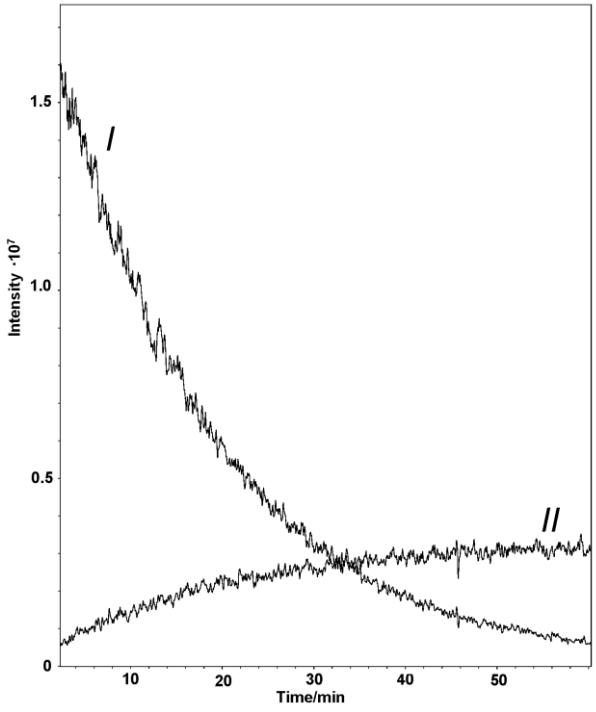

Fig. 2 Time evolution of the ESI-MS signals for a reaction of [(n-Bu_4N)($ReOCl_4$)] with pyrogallol in acetonitrile; 2 equivalents of TEA are added to reaction mixture. Extracted ion current (EIC) at m/z 451 exponentially decreases in favor to EIC at m/z 450, as complex *I* is converted to *II*. Initial concentration: [(n-Bu_4N)($ReOCl_4$)] (1.76 mg, 1.0 μmol) and pyrogallol (0.76 mg, 2.0 μmol).

$[Re^{V}(O)(PG)_2]^-$ complex (*I*) is formed almost immediately, followed by its exponential decay in favor to $[Re^{VI}(O)(PG)_2]^-$ (compound *II*) within 60 minutes. The same process is documented by UV-VIS absorption spectra (Fig. 3).

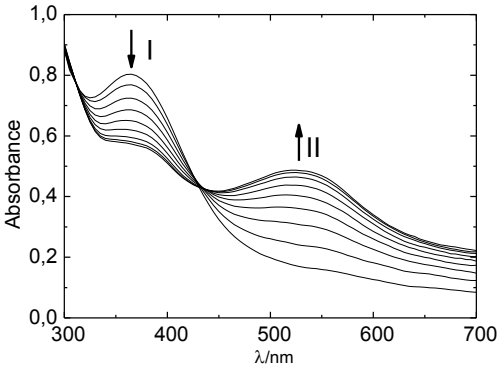

Fig. 3 UV-VIS absorption spectra depicting the conversion of a yellowish complex *I* to carmine colored complex *II*; 2 equivalents of TEA are present in reaction mixture. Arrows indicate increase and/or decrease of absorption maxima of both species. Spectra are collected within 60 minutes and shown at time differences 6 min. Initial concentration: $[(n\text{-}Bu_4N)(ReOCl_4)]$ (1.76 mg, 1.0 μmol) and pyrogallol (0.76 mg, 2.0 μmol).

Initial yellowish color of the reaction mixture given by dominant $[Re^{V}(O)(PG)_2]^-$ complex changes to carmine solution with prevailing $[Re^{VI}(O)(PG)_2]^-$ as a stable reaction intermediate. Within 60 minutes, the absorption maximum at 370 nm almost completely disappears in favor to arising 530 nm peak. Well defined isosbestic point at 425 nm shows at simple reaction mechanism of $[Re^{V}(O)(PG)_2]^-$ – $[Re^{VI}(O)(PG)_2]^-$ chemical transformation. Higher concentrations of TEA significantly accelerate subsequent oxidation to $[Re^{VII}(O)_2(PG)_2]^-$. It was observed that for TEA concentrations higher than 4 equivalents, $[Re^{VII}(O)_2(PG)_2]^-$ is a dominant product in a reaction mixture. UV-VIS reaction monitoring documenting this process in presence of 8 equivalents of TEA is shown in Fig. 4.

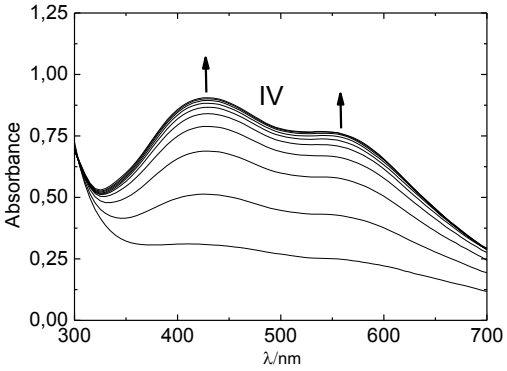

Fig. 4 UV-VIS absorption spectra depicting the conversion of carmine complex *II* to brown colored complex *IV*; 8 equivalents of TEA are present in reaction mixture. Arrows indicate increase and/or decrease of absorption maxima of both species. Spectra are collected within 60 minutes and shown at time differences 6 min. Initial concentration: [(n-Bu_4N)($ReOCl_4$)] (1.76 mg, 1.0 μmol) and pyrogallol (0.76 mg, 2.0 μmol).

Simultaneously arising absorption maxima at 430 and 560 nm indicate the formation of stable brown colored $[Re^{VII}(O)_2(PG)_2]^-$. More detailed dependence of the rate of reaction yielding $[Re^{VII}(O)_2(PG)_2]^-$ complex on the molar excess of TEA is else documented in Fig. 5. Time based dependence of the height of absorption maximum at 430 nm confirms the significant influence of TEA up to the molar excess of 12 equivalents; higher concentrations do not else accelerate the reaction.

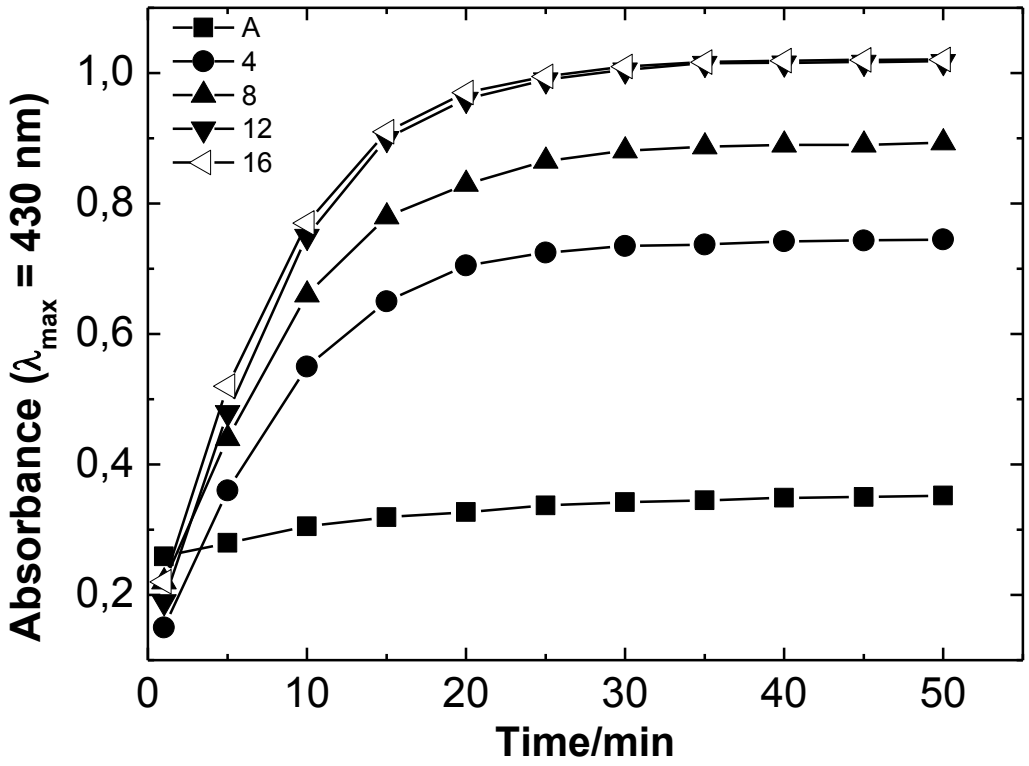

Fig. 5 Time based dependencies of the height of absorption maximum at λ=430 nm (λ_{max} of compound *IV*) in a [(n-Bu_4N)($ReOCl_4$)] – PG reaction mixture with 2 to 16 equivalents of TEA added. Initial concentration: [(n-Bu_4N)($ReOCl_4$)] (1.76 mg, 1.0 μmol) and pyrogallol (0.76 mg, 2.0 μmol).

Different reaction route was observed within long-term UV-VIS monitoring of the reaction in absence of TEA and were collected three months at time 0; 0.5; 1.0; 4.8; 5.6; 6.9; 18.8; 43.6; 219; 381; 573; 693; 1076 and 2542 hours. As it is visible in Fig. 6 part (a), the formation of $[Re^{VI}(O)(PG)_2]^-$ complex is significantly prolonged, the maximum peak height at 530 nm is achieved within tens of hours.

a b

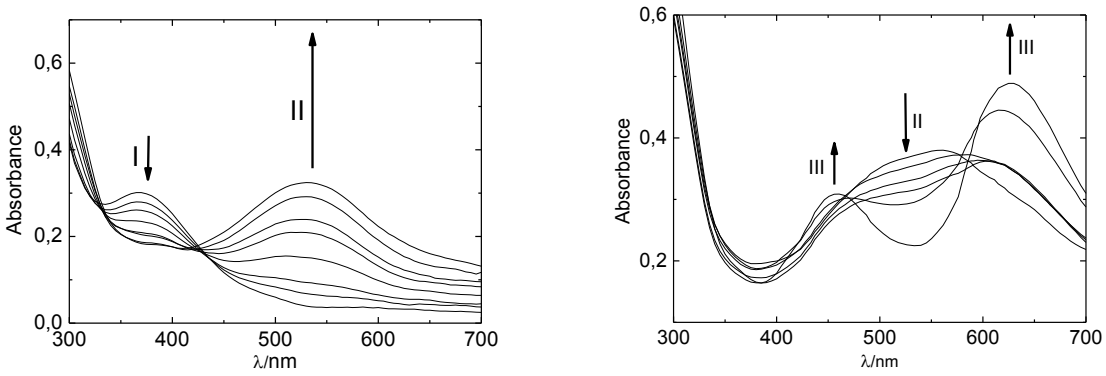

Fig. 6 UV-VIS absorption spectra depicting the reaction of [(n-Bu_4N)($ReOCl_4$)] with pyrogallol in absence of TEA. Immediately formed yellow complex *I* (λ_{max} =370 nm) is converted to cyan colored complex *II* **(**λ_{max} = 530 mn). Arrows indicate increase and/or decrease of absorption maxima of both species. Spectra are shown within time interval 0.0 – 43.6 h (a) and 219-2542 h (b). Initial concentration: [(n-Bu_4N)($ReOCl_4$)] (1.76 mg, 1.0 μmol) and pyrogallol (0.76 mg, 2.0 μmol).

Further long term conversion of $[Re^{VI}(O)(PG)_2]$ involves ligand exchange reaction with Cl^- ions as a by-product of the reaction between [(n-Bu_4N)($ReOCl_4$)] and PG. The oxidation of rhenium ion is accompanied by a cleavage of a single ligand, yielding blue-green $[Re^{VII}(O)_2Cl(PG)]^-$ as a final reaction product. This is evident from Fig. 6 part (b) where absorption maximum at 530 nm diminishes in favor to simultaneously arising maxima at 460 nm and 630 nm.

The structures of the complexes arising in [(n-Bu_4N)($ReOCl_4$)] – PG reaction mixture were confirmed with ESI-MS spectra shown in Fig. 7. Spectrum A reflects the composition of a reaction mixture with two equivalents of TEA immediately after its initialization. Dominant molecular ion cluster of $[Re^{V}(O)(PG)_2]^-$ at m/z 451 was observed. Spectrum B reflects the composition of the same reaction mixture 60 minutes after its initialization. Dominant peak cluster at m/z 450 corresponds to prevailing deprotonated $[Re^{VI}(O)(PG)_2]^-$ complex. Minor peak cluster at m/z 467 visible both in spectra A and B corresponds to traces of $[Re^{VII}(O)_2(PG)_2]^-$ complex at early stages of its formation. In spectrum C peak cluster at m/z 467 confirms the presence of $[Re^{VII}(O)_2(PG)_2]^-$ as a major reaction mixture constituent in a reaction mixture with 8 equivalents of TEA, 60 minutes after its initialization. Peak cluster at m/z 343 corresponds to a fragment ion $[Re^{VII}(O)_2\ (PG)]^-$ as a product of elimination of a single ligand moiety. Last spectrum D reflects the composition of the same reaction mixture after three months. Peak cluster at m/z 377 documents the presence of deprotonated $[Re^{VII}(O)_2Cl(PG)]^-$ as a final and else stable reaction product. Elemental composition

of all observed Re – PG complexes was verified by a comparison of theoretical and experimental molecular ion isotopic patterns, that all possess close resemblance. The difference in peak cluster between complexes $[Re^{V}(O)(PG)_2]^-$ and $[Re^{VI}(O)(PG)_2]^-$ is documented in Fig. 8.

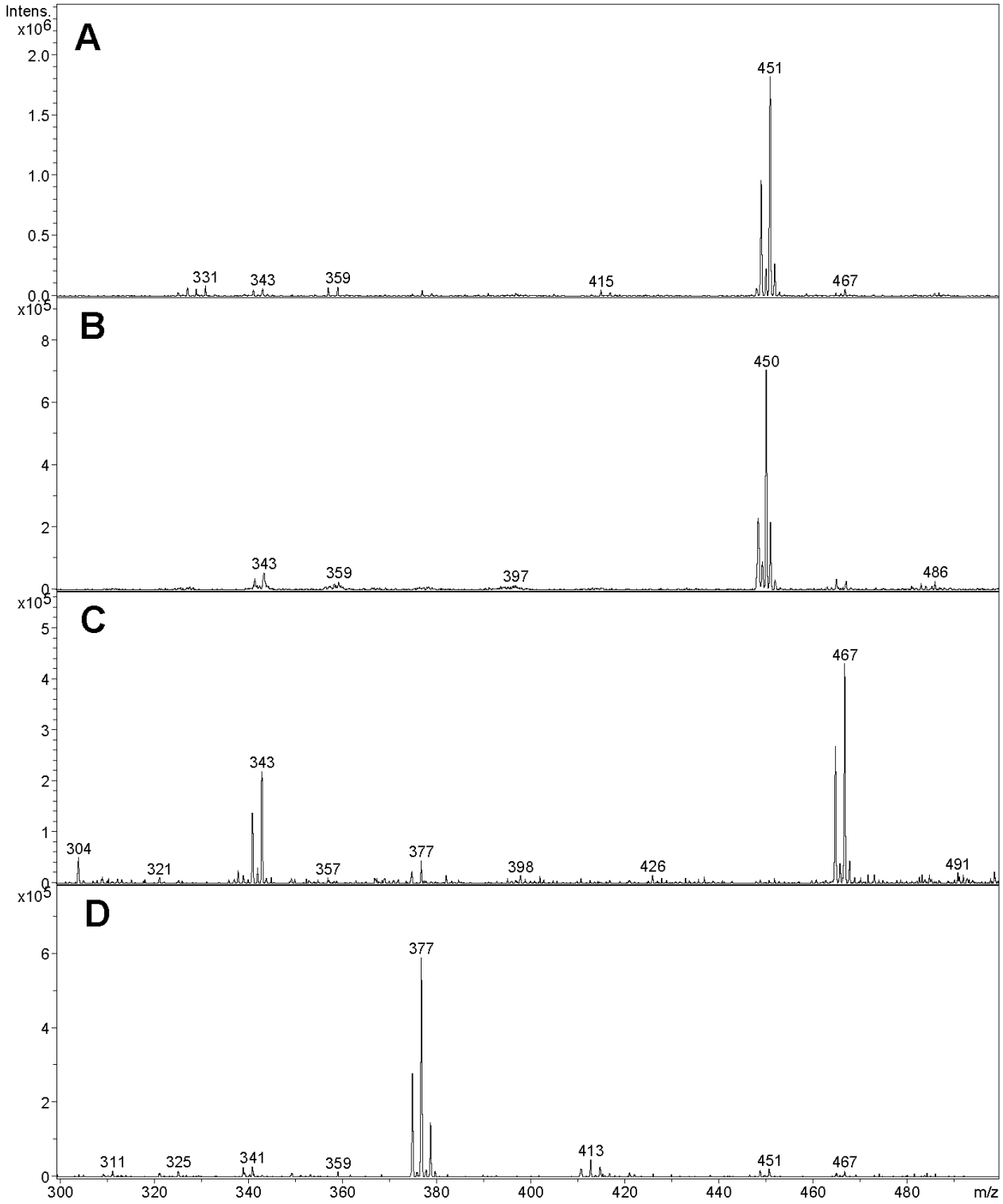

Fig. 7 Direct injected negative ESI-MS spectra reflecting the composition of [(n-Bu_4N)($ReOCl_4$)] – PG reaction mixture sampled and analyzed in a stage with (A) prevailing complex *I*; (B) prevailing complex *II*; (C) prevailing complex *IV* and (D) prevailing complex *III*. Details are given in a supporting text.

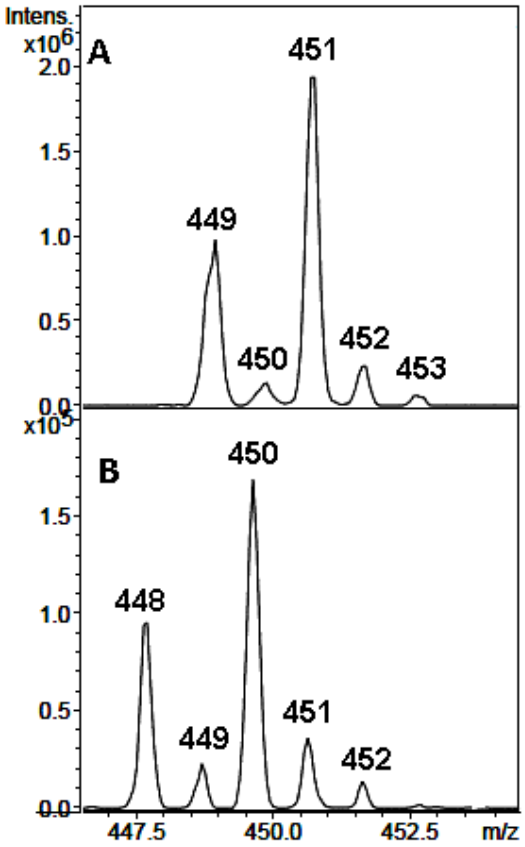

Fig. 8 Experimentally obtained direct injected negative ESI-MS isotopic patterns of compounds *I* (part A) and *II* (part B) molecular ion cluster.

Rhenium - catechol complexes

Comparative kinetic measurements monitoring the formation and subsequent chemical transformations of the complexes arising in catechol (Cat) – [(n-Bu_4N)($ReOCl_4$)] reaction mixture were performed. As in previous experiments, the decisive role of TEA on complex formation and consecutive transformations was confirmed. Proposed reaction scheme based on UV-VIS and ESI-MS measurements, described below, is shown in Fig. 9. Molar ratio of TEA to [(n-Bu_4N)($ReOCl_4$)]

higher than 4 equivalents immediately yields $[Re^{V}(O)(Cat)_2]^-$ (compound *V*) that is consequently converted to stable $[Re^{VII}(O)_2(Cat)_2]^-$ (compound *IX*) as a final oxidation product. Corresponding reaction rates are comparable to those observed with PG as a ligand.

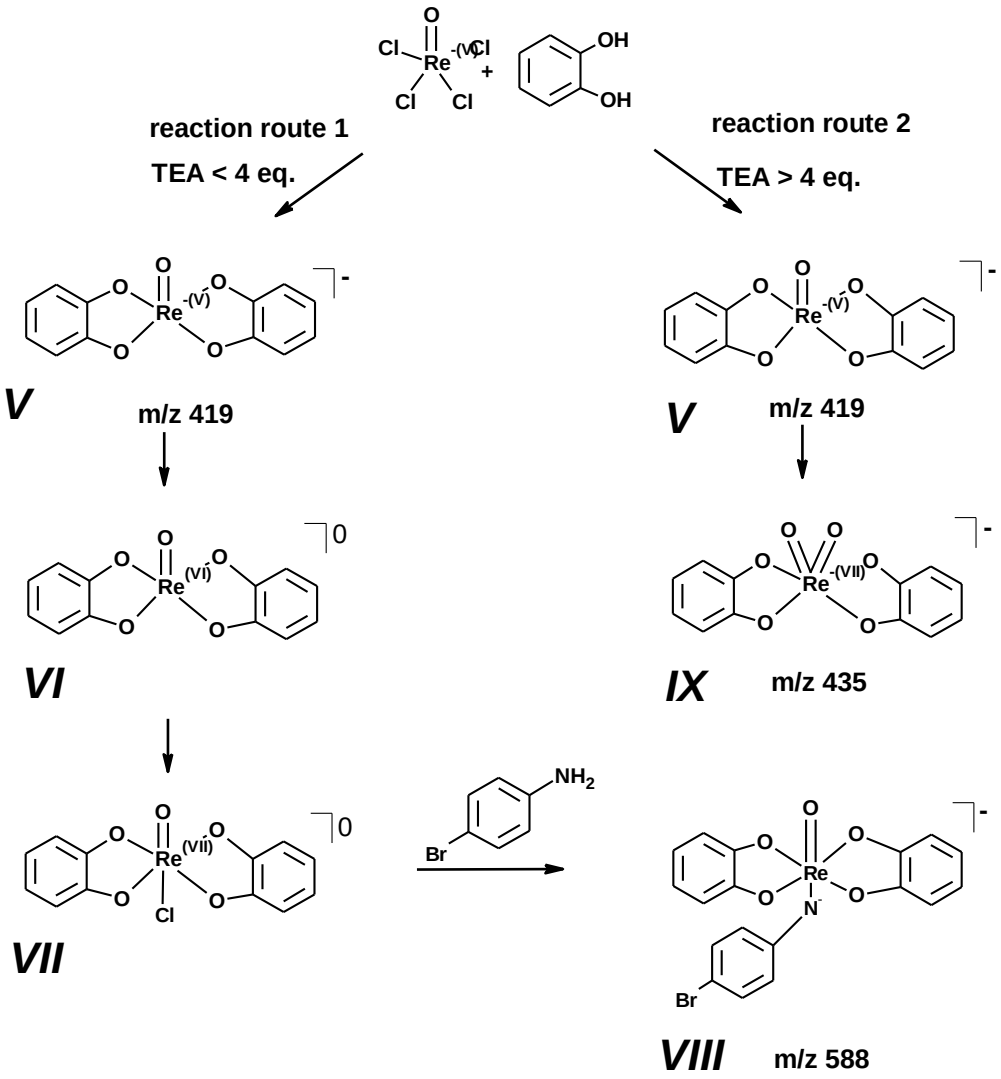

Fig. 9 Scheme of possible reactions between [(n-Bu_4N)($ReOCl_4$)] and catechol in presence of various amounts of TEA.

Absorption spectra shown in Fig. 10 document the rate of $[Re^{V}(O)(Cat)_2]^-$ to $[Re^{VII}(O)_2(Cat)_2]^-$ complex oxidation in presence of 8 equivalents of TEA. The conversion to $[Re^{VII}(O)_2Cat)_2]^-$ is accomplished within 60 minutes, the initial pale yellow color of reaction mixture stains to deep magenta as the concentration of oxidized product with absorption maxima at 365 nm, 460 nm and 540 nm increases.

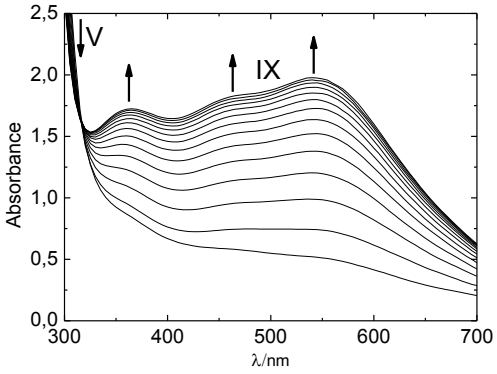

Fig. 10 UV-VIS absorption spectra depicting the conversion of pale yellow complex *I* to deep magenta complex *IX*; 8 equivalents of TEA are present in reaction mixture. Arrow indicate an increase of absorption maxima at λ = 365 nm, 460 nm and 540 nm, characteristic for complex *IX*. Spectra are collected within 60 minutes and shown at time differences 6 min. Initial concentration: [(n-Bu_4N)($ReOCl_4$)] (1.76 mg, 1.0 μmol) and catechol (0.66 mg, 2.0 μmol).

The difference between Cat and PG ligands, in terms of the structures of formed complexes and the rates of individual reactions, becomes significant for TEA concentrations lower than 4 equivalents, markedly, in its absence in reaction mixture. As it is evident from UV-VIS absorption spectra shown in Fig. 11, the rate of the conversion of initially formed $[Re^{V}(O)(Cat)_2]^-$ to $[Re^{VI}(O)(Cat)_2]^0$ intermediate (compound *VI*) (λ_{max} = 510 nm) in presence of 2 equivalents of TEA is significantly prolonged.

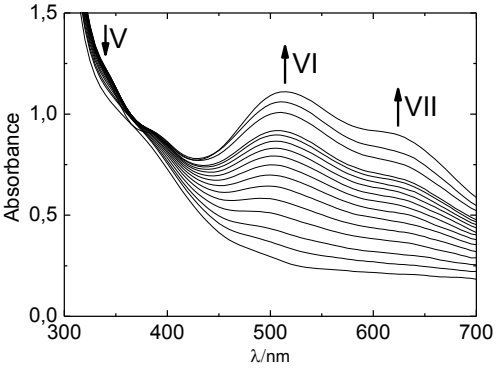

Fig. 11 UV-VIS absorption spectra depicting the conversion of a complex *V* to purple complex *VI* (λ_{max} = 510 nm). The second arising absorption maximum at λ = 620 nm indicate the formation of complex *VII* as a product of concomitant Re oxidation and ligand exchange reaction; 2 equivalents of TEA are present in reaction mixture. Arrows indicate increase and/or decrease of absorption maxima of both species. Spectra are collected within 60 minutes and shown at time differences 6 min. Initial concentration: [(n-Bu_4N)($ReOCl_4$)] (1.76 mg, 1.0 μmol) and catechol (0.66 mg, 2.0 μmol).

Unlike pyrogallol, catechol lacks the free dissociable hydroxyl group after complexation with rhenium, therefore $[Re^{VI}(O)(Cat)_2]^0$ intermediate remains uncharged in ESI, APPI and APCI and its structural characterization by MS is impossible. Its presence in reaction mixture is presumed entirely from a similarity between absorption spectra describing the formation of deprotonated $[Re^{VI}(O)(PG)_2]^-$ and those corresponding to the formation of $[Re^{VI}(O)(Cat)_2]^0$ analogue. Its further and relatively slow oxidation is accompanied by a ligand exchange reaction with residual Cl^- ions present in reaction mixture, yielding $[Re^{VII}(O)Cl(Cat)_2]^0$ (compound *VII*) as a final and stable reaction product. It's formation documents the rise of second maximum at 620 nm. Rate and overall extent of the conversion of $[Re^{VI}(O)(Cat)_2]^0$ to $[Re^{VII}(O)Cl(Cat)_2]^0$ is documented in a series of absorption spectra shown in Fig. 12. Absorption maximum at 510 nm diminishes in favor to increasing maximum at 620 nm. The color of reaction mixture consequently changes from magenta to blue. It should be noted that complex $[Re^{VII}(O)Cl(Cat)_2]^0$ is also neutral, however, its ESI-MS structure identification is possible after the reaction with *p*-bromoaniline yielding complex *N*-[Re(O)$(Cat)_2$]-*p*-bromoaniline (compound *VIII*) as ESI ionizable reaction product.

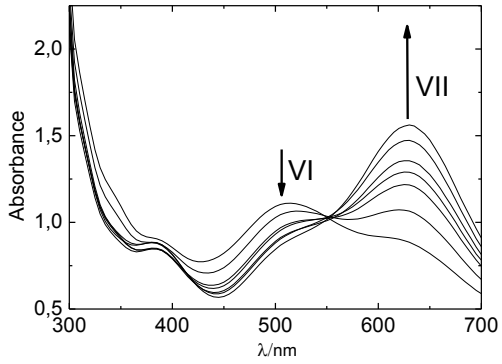

Fig. 12 UV-VIS absorption spectra depicting long-term transformation of complex *VI* to blue complex *VII* (**λ_{max}** = 620 nm). Arrows indicate increase and/or decrease of absorption maxima of both species. Spectra are shown within time interval 0.0 – 43 h. Initial concentration: [(n-Bu_4N)($ReOCl_4$)] (1.76 mg, 1.0 μmol) and catechol (0.66 mg, 2.0 μmol).

ESI-MS spectra depicting the structure of complexes arising in Cat – [(n-Bu_4N)($ReOCl_4$)] reaction mixture are shown in Fig. 13. Spectrum A reflects the composition of a reaction mixture with 8 equivalents of TEA immediately after its initialization. Abundant molecular ion cluster at m/z 419 reflects the dominance of $[Re^{V}(O)(Cat)_2]^-$ complex. Spectrum B with a dominant ion cluster at m/z 435 and fragment ion at m/z 327 documents the composition of the same reaction mixture 60 minutes after its initialization, where complex $[Re^{VII}(O)_2Cat)_2]^-$ predominates. Spectrum C reflects the final composition of a reaction mixture with 2 equivalents of TEA, where the presence of $[Re^{VII}(O)Cl(Cat)_2]^0$ is confirmed by a dominant molecular ion cluster at m/z 588, and fragment at m/z 480, corresponding to reaction product with *p*-bromoaniline.

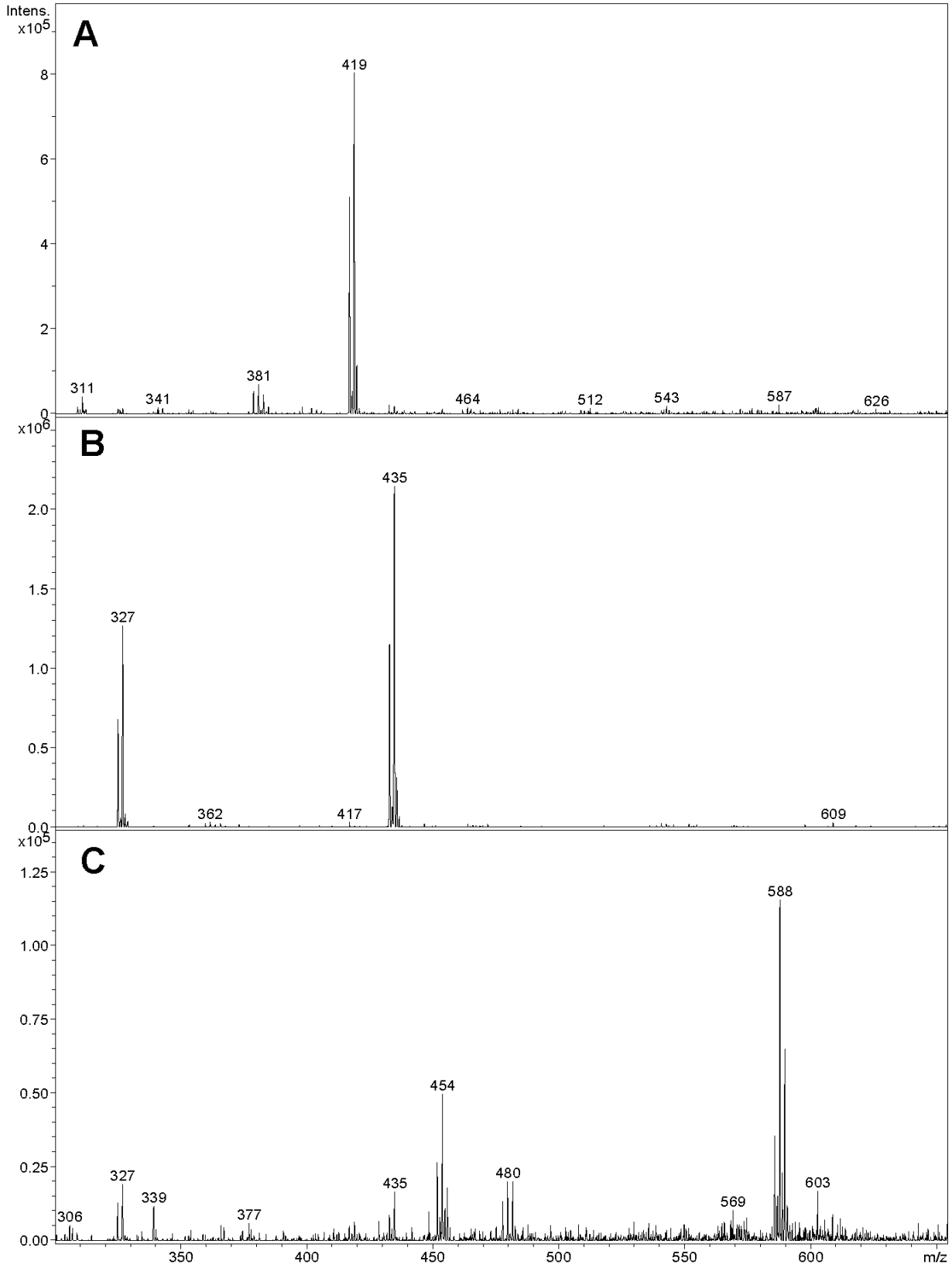

Fig. 13 Direct injected negative ESI-MS spectra reflecting the composition of [(n-Bu_4N)($ReOCl_4$)] – Cat reaction mixture sampled and analyzed in a stage with (A) prevailing complex *V*; (B)

prevailing complex *IX*; (C) prevailing complex *VII* identified after its derivatization with *p*-bromoaniline as complex *VIII*.

Elemental composition of all observed complexes was verified by a comparison of theoretical and experimental molecular ion isotopic patterns, that all possess close resemblance. Tables 2 summarizes theoretical monoisotopic and obtained masses of rhenium complexes observed and identified in negative ESI-MS spectra complemented by colors of individual complexes, oxidation states of central rhenium ion and calculated values of similarity indexes SI. The values of SI indicate significant conformity between calculated and experimental spectra and correct assignment of elemental composition to m/z values of observed ions.

Table 2. Theoretical monoisotopic and measured molecular ion masses of studied rhenium complexes. Additional descriptors covering the properties of individual complexes (Re oxidation state, observed color) and reliability of MS structure identification (similarity index) are enclosed.

Entry	Theoretical monoisotopic m/z	Measured m/z	Rhenium oxidation state	Solution color	Similarity index
I	450.9	451	V	yellow	
II	449.9	450	VI	cyan	
III	376.8	377	VII	green	
IV	466.9	467	VII	brown	
V	418.9	419	V	yellow	
VI	-	-	VI	purple	
VII	-	-	VII	blue	
VIII	587.9	588		yellow	
IX	434.9	435	VII	deep magneta	

- Uncharged species

Conclusions

This study documents the diversity of chemical reactions between rhenium precursor tetrabutylammonium-tetrachlorooxorhenate and pyrogallol (PG) or catechol (Cat) as strongly bound, structurally similar ligands. Irrespective of the selected ligand, observed reactions can be diversified to fast ones, involving immediate formation of Re(V) complex, and the slower ones, involving oxidation of central rhenium ion accompanied with possible ligand exchange reactions.

While the former mentioned do not depend on the actual ligand structure, the later ones show the dependence on exact ligand structure and the actual composition of a reaction mixture.

The presence of triethylamine (TEA) in reaction mixture plays a decisive role in observed reaction schemes and their actual rates. TEA molar ratio higher than 4 equivalents results in formation of $[Re^{VII}(O_2)(PG)_2]^-$ and $[Re^{VII}(O_2)(Cat)_2]^-$ complexes as dominant reaction products. Lower amount or even the absence of TEA decelerates the rates of the reactions and increases the probability of ligand exchange reactions. Within long term reaction monitoring with less than four equivalents of TEA, we identified deprotonated $[Re^{VII}(O_2)Cl(PG)]^-$ and $[Re^{VII}(O)Cl(Cat)_2]^0$ as dominant and stable reaction products.

The absence of free chargeable group in a complex prohibits its structure identification with ESI-MS. Unlike pyrogallol complexes, Re(VI) and Re(VII) catechol analogues remain often uncharged and thus hidden for ESI-MS. However, the final $[Re^{VII}(O)Cl(Cat)_2]^0$ complex was successfully converted to a chargeable product via derivatization with *p*-bromoaniline.

This research was carried out within the framework of the project of the Specific University Research (SVV 260317). The Norwegian Financial Mechanism project CZ01116 is gratefully acknowledged.

Symbols

SI similarity index

Subscripts

PG pyrogallol
Cat catechol
Re rhenium
O oxygen
Cl chlorine
Bu butyl
ESI-MS mass spectrometry with electrospray ionization
TEA triethylamine
UV-VIS ultraviolet-visible absorption spectrometry

EIC Extracted ion current

References

Abrams, M. J., & Murrer, B. A. (1993). Metal compounds in therapy and diagnosis. *Science*, *261*, 725-730. DOI: 10.1126/science.8102010.

Colton R. (1965). *The Chemistry of Rhenium and Technetium*. London, UK: Interscience.

Day E. F., Payne T. A., & Holt C. A. (2007). Mass spectrometric study of dirhenium biscarboxylate:purine dinucleotide complexes. *Rapid Communications in Mass Spectrometry*, *21*, 903-910. DOI: 10.1002/rcm.2910.

Fedorova G., Nebesky V., Randak T., & Grabic R. (2014). Simultaneous determination of 32 antibiotics in aquaculture products using LC-MS/MS. *Chemical Papers*, *68*, 29-36. DOI: 10.2478/s11696-013-0428-3.

Gerloch M., & Constable E. G. (1994). *Transition Metal Chemistry*. Weinheim, Germany: VCH Verlagsgessellschaft mbH.

Henderson V., Nicholson B. K., & McCaffrey L. J. (1998). Applications of electrospray mass spectrometry inorganometallic chemistry. *Polyhedron*, *17*, 4291-4313. DOI: 10.1016/S0277-5387(98)00246-0.

Hori H., Ishitani O., Koike K., & Takeuchi K. (1996). Electrospray Mass Spectrometric Detection of Unstable Rhenium Complexes as Reaction Intermediates of Photochemical CO_2-Fixation. *Analytical Sciences*, *12*, 587-590. DOI: http://doi.org/10.2116/analsci.12.587.

Hori H., Ishihara J., Koike K., Takeuchi K., Ibusuki T., & Ishitani O. (1997). Electrospray Mass Spectrometric Detection of Neutral Rhenium Bipyridine Complexes Using $NaNO_3$ as an Ionization Agent. *Chemistry Letters*, *3*, 273-274. DOI: http://doi.org/10.1246/cl.1997.273.

Kohlickova-Koudelkova M., Jedinakova-Krizova V., & Deyl Z. (2002). Study of perrhenate reduction by capillary electrophoresis. *Electrophoresis*, *23*, 245-248. DOI: 10.1002/1522-2683(200202)23:2<245::AID-ELPS245>3.0.CO;2-D.

Kohlickova M., Jedinakova-Krizova V., & Konirova R. (1999). Chromatographic study of ^{186}Re complexes with various ligands. *Journal Radioanalytical Nuclear Chemistry*, *242*, 545-549. DOI: 10.1007/BF02345591.

Konirova R., Ernestova M., Jedinakova-Krizova V., & Kral V. (2003). Radioactive labeled porphyrin derivates. *Czechoslovak Journal of Physics*, *53*, 755-761. DOI: 10.1007/s10582-003-0098-4.

Koudelkova M., & Jedinakova-Krizova V. (2003). Capillary electrophoretic and thin-layer chromatographic characterization of rhenium complexation with 1-hydroxyethylidenediphosphonic acid. *Journal of Chromatography* A, *990*, 317-323. DOI: 10.1016/S0021-9673(02)01798-3.

Kowalczyk L., & Szynkowska M. I. (2012). Oxidation of ammonia using modified TiO2 catalyst and UV-VIS irradiation. *Chemical Papers, 66*, 607-611. DOI: 10.2478/s11696-012-0159-x.

Nicholson T., Kramer D. J., Davison A., & Jones A. G. (2003). The substitution chemistry of a useful new synthon with neutral donor ligands. The reactions of $[TcCl_3(N{=}NPh_2)(PPh_3)_2]$ with phosphine ligands. The X-ray crystal structures of $[TcCl_2(N{=}NPh_2)(PMe_2Ph)_3][PF_6]$, $[TcCl(N{=}NPh_2)(dppe)_2][PF_6]_2$ and $[TcCl_2(N{=}NPh_2)(TRIPHOS)][BPh_4]$. *Inorganica Chimica Acta*, *353*, 177-182. DOI: 10.1016/S0020-1693(03)00228-7.

Petroselli G., Mandal M. K., Chen L. C., Ruiz G. T., Wolcan E., Hiraoka K., Nonami H., & Erra-Balsells R. (2012). Mass spectrometry of rhenium complexes: a comparative study by using LDI-MS, MALDI-MS, PESI-MS and ESI-MS**.** *Journal of Mass Spectrometry*, *47*, 313-321. DOI: 10.1002/jms.2965.

Schrotterova D., & Nekovar P. (2006). Extraction of Re(VII) by neutral and basic extractants. *Chemical Papers, 60*, 427-431. DOI: 10.2478/s11696-006-0078-9.

Shaker S. A., Khaledi H., & Mohd Ali H. (2010). Spectroscopic investigations and physic-chemical characterization of newly synthetized mixed-ligand complexes of 2-methylbenzimidazole with metal ions. *Chemical Papers, 65*, 299-307. DOI: 10.2478/s11696-011-0003-8.

Sticha M., Jelinek I., Polakova J., & Kaliba D. (2015). Characterization of Rhenium(V) Complexes with Phenols Using Mass Spectrometry with Selected Soft Ionization Techniques. *Analytical Letters*, 48, 2329-2342. DOI: 10.1080/00032719.2015.1038552.

Tisato F., Bolzati C., Porchia M., & Refosco F. (2004). Contribution of electrospray mass spectrometry for the characterization, design, and development of nitrido technetium and rhenium heterocomplexes as potential radiopharmaceuticals. *Spectrometry Reviews*, *23*, 309-332. DOI: 10.1002/mas.20000.

Valliant J. F., Riddoch R. W., Hughes D. W., Roe D. G., Farconnier T. K., & Thornback J. R. (2001). The solid phase synthesis and NMR spectroscopy of a ^{99}Tc chelate–bombesin derived peptide conjugate. *Inorganica Chimica Acta*, *325*, 155-163. DOI: 10.1016/S0020-1693(01)00637-5.

Van Berkel G. J. (2003). An overview of some recent developments in ionization methods for mass spectrometry. *European Journal of Mass Spectrometry*, *9*, 539-562. DOI: http://dx.doi.org/10.1255/ejms.586.

Wan, K. X., I. Vidavsky, & M. L. Gross. (2002). Comparing similar spectra: From similarity index to spectral contrast angle. *Journal of the American Society for Mass Spectrometry*, *13*, 85–88. DOI:10.1016/s1044-0305(01)00327-0

Wyatt M. F. (2011). MALDI-TOFMS analysis of coordination and organometallic complexes: a nic(h)e area to work in. *Journal of Mass Spectrometry*, *46*, 712-719. DOI: 10.1002/jms.1957.

Wyatt M. F., Stein B. K., & Brenton A. G. (2006). Characterization of Various Analytes Using Matrix-Assisted Laser Desorption/Ionization Time-of-Flight Mass Spectrometry and 2-[(2*E*)-3-(4-*tert*-Butylphenyl)-2-methylprop-2- enylidene]malononitrile Matrix. *Analytical Chemistry*, *78*, 199-206. DOI: 10.1021/ac050732f.

PUBLIKACE III

Synthesis of phosphinoferrocene amides and thioamides from carbamoyl chlorides and the structural chemistry of Group 11 metal complexes with these mixed-donor ligands

Fernandes, TA ; Solarova, H; Cisarova, I; Uhlik, F; Sticha, M ; Stepnicka, P

DALTON TRANSACTIONS, 44 (7): 3092-3108 2015

Dalton Transactions

PAPER

View Article Online
View Journal | View Issue

Cite this: *Dalton Trans.*, 2015, **44**, 3092

Synthesis of phosphinoferrocene amides and thioamides from carbamoyl chlorides and the structural chemistry of Group 11 metal complexes with these mixed-donor ligands†

Tiago A. Fernandes,[a] Hana Solařová,[a] Ivana Císařová,[a] Filip Uhlík,[b] Martin Štícha[c] and Petr Štěpnička*[a]

The reaction of *in situ* generated 1′-(diphenylphosphino)-1-lithioferrocene with carbamoyl chlorides, ClC(E)NMe_2, affords the corresponding (thio)amides, $Ph_2PfcC(E)NMe_2$ (E = O (**2**), S (**3**); fc = ferrocene-1,1′-diyl). These compounds as well as their analogues, $Ph_2PfcC(O)NHMe$ (**4**) and $Ph_2PfcC(O)NH_2$ (**5**), prepared from 1′-(diphenylphosphino)ferrocene-1-carboxylic acid (Hdpf) were studied as ligands for the Group 11 metal ions. In the reactions with $[Cu(MeCN)_4][BF_4]$, the amides give rise to bis-chelate complexes of the type $[Cu(L\text{-}\kappa^2O,P)_2][BF_4]$. Similar products, $[Ag(L\text{-}\kappa^2O,P)_2]ClO_4$, are obtained from silver(I) perchlorate and **2**, **4** or **5**. In contrast, the reaction of $AgClO_4$ with **3** produces a unique molecular dimer $[Ag(\mathbf{3})(ClO_4\text{-}\kappa O)]_2$, where the metal centres are bridged by the sulfur atoms of the P,S-chelating thioamides. The reactions of **2**–**5** with [AuCl(tht)] (tht = tetrahydrothiophene) afford the expected gold(I)–phosphine complexes, [AuCl(L-κ*P*)], containing uncoordinated (thio)amide moieties. Hemilabile coordination of the phosphinoamide ligands in complexes with the soft Group 11 metal ions is established by the crystal structure of a solvento complex, $[Cu(\mathbf{5}\text{-}\kappa^2O,P)(\mathbf{5}\text{-}\kappa P)(CHCl_3\text{-}\kappa Cl)][BF_4]$, which was isolated serendipitously during an attempted crystallisation of $[Cu(\mathbf{5}\text{-}\kappa^2O,P)_2][BF_4]$. All of the compounds are characterised by spectroscopic methods, and the structures of several representatives of both the free phosphinoamides and their complexes are determined by X-ray diffraction analysis and further studied by DFT calculations and cyclic voltammetry.

Received 24th October 2014,
Accepted 22nd December 2014

DOI: 10.1039/c4dt03279a

www.rsc.org/dalton

Introduction

Phosphine donors modified with carboxamide substituents have evolved into a specific class of functional phosphine ligands with applications in coordination and supramolecular chemistry, catalysis, biomedical research, *etc.*[1,2] The attractiveness of these compounds lies mainly in their structural modularity and facile synthesis, especially *via* amide coupling reactions.[1]

During our studies[3] on phosphinoferrocene carboxamides, we have also typically relied on the amide coupling reactions,[4] employing 1′-(diphenylphosphino)ferrocene-1-carboxylic acid (Hdpf),[5] suitable functional amines and conventional peptide coupling agents (route A in Scheme 1). Although this synthetic strategy proved very efficient, we felt that the search for alternative synthetic routes that are more straightforward and avoid the use of expensive stoichiometric reagents was still desirable. Thus far, we have demonstrated that phosphinoferrocene carboxamides can be synthesised equally well by lithiation of 1′-(diphenylphosphino)-1-bromoferrocene (**1**)[6] and subsequent reaction of the lithiated intermediate with isocyanates (route B in Scheme 1).[7]

In an attempt to extend this preparative strategy, we decided to replace isocyanates with carbamoyl chlorides (route C in Scheme 1).[8] Although the choice of substituents is inherently limited in carbamoyl halides because of their high reactivity, we reasoned that a reaction of lithiated intermediates with these reagents[9] could possibly offer an alternative *direct*

[a]*Department of Inorganic Chemistry, Faculty of Science, Charles University in Prague, Hlavova 2030, 12840 Prague 2, Czech Republic. E-mail: stepnic@natur.cuni.cz*
[b]*Department of Physical and Macromolecular Chemistry, Faculty of Science, Charles University in Prague, Hlavova 2030, 12840 Prague 2, Czech Republic*
[c]*Department of Organic Chemistry, Faculty of Science, Charles University in Prague, Hlavova 2030, 12840 Prague 2, Czech Republic*

†Electronic supplementary information (ESI) available: Summary of crystallographic parameters, an overlap of the two independent molecules in the structure of **8d**, displacement ellipsoid plots for all structurally characterised compounds, comparison of the DFT optimised and experimental structures of **2** and **3**, and DFT calculated coordinates for compounds **2**, **3** and $FcC(E)NR_2$ (E = O, S; R = H, Me) as XYZ files. CCDC 1029509–1029520. For ESI and crystallographic data in CIF or other electronic format see DOI: 10.1039/c4dt03279a

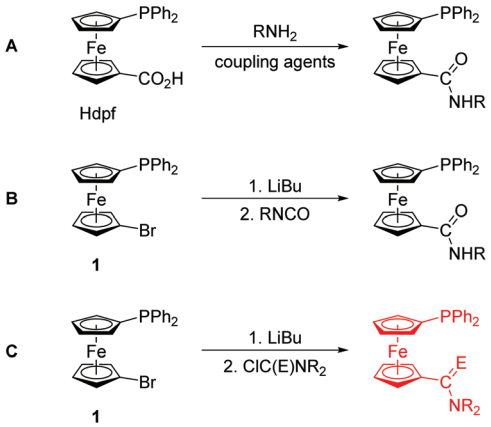

Scheme 1 Synthetic routes to phosphinoferrocene carboxamides: conventional amidation (A) and lithiation/electrophilic quenching (B and C; E = O and S).

route to phosphinoamides and their corresponding thioamides that do not require protection of the already present phosphine moiety from an undesired oxidation.[10] In this regard, a practical synthesis of phosphine-thioamides is particularly attractive as it may provide access to this type of mixed-donor ligands and thus initiate investigations into their coordination properties, which still remain largely unexplored.[11] To the best of our knowledge, there is only one report on the synthesis of a phosphine-thioamide donor *via* the rather unconventional Diels–Alder [4 + 2]-cycloaddition of *N*,*N*-dimethylthioacrylamide across 3,4-dimethyl-1-phenyl-1*H*-phosphole bonded to a Pd(II) centre.[12] This solitary example markedly contrasts with the numerous studies that focus on the chemistry of phosphine-carbothioamides, $Ph_2PC(S)NR_2$.[13]

In this contribution, we describe the synthesis of a phosphinoferrocene carboxamide and thioamide *via* lithiation and electrophilic functionalisation of **1**, and their model compounds obtained by the conventional amidation of Hdpf. The resulting hybrid ligands[14] are structurally characterised through a combination of physicochemical and computational methods and further employed as donors for the soft Group 11 metal ions in order to investigate their coordination properties.

Results and discussion

Preparation and characterisation of phosphino-amide donors

Phosphinoferrocene carboxamide **2** and thioamide **3** were prepared from **1** *via* a one-pot, two-step procedure consisting of lithiation and subsequent quenching of the *in situ* generated lithio intermediate with *N*,*N*-dimethylcarbamoyl chloride and *N*,*N*-dimethylthiocarbamoyl chloride, respectively (Scheme 2). The targeted amides were purified by column chromatography and isolated in moderate to good yields (**2**: 46%; **3**: 81%).

In view of the intended coordination study, the series of phosphinoamide donors was extended by the homologous secondary amide **4** (Scheme 3) and the known primary amide

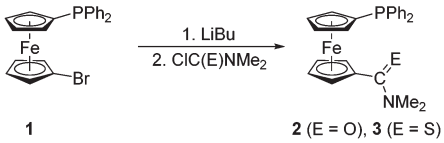

Scheme 2 Preparation of phosphinoferrocene amide **2** and thioamide **3** from **1** and the corresponding carbamoyl halides.

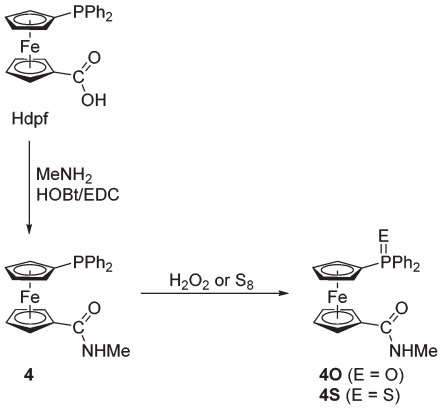

Scheme 3 Preparation of amide **4** and its corresponding P-oxide and P-sulfide. Legend: EDC = 1-ethyl-3-[3-(dimethylamino)propyl]carbodiimide, HOBt = 1-hydroxybenzotriazole.

1′-(diphenylphosphino)-1-(aminocarbonyl)ferrocene (**5**)[7] for the purpose of comparison. The former compound was synthesised by the conventional amidation of Hdpf with methylamine in the presence of 1-ethyl-3-[3-(dimethylamino)propyl]-carbodiimide (EDC) and 1-hydroxybenzotriazole (HOBt), resulting in an 87% yield after isolation by column chromatography. Amide **4** was further converted to the corresponding phosphine oxide (**4O**) and sulfide (**4S**) *via* standard oxidations with hydrogen peroxide and elemental sulfur, respectively.

Amides **2–4** have been characterised by multinuclear NMR and IR spectroscopy, electrospray ionisation (ESI) mass spectrometry and elemental analysis. Phosphines **2–4** display singlets in their $^{31}P\{^1H\}$ NMR spectra at δ_P *ca.* 17, close to that of Hdpf itself,[5] while the signals of the P-oxidised derivatives appear shifted to lower fields (δ_P *ca.* 32 and 43 for **4O** and **4S**, respectively).[5,15] The ^1H and $^{13}C\{^1H\}$ NMR spectra reveal signals typical for the 1′-(diphenylphosphino)ferrocenyl moieties. The amide resonances are observed at δ_C *ca.* 170 for the amides and at δ_C 199 for thioamide **3**. As a result of the limited molecular mobility typical for conjugated amides, the signals of the methyl substituents in the spectra of the tertiary amides are observed either as a broadened singlet (**2**) or a pair of non-equivalent signals (**3**) at room temperature. On the contrary, the ^1H NMR signals of the methyl groups in the spectra of secondary amides **4**, **4O** and **4S** are seen as NH-coupled doublets associated with quartets attributed to the NH proton at a lower field.

The type of amide pendant is manifested in the IR spectra, showing bands resulting from the C–N and C=E[16] stretching vibrations (**2**: 1502 and 1650 cm^{-1}, **3**: 1508 cm^{-1}). The spectra

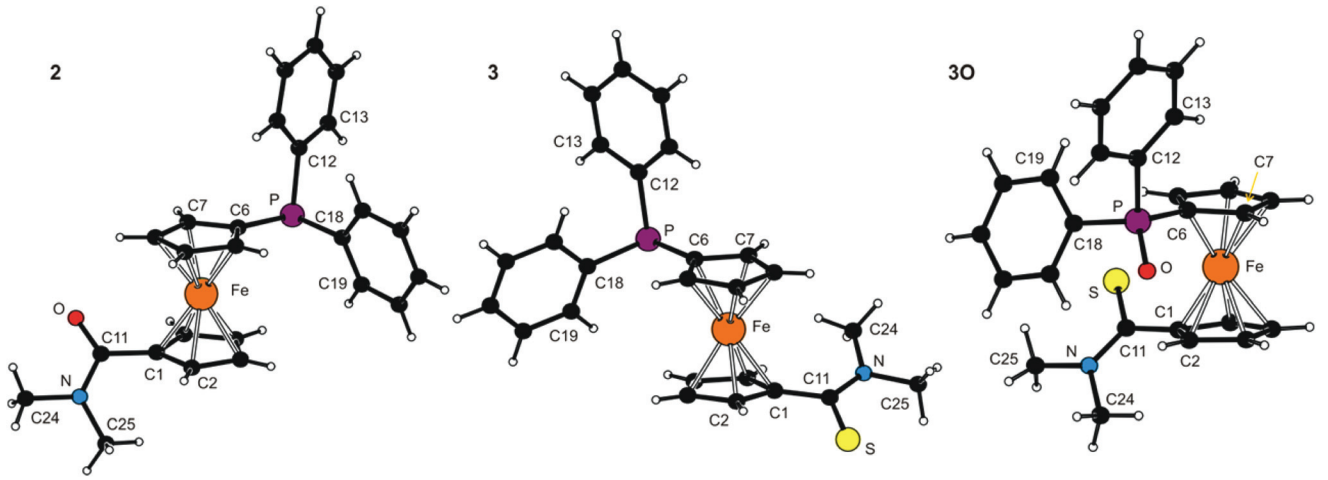

Fig. 1 PLATON plots of the molecular structures of **2**, **3** and **3O** (for displacement ellipsoid plots, see ESI†).

of the secondary amides further display bands due to NH stretching modes above 3000 cm^{-1}. Additional characterisation of **2** and **3** by DFT computations, UV-vis spectroscopy and by cyclic voltammetry are described below.

Molecular structures of uncoordinated amides

The molecular structures of all tertiary amides (**2**, **3** and **3O**) and secondary amides (**4**, **4O**·$CHCl_3$ and **4S**) have been determined by single-crystal X-ray diffraction analysis. The crystals of **3O** were isolated during an attempted complexation experiment with **3**, whereas those of all other compounds were grown by crystallisation of authentic samples.

The molecular structures of **2**, **3** and **3O** are depicted in Fig. 1. Selected geometric parameters are summarised in Table 1. The ferrocene units in the structures of these tertiary amides exert the typical regular geometries with similar Fe–C distances and tilt angles below *ca.* 6° (maximum: 5.8(1)° for **3**). The ferrocene cyclopentadienyl rings in **2** and **3** assume similar anticlinal eclipsed conformations that divert the substituents into mutually distant positions. The amide plane in **2** is rotated by as much as 47.4(2)° from an arrangement coplanar with its parent cyclopentadienyl ring (Cp1) with the NMe_2 group pointing away from the ferrocene unit and the PPh_2 substituent. The thioamide moiety in **3** is twisted considerably less (26.7(2)°) and adopts the opposite orientation with respect to the PPh_2 moiety (*i.e.*, with the C═S bond more distant). In contrast, the ferrocene unit in **3O** has a synclinal eclipsed conformation, which results in a rather compact structure in which both substituents are located on the same side of the ferrocene scaffold. Consequently, the rotation of the thioamide plane is increased to 41.8(2)° and the orientation of the C(S) NMe_2 pendant unit is changed so that the more bulky NMe_2 unit is directed away from the ferrocene unit (though on the same side as the phosphine substituent). Parameters pertaining to the amide/thioamide and (diphenylphosphino)-ferrocenyl moieties appear unexceptional in view of the data reported earlier for $FcCSNH_2$,[17] $fc[CSNMe_2]_2$,[9a] Hdpf and its P-oxide,[5] $Ph_2P(O)fcCONHCy$,[7] and bromide **1**[18] (Fc = ferrocenyl, fc = ferrocene-1,1′-diyl).

Table 1 Selected geometric data for tertiary amides **2**, **3** and **3O** (in Å and °)[a]

Parameter	**2** (E = O)	**3** (E = S)	**3O** (E = S)[b]
Fe–Cg1	1.6462(8)	1.6544(8)	1.6413(7)
Fe–Cg2	1.6464(8)	1.6486(8)	1.6402(7)
∠Cp1, Cp2	2.8(1)	5.8(1)	4.12(9)
τ	−151.1(1)	143.5(1)	71.8(1)
C11═E	1.225(2)	1.689(2)	1.672(2)
C11–N	1.356(2)	1.333(2)	1.337(2)
E═C11–N	121.7(2)	121.4(1)	122.3(1)
φ	47.4(2)	26.7(2)	41.8(2)
N–C24	1.460(2)	1.465(2)	1.468(2)
N–C25	1.460(2)	1.464(2)	1.461(2)
C24–N–C25	116.3(1)	113.7(2)	113.0(2)
P–C6	1.820(2)	1.811(2)	1.788(2)
P–C12	1.832(2)	1.835(2)	1.811(2)
P–C18	1.841(2)	1.839(2)	1.808(2)

[a] Definitions: Cp1 and Cp2 are the cyclopentadienyl rings C(1–5) and C(6–10), respectively. Cg1/2 denote their centroids. τ is the torsion angle C1–Cg1–Cg2–C6 and φ is the dihedral angle subtended by the amide unit (C11, E, N) and the plane of its parent ring Cp1. [b] Further data: P═O = 1.536(1) Å.

Molecular structures of the secondary amides **4**, **4O**·$CHCl_3$ and **4S** are shown in Fig. 2. Principal geometric data are given in Table 2. The molecular parameters compare well with those reported for other structurally characterised secondary amides derived from Hdpf.[19] Similar to the tertiary amides, the ferrocene units in the structures of the secondary amides are typical with tilt angles not exceeding *ca.* 5°. A most notable difference observed across the series is again associated with the mutual orientation of the ferrocene substituents, which are near synclinal eclipsed in **4** and **4O**, staggered anticlinal in molecule 2 of **4S**, or assume an intermediate conformation between anticlinal staggered and eclipsed anticlinal eclipsed (molecule 1 of **4S**).

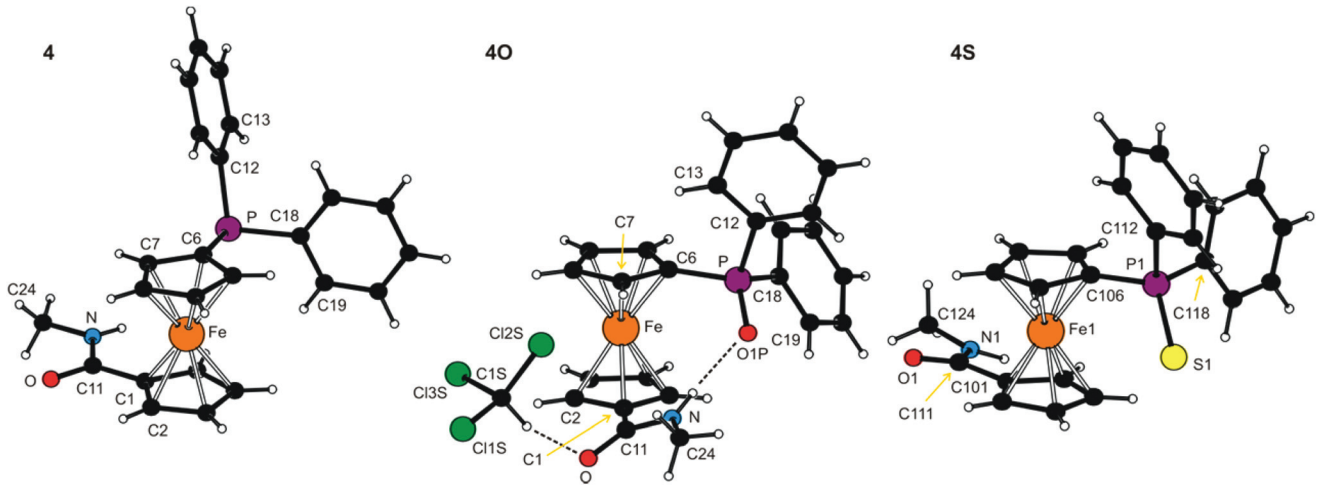

Fig. 2 PLATON plots of the molecular structures of **4**, **4O**·$CHCl_3$ and **4S** (molecule 1). Labelling of the second independent molecule in the structure of **4S** is strictly analogous. Displacement ellipsoid plots are available in the ESI.† The N–H···O and C–H···Cl hydrogen bonds in the structure of **4O**·$CHCl_3$ are shown as dashed lines.

Table 2 Selected geometric parameters for the secondary amides **4**, **4O** and **4S** (in Å and °)[a]

Parameter	**4** (E = void)	**4O** (E = O1P)[b]	**4S** (E = S1/S2)[c]
Fe–Cg1	1.6462(8)	1.650(1)	1.640(4)/1.662(4)
Fe–Cg2	1.6420(7)	1.641(1)	1.643(4)/1.639(4)
∠Cp1, Cp2	3.2(1)	1.2(1)	3.2(5)/4.7(5)
τ	−82.6(1)	71.3(2)	−162.3(5)/145.4(5)
C11═O	1.242(2)	1.233(3)	1.222(6)/1.233(7)
C11–N	1.330(2)	1.343(3)	1.326(8)/1.309(7)
O–C11–N	122.1(2)	123.3(2)	123.6(5)/121.9(6)
φ	6.1(2)	25.3(3)	11.3(8)/13.6(7)
N–C24	1.453(2)	1.456(3)	1.457(9)/1.45(1)
P═E	n.a.	1.495(2)	1.951(3)/1.960(3)
P–C6	1.822(2)	1.785(2)	1.785(8)/1.792(8)
P–C12	1.835(2)	1.809(2)	1.826(9)/1.813(9)
P–C18	1.839(2)	1.809(2)	1.819(7)/1.818(7)

[a] The parameters are defined as for the tertiary amides (see Table 1). n.a. = not applicable. [b] The compound crystallised in the form of stoichiometric solvate **4O**·$CHCl_3$. [c] Data for the two structurally independent molecules (molecule 1/molecule 2).

The rotation of the amide unit with respect to the parent cyclopentadienyl ring varies from *ca.* 6° in amide **4** to *ca.* 25° in **4O**. However, these structural changes seem to be (at least partly) induced by different intermolecular interactions because, unlike the tertiary amides whose solid-state structures are essentially molecular,[20] the molecules of the *secondary* amides associate in the solid state by means of hydrogen bonds formed by the NH hydrogens. Compounds **4** and **4S** assemble into infinite chains consisting of molecules located around the crystallographic glide planes *via* N–H···O═C hydrogen bonds (N···O = 2.835(2) Å for **4** and 2.797(6)/2.834(6) for molecules 1/2 of **4S**). Conversely, the solvated phosphine oxide **4O** forms an intramolecular hydrogen N–H···O═P bond towards the highly polarised[21] phosphoryl oxygen (N···O = 2.838(2) Å) rather than the amide C═O moiety, while the C═O group is employed in binding the solvent molecule *via* the soft C–H···O interaction (Cl_3C–H···O═C, C···O = 3.013(3) Å).

DFT and electrochemical study of amides 2 and 3

Geometries of **2** and **3** computed by DFT methods for isolated molecules in vacuum reproduce very well those determined by X-ray crystallography in the solid state (for an overlap of the computed and experimentally determined molecular structures, see ESI†). Whereas the calculated interatomic distances differ from the experimental ones by less than *ca.* 0.04 Å (the mean difference being only 0.01 Å), the interatomic angles show more pronounced variation (maximum 14°, average difference: 1–3°) due to changes in conformation.[22] The dihedral angle of the cyclopentadienyl planes and τ parameter calculated for amide **2** are 2° and −174°, respectively. The amide moiety in the DFT optimised structure has similar orientation to the solid state structure with twist angle φ of 39°. In the case of thioamide **3**, the τ and φ angles of 149° and 26°, respectively, correspond also well with the crystal structure data (*cf.* data in Table 1).

The LUMO, HOMO and two next molecular orbitals below HOMO are depicted in Fig. 3. In the case of **2**, the HOMO and HOMO−1 show dominant contributions from d orbitals on Fe, while for **3**, the HOMO consists mainly of non-bonding orbital located on sulfur (lone pair). The next two lower molecular orbitals of **3** are of similar nature as HOMO and HOMO−1 of **2** (similar to diagonal relationship), but with certain contribution from atomic orbitals located on the sulfur atom and with somewhat lower energies. This corresponds well with the lower ionisation potential and higher softness of sulfur with respect to oxygen. This principal difference in the structure of the highest occupied molecular orbitals is most likely responsible for the different electrochemical behaviour of **2** and **3** (*vide infra*).

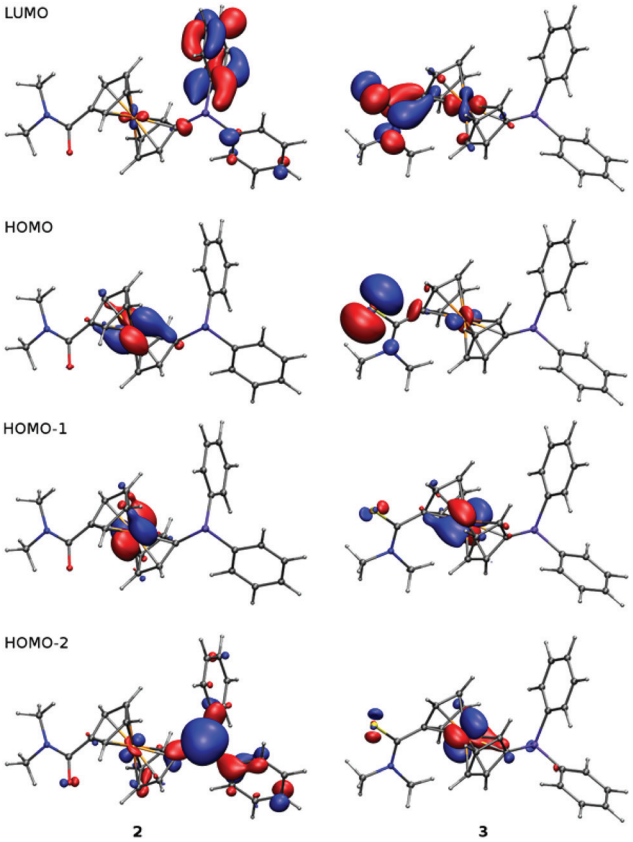

Fig. 3 Plots of LUMO, HOMO and two lower molecular orbitals of **2** and **3** showing contours at the ±0.05 a.u. level.

Changes in electronic structure associated with the (formal) replacement of the amide oxygen with sulfur prompted us to investigate the representative amides **2** and **3** by UV-vis spectroscopy and by electrochemical methods. The UV-vis spectra (Fig. 4) comprise single bands (with a shoulder at lower energies) located at the foot of a more intense bands extending from the UV region. This band in the spectrum of **2**

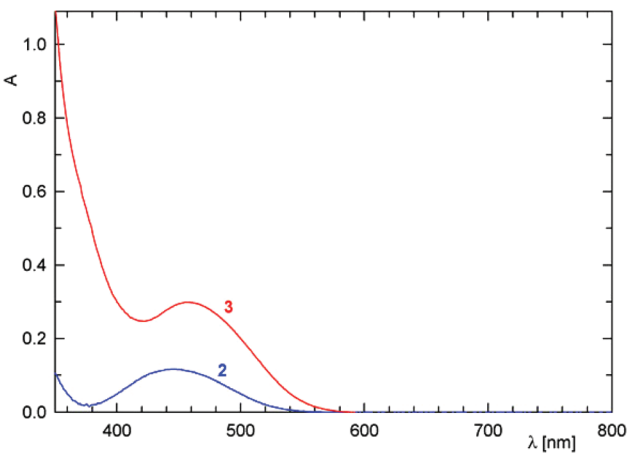

Fig. 4 UV-vis spectra of **2** (blue line) and **3** (red line) recorded in 1,2-dichloroethane solutions (c = 5 × 10^{-4} M, optical path 10 mm).

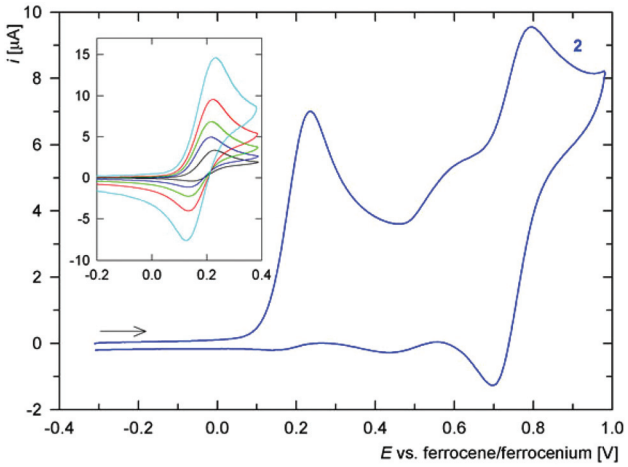

Fig. 5 Cyclic voltammogram of amide **2** as recorded at Pt disc electrode in 1,2-dichloroethane at 0.1 V s^{-1} scan rate (the arrow indicates the scan direction). The inset shows partial cyclic voltammograms recorded at different scan rates (black: 20 mV s^{-1}, blue: 50 mV s^{-1}, green: 0.1 mV s^{-1}, red: 0.2 V s^{-1}, and cyan: 0.5 V s^{-1}).

is observed at 445 nm, shifted slightly to lower energies as compared with ferrocene itself (440 nm; forbidden d–d transition).[23] In the spectrum of **3**, the absorption band is significantly red-shifted (458 nm) and also more intense, presumably owing to a more extensive conjugation.[24]

Cyclic voltammogram of amide **2** (Fig. 5) displays a one-electron oxidation at $E^{o\prime}$ *ca.* 0.17 V *vs.* ferrocene/ferrocenium. The oxidation, which can be attributed to the Fe^{II}/Fe^{III} couple (electron removal from HOMO located predominantly at the ferrocene unit, see above), is associated with some follow-up processes that render it quasi-reversible and also give to rise to additional redox waves at higher potentials. Nonetheless, chemical reactions of the electrochemically generated species are relatively slow because the ratio of the cathodic and anodic peak currents (i_{pc}/i_{pa}) significantly increases with increasing scan rate (see inset in Fig. 5), limiting to unity. Such behaviour resembles that of the parent acid Hdpf.[5] The fact that the oxidation of the ferrocene unit is shifted to less positive potential than that of Hdpf ($E^{o\prime}$ *ca.* 0.31 V in MeCN) is in accordance with the lower electron-withdrawing ability of the amide moiety as compared with the carboxyl group (*cf.* the Hammett σ_p constants: 0.36 for $CONH_2$, and 0.45 for CO_2H).[25]

The redox behaviour of thioamide **3** is much less clear-cut (Fig. 6). The compound undergoes an irreversible oxidation at *ca.* 0.02 V (anodic peak potential, E_{pa}, is given), which is followed by several ill-defined irreversible oxidations that replace the original composite oxidative wave during the second and following scans (even at 1 V s^{-1}). Such a response may well correspond with the properties of the HOMO orbital, which encompasses both ferrocene unit and the thioamide moiety.

DFT study of amide group conformation

The relatively high and varying twisting of the amide pendant observed in the solid-state structures of free phosphinoamides

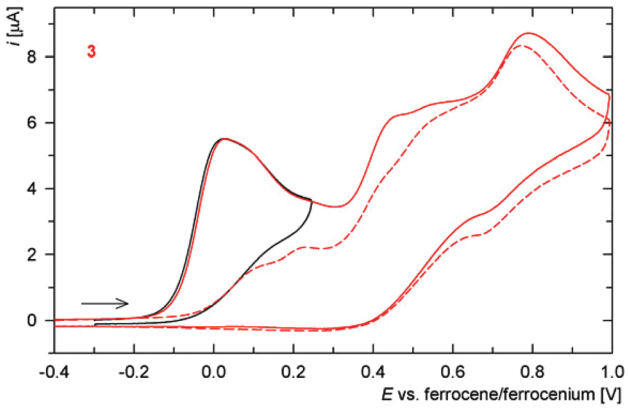

Fig. 6 Full (red line) and partial (black line) cyclic voltammograms of **3** as recorded at Pt disc electrode in 1,2-dichloroethane at 0.1 V s^{-1} scan rate. The arrow indicates the scan direction and the second scan is distinguished by a dashed line.

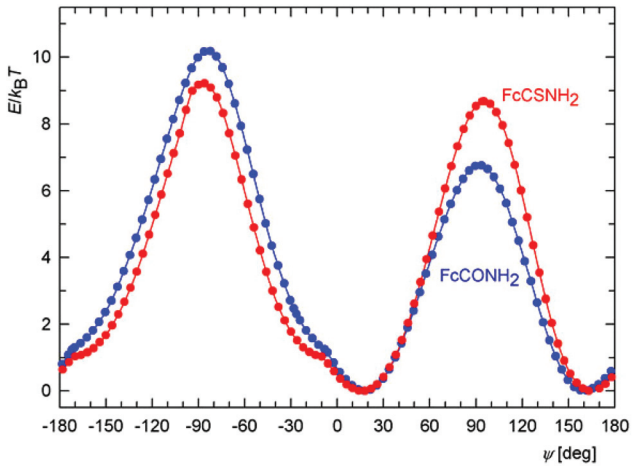

Fig. 7 Calculated energy dependence on the torsion angle ψ for $FcCONH_2$ (blue) and $FcCSNH_2$ (red) at T = 300 K.

led us further to investigate the influence of the dihedral angle subtended by the amide plane {C, N, E} and its parent cyclopentadienyl ring on the overall energy of the isolated model molecules of $FcCONR_2$ and $FcCSNR_2$ (R = H and Me) by DFT calculations. Attention was paid to this parameter mainly because it could significantly affect the coordination properties of the phosphinoamides, being responsible for an efficient approach of the amide moieties to a metal centre.

For the sake of a simpler definition, the dihedral angle φ was replaced with the torsion angle C2–C1–C11–E (ψ). The energy profiles calculated as a function of this angle for $FcCONH_2$ and $FcCSNH_2$ (Fig. 7) show two equivalent minima corresponding to enantiomers. The maxima belong to conformations with amide groups perpendicular to the parent cyclopentadienyl rings, with the higher in energy corresponding to the conformation in which the NH_2 unit is directed closer to the Fe atom. The practically coincident minima for both amides exhibit twists of the amide group of 18°. In the case of the more bulky *N*,*N*-dimethyl derivatives, $FcC(E)NMe_2$, the twisting increases to 35° and 37° for E = O and S, respectively, presumably for steric reasons. The former value corresponds with that determined in the solid state ($FcCONMe_2$: 36/37° for two independent molecules).[26,27]

Importantly, the curvature of the energy landscape near the minima for both $FcCONH_2$ and $FcCSNH_2$ allows for an essentially free change of ψ by approximately 20° in both directions at room temperature, *i.e.*, within the energy change of 1 k_BT (where k_B is the Boltzmann constant). In this interval, the twist angle can thus be controlled *via* an interplay between energy changes reflecting the extent of conjugation, steric effects, coordination and intermolecular interactions (the latter in the solid state).

Another notable feature in the energy profiles concerns small changes in the slope for conformers whose amide groups are nearly coplanar with their bonding cyclopentadienyl rings ($\psi \approx 10°$). These changes result from the potential energy surface (PES) crossing other surface corresponding to an inversion of the pyramidal NH_2 moiety because the two surfaces coincide for the planar arrangement of the NH_2 groups (for clarity, only the PES with the lower energy is shown in Fig. 7).

Synthesis of copper(I) and silver(I) complexes

In order to fully exploit the donor moieties available in **2–5**, coordination study with the soft Cu(I) and Ag(I) ions was undertaken using metal precursors devoid of any firmly bound ligands (*e.g.*, halides) and coordinating anions that could possibly compete with the donor groups offered by the amidophosphine ligands. Hence, the complexation reactions were performed at the ligand-to-metal ratio of 2 : 1 using $[Cu(MeCN)_4][BF_4]$ and $AgClO_4$ as the metal sources (Scheme 4).

These precursors reacted identically with all of the *amides* to afford bis-chelate complexes of the type $[M(L\text{-}\kappa^2O,P)_2]X$. The reaction of thioamide **3** with $[Cu(MeCN)_4][BF_4]$ afforded an analogous compound **6d**, the structure of which, together with other representatives (**6b**, **7b** and **6d**; *vide infra*), was unambiguously confirmed by single-crystal X-ray diffraction analysis. In contrast, the reaction of **3** with silver(I) perchlorate produced an evidently different product (**7d**) exhibiting properties very different from those of the rest of the series: the compound readily precipitated from the reaction mixture and was practically insoluble in common organic solvents (including DMSO-d_6), which in turn precluded its detailed characterisation by solution techniques (*e.g.*, NMR spectroscopy). This finding alerted us to investigate this material in more detail. Fortunately, X-ray quality crystals were obtained when the educts were allowed to mix slowly by liquid-phase diffusion. The isolated crystals proved to be identical with **7d** obtained by direct mixing of the starting materials, as evidenced by the IR spectra.

The structure determination revealed **7d** to be a "dimer", wherein the thioamide coordinates in a P,S-bidentate fashion to one silver(I) centre and simultaneously acts as a bridge towards the other Ag(I) ion through its sulfur atom. The coordi-

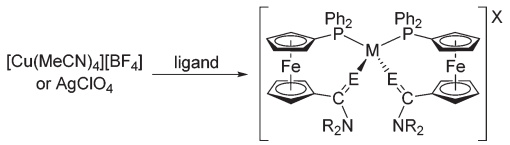

6a-d, 7a-c

complex	M	E	NR_2	X
6a	Cu	O	NH_2	BF_4
6b	Cu	O	NHMe	BF_4
6c	Cu	O	NMe_2	BF_4
6d	Cu	S	NMe_2	BF_4
7a	Ag	O	NH_2	ClO_4
7b	Ag	O	NHMe	ClO_4
7c	Ag	O	NMe_2	ClO_4

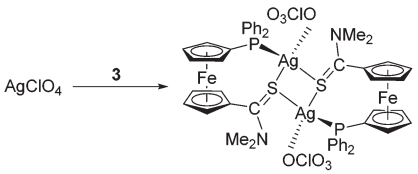

7d

Scheme 4 Synthesis of Cu(I) and Ag(I) complexes.

nation sphere is completed by O-bonded perchlorate, resulting in tetrahedral coordination around the chemically equivalent metal centres. As the consequence, the complex has an overall 1 : 1 ligand-to-metal stoichiometry, which clearly differentiates **7d** from the rest of the Cu(I) and Ag(I) complexes.

Complexes **6** and **7** were characterised by elemental analysis, IR and NMR spectroscopy, and ESI MS spectrometry. The coordination of the amidophosphine ligands in these compounds is clearly manifested in the ^{31}P NMR spectra *via* a shift of the ^{31}P NMR signal to lower fields. The ^{31}P NMR signals are observed as singlets at approximately −11 ppm for the Cu(I) complexes **6a–d**, and as $^{107/109}Ag$-coupled doublets at *ca.* 3–4 ppm for **7a–c**. Compound **7d** gives rise to a broad doublet at δ_P −0.3 with $^1J(Ag,P) \approx 510$ Hz. It is also noteworthy that the ^{31}P and ^1H NMR signals are typically broadened, indicating that some dynamic processes are taking place in the solution. In their ESI mass spectra, the "mononuclear" complexes **6a–d** and **7a–c** exhibit signals of the cations $[ML_2]^+$ and their fragments $[ML]^+$. The spectrum of the disilver(I) species **7d** is dominated by the ions due to $[Ag(\mathbf{3})]^+$ at *m*/*z* 563/566 and further shows additional signals attributable to $[Ag(\mathbf{3})(CH_3OH)]^+$ (*m*/*z* 596/599). All these results (shifts of the ^1H and ^{31}P NMR signals and species observed in the ESI MS spectra) suggest the solid state structures to be retained even in solution, though perhaps with some structural dynamics.

Finally, the presence of the counter anions is reflected in the IR spectra, showing composite intense bands resulting from the ν_3 vibrations[28] of the tetrahedral ions BF_4^- and ClO_4^- at *ca.* 1030–1095 cm^{-1} and 1050–1130 cm^{-1}, respectively.

The anticipated dynamic and possibly hemilabile coordination[29] of the phosphinoamide donors was proven by a serendipitous isolation of several crystals of a solvento complex, $[Cu(\mathbf{5}\text{-}\kappa^2O,P)(\mathbf{5}\text{-}\kappa P)(CHCl_3\text{-}\kappa Cl)][BF_4]$ (**6a′**), which was isolated during an attempted crystallisation of **6a** and structurally characterised. It is noteworthy that this solvento complex ensued from a copper(I) complex whose amide substituents (NH_2) provide the lowest steric protection and donating ability among the amides studied and comprise oxygen as a hard donor atom (N.B. Cu(I) is softer than Ag(I) according to the absolute hardness scale[30]).

Molecular structures of the Cu(I) and Ag(I) complexes

Crystallisation of the "bulk" samples provided single crystals of **6b**·1/4$CHCl_3$, **6d**·2$CHCl_3$, and **7b**·$CHCl_3$, which were used for structure determination. The crystals of **7d** had to be grown by reactive diffusion because of poor solubility, making any recrystallisation impossible (see Experimental), whereas those of **6a′**·$CHCl_3$ were obtained unintentionally upon attempted crystallisation of **6a**.

As indicated by the formulae given above, the compounds tend to retain crystallisation solvents in their structure, which often become disordered in structural voids defined by the bulky complex molecules. A similar effect affects the counter anions, which are considerably smaller than the cations they are associated with, and even some peripheral molecular parts (*e.g.*, phenyl rings).

The crystal structure of **6d**·2$CHCl_3$ is shown in Fig. 8 (structural drawings of the analogous complexes **6b**·1/4$CHCl_3$ and **7b**·$CHCl_3$ are presented in the ESI†). Relevant geometric parameters for all three complexes are provided in Table 3. The structures support the formulation, revealing tetrahedral coordination environments around the metal centres constituted by two P,E-chelating (E = O or S) amidophosphine ligands. An inspection of the interligand angles reveals pronounced angular distortion of the coordination sphere resulting from the different steric demands of the donor moieties. In the pair of complexes derived from ligand **4** (*i.e.*, **6b**·1/4$CHCl_3$ and **7b**·$CHCl_3$), the interligand angles increase from O–M–O *via* O–M–P to P–M–P. Such a feature, as well as the

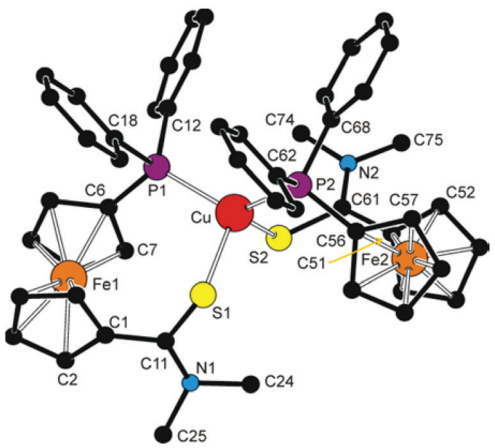

Fig. 8 View of the cation in the structure of **6d**·2$CHCl_3$. The hydrogen atoms are omitted for clarity.

Table 3 Selected geometric data for the bis-chelates **6b**·1/4$CHCl_3$, **6d**·2$CHCl_3$ and **7b**·$CHCl_3$ and for the related solvento complex **6a′**·$CHCl_3$ (in Å and °)[a]

Compound	**6b**·1/4$CHCl_3$ (M/E = Cu/O1, O2)		**6d**·2$CHCl_3$ (M/E = Cu/S1, S2)		**7b**·$CHCl_3$ (M/E = Ag/O)	**6a′**·$CHCl_3$ (M/E = Cu/O1, O2)[c]	
Parameter	Ligand 1	Ligand 2	Ligand 1	Ligand 2	Ligand 1[b]	Ligand 1[d]	Ligand 2[d]
M–P	2.2469(7)	2.2256(8)	2.2842(5)	2.2636(5)	2.4256(6)	2.251(1)	2.233(1)
M–E	2.174(2)	2.102(2)	2.3866(6)	2.3951(7)	2.468(2)	n.a.	2.006(3)
P–M–P [E–M–E]	125.79(3)	[93.06(9)]	127.32(2)	[108.24(2)]	142.99(3) [80.20(6)]	128.17(4)	n.a.
P–M–E1	104.09(6)	109.40(6)	105.59(2)	100.17(2)	115.50(5)	n.a.	n.a.
P–M–E2	101.29(7)	117.74(6)	104.98(2)	109.33(2)	93.16(5)	110.95(9)	118.04(9)
Fe–Cg1	1.645(2)	1.648(1)	1.647(1)	1.643(1)	1.651(1)	1.652(2)	1.652(2)
Fe–Cg2	1.639(1)	1.646(1)	1.644(1)	1.647(1)	1.640(1)	1.649(2)	1.646(2)
∠Cp1, Cp2	1.0(2)	4.0(2)	3.5(2)	7.5(2)	1.0(2)	2.7(2)	2.2(2)
τ	−49.4(2)	−68.2(2)	−59.5(2)	−15.2(2)	−69.5(2)	101.0(3)	−59.4(3)
C═E (amide)	1.240(4)	1.228(3)	1.711(2)	1.714(2)	1.231(3)	1.250(4)	1.271(3)
C–N (amide)	1.324(4)	1.331(3)	1.325(3)	1.323(3)	1.337(4)	1.320(5)	1.312(4)
E═C–N (amide)	121.1(3)	121.4(2)	120.0(2)	121.1(2)	122.0(2)	121.9(3)	118.6(3)
φ	19.3(4)	27.9(3)	11.1(2)	39.1(2)	15.5(3)	9.0(4)	19.8(3)

[a] Definitions: Cp1 and Cp2 are the amide- and phosphine-substituted cyclopentadienyl rings, respectively. Cg1/2 are their centroids. τ is the torsion angle C1–Cg1–Cg2–C6 and φ is the dihedral angle subtended by the amide unit (E═C1–N) and the plane of its parent ring Cp1. n.a. = not applicable. [b] Only one set of distances and angles available because of the imposed symmetry. [c] Further data: Cu–Cl1 = 3.138(2); Cl1–Cu–P1 = 107.90(4), Cl1–Cu–P2 = 86.96(4), Cl1–Cu–O2 = 91.8(1). [d] Ligand 1 = P-monodentate **5**, ligand 2 = O,P-chelating **5**.

individual ligand–donor bond lengths, correspond with those reported for $[Cu(Ph_2PfcCONHCH_2CO_2Me\text{-}\kappa^2O,P)_2](CF_3SO_3)$.[31]

Upon going from **6b**·1/4$CHCl_3$ to **7b**·$CHCl_3$, a lengthening of the M–P (by *ca*. 0.2 Å) and, particularly, the M–O bonds (from *ca*. 2.10/2.17 Å for Cu(I) to 2.47 Å for Ag(I)) is observed owing to the presence of a larger central atom in the Ag(I) complex. The fact that the Cu–O distances in the structure of the former compound differ significantly (0.07 Å) can be associated with a relatively weaker coordination of the hard donor group, which may in turn allow for structural distortions without any dramatic destabilisation (increase in the overall energy; *cf*. the DFT calculations above). On the other hand, the bond lengths within the amide pendant change only marginally upon coordination (see the data for **4** above) but the ligand undergoes conformational reorganisation. The ferrocene-bound donor moieties are rotated closer to each other and the amide planes are twisted so as their oxygen atoms can reach the metal centre.

The Cu(I) complex bearing the thioamide ligands, **6d**·2$CHCl_3$, also possesses a tetrahedral structure, but because of longer Cu–S bonds, it appears to be more sterically relaxed. This is manifested in the interligand angles among which the S–Cu–S is no longer the most acute. Notably, the two structurally independent P,S-chelating ligands in the structure of **6d** differ by conformation as evidenced by the τ and φ angles (Table 3; N.B. similar though less pronounced differences can be observed in the structure of **6b**).

Opening of one of the chelate rings, such in the structure of **6a′**·$CHCl_3$ (Fig. 9 and Table 3), does not result in an equalisation of the interligand angles (*ca*. 87–128°), presumably because the amide oxygen is replaced with a relatively bulky chloroform molecule. The Cu–Cl1 distance of 3.138(2) Å approaches the threshold of the van der Waals contacts (3.15 Å[32]). According to a search in the Cambridge Structural Database (CSD),[33] analogous Cu···Cl–$CHCl_2$ interactions are rare and can be detected in the crystal structures of chloroform solvates of molecular triangles (Cu_3)[34] and squares (Cu_4)[35] built up from bis(acetylacetonate) ligands and Cu(II) ions, in which the chloroform occupies an apical position in a square pyramid around the Cu(II) ions (Cu···Cl ≈ 3.11–3.25 Å).

The different roles that the two amidophosphine ligands play in the complex cation of **6a′** are reflected in their conformations. Thus, the donor substituents in the chelating ligand adopt a conformation between synclinal staggered and synclinal eclipsed ($\tau \approx -59°$), and the amide planes are rotated by *ca*. 20° with respect to the parent cyclopentadienyl ring. On the other hand, the P-bound ligand assumes a more opened anticlinal conformation ($\tau \approx 101°$) and the amide plane is twisted by only *ca*. 9°. The C═O distances are affected only marginally but in the expected manner as the coordinated C═O bond is *ca*. 0.02 Å longer than the uncoordinated one.

NH protons in the structures of complexes with coordinated **4** (*i.e.*, **6b** and **7b**) are involved in hydrogen bonding to the respective counter anion in the crystal state. Those in molecules of **6a′** interconnect the complex units into dimers positioned around the inversion centres (Fig. 9). In the latter case, each P-bound ligand is linked to its inversion-related counterpart *via* a pair of N–H···O═C hydrogen bonds from the NH hydrogen closer to the amide oxygen, whereas the other hydrogen forms an N–H···F hydrogen bridge to one of the BF_4^- anions. Amide hydrogens in the P,O-chelating ligand participate in similar interactions towards the oxygen in the P-monodentate ligand (O1) bonded to the same metal centre and towards another BF_4 fluorine, respectively.

As it was stated above, complex **7d** (Fig. 10 and Table 4) is a dimer, in which the phosphinoamide ligands coordinate in a

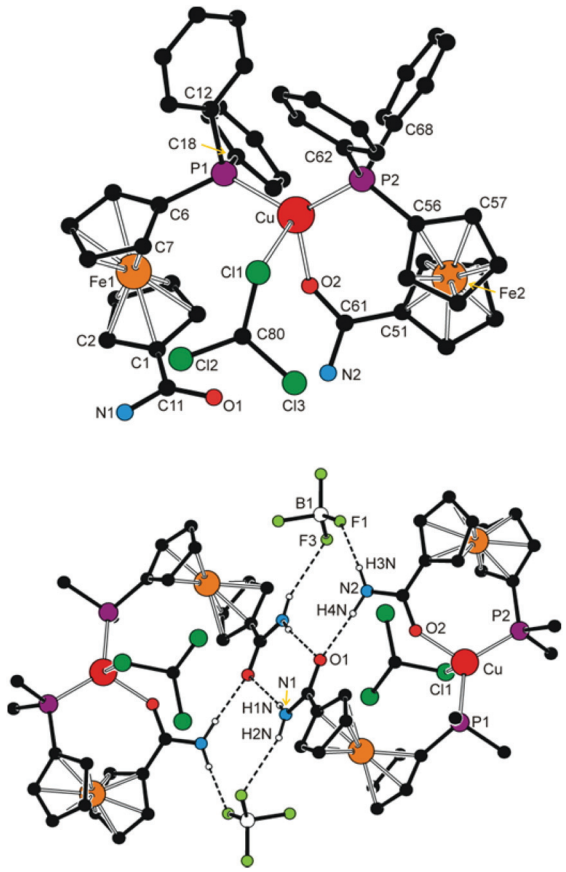

Fig. 9 Top: view of the complex molecule in the structure of **6a**′·$CHCl_3$. All CH hydrogen atoms are omitted for clarity. Bottom: packing diagram for **6a**′·$CHCl_3$. Only the pivotal carbon atoms from the phenyl rings and NH hydrogens are shown for clarity. Hydrogen bond parameters are as follows (in Å and °): N1–H1N···O1, N1···O1 = 2.914(5), angle at H1N = 158; N1–H2N···F3, N1···F3 = 3.15(1), angle at H2N = 160; N2–H4N···O1, N2···O1 = 2.914(4), angle at H4N = 152; N2–H3N···F1, N2···F1 = 2.872(8), angle at H3N = 152.

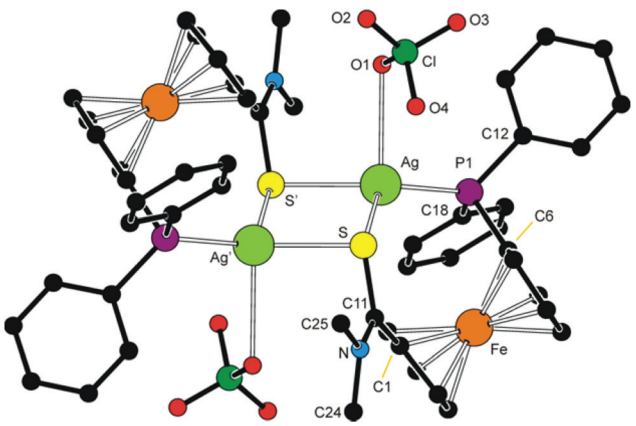

Fig. 10 View of the molecular structure of **7d**. The prime-labelled atoms are generated by the crystallographic inversion.

chelating manner and are further involved in bridging of the "other" Ag(I) ion through the sulfur atom. The donor set around each Ag(I) is supplemented with an O-bonded perchlorate anion into a distorted tetrahedron. The Ag–O distance of 2.814(6) Å falls well below the sum of the van der Waals radii (3.24 Å), suggesting a relatively weaker yet significant interaction between the anion and Ag(I).

Table 4 Selected distances and angles for **7d** (in Å and °)[a]

Ag–P	2.426(1)	P–Ag–S	121.68(4)
Ag–S	2.663(1)	P–Ag–S′	143.55(5)
Ag–S′	2.572(1)	P–Ag–O1	95.9(1)
Ag–O1	2.814(6)	S–Ag–S′	85.44(4)
Ag···Ag′	3.8469(7)	S–Ag–O1	117.6(1)
S···S′	3.552(2)	S′–Ag–O1	90.9(1)
Fe–Cg1	1.647(2)	∠Cp1, Cp2	5.1(3)
Fe–Cg2	1.651(2)	τ	−80.9(3)
C11═S	1.719(4)	S–C11–N	120.3(3)
C11–N	1.306(6)	φ	37.8(5)

[a] All parameters are defined as for the free ligand (see Table 1). The prime-labelled atoms are generated by the $(1 - x, 2 - y, 2 - z)$ symmetry operation.

The Ag–S distance pertaining to the sulfur atom from the chelating ligand is *ca.* 0.1 Å longer than the Ag–S distance to the bridging sulfur, and the central Ag_4S_4 ring has a twisted rhomboidal shape (S–Ag–S′ = 85.44(4)°, Ag–S–Ag′ = 94.56(4)°). The ferrocene ligands adopt a conformation near to synclinal eclipsed (ideal value: τ = 72°) and their amide pendants are twisted by *ca.* 38°.

Synthesis of chloridogold(I) complexes

For the sake of completeness, we have synthesised a series of chloridogold(I) complexes of the type [AuCl(L-κ*P*)] (**8**; L = **2–5**, Scheme 5), in which the amidophosphine ligands employ only their phosphorus donor moieties for coordination. These compounds were readily prepared *via* displacement of the tetrahydrothiophene (tht) ligand in [AuCl(tht)] by the stoichiometric amount of the respective amidophosphine, resulting in good to excellent yields depending on the isolation procedure.

Compounds **8a–d** were characterised similarly to the Cu(I) and Ag(I) complexes discussed above. In addition, the molecular structure of **8d** was determined by single-crystal X-ray diffraction analysis. The ^{1}H and ^{31}P{^{1}H} NMR spectra of **8a–d** show signals of the phosphinoferrocene ligands and sharp singlets at *ca.* δ_P +29, respectively. The ESI MS spectra of these complexes display signals attributable to cationic fragments resulting from the loss of chloride ion ($[M - Cl]^+$) and, for **8a–c**, also the signals due to the pseudomolecular ions ($[M + Na]^+$ and $[M + K]^+$).

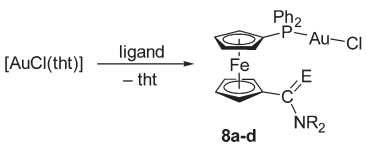

complex	E	NR_2
8a	O	NH_2
8b	O	NHMe
8c	O	NMe_2
8d	S	NMe_2

Scheme 5 Synthesis of Au(I) complexes **8a–d** (tht = tetrahydrothiophene).

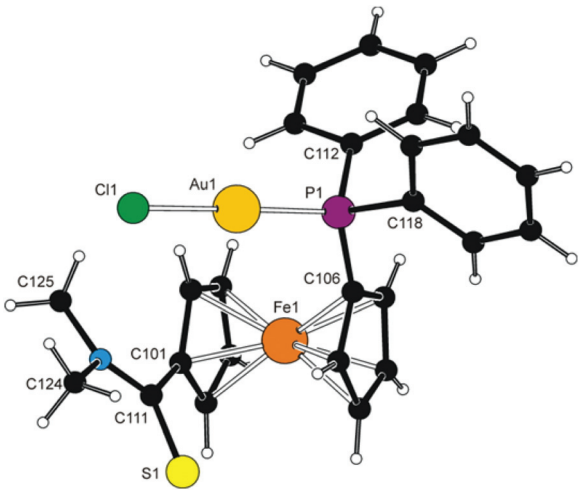

Fig. 11 View of molecule 1 in the crystal structure of **8d**. The labelling of molecule 2 is analogous with the respective labels having 2 as the first numeral. Selected distances and angles (in Å and °) for molecule 1 [molecule 2]: Au–Cl 2.294(2) [2.278(2)], Au–P 2.230(2) [2.226(2)], Cl–Au–P 178.3(1) [174.91(7)], Fe–Cg1 1.653(4) [1.654(4)], Fe–Cg2 1.640(3) [1.628(4)], τ −78.9(5) [−83.0(5)], C═S 1.663(9) [1.669(8)], C–N 1.34(1) [1.34(1)], S–C–N 123.2(6) [122.1(6)], φ 33.2(8) [39.9(8)]. Note: the parameters are defined as for the free ligand.

Molecular structure of 8d

Complex **8d** (Fig. 11) crystallises with two independent but otherwise similar[36] molecules per asymmetric unit (for an overlap, see ESI†). The molecules comprise the typical, practically linear Cl–Au–P moieties with the Au–P and Au–Cl bond lengths being close to those previously determined for $[AuCl(FcPPh_2)]$[37] and the related AuCl complexes with 1′-functionalised phosphinoferrocene ligands.[38]

The amidophosphine ligands in the two molecules exert negligible tilting on the ferrocene unit (1.9(5)° and 3.4(5)°) and adopt conformations close to synclinal eclipsed (*cf.* τ with the ideal value of 72°). The amide substituents are rotated by *ca.* 33° and 40° (for molecules 1/2) from the planes of their parent cyclopentadienyl rings so that the bulky NMe_2 unit are directed away from the ferrocene unit. The structure of **8d** is essentially molecular; no Au···Au contacts indicative of possible aurophilic interactions[39] were detected.

Electrochemical study of representative complexes

In addition to the characterization discussed above, complexes **6c**, **6d**, **7c** and **8c** as the representatives were studied by voltammetric methods similarly to the free ligands. Attention was paid mostly to the behaviour in the anodic region.

Thus, in cyclic voltammetry, compound **6c** undergoes an oxidation which can be tentatively attributed to the oxidation of its ferrocene ligands (Fig. 12). However, the observed redox wave is composite, presumably owing to a convolution of two narrow-spaced oxidations (peak potentials: anodic 0.49 V, cathodic 0.34 V). This is clearly manifested in differential pulse voltammograms (see Figure in the ESI†). The associated redox process appears to be reversible, though only when the wave is scanned separate over a narrow range. If the scan is extended beyond this first redox event, an irreversible oxidative and two reduction waves appear, replacing the original redox response during the second and following scans (Fig. 12). The response of the analogous Ag(I) complex **7c** in cyclic voltammetry is very similar (peak potentials for the composite wave: approx. 0.50 and 0.37 V).

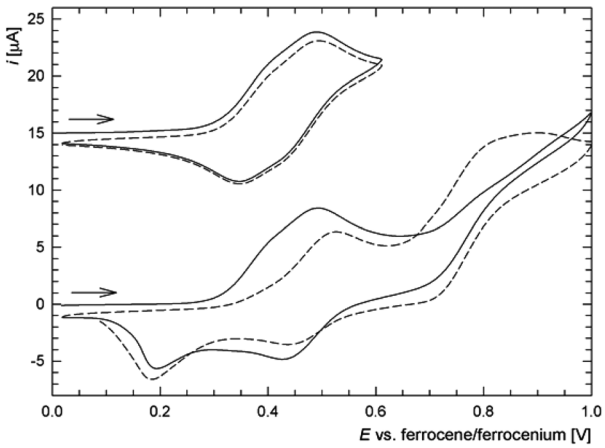

Fig. 12 Full (bottom) and partial (top) cyclic voltammograms of **6c** as recorded at a glassy carbon electrode and with 0.1 V s^{-1} scan rate (second scans are shown as dashed lines). For clarity, the partial cyclic voltammogram is shifted by +15 μA (to avoid overlaps) and the scan direction is indicated with an arrow.

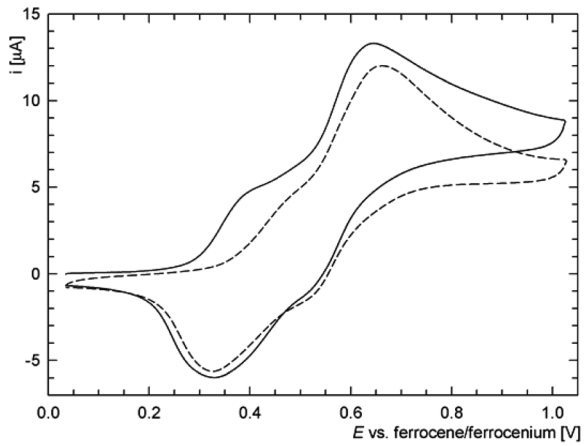

Fig. 13 Representative cyclic voltammograms of **6d** as recorded at a glassy carbon electrode and 0.1 V s^{-1} scan rate (the second scan is shown as a dashed line).

On the other hand, the redox behaviour of the Cu(I)–thioamide complex **6d** differs from that of **6c** (Fig. 13) in that compound **6d** undergoes an irreversible oxidation at *ca.* 0.41 V (peak potential). When the scan window is enlarged, a pair of redox waves appears at *ca.* 0.66 and 0.32 V that practically supersede the original oxidative wave. Finally, the gold(I) monophosphine complex **8c** undergoes a standard one-electron oxidation at $E^{\circ\prime}$ = 0.375 V. It is noteworthy that the wave, which can be ascribed to the ferrocene/ferrocenium couple, is

electrochemically reversible, very likely because the lone pair at phosphorus as a reactive site is no longer available.[5] The shift of the redox wave towards more positive potential with respect to free **2** corresponds with the expected electron density lowering at the ferrocene unit associated with coordination.

Conclusions

The results presented in this paper demonstrate that the reaction of 1′-(diphenylphosphino)-1-lithioferrocene with carbamoyl and thiocarbamoyl chlorides is a viable synthetic route to new phosphinoamide ligands, offering an alternative to other commonly employed preparative methods such as the amidation of carboxylic acids. The reaction appears to be particularly attractive for the synthesis of phosphine-thioamides because it eliminates the additional protection/deprotection steps required during the conventional thionations.

As evidenced by the structures of the free donors and their complexes, the molecules of 1′-(diphenylphosphino)ferrocene amides and thioamides are flexible, allowing for a pre-organisation of the donor moieties into positions suitable for coordination *via* rotation of the ferrocene cyclopentadienyls and twisting of the amide unit around the pivotal C–C bond at no substantial energy cost. The hybrid nature of these donors, particularly the amides combining hard and soft donor groups, results in hemilabile coordination in complexes with the soft Group 11 metal ions that in turn affects the stability and structural dynamics of these coordination compounds. The coordination variability is in no way reduced upon the replacement of amide oxygen with the soft sulfur atom. The thioamides may thus not only simply parallel the behaviour of their amide analogues but can also behave differently, taking advantage of the specific qualities of the thioamide moiety (longer C═S bond, softer and less electronegative donor atom, *etc.*) and thus give rise to new and unique structural motifs (*cf.* the structure of **7d**). All of these factors render the coordination chemistry of phosphino-thioamides an attractive research target that has not yet been explored in great detail.

Experimental

Materials and methods

All syntheses were performed under an argon atmosphere in the absence of direct daylight. Compounds **1**[40] and [AuCl(tht)][41] were synthesised according to the literature. Dichloromethane and tetrahydrofuran were dried with a Pure Solv MD-5 Solvent Purification System (Innovative Technology, USA). Benzene and toluene were dried over sodium metal and distilled under argon. Other chemicals and solvents utilised for crystallisations and during column chromatography were used as received (Sigma-Aldrich; solvents from Lachner, Czech Republic).

IR spectra were recorded with an FTIR Nicolet 760 instrument in the range 400–4000 cm^{-1}. NMR spectra were obtained on a Varian UNITY Inova 400 spectrometer at 25 °C unless noted otherwise. Chemical shifts (δ/ppm) are referenced to internal tetramethylsilane (for ^{1}H and ^{13}C NMR spectra) and external 85% aqueous H_3PO_4 (^{31}P NMR spectra). Alongside the standard notation of signal multiplicity, vq and vt are used to distinguish virtual quartets and triplets arising from the magnetically non-equivalent protons at the phosphine- and carbamoyl-substituted cyclopentadienyl rings, respectively.

Electrospray ionisation mass spectra (ESI MS) were recorded with a Bruker Esquire 3000 spectrometer using samples dissolved in HPLC-grade methanol. High-resolution (HR) ESI mass spectra were measured on a LTQ Orbitrap XL spectrometer. UV-vis spectra were recorded with a Unicam UV300 spectrometer in 1,2-dichloroethane. Elemental analyses were determined with a PE 2400 Series II CHNS/O Elemental Analyser (Perkin Elmer). The amount of clathrated solvent (if any) was verified by NMR analysis.

Safety note. Caution! Although we have not encountered any problems, it must be noted that perchlorate salts of complexes with organic ligands are potentially explosive and should be handled with care and only in small quantities.

Synthesis of the amidophosphine ligands

1′-(Diphenylphosphino)-1-[(dimethylamino)carbonyl]ferrocene (2). 1′-(Diphenylphosphino)-1-bromoferrocene (**1**; 0.90 g, 2.0 mmol) was placed in a two-necked, round bottom flask and dissolved in dry tetrahydrofuran (10 mL). The orange solution was cooled for 10 minutes in a dry ice/ethanol bath before BuLi (1.0 mL of 2.5 M in hexanes, 2.5 mmol) was slowly introduced, causing the reaction mixture to darken. After stirring for 15 min, neat *N*,*N*-dimethylcarbamoyl chloride (0.39 g, 3.6 mmol) was slowly added to the reaction mixture at −78 °C and the stirring was continued at room temperature for 90 min. Saturated aqueous $NaHCO_3$ (*ca.* 20 mL) was introduced and the resulting mixture was stirred for an additional 15 min. Then, the mixture was extracted with Et_2O (3 × 10 mL), and the combined organic layers were washed with brine and dried over $MgSO_4$. Following solvent removal, the crude product was purified by repeated column chromatography over silica gel using dichloromethane–methanol (50 : 1) and then ethyl acetate–hexane (3 : 1) as the eluents. Subsequent evaporation under vacuum afforded amide **2** as an orange solid. Yield: 0.41 g (46%).

^{1}H NMR (399.95 MHz, $CDCl_3$): δ 3.04 (br s, 6 H, NMe_2), 4.14 (vq, $J' \approx 1.7$ Hz, 2 H, fc), 4.19 (vt, $J' = 1.9$ Hz, 2 H, fc), 4.47 (vt, $J' \approx 1.9$ Hz, 2 H, fc), 4.52 (vt, $J' \approx 1.9$ Hz, 2 H, fc), 7.28–7.39 (m, 10 H, PPh_2). $^{31}P\{^{1}H\}$ NMR (161.90 MHz, $CDCl_3$): δ −16.8 (s). $^{13}C\{^{1}H\}$ NMR (100.58 MHz, $CDCl_3$): δ 37.5 (very br, NMe_2), 70.73 (CH of fc), 71.44 (CH of fc), 73.46 (d, J_{PC} = 4 Hz, CH of fc), 74.18 (d, J_{PC} = 15 Hz, CH of fc), 79.20 (*C*-$CONMe_2$ of fc), 128.17 (d, $^{3}J_{PC}$ = 7 Hz, PPh_2 CH_{meta}), 128.58 (PPh_2 CH_{para}), 133.43 (d, $^{2}J_{PC}$ = 20 Hz, PPh_2 CH_{ortho}), 138.60 (d, $^{1}J_{PC}$ = 9 Hz, PPh_2 C_{ipso}), 170.07 (C═O). The signal due to *C*-PPh_2 was not observed. IR (Nujol): ν_{max} 1615 vs (amide I), 1502 s (amide II)

cm^{-1}. ESI+ MS: *m*/*z* 442 ([M + H]$^+$). HR MS (ESI) calcd for $C_{25}H_{25}FeNOP$ ([M + H]$^+$) 442.1018, found 442.1019. Anal. Calcd for $C_{25}H_{24}FeNOP$ (441.3): C 68.04, N 3.17, H 5.48%. Found: C 67.74, N 3.04, H 5.32%.

1′-(Diphenylphosphino)-1-[(dimethylamino)thiocarbonyl]-ferrocene (3). Thioamide **3** was prepared similarly to **2** using bromide **1** (0.90 g, 2.0 mmol) and *N*,*N*-dimethylthiocarbamoyl chloride (0.45 g, 3.6 mmol). An aqueous work-up as described above afforded an oily crude product, which was purified by column chromatography over silica gel using dichloromethane–methanol (50 : 1) and (in the second run) pure dichloromethane as the eluents. Following evaporation under vacuum, thioamide **3** was isolated as an a dark orange-red solid. Yield: 0.74 g, 81%.

^{1}H NMR (399.95 MHz, $CDCl_3$): δ 3.31 (br s, 3 H, NMe), 3.43 (br s, 3 H, NMe), 4.12 (vq, $J' \approx 1.8$ Hz, 2 H, fc), 4.24 (vt, $J' \approx 1.9$ Hz, 2 H, fc), 4.50 (vt, $J' \approx 1.8$ Hz, 2 H, fc), 4.59 (vt, $J' \approx 1.9$ Hz, 2 H, fc), 7.29–7.39 (m, 10 H, PPh_2). ^{31}P{^{1}H} NMR (161.90 MHz, $CDCl_3$): δ −16.8 (s). ^{13}C{^{1}H} NMR (100.58 MHz, $CDCl_3$): δ 44.19 (NMe), 45.08 (NMe), 70.62 (CH of fc), 72.99 (CH of fc), 75.39 (d, J_{PC} = 14 Hz, CH of fc), 75.81 (d, J_{PC} = 4 Hz, CH of fc), 88.02 (*C*-CSNMe$_2$ of fc), 128.17 (d, $^3J_{PC}$ = 7 Hz, PPh_2 CH_{meta}), 128.57 (PPh_2 CH_{para}), 133.46 (d, $^2J_{PC}$ = 20 Hz, PPh_2 CH_{ortho}), 138.73 (d, $^1J_{PC}$ = 10 Hz, PPh_2 C_{ipso}), 199.24 (C═S). The signal due to *C*-PPh_2 was not observed. IR (Nujol): ν_{max} 1508 (ν_{C-N}) cm^{-1}. ESI+ MS: *m*/*z* 480 ([M + Na]$^+$). HR MS (ESI) calcd for $C_{25}H_{25}NSPFe$ ([M + H])$^+$ 458.0789, found 458.0789.

1′-(Diphenylphosphino)-1-[(methylamino)carbonyl]ferrocene (4). Neat 1-[3-(dimethylamino)propyl]-3-ethylcarbodiimide (EDC; 0.40 mL, 2.4 mmol) was added to a mixture of 1′-(diphenylphosphino)ferrocene-1-carboxylic acid (Hdpf; 0.83 g, 2.0 mmol), 1-hydroxybenzotriazole (0.33 g, 2.40 mmol) and tetrahydrofuran (5 mL) while stirring and cooling in ice. After stirring at 0 °C for 30 min, dimethylamine solution (1.2 mL of 2 M in THF, 2.4 mmol) was introduced and the resultant mixture was stirred at 0 °C for 30 min and then at room temperature overnight. The reaction was terminated by addition of a saturated aqueous $NaHCO_3$ solution (20 mL) and stirring for additional 15 min. The organic phase was separated and the aqueous layer was extracted with diethyl ether (3 × 10 mL). The combined organic layers were washed with brine and dried over $MgSO_4$. The crude product resulting after evaporation was purified by column chromatography on silica gel with dichloromethane–methanol (20 : 1) as the eluent. The first minor band was discarded and the second one was collected and evaporated to afford amide **4** as an orange yellow solid. Yield: 0.75 g, 87%.

^{1}H NMR (399.95 MHz, $CDCl_3$): δ 2.83 (d, $^3J_{HH}$ = 4.9 Hz, 3 H, NMe), 4.07 (vq, $J' \approx 1.9$ Hz, 2 H, fc), 4.22 (vt, $J' \approx 1.9$ Hz, 2 H, fc), 4.44 (vt, $J' \approx 1.8$ Hz, 2 H, fc), 4.55 (vt, $J' \approx 1.9$ Hz, 2 H, fc), 5.60 (br q, $^3J_{HH} \approx 5$ Hz, 1 H, NH), 7.31–7.41 (m, 10 H, PPh_2). ^{31}P{^{1}H} NMR (161.90 MHz, $CDCl_3$): −16.7 (s). ^{13}C{^{1}H} NMR (100.58 MHz, $CDCl_3$): δ 26.50 (NMe), 69.38 (CH of fc), 71.31 (CH of fc), 72.71 (d, J_{PC} = 4 Hz, CH of fc), 74.31 (d, J_{PC} = 14 Hz, CH of fc), 128.30 (d, $^3J_{PC}$ = 7 Hz, PPh_2 CH_{meta}), 128.80 (PPh_2 CH_{para}), 133.48 (d, $^2J_{PC}$ = 20 Hz, PPh_2 CH_{ortho}), 138.34 (d, $^1J_{PC}$ = 9 Hz, PPh_2 C_{ipso}), 170.30 (C═O). Signals due to ferrocene C_{ipso} were not observed. IR (Nujol): ν_{max} 3308 m (ν_{N-H}), 1628 s (amide I), 1545 s (amide II) cm^{-1}. ESI+ MS: *m*/*z* 428 ([M + H]$^+$). HR MS (ESI) calcd for $C_{24}H_{22}FeNNaOP$ ([M + Na]$^+$) 450.0681, found 450.0680. Anal. Calcd for $C_{24}H_{22}FeNO$ (427.3): C 67.46, N 3.28, H 5.19%. Found: C 67.07, N 3.24, H 5.03%.

1′-(Diphenylphosphinyl)-1-[(methylamino)carbonyl]ferrocene (4O). Aqueous hydrogen peroxide (2 drops of 30% solution) was added to a solution of amide **4** (48 mg, 0.11 mmol) in acetone (8 mL) while stirring and cooling in ice. The reaction mixture was stirred at 0 °C for 30 min and then diluted with water (5 mL). The organic solvent was removed under reduced pressure and the aqueous residue was extracted with dichloromethane (3 × 5 mL). The organic washings were combined, dried over $MgSO_4$ and evaporated. The residue was dissolved in dichloromethane (2 mL) and the solution was passed through a plug of silica gel eluted with dichloromethane–methanol (10 : 1). Following evaporation, phosphine oxide **4O** was isolated as a dark yellow solid. Yield: 40 mg, 82%.

^{1}H NMR (399.95 MHz, $CDCl_3$): δ 2.93 (d, $^3J_{HH}$ = 4.7 Hz, 3 H, NMe), 4.07 (vt, $J' \approx 1.9$ Hz, 2 H, fc), 4.14 (vq, $J' \approx 1.9$ Hz, 2 H, fc), 4.58 (vq, $J' \approx 1.8$ Hz, 2 H, fc), 4.99 (vt, $J' \approx 1.9$ Hz, 2 H, fc), 7.44–7.58 (m, 6 H, PPh_2), 7.65–7.73 (m, 4 H, PPh_2), 8.76 (br q, $^3J_{HH}$ *ca.* 4.5 Hz, 1 H, NH). ^{31}P{^{1}H} NMR (161.90 MHz, $CDCl_3$): δ 31.6 (s). ^{13}C{^{1}H} NMR (100.58 MHz, $CDCl_3$): δ 26.46 (NMe), 70.26 (CH of fc), 70.74 (CH of fc), 72.56 (d, J_{PC} = 11 Hz, CH of fc), 73.07 (d, $^1J_{PC}$ = 114 Hz, *C*-PPh_2 of fc), 74.91 (d, J_{PC} = 13 Hz, CH of fc), 79.63 (*C*-CONH of fc), 128.45 (d, J_{PC} = 12 Hz, PPh_2 CH), 131.43 (d, J_{PC} = 10 Hz, PPh_2 CH), 131.94 (d, $^4J_{PC}$ = 2 Hz, PPh_2 CH_{para}), 133.10 (d, $^1J_{PC}$ = 108 Hz, PPh_2 C_{ipso}), 170.35 (C═O). IR (Nujol): ν_{max} 3246 m, 1657 s (amide I), 1556 s (amide II) cm^{-1}. ESI+ MS: *m*/*z* 466 ([M + Na]$^+$). HR MS (ESI) calcd for $C_{24}H_{23}FeNO_2P$ ([M + H]$^+$) 444.0810, found 444.0809. Anal. Calcd for $C_{24}H_{22}FeNO_2 \cdot 1/4CH_2Cl_2$ (464.5): C 62.71, N 3.02, H 4.88%. Found: C 62.70, N 2.81, H 4.73%.

1′-(Diphenylphosphinothioyl)-1-[(methylamino)carbonyl]-ferrocene (4S). Amide **4** (61 mg, 0.14 mmol) and elemental sulfur (5.0 mg, 0.16 mmol) were dissolved in dry toluene (5 mL) and the resulting solution was heated at 80 °C for 90 min. Subsequent evaporation afforded a yellow brown residue, which was taken up with dichloromethane (2 mL) and filtered through a plug of silica gel eluted with dichloromethane–methanol (50 : 1). Subsequent evaporation afforded the product as a yellow glassy solid. Yield of **4S**: 40 mg, 62%.

^{1}H NMR (399.95 MHz, $CDCl_3$): δ 2.92 (d, $^3J_{HH}$ = 4.8 Hz, 3 H, NMe), 3.96 (vt, $J' \approx 2.0$ Hz, 2 H, fc), 4.23 (vq, $J' \approx 2.0$ Hz, 2 H, fc), 4.62 (vq, $J' \approx 2.0$ Hz, 2 H, fc), 4.90 (vt, $J' \approx 2.0$ Hz, 2 H, fc), 7.41 (br q, $^3J_{HH} \approx 5$ Hz, 1 H, NH), 7.43–7.56 (m, 6 H, PPh_2), 7.68–7.76 (m, 4 H, PPh_2). ^{31}P{^{1}H} NMR (161.90 MHz, $CDCl_3$): δ 42.9 (s). ^{13}C{^{1}H} NMR (100.58 MHz, $CDCl_3$): δ 26.13 (NMe), 70.86 (CH of fc), 71.00 (CH of fc), 73.05 (d, J_{PC} = 10 Hz, CH of fc), 74.81 (d, J_{PC} = 12 Hz, CH of fc), 75.98 (d, $^1J_{PC}$ = 97 Hz, *C*-PPh_2 of fc), 79.01 (*C*-CONH of fc), 128.40 (d, J_{PC} = 13 Hz, PPh_2 CH), 131.60 (d, J_{PC} = 10 Hz, PPh_2 CH), 131.62 (d, $^4J_{PC}$ = 4 Hz, PPh_2 CH_{para}), 133.51 (d, $^1J_{PC}$ = 88 Hz, PPh_2 C_{ipso}), 169.88 (C═O). IR (Nujol): ν_{max} 3298 m, 3229 m, 1628 s (amide I),

1558 s (amide II) cm^{-1}. ESI+ MS: *m*/*z* 482 ($[M + Na]^+$). HR MS (ESI) calcd for $C_{24}H_{23}FeNOPS$ ($[M + H]^+$) 460.0582, found 460.0583. Anal. Calcd for $C_{24}H_{22}FeNOPS{\cdot}1/2CH_2Cl_2$ (501.2): C 58.64, N 2.79, H 4.62%. Found C 58.57, N 2.71, H 4.53%.

Synthesis of Cu(I) complexes

$[Cu(7\text{-}\kappa P)_2][BF_4]$ (6a). 1′-(Diphenylphosphino)-1-(aminocarbonyl)ferrocene (**5**; 80 mg, 0.19 mmol) and $[Cu(MeCN)_4][BF_4]$ (29 mg, 0.092 mmol) were dissolved in dry dichloromethane (2 mL), and the resulting orange solution was stirred for 4 h at room temperature in the dark. The separated solid was filtered off, washed with pentane and dried under vacuum. Yield: 84 mg (93%), yellow solid.

^1H NMR (399.95 MHz, dmso-d_6): δ 4.15 (br s, 2 H, fc), 4.19 (vt, 2 H, J' = 1.7 Hz, fc), 4.51 (vt, 2 H, J' = 1.7 Hz, fc), 4.82 (br s, 2 H, fc), 7.40 (s, 1 H, NH_2), 7.42–7.52 (m, 10 H, PPh_2), 7.71 (s, 1 H, NH_2). $^{31}P\{^1H\}$ (161.90 MHz, dmso-d_6): δ −10.1 (br s). IR (Nujol): ν_{max} 3450 (m), 3362 (m), 1650 (s) 1583 (s), 1481 (m), 1437 (m), 1405 (m), 1167 (m), 1095 (s), 1069 (s), 1029 (s), 837 (m), 748 (m), 697 (m), 517 (m), 502 (m) cm^{-1}. ESI+ MS: *m*/*z* 889 ($[Cu(\mathbf{5})_2]^+$), 476 ($[Cu(\mathbf{5})]^+$). Anal. calcd for $C_{46}H_{40}BCuF_4Fe_2N_2O_2P_2{\cdot}1/2CH_2Cl_2$ (1019.3): C 54.79; N 2.75, H 4.05%. Found C 54.51; N 3.00, H 4.27%.

$[Cu(4\text{-}\kappa P)_2][BF_4]$ (6b). Amide **4** (60 mg, 0.14 mmol) and $[Cu(MeCN)_4][BF_4]$ (22 mg, 0.070 mmol) were dissolved in dry dichloromethane (3 mL). The resulting yellow solution was stirred at room temperature for 18 h, filtered through a PTFE syringe filter (0.45 μm pore size), and the filtrate was precipitated by addition of pentane (4 mL). The yellow precipitate was filtered off, washed with pentane and dried under vacuum. Yield: 44 mg (63%), yellow powder.

^1H NMR (399.95 MHz, dmso-d_6): δ 2.73 (d, $^3J_{HH}$ = 4.5 Hz, 3 H, NMe), 4.15 (vt, J' = 1.8 Hz, 2 H, fc), 4.18 (vt, J' = 1.8 Hz, 2 H, fc), 4.52 (vt, J' = 1.8 Hz, 2 H, fc), 4.75 (vt, J' = 1.8 Hz, 2 H, fc), 7.38–7.50 (m, 10 H, PPh_2), 8.24 (br d, $^3J_{HH} \approx$ 4.5 Hz, 1 H, NH). $^{31}P\{^1H\}$ NMR (161.90 MHz, dmso-d_6): δ −11.5 (br s). IR (Nujol): ν 3397 (m), 1618 (s), 1601 (w), 1558 (s), 1435 (m), 1411 (m), 1310 (m), 1165 (w), 1061 (s), 1029 (s), 830 (m), 816 (m), 747 (s), 699 (s), 519 (s), 510 (m), 488 (s), 462 (m) cm^{-1}. ESI+ MS: *m*/*z* 917 ($[Cu(\mathbf{4})_2]^+$), 490 ($[Cu(\mathbf{4})]^+$). Anal. Calcd for $C_{48}H_{44}BCuF_4Fe_2N_2O_2P_2{\cdot}CH_2Cl_2$ (1089.8): C 54.00, N 2.57, H 4.25%. Found C 54.28, N 2.47, H 4.20%.

$[Cu(2\text{-}\kappa P)_2][BF_4]$ (6c). Complex **6c** was prepared similarly starting with amide **2** (50 mg, 0.11 mmol) and $[Cu(MeCN)_4][BF_4]$ (18 mg, 0.057 mmol) in 2 mL of dichloromethane. The reaction mixture was stirred for only 4 h prior to the filtration and precipitation. Yield: 44 mg (75%), fine yellow powder.

^1H NMR (399.95 MHz, dmso-d_6): δ 2.93 (br s, 3 H, NMe), 3.02 (br s, 3 H, NMe), 4.19 (vt, J' = 1.8 Hz, 2 H, fc), 4.21 (vt, J' = 1.8 Hz, 2 H, fc), 4.53 (br s, 2 H, fc), 4.60 (vt, J' = 1.8 Hz, 2 H, fc), 7.42–7.53 (m, 10 H, PPh_2). $^{31}P\{^1H\}$ NMR (161.90 MHz, dmso-d_6): δ −10.5 (br s). IR (Nujol): ν_{max} 1582 (s), 1575 (s), 1505, (m), 1435 (w), 1401 (m), 1377 (m), 1112 (m), 1096 (m), 1050 (s) 1032 (s), 745 (m), 696 (s), 511 (s), 495 (s) cm^{-1}. ESI+ MS: *m*/*z* 945 ($[Cu(\mathbf{2})_2]^+$), 504 ($[Cu(\mathbf{2})]^+$). Anal. calcd for $C_{50}H_{48}BCuF_4Fe_2N_2O_2P_2$ (1032.9): C 58.14, N 2.71; H 4.68%. Found: C 58.63, N 2.52, H 4.94%.

$[Cu(3\text{-}\kappa P)_2][BF_4]$ (6d). Compound **6d** was prepared and isolated analogously to **6c** using thioamide **3** (38 mg, 0.083 mmol) and $[Cu(MeCN)_4][BF_4]$ (13 mg, 0.041 mmol) as the starting materials. Yield of **6d**: 38 mg (87%), orange solid.

^1H NMR (399.95 MHz, dmso-d_6, 25 °C): δ 3.28 (br s, 3 H, NMe), 3.53 (s, 3 H, NMe), 4.15 (br s, 2 H, fc), 4.35 (br s, 2 H, fc), 4.60 (br s, 2 H, fc), 4.64 (br s, 2 H, fc), 7.30–7.52 (m, 10 H, PPh_2). ^1H NMR (399.95 MHz, dmso-d_6, 50 °C): δ 3.19 (s, 3 H, NMe), 3.53 (s, 3 H, NMe), 4.16 (br s, 2 H, fc), 4.35 (vt, J' = 1.9 Hz, 2 H, fc), 4.59 (vt, J' = 1.9 Hz, 2 H, fc), 4.74 (br s, 2 H, fc), 7.35–7.50 (m, 10 H, PPh_2). $^{31}P\{^1H\}$ NMR (161.90 MHz, dmso-d_6, 25 °C): δ −11.0 (br s). IR (Nujol): ν_{max} 1712 (w), 1526 (m), 1436 (w), 1277 (m), 1059 (s) 1135 (m), 825 (m) 745 (m), 697 (m), 511 (m), 491 (w) cm^{-1}. ESI+ MS: *m*/*z* 977 ($[Cu(\mathbf{3})_2]^+$), 520 ($[Cu(\mathbf{3})]^+$). Anal. Calcd for $C_{50}H_{48}BCuF_4Fe_2N_2P_2S_2{\cdot}1/4CH_2Cl_2$ (1086.3): C 55.56, N 2.58, H 4.50%. Found: C 55.53, N 2.57, H 4.77%.

Synthesis of Ag(I) complexes

$[Ag(7\text{-}\kappa P)_2]ClO_4$ (7a). A solution of silver(I) perchlorate (6.0 mg, 0.029 mmol) in dry benzene (2 mL) was added to solid amide **5** (25 mg, 0.061 mmol) and the resultant mixture was diluted with dry dichloromethane (4 mL). The reaction mixture was stirred at room temperature for 4 h, whereupon it deposited a light orange solid, which was filtered off, washed with pentane and dried under vacuum. Yield of **7a**: 28 mg (87%), light orange powder.

^1H NMR (399.95 MHz, $CDCl_3$): δ 4.11 (br vt, J' = 1.9 Hz, 2 H, fc), 4.46 (br s, 2 H, fc), 4.72 (vt, J' = 1.9 Hz, 2 H, fc), 4.84 (br vt, J' = 1.8 Hz, 2 H, fc), 6.24 (br s, 1 H, NH), 6.75 (br s, 1 H, NH), 7.39–7.56 (m, 10 H, PPh_2). $^{31}P\{^1H\}$ NMR (161.90 MHz, $CDCl_3$): δ 3.1 (broad d, $^1J(^{107/109}Ag, ^{31}P) \approx$ 510 Hz). IR (Nujol): ν_{max} 3444 (m), 3340 (m), 1645 (s), 1591 (s), 1555 (m), 1479 (w), 1436 (s), 1396 (m), 1168 (m), 1098 (br s), 1027 (s), 910 (m), 837 (m), 826 (m), 747 (s), 735 (s), 697 (s), 624 (m), 532 (w), 506 (s), 489 (m), 465 (m) cm^{-1}. ESI+ MS: *m*/*z* 933 ($[Ag(\mathbf{5})_2]^+$), 520 ($[Ag(\mathbf{5})]^+$). Anal. Calc. for $C_{46}H_{40}AgClFe_2N_2O_6P_2{\cdot}CH_2Cl_2$ (1118.7): C 50.46, H 3.76, N 2.50%. Found: C 49.95, H 3.58, N 2.62%.

$[Ag(4\text{-}\kappa P)_2]ClO_4$ (7b). Amide **4** (26 mg, 0.061 mmol) and $AgClO_4$ (6.0 mg, 0.029 mmol) were reacted in a mixture of benzene (1 mL) and dichloromethane (3 mL) for 20 h as described above. The yellow solid that formed was filtered off, washed with Et_2O and dried under vacuum to give **7b** as a yellow powder (26 mg, 78%).

^1H NMR (399.95 MHz, dmso-d_6): δ 2.67 (d, $^3J_{HH}$ = 4.6 Hz, 3 H, NMe), 4.12 (vt, J' = 1.9 Hz, 2 H, fc), 4.29 (vt, J' = 1.9 Hz, 2 H, fc), 4.60 (vt, J' = 1.9 Hz, 2 H, fc), 4.85 (vt, J' = 1.9 Hz, 2 H, fc), 7.44–7.60 (m, 10 H, PPh_2), 8.09 (q, $^3J_{HH}$ = 4.6 Hz, 1 H, NH). $^{31}P\{^1H\}$ NMR (161.90 MHz, dmso-d_6): δ 2.6 (pair of d, $^1J(^{107}Ag, ^{31}P)$ = 543 Hz, $^1J(^{109}Ag, ^{31}P)$ = 471 Hz). IR (Nujol): ν_{max} 3389 (m), 3079 (w), 1629 (s), 1615 (s), 1544 (s), 1480 (w), 1435 (m), 1412 (m), 1301 (m), 1194 (m), 1174 (m), 1095 (s), 1067 (br s), 1050 (w), 1031 (m), 914 (m), 816 (m), 748 (s), 697 (s), 623 (m), 529 (m), 509 (s), 492 (m), 467 (m) cm^{-1}. ESI+ MS: *m*/*z* 961

([Ag(**4**)$_2$]$^+$), 534 ([Ag(**4**)]$^+$). Anal. Calc. for $C_{48}H_{44}AgClFe_2N_2O_6P_2{\cdot}CH_2Cl_2$ (1146.7): C 51.32, H 4.04, N 2.44%. Found: C 50.90, H 3.75, N 2.13%.

[Ag(2-κ*P*)$_2$]ClO$_4$ (7c). Silver(I) perchlorate (25 mg, 0.12 mmol) and amide **2** (107 mg, 0.24 mmol) were reacted in benzene (2 mL) and dichloromethane (4 mL) for 4 h as described above. The solid product was filtered off, washed with diethyl ether and dried under vacuum. Yield of **7c**: 84 mg (62%), yellow-brown solid.

^{1}H NMR (399.95 MHz, dmso-d$_6$): δ 2.91 (br s, 3 H, NMe), 2.99 (br s, 3 H, NMe), 4.22 (br s, 2 H, fc), 4.32 (br s, 2 H, fc), 4.61 (vt, J' = 1.9 Hz, 2 H, fc), 4.65 (vt, J' = 1.9 Hz, 2 H, fc), 7.49–7.56 (m, 10 H, PPh$_2$). ^{31}P{^{1}H} NMR (161.90 MHz, dmso-d$_6$): δ 4.2 (pair of concentric d, ^1J(^{107}Ag, ^{31}P) = 770 Hz, ^1J (^{109}Ag, ^{31}P) = 685 Hz). IR (Nujol): ν_{max} 1557 (s), 1492 (s), 1436 (m), 1127 (m), 1109 (s), 1097 (m), 1071 (w), 1050 (s), 824 (w), 758 (m), 747 (m), 695 (m), 679 (s), 623 (s), 514 (w), 503 (w), 490 (m), 467 (w) cm^{-1}. ESI+ MS: *m*/*z* 989 ([Ag(**2**)$_2$]$^+$), 548 ([Ag(**2**)]$^+$). Anal. Calc. for $C_{50}H_{48}AgClFe_2N_2O_6P_2{\cdot}1/2CH_2Cl_2$ (1132.3): C 53.56, H 4.36, N 2.47%. Found: C 53.30, H 4.15, N 2.35%.

[Ag$_2$(ClO$_4$)$_2$(μ-3)$_2$] (7d). Thioamide **3** (50 mg, 0.11 mmol) and $AgClO_4$ (10 mg, 0.048 mmol) were reacted in benzene (2 mL) and dichloromethane (6 mL) as described above. The solid product was filtered off, washed with pentane and dried under vacuum. Yield of **7d**: 52 mg (81%), red solid. Crystals suitable for X-ray diffraction analysis were grown by the reactive diffusion approach as follows. A solution of ligand **3** (46 mg, 0.1 mmol) in dichloromethane (2 mL) was layered with pure solvent (1 mL of dichloromethane) and then with a solution of $AgClO_4$ (10.5 mg, 0.051 mmol) in benzene (3 mL). The mixture was allowed to stand undisturbed for several days during which time red crystals deposited in the phase boundary region. These crystals were directly used for the X-ray measurements. IR analysis of the isolated material confirmed it to be identical to the authentic (bulk) sample of **7d**.

^{1}H NMR (399.95 MHz, dmso-d$_6$): δ 3.39 (s, 3 H, NMe), 3.56 (s, 3 H, NMe), 4.12 (dt, J = 3.0, 1.8 Hz, 2 H, fc), 4.30 (vt, J' = 1.9 Hz, 2 H, fc), 4.73 (vt, J' = 1.8 Hz, 2 H, fc), 5.06 (vt, J' = 1.9 Hz, 2 H, fc), 7.50–7.57 (m, 10 H, PPh$_2$). ^{31}P{^{1}H} NMR (161.90 MHz, dmso-d$_6$): δ −0.3 (broad d, ^1J($^{107/109}$Ag, ^{31}P) ≈ 510 Hz). IR (Nujol): ν_{max} 1551 (s), 1436 (m), 1280 (m), 1144 (m), 1108 (s), 1096 (s), 1061 (m), 1030 (m), 979 (m), 851 (m), 818 (w), 749 (m), 695 (m), 623 (m), 507 (m), 465 (m) cm^{-1}. ESI+ MS: *m*/*z* 564 ([Ag(**3**)]$^+$), 597 ([Ag(**3**)(CH$_3$OH)]$^+$). Anal. Calc. for $C_{50}H_{48}Ag_2Cl_2Fe_2N_2O_8P_2S_2$ (1329.3): C 45.17, H 3.64, N 2.11%. Found: C 44.83, H 3.81, N 1.90%.

Synthesis of chloridogold(I) complexes

[AuCl(5-κ*P*)] (8a). Amide **5** (71 mg, 0.17 mmol) and chlorido(tetrahydrothiophene)gold(I) (55 mg, 0.17 mmol) were dissolved in dry dichloromethane (2 mL). The resulting solution was stirred at room temperature for 4 h, whereupon it deposited a yellow solid. This solid was filtered off, washed with pentane and dried under vacuum to afford **8a** as a yellow solid. Yield: 102 mg (92%).

^{1}H NMR (399.95 MHz, dmso-d$_6$): δ 4.28 (vt, J' = 1.9 Hz, 2 H, fc), 4.48 (dt, J = 3.0, 1.9 Hz, 2 H, fc), 4.59–4.61 (m, 2 H, fc), 4.78 (vt, J' = 1.9 Hz, 2 H, fc), 7.02 (br s, 1 H, NH), 7.37 (br s, 1 H, NH), 7.54–7.64 (m, 10 H, PPh$_2$). ^{31}P{^{1}H} NMR (161.90 MHz, dmso-d$_6$): δ 28.7 (s). IR (Nujol): ν_{max} 3421 (m), 1667 (s), 1612 (m), 1432 (m), 1349 (m), 1176 (m), 1099 (m), 1027 (m), 843 (m), 822 (m), 745 (m), 688 (s), 526 (m), 511 (m), 496 (w), 477 (s) cm^{-1}. ESI+ MS: *m*/*z* 610 ([**8a** − Cl]$^+$), 668 ([**8a** + Na]$^+$), 684 ([**8a** + K]$^+$). Anal. Calcd for $C_{23}H_{20}AuClFeNOP$ (645.6): C 41.75, N 2.12, H 3.05%. Found: C 41.56, N 1.93, H 2.96%.

[AuCl(4-κ*P*)] (8b). Amide **4** (90 mg, 0.22 mmol) and [AuCl(tht)] (68 mg, 0.21 mmol) were reacted in 2 mL of dichloromethane as described above to furnish **8b** as a yellow powder. Yield: 126 mg (91%).

^{1}H NMR (399.95 MHz, $CDCl_3$): δ 2.93 (d, $^3J_{HH}$ = 4.8 Hz, 3 H, NMe), 4.19 (vt, J' = 1.8 Hz, 2 H, fc), 4.23 (dt, J = 2.9, 1.9 Hz, 2 H, fc), 4.68–4.70 (m, 2 H, fc), 4.87 (vt, J' = 1.9 Hz, 2 H, fc), 6.07 (q, $^3J_{HH}$ = 4.8 Hz, 1 H, NH), 7.44–7.61 (m, 10H, PPh$_2$). ^{31}P{^{1}H} NMR (161.90 MHz, $CDCl_3$): δ 28.8 (s). IR (Nujol): ν_{max} 3369 (m), 1628 (s), 1544 (m), 1440 (m), 1298 (m), 1173 (m), 1103 (w), 1029 (m), 1000 (w), 842 (m), 743 (m), 691 (m), 628 (w), 555 (w), 529 (w), 515 (w), 494 (w), 480 (w) cm^{-1}. ESI+ MS: *m*/*z* 624 ([**8b** − Cl]$^+$), 680 ([**8b** + Na]$^+$), 698 ([**8b** + K]$^+$). Anal. Calcd for $C_{24}H_{22}AuClFeNOP{\cdot}1/2CHCl_3$ (719.3): C 40.90, N 1.95, H 3.15%. Found C 41.04, N 1.79, H 3.09% (analytical sample crystallised from chloroform/pentane).

[AuCl(2-κ*P*)] (8c). Amide **2** (55 mg, 0.12 mmol) and [AuCl(tht)] (40 mg, 0.12 mmol) were dissolved in dichloromethane (2 mL). After stirring for 4 h, the solution was precipitated with diethyl ether and the product was filtered off and dried under vacuum. Yield of **8c**: 61 mg (73%), yellow powder.

^{1}H NMR (399.95 MHz, dmso-d$_6$): δ 2.85 (s, 3 H, NMe), 3.00 (s, 3 H, NMe), 4.30 (vt, J' = 1.9 Hz, 2 H, fc), 4.43 (dt, J = 3.0, 1.8 Hz, 2 H, fc), 4.61 (vt, J' = 1.8 Hz, 2 H, fc), 4.73–4.76 (m, 2 H, fc), 7.54–7.65 (m, 10 H, PPh$_2$). ^{31}P{^{1}H} NMR (161.90 MHz, dmso-d$_6$): δ 28.9 (s). IR (Nujol): ν_{max} 3103 (m), 1622 (s), 1585 (m), 1499 (m), 1439 (s), 1393 (m), 1308 (m), 1265 (m), 1225 (m), 1180 (m), 1173 (m), 1107 (s), 1039 (m), 1032 (m), 840 (m), 821 (m), 758 (s), 752 (s), 704 (s), 558 (m), 535 (m), 526 (s), 504 (s), 490 (s), 474 (m) cm^{-1}. ESI+ MS: *m*/*z* 638 ([**8c** − Cl]$^+$), 696 ([**8c** + Na]$^+$), 712 ([**8c** + K]$^+$). Anal. Calcd for $C_{25}H_{24}$-AuClFeNOP (673.7): C 44.57, N 2.08, H 3.59%. Found: C 44.22, N 2.01, H 3.50%.

[AuCl(3-κ*P*)] (8d). Ligand **3** (38 mg, 0.083 mmol) and [AuCl(tht)] (26 mg, 0.081 mmol) were reacted in CH_2Cl_2 (2 mL) overnight. The separated solid was filtered off, washed with diethyl ether and dried under vacuum to afford **8d** as a dark orange solid. Yield: 36 mg (64%).

^{1}H NMR (399.95 MHz, dmso-d$_6$): δ 3.27 (s, 3 H, NMe), 3.29 (s, 3 H, NMe), 4.34 (vt, J' = 1.9 Hz, 2 H, fc), 4.35 (dt, J = 3.0, 1.8 Hz, 2 H, fc), 4.73 (vt, J' = 1.9 Hz, 2 H, fc), 4.76–4.79 (m, 2 H, fc), 7.54–7.65 (m, 10 H, PPh$_2$). ^{31}P{^{1}H} NMR (161.90 MHz, dmso-d$_6$): δ 28.7 (s). IR (Nujol): ν_{max} 1712 (w), 1512 (s), 1435 (m), 1309 (m), 1274 (m) 1174 (m), 1138 (m), 1101 (s),

1062 (w), 1034 (w), 1025 (w), 989 (w), 973 (w), 838 (m), 824 (m), 814 (w), 764 (w), 749 (m), 695 (s), 556 (m), 530 (m), 509 (s), 498 (w), 477 (m) cm^{-1}. ESI+ MS: *m*/*z* 654 ([**8d** − Cl]$^+$. Anal. calcd for $C_{25}H_{24}AuClFeNPS$ (689.8): C 43.53, N 2.03, H 3.51%. Found: C 43.88, N 1.87, H 3.45%.

X-ray crystallography

Crystallisation conditions are described in the ESI.† Full set diffraction data ($\pm h \pm k \pm l$, θ_{max} = 26.0–27.5°, completeness ≥99.3%) were collected with a Nonius Kappa CCD diffractometer equipped with an Apex II image plate detector and Cryostream Cooler (Oxford Cryosystems) using graphite monochromated Mo Kα radiation (λ = 0.71073 Å). The data were analysed and corrected for absorption by methods included in the diffractometer software. Details on the data collection, structure solution and refinement are available in the ESI (Table S1†), which also contains conventional displacement ellipsoid plots.

All structures were solved by direct methods (SHELXS97[42]) and refined by full-matrix least-squares based on F^2 (SHELXL97[42]). The non-hydrogen atoms were refined with anisotropic displacement parameters. The amide hydrogen atoms (NH; if present) were located on the difference electron density maps and refined as riding atoms with U_{iso}(H) set to a 1.2U_{eq}(N). Hydrogens residing on the carbon atoms were included in their calculated positions and refined similarly with U_{iso}(H) = 1.5U_{eq}(C) for the methyl groups and 1.2U_{eq}(C) for all other CH_n moieties. Particular details of the structure refinement are as follows.

Compound **4S** crystallises in the chiral *Pc* space group with two molecules per asymmetric unit. However, all atoms except for the *amide* moiety in these two independent molecules match each other because of an inversion centre from the space group $P2_1/c$ (the maximum distance of the overlapping atoms in the phosphinoferrocenyl units is 0.53 Å). Such a virtually higher symmetry results in large correlations during the refinement and, therefore, restrictions to anisotropic displacement parameters had to be applied to several atoms.

Parts of some structures (**7b**·$CHCl_3$: the solvent and the perchlorate anion; **6b**·1/4$CHCl_3$ and **6a′**·$CHCl_3$: one of the phosphorus-bound phenyl rings and the BF_4^- anion) are disordered and were refined over two positions (with isotropic displacement parameters, if necessary). Moreover, the solvating molecules in the structures of **6b**·1/4$CHCl_3$ and **6a′**·$CHCl_3$ are severely disordered in structural voids and were modelled by PLATON/SQUEEZE.[43]

All geometric calculations were performed and the diagrams were obtained with the PLATON program.[44] All numerical values were rounded with respect to their estimated deviations (ESDs) given to one decimal place. Parameters relating to atoms in constrained positions (hydrogens) are given without ESDs.

DFT computations

Calculations were performed using the density-functional theory (DFT) with Becke's three-parameter functional[45] employing the non-local Lee–Yang–Parr correlation functional (B3LYP)[46] and the 6-31G* basis set for $FcC(E)NH_2$ and 6-311G** for **2** and **3** with an analytically constructed energy gradient as implemented in the Gaussian 09 program package.[47] Geometry optimisations were started from the experimentally determined solid-state structures of **2**, **3** and $FcCONH_2$.[27b] The stationary points of the potential energy surface (PES) were located and harmonic vibrational analysis was performed using the analytically calculated force-constant matrix. For the case of $FcC(E)NH_2$ (E = O, S), relaxed PES scan using ψ as a single variable was performed, starting from the respective stationary points.

Electrochemistry

Electrochemical measurements were carried out with a μAUTOLAB III instrument (Eco Chemie) at room temperature (23 °C) using a standard three-electrode cell (Metrohm) equipped with a glassy carbon disc working electrode (2 mm diameter), platinum sheet auxiliary electrode, and a double-junction Ag/AgCl (3 M KCl) reference electrode. The samples were dissolved in anhydrous 1,2-dichloroethane (Sigma-Aldrich; absolute) to give a solution containing 1×10^{-3} M of the analysed compound and 0.1 M $Bu_4N[PF_6]$ (Fluka, p. a. for electrochemistry). The solutions were deaerated by bubbling with argon and then kept under an argon blanket during the measurement. The redox potentials are given relative to the ferrocene/ferrocenium reference.

Acknowledgements

This research was supported through the grants from the Czech Science Foundation (project no. 13-08890S) and the Grant Agency of Charles University in Prague (project no. 643012).

Notes and references

1 P. Štěpnička, *Chem. Soc. Rev.*, 2012, **41**, 4273.
2 For recent examples, see: (*a*) N. Nasser, P. D. Boyle and R. J. Puddephatt, *Organometallics*, 2013, **32**, 5504; (*b*) N. Nasser and R. J. Puddephatt, *Inorg. Chim. Acta*, 2014, **409**, 238; (*c*) E. C. Constable, N. Hostettler, C. E. Housecroft, N. S. Murray, J. Schönle, U. Soydaner, R. M. Walliser and J. A. Zampese, *Dalton Trans.*, 2013, **42**, 4970; (*d*) N. Ye and W.-M. Dai, *Eur. J. Org. Chem.*, 2013, 831; (*e*) I. Philipova, G. Stavrakov and V. Dimitrov, *Tetrahedron: Asymmetry*, 2012, **23**, 927.
3 For recent examples, see: (*a*) J. Schulz, I. Císařová and P. Štěpnička, *Organometallics*, 2012, **31**, 729; (*b*) J. Tauchman, B. Therrien, G. Süss-Fink and P. Štěpnička, *Organometallics*, 2012, **31**, 3985; (*c*) J. Schulz, I. Císařová and P. Štěpnička, *Eur. J. Inorg. Chem.*, 2012, 5000; (*d*) J. Tauchman, I. Císařová and P. Štěpnička, *Dalton Trans.*, 2011, **40**, 11748; (*e*) P. Štěpnička, B. Schneiderová,

J. Schulz and I. Císařová, *Organometallics*, 2013, **32**, 5754; (*f*) J. Schulz, J. Tauchman, I. Císařová, T. Riedel, P. J. Dyson and P. Štěpnička, *J. Organomet. Chem.*, 2014, **751**, 604; (*g*) P. Štěpnička, M. Verníček, J. Schulz and I. Císařová, *J. Organomet. Chem.*, 2014, **755**, 41; (*h*) M. Semler, J. Čejka and P. Štěpnička, *Catal. Today*, 2014, **227**, 207; (*i*) H. Solařová, I. Císařová and P. Štěpnička, *Organometallics*, 2014, **33**, 4131; (*j*) J. Tauchman, I. Císařová and P. Štěpnička, *Dalton Trans.*, 2014, **43**, 1599.

4 (*a*) A. El-Faham and F. Albericio, *Chem. Rev.*, 2011, **111**, 6557; (*b*) E. Valeur and M. Bradley, *Chem. Soc. Rev.*, 2009, **38**, 606.

5 J. Podlaha, P. Štěpnička, J. Ludvík and I. Císařová, *Organometallics*, 1996, **15**, 543.

6 This method represents a versatile route to phosphinoferrocenes functionalised in position 1′ of the ferrocene unit. For examples, see: (*a*) I. R. Butler and R. L. Davies, *Synthesis*, 1996, 1350; (*b*) P. Štěpnička, in *Ferrocenes: Ligands, Materials and Biomolecules*, Wiley, Chichester, 2008, ch. 5, pp. 177–204.

7 P. Štěpnička, H. Solařová, M. Lamač and I. Císařová, *J. Organomet. Chem.*, 2010, **695**, 2423.

8 For representative examples of (thio)amide synthesis from organolithium reagents and (thio)carbamoyl halides, see: (*a*) E. G. Doadt and V. Snieckus, *Tetrahedron Lett.*, 1985, **26**, 1149; (*b*) M. P. Sibi, S. Chattopadhyay, J. W. Dankwardt and V. Snieckus, *J. Am. Chem. Soc.*, 1985, **107**, 6312; (*c*) E. J. Bures and B. A. Keay, *Tetrahedron Lett.*, 1988, **29**, 1247; (*d*) R. J. Mills, N. J. Taylor and V. Snieckus, *J. Org. Chem.*, 1989, **54**, 4372; (*e*) D. L. Comins and H. Hong, *J. Am. Chem. Soc.*, 1991, **113**, 6672; (*f*) P. Gros, Y. Fort, G. Queguiner and P. Caubere, *Tetrahedron Lett.*, 1995, **36**, 4791; (*g*) J. Clayden, N. Westlund and F. X. Wilson, *Tetrahedron Lett.*, 1999, **40**, 7883; (*h*) F. Wudl, S. D. Cox and D. E. Wellman, *Mol. Cryst. Liq. Cryst.*, 1985, **125**, 181.

9 For examples of the reactions of lithioferrocenes with thiocarbamoyl chlorides, see: (*a*) K. Hamamura, M. Kita, M. Nonoyama and J. Fujita, *J. Organomet. Chem.*, 1993, **463**, 169; (*b*) S. Jautze, P. Seiler and R. Peters, *Angew. Chem., Int. Ed.*, 2007, **46**, 1260; (*c*) S. Jautze, P. Seiler and R. Peters, *Chem. – Eur. J.*, 2008, **14**, 1430; (*d*) T. Hellmuth, S. Rieckhoff, M. Weiss, K. Dorst, W. Frey and R. Peters, *ACS Catal.*, 2014, **4**, 1850 N.B. The amidation of ferrocene with carbamoyl chlorides has been typically achieved through Friedel–Crafts reactions: (*e*) W. F. Little and R. Eisenthal, *J. Am. Chem. Soc.*, 1960, **82**, 1577; (*f*) J. Hu, L. J. Barbour and G. W. Gokel, *New J. Chem.*, 2004, **28**, 907.

10 Thioamides are typically synthesised through thionation of amides with Lawesson's reagent or P_2S_5 which, however, convert phosphines to phosphine sulfides: (*a*) M. Jesberger, T. P. Davis and L. Barner, *Synthesis*, 2003, 1929; (*b*) T. Ozturk, E. Ertas and O. Mert, *Chem. Rev.*, 2010, **110**, 3419; (*c*) A. B. Charette and M. Grenon, *J. Org. Chem.*, 2003, **68**, 5792 and references cited therein.

11 This contrasts with the attention dedicated to simple and multi-donor (non-phosphine) thioamide donors. For selected examples, see: E. S. Raper, *Coord. Chem. Rev.*, 1994, **129**, 91; W. Zhang and M. Shi, *Synlett*, 2007, 19; K. Belhamel, T. K. D. Nguyen, M. Benamor and R. Ludwig, *Eur. J. Inorg. Chem.*, 2003, 4110; M. A. Hossain, S. Lucarini, D. Powell and K. Bowman-James, *Inorg. Chem.*, 2004, **43**, 7275; R. A. Begum, D. Powell and K. Bowman-James, *Inorg. Chem.*, 2006, **45**, 964; N. K. Singh, M. Singh, P. Tripathi, A. K. Srivastava and R. J. Butcher, *Polyhedron*, 2007, **27**, 375; K. Ahlford, M. Livendahl and H. Adolfsson, *Tetrahedron Lett.*, 2009, **50**, 6321; J. Kulesza, M. Guzinski, V. Hubscher-Bruder, F. Arnaud-Neu and M. Bocheńska, *Polyhedron*, 2011, **30**, 98; T. Teratani, T. Koizumi, T. Yamamoto, K. Tanaka and T. Kanbara, *Dalton Trans.*, 2011, **40**, 8879 and references therein; T. Suzuki, Y. Kajita and H. Masuda, *Dalton Trans.*, 2014, **43**, 9732.

12 P.-H. Leung, Y. Qin, G. He, K. F. Mok and J. J. Vittal, *J. Chem. Soc., Dalton Trans.*, 2001, 309.

13 For representative examples, see: (*a*) K. Issleib and G. Harzfeld, *Chem. Ber.*, 1964, **97**, 3430; (*b*) K. Issleib and G. Harzfeld, *Z. Anorg. Allg. Chem.*, 1967, **351**, 18; (*c*) E. W. Abel and I. H. Sabherwal, *J. Chem. Soc. A*, 1968, 1105; (*d*) A. W. Gal, J. W. Gosselink and F. A. Vollenbroek, *J. Organomet. Chem.*, 1977, **142**, 357; (*e*) H. P. M. M. Ambrosius, F. A. Cotton, L. R. Falvello, H. T. J. M. Hintzen, T. J. Melton, W. Schwotzer, M. Tomas and J. G. M. Van der Linden, *Inorg. Chem.*, 1984, **23**, 1611; (*f*) U. Kunze, H. Jawad, R. Burghardt, R. Tittmann and V. Kruppa, *J. Organomet. Chem.*, 1986, **302**, C30 and previous articles in this series; (*g*) A. Gutierrez-Alonso, L. Ballester-Reventos, V. Perez-Garcia and C. Ruiz-Valero, *Polyhedron*, 1990, **9**, 2163; (*h*) D. Clajus, R. Kramolowsky, G. Siasios and E. R. T. Tiekink, *Inorg. Chim. Acta*, 1998, **281**, 64; (*i*) O. Crespo, E. J. Fernandez, P. G. Jones, A. Laguna, J. M. Lopez de Luzuriaga, M. Monge, M. E. Olmos and J. Perez, *Dalton Trans.*, 2003, 1076; (*j*) A. C. Behrle and J. A. R. Schmidt, *Organometallics*, 2013, **32**, 1141.

14 (*a*) A. Bader and E. Lindner, *Coord. Chem. Rev.*, 1991, **108**, 27; (*b*) C. S. Slone, D. A. Weinberger and C. A. Mirkin, *Prog. Inorg. Chem.*, 1999, **48**, 233; (*c*) P. Braunstein and F. Naud, *Angew. Chem., Int. Ed.*, 2001, **40**, 680.

15 P. Štěpnička, J. Schulz, I. Císařová and K. Fejfarová, *Collect. Czech. Chem. Commun.*, 2007, **72**, 453.

16 The C═S stretching band is probably obscured by Nujol. See, for instance, the data for $PhC(S)NC_5H_{10}$: K. A. Jensen and P. H. Nielsen, *Acta Chem. Scand.*, 1966, **20**, 597.

17 D. Plażuk, J. Zakrzewski, A. Rybarczyk-Pirek and S. Domagała, *J. Organomet. Chem.*, 2005, **690**, 4302.

18 P. Štěpnička and I. Císařová, *J. Organomet. Chem.*, 2006, **691**, 2863.

19 (*a*) J. Kühnert, M. Dušek, J. Demel, H. Lang and P. Štěpnička, *Dalton Trans.*, 2007, 2802; (*b*) J. Kühnert, I. Císařová, M. Lamač and P. Štěpnička, *Dalton Trans.*, 2008, 2454; (*c*) J. Schulz, I. Císařová and P. Štěpnička, *J. Organomet. Chem.*, 2009, **694**, 2519; (*d*) J. Tauchman, I. Císařová and P. Štepnička, *Organometallics*, 2009, **28**, 3288 and also ref. 3*a*, *c* and *e*.

20 A C7–H7···S═C interaction between molecules related by elemental translation along the crystallographic *a*-axis can be found in the structure of **3O**: C7···S = 3.689(2) Å, angle at H7 = 151°.
21 The difference in electronegativity is considerably higher in the P/O pair than in the C/O pair.
22 Change in the mutual orientation of the cyclopentadienyl ring (*i.e.*, conformation of the 1,1′-disubstited ferrocene scaffold) results in changes in the C(ring1)–Fe–C(ring2) angles, which is also the present case. This concerns mainly amide **2**; the maximum difference in interatomic angles for **3** is only 5°.
23 (*a*) D. R. Scott and R. S. Becker, *J. Chem. Phys.*, 1961, **35**, 516 (erratum: D. R. Scott and R. S. Becker, *J. Chem. Phys.*, 1961, **35**, 2246
(*b*) U. Salzner, *J. Chem. Theor. Comput.*, 2013, **9**, 4064.
24 The position of the absorption band is of course reflected in the colours of the compounds. Whereas amide **2** is orange (orange brown as a bulk solid), thioamide **3** is intensely red-orange (red in the solid state).
25 C. Hansch, A. Leo and R. W. Taft, *Chem. Rev.*, 1991, **91**, 165.
26 J. A. S. Howell, P. C. Yates, N. Fey, P. McArdle, D. Cunningham, S. Parsons and D. W. H. Rankin, *Organometallics*, 2002, **21**, 5272 (Note: the value was calculated from the data deposited in CSD).
27 In the case of primary amides, $FcC(E)NH_2$, the comparison is not possible because the individual molecules are involved in hydrogen-bonding interactions that influence molecular conformations. For instance, the ψ angles determined from the crystal structure data of $FcCONH_2$ are −13.9°, −9.7(2)° and −8.4(2) ° for different polymorphs: (*a*) D. Salazar-Mendoza, S. A. Baudron, M. W. Hosseini, N. Kyritsakas and A. De Cian, *Dalton Trans.*, 2007, 565 (Note: the first value was calculated from the data deposited with CCDC); (*b*) P. Štěpnička, I. Císařová, D. Nižňanský and S. Bakardjieva, *Polyhedron*, 2010, **29**, 134. The corresponding thioamide $FcCSNH_2$ shows a lower tilting in the solid state ($\psi \approx -3.7°$; ref. 17, Note: the value was calculated from the data deposited with CCDC).
28 K. Nakamoto, in *Infrared and Raman Spectra of Inorganic and Coordination Compounds*, Wiley, New York, 5th edn, 1997, Part A: Theory and Applications in Inorganic Chemistry, ch. II-6, pp. 189–201, and Part B: Applications in Coordination, Organometallic and Bioinorganic Chemistry, ch. III-12, pp. 82–83.
29 The M–P bonds between the soft phosphine donor group and the soft metal centre can be expected to be stronger than the M–O bonds involving the amide moiety.
30 R. G. Parr and R. G. Pearson, *J. Am. Chem. Soc.*, 1983, **105**, 7512.
31 J. Tauchman, I. Císařová and P. Štěpnička, *Eur. J. Org. Chem.*, 2010, 4276.
32 A. Bondi, *J. Phys. Chem.*, 1964, **68**, 441.
33 Cambridge Structural Database version 5.35 of November 2013 with updates from November 2013, February 2014 and May 2014.
34 C. Pariya, F. R. Fronzek and A. W. Maverick, *Inorg. Chem.*, 2011, **50**, 2748.
35 C. Paryia, C. R. Sparrow, C.-K. Back, G. Sandí, F. R. Fronczek and A. W. Maverick, *Angew. Chem., Int. Ed.*, 2007, **46**, 6305.
36 The molecules differ by the overall conformation, mainly the phenyl rings (see an overlap in the ESI†).
37 K. Rössler, T. Rüffer, B. Walfort, R. Packheiser, R. Holze, M. Zharnikov and H. Lang, *J. Organomet. Chem.*, 2007, **692**, 1530.
38 (*a*) J. E. Aguado, S. Canales, M. C. Gimeno, P. G. Jones, A. Laguna and M. D. Villacampa, *Dalton Trans.*, 2005, 3005; (*b*) J. Kühnert, P. Ecorchard and H. Lang, *Eur. J. Inorg. Chem.*, 2008, 5125; (*c*) A. Hildebrandt, N. Wetzold, P. Ecorchard, B. Walfort, T. Rüffer and H. Lang, *Eur. J. Inorg. Chem.*, 2010, 3615; (*d*) U. Siemeling, T. Klemann, C. Bruhn, J. Schulz and P. Štěpnička, *Z. Anorg. Allg. Chem.*, 2011, **637**, 1824; (*e*) P. Štěpnička, M. Zábranský and I. Císařová, *ChemistryOpen*, 2012, **1**, 71.
39 H. Schmidbaur and A. Schier, *Chem. Soc. Rev.*, 2012, **41**, 370 and references cited therein.
40 I. R. Butler and R. L. Davies, *Synthesis*, 1996, 1350.
41 R. Uson, A. Laguna and M. Laguna, *Inorg. Synth.*, 1989, **26**, 85.
42 G. M. Sheldrick, *Acta Crystallogr., Sect. A: Found. Crystallogr.*, 2008, **64**, 112.
43 P. van der Sluis and A. L. Spek, *Acta Crystallogr., Sect. A: Found. Crystallogr.*, 1990, **46**, 194.
44 A. L. Spek, *J. Appl. Crystallogr.*, 2003, **36**, 7.
45 A. D. Becke, *J. Chem. Phys.*, 1993, **98**, 5648.
46 C. Lee, W. Yang and R. G. Parr, *Phys. Rev. B: Condens. Matter*, 1988, **37**, 785.
47 M. J. Frisch, G. W. Trucks, H. B. Schlegel, G. E. Scuseria, M. A. Robb, J. R. Cheeseman, G. Scalmani, V. Barone, B. Mennucci, G. A. Petersson, H. Nakatsuji, M. Caricato, X. Li, H. P. Hratchian, A. F. Izmaylov, J. Bloino, G. Zheng, J. L. Sonnenberg, M. Hada, M. Ehara, K. Toyota, R. Fukuda, J. Hasegawa, M. Ishida, T. Nakajima, Y. Honda, O. Kitao, H. Nakai, T. Vreven, J. A. Montgomery Jr., J. E. Peralta, F. Ogliaro, M. Bearpark, J. J. Heyd, E. Brothers, K. N. Kudin, V. N. Staroverov, T. Keith, R. Kobayashi, J. Normand, K. Raghavachari, A. Rendell, J. C. Burant, S. S. Iyengar, J. Tomasi, M. Cossi, N. Rega, J. M. Millam, M. Klene, J. E. Knox, J. B. Cross, V. Bakken, C. Adamo, J. Jaramillo, R. Gomperts, R. E. Stratmann, O. Yazyev, A. J. Austin, R. Cammi, C. Pomelli, J. W. Ochterski, R. L. Martin, K. Morokuma, V. G. Zakrzewski, G. A. Voth, P. Salvador, J. J. Dannenberg, S. Dapprich, A. D. Daniels, O. Farkas, J. B. Foresman, J. V. Ortiz, J. Cioslowski and D. J. Fox, *Gaussian 09, Revision C.01*, Gaussian, Inc, Wallingford CT, 2010.

4. Sledování významných biomarkerů pomocí hmotnostní spektrometrie

Za biomarker může být považována látka, která poskytuje objektivně a dostatečně přesně měřitelnou charakteristiku indikující biologické nebo patologické procesy. Sledování biomarkerů hrají důležitou úlohu při vývoji léčiv, včasné diagnostice závažných onemocnění, monitorování průběhu léčby a chirurgických zákroků a v mnoha oblastech biolékařského výzkumu. Pochopení vztahu mezi měřitelnými biologickými procesy a klinickými výsledky má zásadní význam pro rozšiřování možností léčby nemocí i pro pochopení normální, zdravé fyziologie. S využitím biomarkerů je možné dosáhnout progresivního pozitivního posunu v oblasti lékařského výzkumu, a proto je této problematice věnována v posledních letech obrovská pozornost [1].

Metody hmotnostní spektrometrie nabízejí jedinečnou podporu při řešení řady biologických otázek a jsou základním nástrojem oborů molekulární biologie. Ve srovnání s ostatními instrumentálními analytickými metodami je informační obsažnost výsledků poskytovaných hmotnostní spektrometrií nesrovnatelně vyšší než u většiny instrumentálních analytických metod. Proto hmotnostní spektrometrie nachází stále širší uplatnění v mnoha oblastech výzkumu, jako je vývoj léčiv, biomedicínský výzkum, a toxikologie. Bouřlivý technologický vývoj v oblasti instrumentace pro hmotnostní spektrometrii značně zvýšil možnosti zapojení této metody v oblasti výzkumu biomarkerů [2].

4.1. Studie redukce bilirubin ditaurátu střevní bakterií *Clostridium perfringens* (publikace IV)

3.1.1. Teoretický úvod

Hem jako součást červeného krevního barviva, hemoglobinu (Hb), je tvořen čtyřmi pyrrolovými jádry s centrálně vázaným atomem železa. Při katabolismu hemu se nejprve odštěpuje železo a následně dochází k regioselektivní oxidaci porfyrinového cyklu na biliverdin, který je následně redukován na bilirubin [3,4]. V zažívacím traktu dochází k redukci bilirubinu za vzniku skupiny hydroderivátů označovaných souborným označením urobilinoidy, ze kterých následnou oxidací vznikají nažloutlé urobiliny [5]. Reakční schéma je uvedeno na obrázku 4.1.

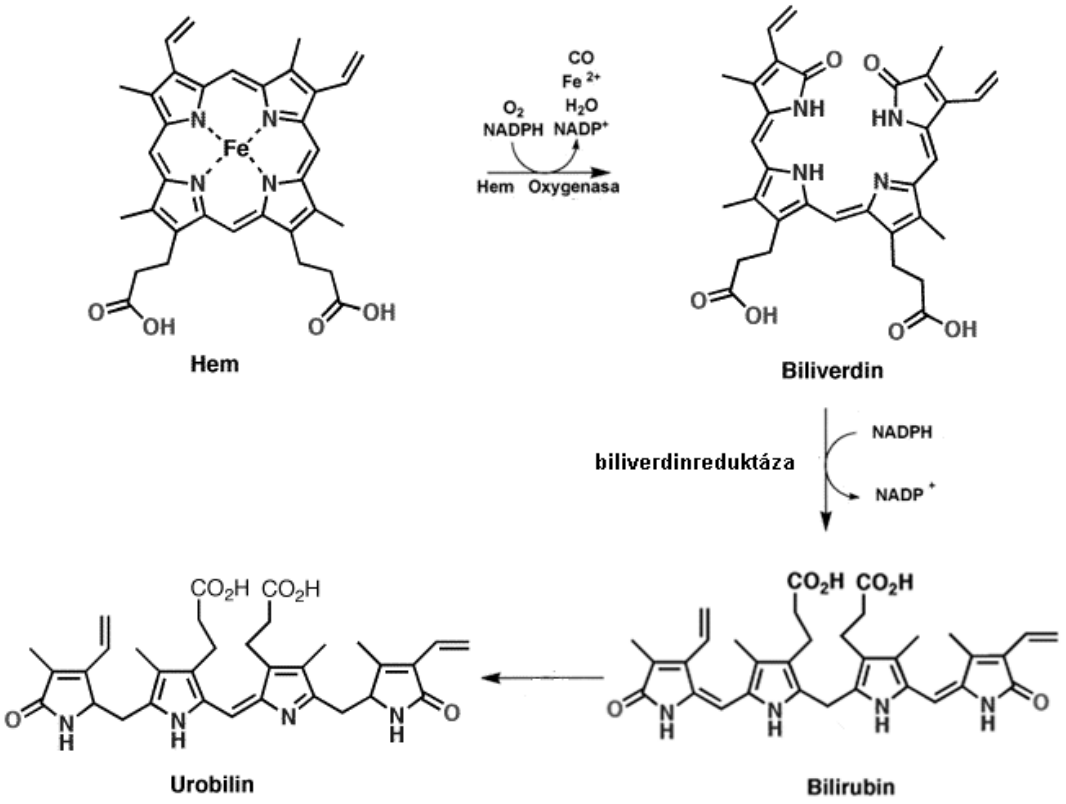

Obr. 4.1 Katabolická dráha přeměny hemu

Cílem dále diskutované práce bylo identifikovat produkty bakteriální redukce bilirubinu a zjistit, zda hladina bilirubin ditaurátu (BDT), který se přirozeně vyskytuje ve žluči nižších obratlovců, může být snížena působením bakterie *Clostridium perfringens* izolované z lidských výkalů novorozenců.

Hmotnostní spektrometrie s ionizací elektrosprejem v negativním módu (ESI-MS) se ukázala, jako vhodná metoda pro charakterizaci produktů mikrobiální degradace bilirubinu. Pro tyto účely dříve používaná technika elektronové ionizace poskytovala bohatá spektra s hlubokou fragmentací, ale často velmi málo intenzivní molekulární ionty, což znesnadňovalo strukturní charakterizaci těchto látek. Značným problémem byla i jejich tepelná nestabilita při teplotách převyšujících 200°C.

4.1.2. Výsledky a diskuse – doplňkový komentář k publikaci

Bylo zjištěno, že bakterie *Clostridium perfringens* dokáží efektivně snižovat hladinu BDT. Při tomto procesu vznikalo několik urobilinoidů, u kterých se ukázalo, že nedochází

k hydrolýze taurinu. Dále bylo zjištěno, že amidová vazba BDT je pravděpodobně rezistentní k hydrolýze enzymy střevní mikroflóry. Překvapivě se však BDT může přeměňovat na urobilinoidy vázané na taurin. Na obrázku 4.2 je uvedeno hmotnostní spektrum volného bilirubinu $C_{33}H_{36}N_4O_6$ zaznamenané v negativním módu za použití elektrosprejové ionizace. Distribuce izotopů u aniontu $[M-H]^-$ m/z 583,3 je v dobré shodě s teoreticky vypočítanými hodnotami.

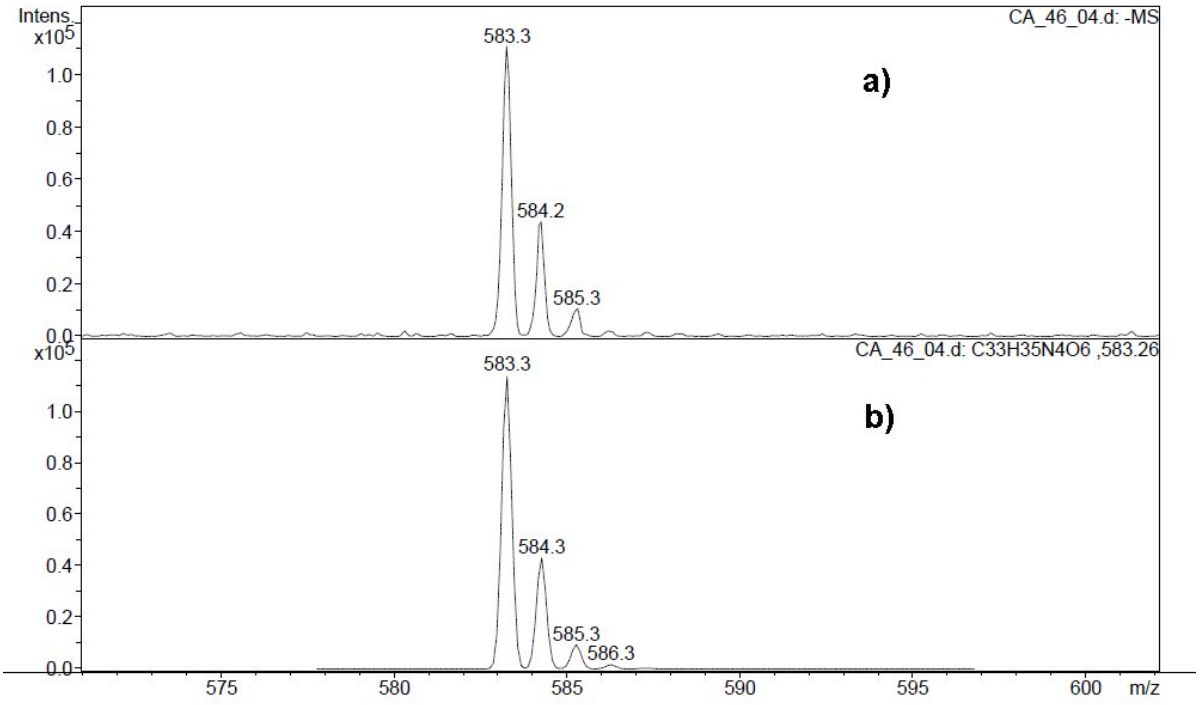

Obr.4.2 Hmotnostní spektrum bilirubinu (m/z = 583,3) **a)** naměřený $[M-H]^-$ ion, **b)** teoretické vypočítané izotopické zastoupení

Na obrázku 4.3 je zachyceno hmotnostní spektrum volného biliverdinu $C_{33}H_{34}N_4O_6$ zaznamenané v negativním módu za použití elektrosprejové ionizace. Distribuce izotopů u aniontu $[M-H]^-$ m/z 581,3 je v dobré shodě s teoreticky vypočítanými hodnotami.

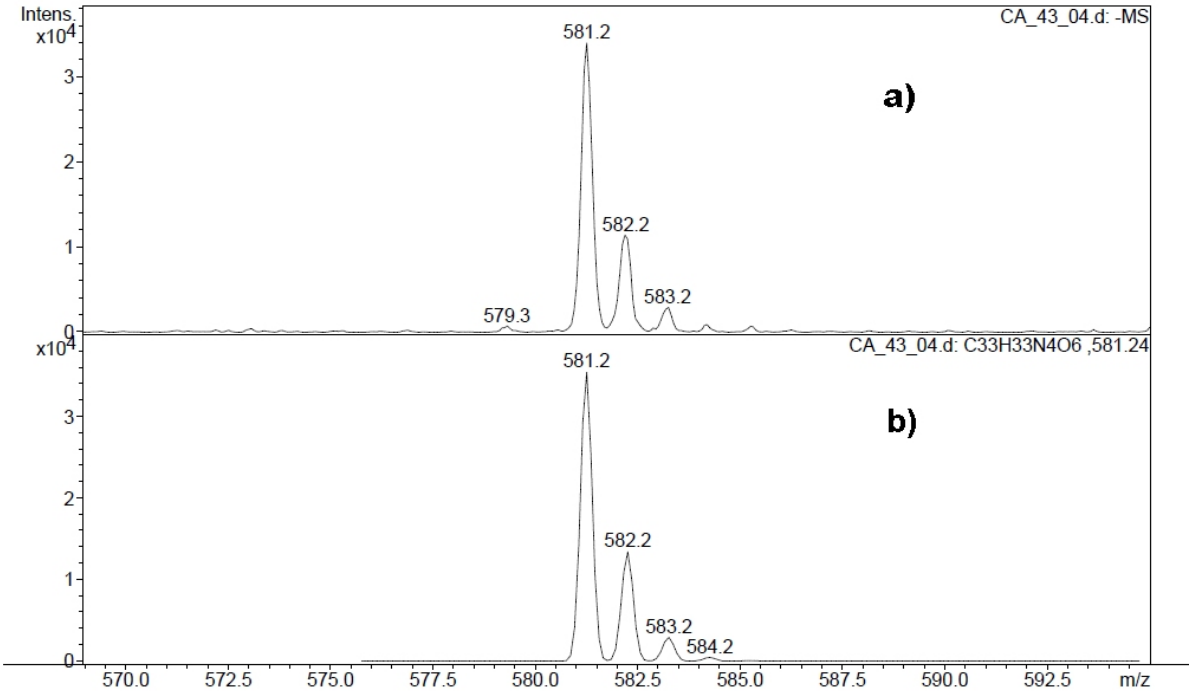

Obr.4.3 Hmotnostní spektrum biliverdinu (m/z = 581,3) **a)** naměřený $[M-H]^-$ ion, **b)** teoretické vypočítané izotopické zastoupení

Hmotnostní spektrometrie díky své vysoké strukturní selektivitě prokázala schopnost jednoznačně rozlišit jednotlivé produkty katabolického rozkladu hemu a prokázala svou nezastupitelnou roli při monitorování strukturních přeměn biologicky významných látek.

4.2. Studie biologického efektu fotoizomerů bilirubinu (publikace V)

4.2.1. Teoretický úvod

Bilirubin je tetrapyrolové žlučové barvivo. Zhruba u 45-65 % zdravých novorozenců pozorujeme zvýšení hladiny bilirubinu v krvi nad 25μmol/L, což se projevuje žlutým zbarvením bělma a později i kůže (novorozenecká žloutenka). Bilirubin je konečným degradačním produktem hemoglobinu a jeho přirozená fyziologická hladina není toxická, jako buněčný jed ale působí volný nekonjugovaný bilirubin, který vzniká dekonjugací ve střevech a následně podléhá redukci bakteriální flórou na urobilinoidy. K eliminaci nežádoucího bilirubinu se využívá fototerapie, která generuje řadu fotoizomerů (PI) [6]. Ačkoliv je tato metoda široce aplikována již řadu let, biologické vlastnosti PI nejsou dosud uspokojivým způsobem prostudovány. Vzniklé izomerní struktury bilirubinů a lumirubinu zobrazené na obrázku 4.4 [7-9], jakož i další oxidační produkty [10,11] se z těla snadno vylučují.

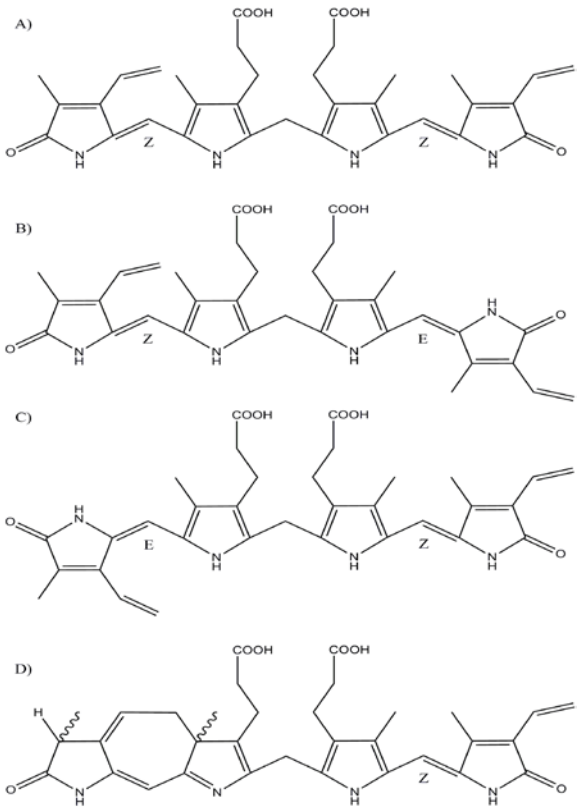

Obr.4.4 .Bilirubin a jeho fotoderiváty. (A) Z,Z-Bilirubin; (B) Z,E-Bilirubin; (C) E,Z-Bilirubin; (D) Z-Lumirubin

Neurotoxicita bilirubinu je přímo spojena s koncentrací frakce, která není navázána na albumin, což samozřejmě závisí na přítomnosti látek, které se mohou vázat konkurenčně [12]. Máme poměrně málo informací o tom, zda interakci s albuminem mohou nějakým způsobem ovlivňovat také fotoizomery vzniklé po aplikaci fototerapie. Také stále existuje nejistota, zda tyto rozkladné produkty nejsou toxické a to nejen pro centrální nervový systém, ale i další orgány. Z tohoto důvodu bylo cílem této studie charakterizovat jednotlivé fotoizomery a následně vyhodnotit jejich vlastnosti a možné biologické účinky.

4.2.2. Výsledky a diskuse – doplňkový komentář k publikaci

S pomocí tenkovrstvé chromatografie, jak ukazuje obrázek 4.5, se podařilo se úspěšně rozdělit 18 různých produktů vznikajících ozařováním bilirubinu, z nichž dva hlavní fotoderiváty označené čísly 1 a 7 bylo možno izolovat v dostatečné čistotě a množství pro účely biologického studia.

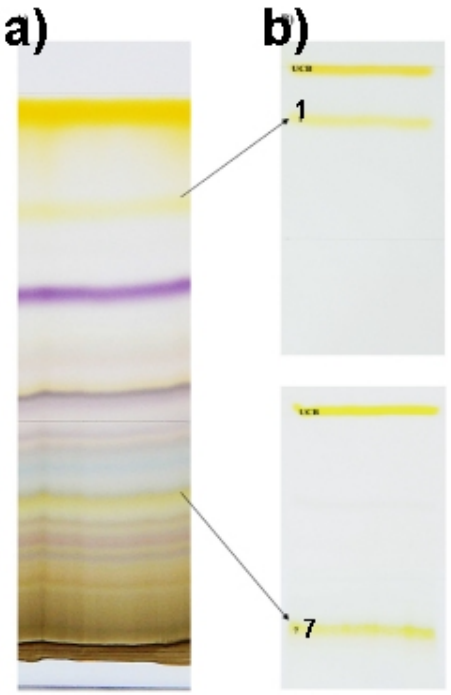

Obr. 4.5. Produkty fototerapie bilirubinu. **a)** celková TLC separace **b)** Nejdůležitější fotoderiváty 1 a 7 byly rechromatografovány s nekonjugovaným bilirubinem. Podmínky TLC: deska 200 x 200 x 0,25 mm Kieselgel 60, mobilní fáze = chloroform : methanol : voda 40: 9: 1, v/v/v,

Bylo prokázáno, že PI nezvyšují hladinu volného bilirubinu a nepřispívají tedy ke zvýšení toxicity. To znamená, že toxický je pouze nekonjugovaný bilirubin, jehož MS/MS spektrum je na obrázku 4.6, a že konformační změny vyvolané ozářením téměř úplně ruší škodlivý účinek barviva.

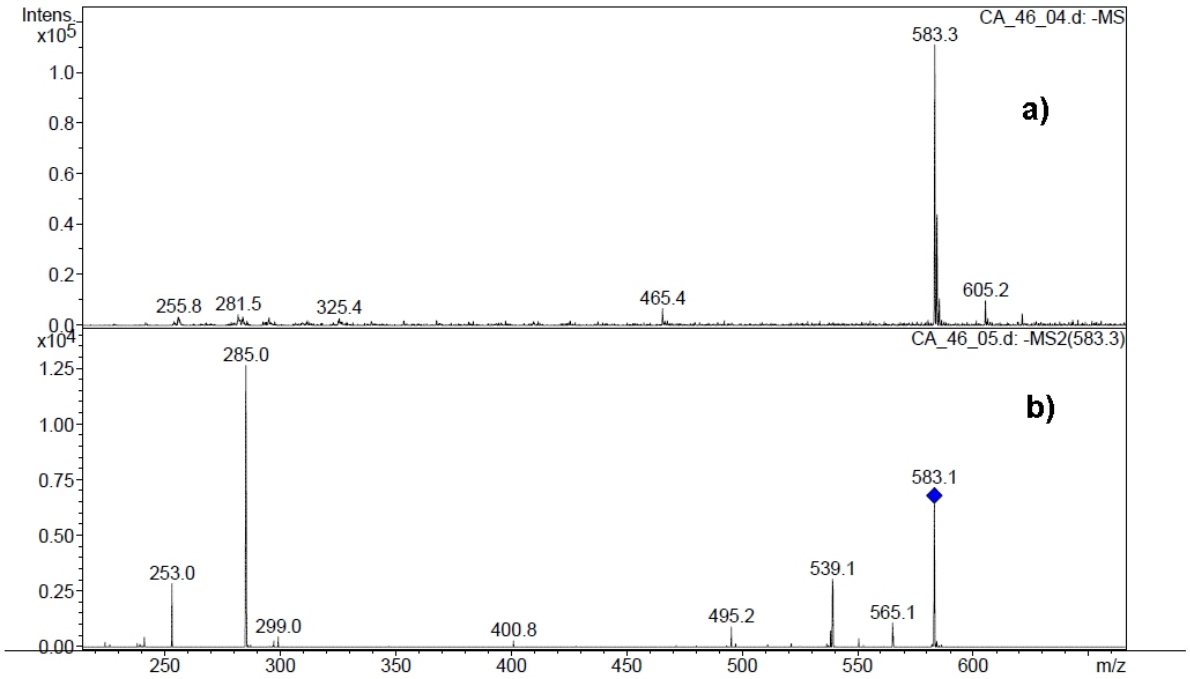

Obr.4.6 Hmotnostní spektrum výchozího bilirubinu (m/z = 583,3) **a)** naměřený $[M-H]^-$ ion, **b)** fragmentové MS^2 spektrum bilirubinu vzniklé z prekurzorového iontu m/z = 583,3.

Podrobným studiem fragmentace bilirubinu byly identifikovány produkty rozpadu prekurzorového iontu. Především se jedná o ion m/z = 565 vznikající ztrátou vody a ion m/z = 539 vznikající ztrátou oxidu uhličitého. Oba tyto ionty pocházejí z fragmentace ethoxykarboxylové skupiny. Bohužel ani nejintenzivnější ion m/z = 285 není možné využít k identifikaci jednotlivých izomerních forem vzniklých ozářením bilirubinu.

Provedená studie umožnila prokázat klinicky významný fakt, že produkty fototerapie jsou biologicky inertní a nevykazují žádné negativní biologické účinky.

4.3. Studie mutageneze vazebných míst pro ubichinon odhalujícíe roli mitochondriálního komplexu II v iniciaci buněčné smrti (publikace VI)

4.3.1.Teoretický úvod

Sukcinátdehydrogenáza (SDH) označovaná též jako komplex II (CII) je enzymatický komplex, který katalyzuje oxidaci sukcinátu na fumarát za současné redukce ubichinonu na ubichinol. SDH je tedy jedním z enzymů citrátového cyklu, ale zároveň má přímé napojení na další fáze buněčného dýchání tím, že se účastní přenosu elektronů [13-16]. Je známo, že inhibice CII naruší přenos elektronů a může vést ke generaci reaktivních forem kyslíku se všemi negativními důsledky pro organizmus. Na druhé straně, cílená inhibice CII působením vitamínu E a jeho analogů, jako je mitochondriálně cílený derivát α-tokoferyl sukcinátu (MitoVES), může preferenčně iniciovat buněčnou smrt rychle rostoucích buněk. Potlačení růstu nádorových buněk tímto způsobem bylo již prokázáno na zvířecích modelech [17-21] a jeví se jako perspektivní i pro použití v humánní medicíně.

4.3.2.Výsledky a diskuse – doplňkový komentář k publikaci

Pro studium role CII v procesu iniciace buněčné smrti byla provedena cílená změna aminokyselin v podjednotce C (SDHC), jak je znázorněno na obrázku 4.7.

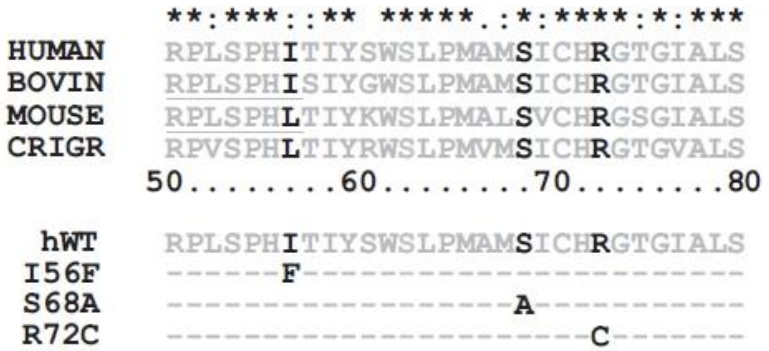

Obr. 4.7 schéma výměny aminokyselin v oblasti SDHC

Jak je tedy z obrázku patrné v případě **I56F** dochází k záměně isoleucinu za fenylalanin, u **S68A** byl vyměněn serin za alanin a v případě **R72C** byl vyměněn arginin za cystein.

Stanovení intracelulární koncentrace sukcinátu byla prováděna metodou LC-ESI/MS. Jednalo se o analýzu na velmi nízkých koncentračních hladinách analytu v komplikované biologické matrici představované ethanolickým extraktem z buněk. Použitá analytická metoda byla vyvinuta modifikací postupu použitého v práci [22]. Metoda je založena na esterifikaci kyseliny jantarové a následné analýze vzniklého málo polárního esteru kapalinovou chromatografií s hmotnostní detekcí. Optimalizovaný postup derivatizace zahrnoval in situ generování kyseliny chlorovodíkové, která katalyzovala esterifikaci benzylalkoholem. Mechanizmus esterifikace je naznačen na obrázku 4.8[23]. Po přidání vnitřního standardu (kyselina šťavelová) byly extrakty buněk vysušeny v proudu argonu. Poté bylo přidáno 50 μl benzylalkoholu a 30 μl TMS-chloridu. Uzavřené zkumavky Eppendorf byly umístěny do v ultrazvukové lázně na 45 min za laboratorní teploty a následně byly vzorky dalších 45 minut inkubovány v sušárně při teplotě 80 ° C.

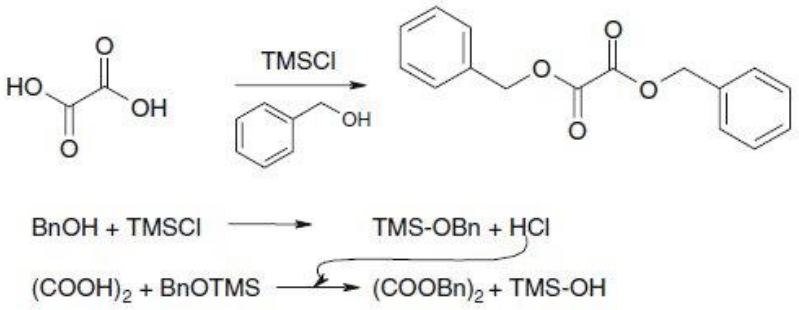

Obr. 4.8 Proces derivatizace nízkomolekulárních organických kyselin

Jednoznačnou výhodou použitého postupu esterifikace s aromatickým alkoholem byla možnost následné separace na reverzní fázi a dále možnost duální detekce s použitím UV spektrofotometrického detektoru a ESI/MS. MS kvantifikace derivatizovaného sukcinátu a oxalátu byla provedena pomocí aduktů se sodíkem. Dibenzyl oxalát poskytoval v pozitivním módu pík $[M+Na]^+$ m/z = 293 a dibenzyl sukcinát poskytoval pík $[M+Na]^+$ m/z = 321. Složený UV chromatogram se sledovanou vlnovou délkou λ = 254 nm s chromatogramy vybraných iontů m/z =293 (pík 1) a m/z = 321 (pík 2) je uveden na Obr. 4.9.

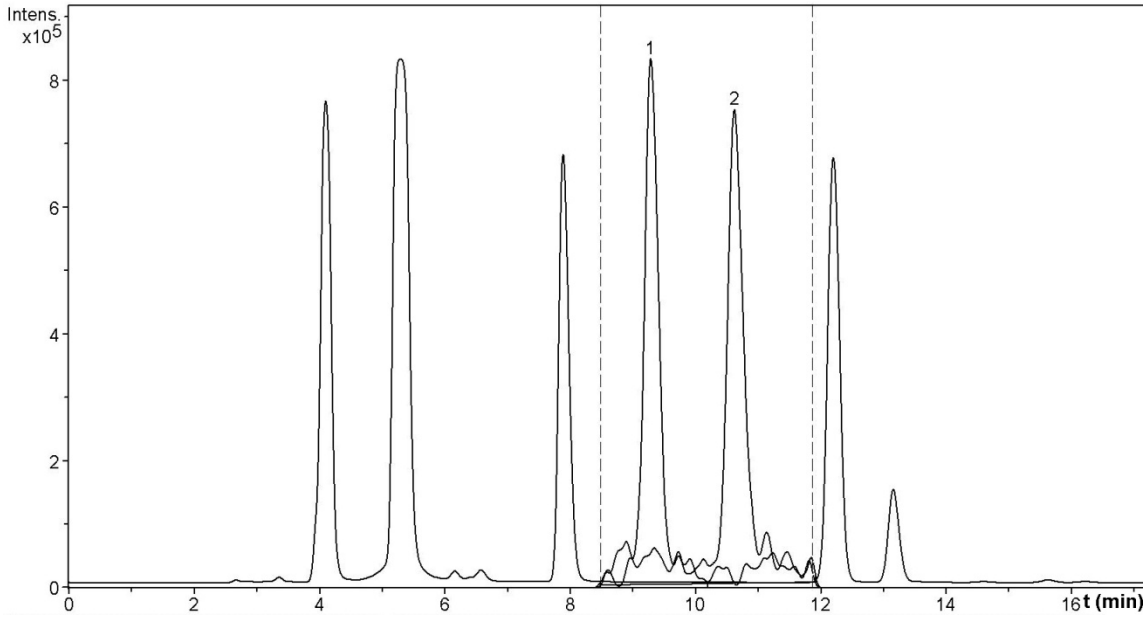

Obr.4.9 LC-MS chromatogram sukcinátu a vnitřního standard po derivatizaci benzylalkoholem. Pík č.1 náleží dibenzyl oxalátu (m/z 293) a pík č.2 patří dibenzyl sukcinátu (m/z 321).

Kalibrační závislost odezvy MS detektoru na benzylsukcinát, která je uvedená na obrázku 4.10, je lineární v celém sledovaném intervalu koncentrací stanovované látky.

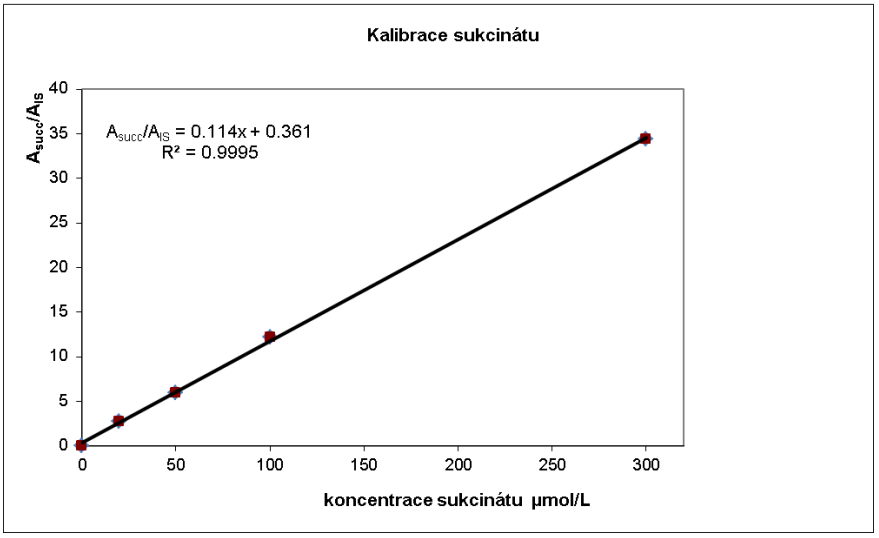

Obr.4.10 Závislost odezvy MS detektoru na koncentraci sukcinátu

Z provedené studie jednoznačně plyne, že inhibice respiračního komplexu II (CII, sukcinát dehydrogenáza, SDH) může indukovat buněčnou smrt a představuje tak potenciálně významný přístup k léčbě nádorových onemocnění. Pro objasnění role reaktivních forem kyslíku (ROS) byl použit CII pozměněný řízenou mutagenezí (SDHC).

Objasnění detailního mechanizmu výše zmíněných mechanizmů včetně specifikace jejich klinického využití bude předmětem dalšího studia. Ze sloupcových grafů na obrázku 4.11 je zřejmé, jak koncentrace intrabuněčného sukcinátu úzce souvisí s funkčností CII a tedy možností buněčného dýchání. Jak je zde ukázáno v případě B9 a R72C buňky nemohly využít sukcinát pro dýchání v důsledku nefunkčnosti enzymu sukcinátdehydrogenázy.

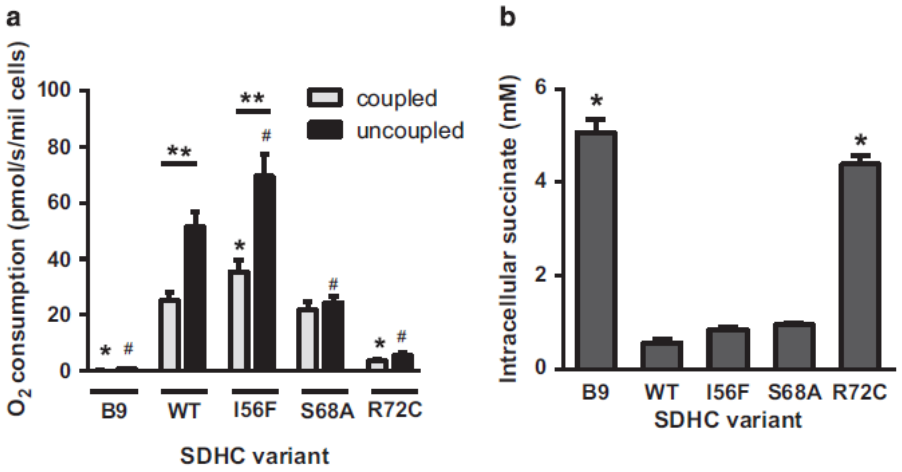

Obr.4.11 Porovnání biologické spotřeby kyslíku a hladiny intrabuněčného sukcinátu

Dále bylo prokázáno, že I56F a S68A SDHC varianty, které podporují zprostředkované dýchání byly méně efektivně inhibovány mitochondriálně cíleným derivátem α-tokoferyl sukcinátu MitoVES, než tomu bylo u typu (WT). Na rozdíl od toho S68A varianta byla mnohem náchylnější k inhibici thenoyltrifluoroacetonem (TTFA) než varianty I56F nebo WT. Varianta R72C, byla odolná vůči MitoVES i TTFA a nedocházelo ke zvyšování ROS. Podobně Atpenin A5 rapidně zvýšil hladinu intracelulárního sukcinátu v buňkách typu WT, ale nevyvolal vznik ROS a buněčnou smrt, na rozdíl od MitoVES a TTFA. Je zřejmé, že iniciace buněčné smrti při inhibici CII závisí na ROS, a že rozsah buněčné smrti koreluje s účinností inhibice v místě vazby ubichinonu. Získané poznatky mohou být velmi cenné zejména s ohledem na terapii nádorových onemocnění.

4.4.Literatura IV –VI

1. Poste, G. Bring on the biomarkers. Nature **2011**, 469, 156–157.
2. General Methods in Biomarker Research and their Applications Editors:Victor R. Preedy, Vinood B. Patel ISBN: 978-94-007-7695-1
3. T Kamachi, Alexander F. Shestakov, K Yoshizawa. J. AM. CHEM. SOC. 2004, 126, 3672 – 3673
4. Sedlak T, Snyder H: Pediatrics 2004, 113 1776-1782
5. Vítek L, Ostrow JD. Curr Pharm Des **15**: 2869–2883(2009)
6. JANOTA J., STRAŇÁK Z.: Neonatologie. 1. vydání. Praha : Mladá fronta, 2013. s. 121-129. ISBN 978-80-204-2994-0.
7. Onishi S, Isobe K, Itoh S, Kawade N, Sugiyama S.:. Biochem J. 1980; 190: 533–536
8. Onishi S, Miura I, Isobe K, Itoh S, Ogino T, Yokoyama T, et al.:. Biochem J. 1984; 218: 667–6764.
9. McDonagh AF, Palma LA.: J Am Chem Soc. 1982; 104: 6867–6869.
10. Lightner DA, McDonagh AF.: Acc Chem Res. 1984; 17: 417–424.
11. Knobloch E, Mandys F, Hodr R, Hujer R, Mader R.: J Chromatogr. 1991; 566: 89 – 99.
12. Ahlfors CE, Wennberg RP.: Semin Perinatol. 2004; 28: 334–339.
13. R. Cammack et al. Oxford dictionary of biochemistry and molecular biology; revised edition. New York : Oxford University press, 2006.
14. Maklashina E, Cecchini G. Biochim Biophys Acta 2010; 1797: 1877–1882.
15. Sun F, Huo X, Zhai Y,Wang A, Xu J, Su D et al. Cell 2005; 121: 1043–1057.
16. Iverson TM. Biochim Biophys Acta 2013; 1827: 648–657.
17. Dong LF, Jameson VJ, Tilly D, Cerny J, Mahdavian E, Marin-Hernandez A et al. J Biol Chem 2011; 286: 3717–3728.
18. Dong LF, Jameson VJ, Tilly D, Prochazka L, Rohlena J, Valis K et al.: Free Radic Biol Med 2011; 50: 1546–1555.
19. Rohlena J, Dong LF, Kluckova K, Zobalova R, Goodwin J, Tilly D et al.: Antioxid Redox Signal 2011; 15: 2923–2935.
20. Rodriguez-Enriquez S, Hernandez-Esquivel L, Marin-Hernandez A, Dong LF, Akporiaye ET, Neuzil J et al.: Biochim Biophys Acta 2012; 1817: 1597–1607.
21. Neuzil J, Dong LF, Rohlena J, Truksa J, Ralph SJ.: Mitochondrion 2013; 13: 199.

22. R. Nakao, K. Oka a T.Fukumoto.: Bull Chem Soc Jpn 54:1267-1268, 1981
23. L. Jaitz, B. Mueller, G. Koellensperger, D. Huber, E. Oburger, M. Puschenreiter, S. Hann.: Anal Bioanal Chem (2011) 400:2587–2596

PUBLIKACE IV

Reduction of bilirubin ditaurate by the intestinal bacterium Clostridium perfringens

Konickova, R; Jiraskova, A ; Zelenka, J ; Leseticky, L ; Sticha, M ;
Vitek, L.

J ACTA BIOCHIMICA POLONICA 59 (2) : 289-291 2012

ACTA ABP BIOCHIMICA POLONICA

Vol. 59, No 2/2012
289–291
on-line at: www.actabp.pl

Regular paper

Reduction of bilirubin ditaurate by the intestinal bacterium *Clostridium perfringens*

Renata Koníčková[1*], Alena Jirásková[1,*], Jaroslav Zelenka[1,#], Ladislav Lešetický[2], Martin Štícha[2] and Libor Vítek[1,3]✉

[1]Institute of Medical Biochemistry and Laboratory Diagnostics, 1st Faculty of Medicine, Charles University in Prague, Prague, Czech Republic; [2]Department of Organic and Nuclear Chemistry, Faculty of Science, Charles University in Prague, Prague, Czech Republic; [3]4th Department of Internal Medicine, 1st Faculty of Medicine, Charles University in Prague, Prague, Czech Republic

Bilirubin is degraded in the human gut by microflora into urobilinoids. In our study we investigated whether the bilirubin-reducing strain of *Clostridium perfringens* can reduce bilirubin ditaurate (BDT), a bile pigment of some lower vertebrates, without hydrolysis of the taurine moiety. *C. perfringes* was incubated under anaerobic conditions with BDT; reduction products were quantified by spectrophotometry and separated by TLC. Based on Rf values of BDT reduction products and synthetic urobilinogen ditaurate, three novel taurine-conjugated urobilinoids were identified. It is likely that bilirubin-reducing enzyme(s) serve for the effective disposal of electrons produced by fermentolytic processes in these anaerobic bacteria.

Key words: *Clostridium perfringens*, bile pigments, bilirubin ditaurate, intestinal metabolism, urobilinoids

Received: 19 November, 2011; revised: 17 January, 2012; accepted: 26 April, 2012; available on-line: 27 April, 2012

INTRODUCTION

Unconjugated bilirubin (UCB), a yellow, poorly water-soluble pigment, is the main heme catabolic product in the intravascular compartment. The predominant source of UCB is the breakdown of heme, originating from senescent or hemolyzed red blood cells. After its biotransformation in the liver, secretion into the bile, and then in the intestinal lumen, bilirubin is rapidly reduced to urobilinoids by the intestinal microflora (Vítek & Ostrow, 2009). The term urobilinoids covers the group of reduction products of bilirubin, including urobilinogen and stercobilinogen, along with their oxidized derivatives urobilins and stercobilins (Moscowitz *et al*., 1970). In the absence of bilirubin-reducing microflora, such as in the early newborn period (Vítek *et al*., 2000), or in patients treated with systemic antibiotics (Vítek *et al*., 2005), UCB may undergo substantial enterohepatic and enterosystemic circulation. Severe unconjugated hyperbilirubinaemia in neonates is of concern because of the potential danger to their central nervous system.

UCB is reduced by multiple sequential reactions into a series of urobilinogens; in turn, these colorless chromogens may be oxidized to urobilins, their respective yellowish oxidation products. These substances are believed to be nontoxic due to their increased polarity. Despite the importance of this catabolic pathway, only a few bacterial strains involved in bilirubin reduction have so far been isolated: *Clostridium ramosum* (Gustafsson & Lanke, 1960), *C. perfringens*, *C. difficile* (Vítek *et al*., 2000), and *Bacteroides fragilis* (Fahmy *et al*., 1972). In our recent study (Vítek *et al*., 2006), we undertook a detailed analysis of the products of the bacterial reduction of bilirubin and its derivatives formed by a novel strain of *C. perfringens* isolated from neonatal feces (Vítek *et al*., 2000). The *C. perfringens* strain reduced a wide variety of bile pigments that differed substantially in both their polarity and structure. The end-catabolic bilirubin products resulting from bacterial reduction were identified as urobilinogen species. The reduction process catalyzed by the bacterial strain studied did not proceed to the production of stercobilinogen (Vítek *et al*., 2006).

The aim of the present study was to assess whether bilirubin ditaurate, a pigment that occurs naturally in the bile of certain lower vertebrates (such as the marine fish *Seriola quinqueradiata*) (Sakai *et al*., 1987), can be reduced by the aforementioned strain of *C. perfringens* isolated from human neonatal feces, and secondly, to characterize the reduction products formed.

MATERIAL AND METHODS

***C. perfringens* cultivation.** The strain of *C. perfringens* used in our studies was isolated from stool of a healthy neonate (Vítek *et al*., 2000). The strain was classified in the National Reference Laboratory for Anaerobic Bacteria (Ostrava, Czech Republic) as non-pathogenic, based on the absence of any toxin production. The strain was incubated with BDT and UCB (both from Frontier Scientific, Inc., Logan, UT, USA) in broth (2% Yeast Extract, Oxoid, GB; prepared in 100 mM phosphate buffer, pH=8). Based on their polarity, UCB was dissolved in dimethylsulfoxide (Sigma, St. Louis, MO, USA) and bilirubin ditaurate (BDT) in the broth; both pigments were added to the late exponential phase *C. perfringens* culture, at the final concentration of 50 μmol/L (final concentration of DMSO was <3%, this concentration was found in separate experiments not to influence the growth of *C. perfringens*). The growth phase was monitored according to the optical density of the culture (spectrophotometry at 600 nm). The conversion rates of both bile pigments were analyzed under exactly the same conditions, and calculated from five independent measurements. Af-

✉e-mail: vitek@cesnet.cz
*These authors contributed equally
#Current address: Institute of Physiology, Academy of Sciences of the Czech Republic, Prague, Czech Republic
Abbreviations: BDT, bilirubin ditaurate; UCB, unconjugated bilirubin

ter incubation for 24 h at 37°C in Anaerostat (Oxoid, GB), the medium was sampled for urobilinoid analyses.

Determination and isolation of urobilinoids. The rate of bile pigment conversion was calculated as the proportion of the urobilinoids produced to the initial bile pigment concentration. Concentrations of the UCB and BDT reduction products were determined spectrophotometrically (UV/Vis Spectrophotometer Lambda 20, Perkin-Elmer, USA) as the oxidation products of zinc complexes of urobilinoids, as previously described (Kotal & Fevery 1991).

The pigments were extracted from the culture medium using an SPE column (Strata C8 500 mg/6 ml, Phenomenex, Torrance, CA, USA). The columns were washed with 1 volume of methanol and distilled water. The urobilinoids were eluted with a minimal volume of MeOH:H_2O (1:1, by vol.). The elution mixture was evaporated; the extracted pigments were dissolved in methanol and separated by TLC.

To check whether the BDT-reducing enzyme(s) were secreted into the medium, BDT was incubated with a cell-free supernatant and a protein extract after a French press disintegration of bacterial cells. A *C. perfringens* culture grown overnight (500 ml) was centrifuged (15 000 × *g*, 10 min, 4°C) and the medium was filter-sterilized (Milipore Millex HV, PVDF 0.45 μm). The cells were re-suspended in a phosphate buffer (0.025 M, pH=8) containing 5 mM $MgCl_2$, 2 mM EDTA and 10% glycerol, and then disintegrated using a French press (6 cycles, 1500 psi, SLM-Aminco, USA). The cell debris was removed by centrifugation (15 000 × *g*, 10 min, 4°C) and the supernatant containing the protein extract was filter-sterilized as above. The cell-free supernatant and the protein extract were incubated separately with BDT, as described above; the production of urobilinoids was again determined.

Thin layer chromatography. Isolated BDT and UCB reduction products were separated by TLC, using HPTLC aluminum plates coated with silica gel (RP-18 W/UV_{254}, Macherey-Nagel, Germany) (solvent system: H_2O:MeOH:CH_3COOH (250:250:1, by vol.)) and examined under both visible and UV light (CAMAG TLC Scanner II, CAMAG, Muttenz, Switzerland). Urobilin (Frontier Scientific, Inc., Logan, UT, USA) and urobilinogen ditaurate were used as standards. Urobilinogen ditaurate was prepared by amalgam reduction of bilirubin ditaurate, as previously described (Watson, 1953); with its structure confirmed by mass spectrometry (Esquire 3000, Bruker Daltonics, Bremen, Germany).

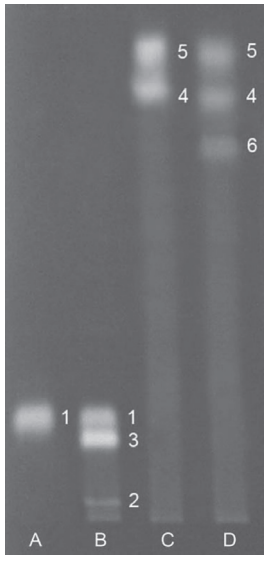

Figure 1. Products of UCB and BDT reduction by *C. perfringens*. The initial pigment concentration in the broth was 50 μmol/L. TLC system specification: HPTLC silica gel plate (RP-18 W/UV_{254}, Macherey-Nagel), solvent system: H_2O:MeOH:CH_3COOH (250:250:1, by vol.). **(Track A)** Urobilin (standard); **(Track B)** Reduction products of UCB; **(Track C)** Urobilinogen ditaurate (standard); **(Track D)** Reduction products of BDT. **(1)** Urobilin; **(2)** Mesobiliviolin; **(3)** Urobilinogen; **(4)** Urobilinogen ditaurate; **(5)** Urobilin ditaurate; **(6)** Mesobiliviolin ditaurate.

RESULTS AND DISCUSSION

The bilirubin-reducing strain of *C. perfringens* isolated from neonatal feces was able to reduce BDT efficiently. The conversion rates were 9±3 and 30±5% in 24 h for BDT and UCB, respectively; this is consistent with our previous findings (Vítek *et al.*, 2006). No reduction of BDT could be detected in cell-free post-culture medium; in contrast, a French press disintegration of the bacterial cells resulted in the release of enzyme(s) capable of reducing BDT, indicating that the BDT reductase is not secreted by the bacteria to the medium.

BDT was reduced by *C. perfringens* into several species of taurine-bound urobilinoids, demonstrating that taurine hydrolysis did not precede the enzymatic reduction (Fig. 1). After TLC separation, no unconjugated urobilinoids derived from BDT could be detected. Based on comparison of the bilirubin reduction products with synthetic urobilinogen ditaurate, three reduction products of BDT were identified: urobilinogen ditaurate, urobilin ditaurate, and (most likely) mesobiliviolin ditaurate (Fig. 1). A more polar taurine-bound urobilin derivative detected in both metabolized BDT and synthetic urobilinogen ditaurate tracks was most likely formed spontaneous oxidation of the urobilinogen ditaurate.

Another bilirubin conjugate, bisglucuronosyl bilirubin, was reduced by the same *C. perfringens* strain into unconjugated urobilinoids; the glucuronoside bond was hydrolyzed prior to the reduction of the tetrapyrroles (Vítek *et al.*, 2006). The amide bond of BDT is presumably resistant to hydrolysis by the enzymes of the intestinal microflora; surprisingly, however, BDT can still be reduced into taurine-bound urobilinoids. These results demonstrate a very broad substrate specificity of the enzyme(s) reducing bilirubin in the human gastrointestinal tract and may help to understand the function of bilirubin reductase. Such a broad substrate specificity of the bilirubin-reducing enzyme(s) presumably serve for the effective disposal of electrons produced by fermentolytic processes in these anaerobic bacteria in a manner similar to that described for microbial bile acid dehydroxylation (Ridlon *et al.*, 2006).

It is interesting to note that despite their ubiquitous occurrence in the human intestinal tract, as well as their high therapeutic potential, the bacterial enzymes responsible for bilirubin reduction have, to date, not been identified.

Acknowledgement

This work was supported by grant CZ:GA CR:P206/11/0836 from the Research Granting Agency of the Czech Republic.

REFERENCES

Fahmy K, Gray CH, Nicholson DC (1972) The reduction of bile pigments by faecal and intestinal bacteria. *Bioch Bioph Acta* **264**: 85–97.

Gustafsson BE, Lanke L (1960) Bilirubin and urobilins in germfree, exgermfree, and conventional rats. *J Exp Med* **112**: 975–981.

Kotal P, Fevery J (1991) Quantitation of urobilinogen in feces, urine, bile and serum by direct spectrophotometry of zinc complex. *Clin Chim Acta* **202**: 1–9.

Moscowitz A, Weimer M, Lightner A, Petryka ZJ, Davis E, Watson CJ (1970) The in vitro conversion of bile pigments to the urobilinoids by a rat clostridia species as compared with the human fecal flora; III. Natural d-Urobilin, synthetic i-urobilin, and synthetic i-urobilinogen. *Biochem Med* **4**: 149–164.

Ridlon JM, Kang DJ, Hylemon PB (2006) Bile salt biotransformations by human intestinal bacteria. *J Lip Res* **47**: 241–259.

Sakai T, Watanabe K, Kawatsu H (1987) Occurrence of ditaurobilirubin, bilirubin conjugated with two moles of taurine, in the gallbladder bile of yellowtail, Seriola quinqueradiata. *J Biochem* **102**: 793–796.

Vítek L, Ostrow JD (2009) Bilirubin chemistry and metabolism; harmful and protective aspects. *Curr Pharm Des* **15**: 2869–2883.

Vítek L, Kotal P, Jirsa M, Malina J, Černá M, Chmelař D, *et al.* (2000). Intestinal colonization leading to fecal urobilinoid excretion may play a role in the pathogenesis of neonatal jaundice. *J Ped Gastroenterol Nutr* **30**: 294–298.

Vítek L, Zelenka J, Zadinová M, Malina J (2005). The impact of intestinal microflora on serum bilirubin levels. *J Hepatol* **42**: 238–243.

Vítek L, Majer F, Muchová L, Zelenka J, Jirásková A, Branny P, *et al.* (2006). Identification of bilirubin reduction products formed by Clostridium perfringens isolated from human neonatal fecal flora. *J Chromat B* **833**: 149–157.

Watson CJ (1953). The direct preparation of crystalline urobilin from bilirubin. *J Biol Chem* **200**: 691–696.

PUBLIKACE V

The biological effect of bilirubin photoisomers

J. Jasprova, M. Dal Ben, E. Vianello, I. Goncharova, M Urbanova, K. Vyroubalova, S. Gazzin, C. Tiribelli, M. Sticha, M. Cerna, L. Vitek.

PLOS ONE 11 (2) Article Number: e0148126 2016

PLOS ONE

RESEARCH ARTICLE

The Biological Effects of Bilirubin Photoisomers

Jana Jasprova[1], Matteo Dal Ben[2], Eleonora Vianello[2], Iryna Goncharova[3], Marie Urbanova[3], Karolina Vyroubalova[1], Silvia Gazzin[2], Claudio Tiribelli[2], Martin Sticha[4], Marcela Cerna[5], Libor Vitek[1,6]*

1 Institute of Medical Biochemistry and Laboratory Diagnostics, 1st Faculty of Medicine, Charles University in Prague, Prague, Czech Republic, **2** Italian Liver Foundation, CSF, Trieste, Italy, **3** Institute of Chemical Technology Prague, Prague, Czech Republic, **4** Faculty of Science, Charles University in Prague, Prague, Czech Republic, **5** The Institute for Mother and Child, Prague, Czech Republic, **6** 4th Department of Internal Medicine, 1st Faculty of Medicine, Charles University in Prague, Prague, Czech Republic

* vitek@cesnet.cz

Citation: Jasprova J, Dal Ben M, Vianello E, Goncharova I, Urbanova M, Vyroubalova K, et al. (2016) The Biological Effects of Bilirubin Photoisomers. PLoS ONE 11(2): e0148126. doi:10.1371/journal.pone.0148126

Editor: Reza Khodarahmi, Kermanshah University of Medical Sciences, ISLAMIC REPUBLIC OF IRAN

Received: May 12, 2015

Accepted: January 13, 2016

Published: February 1, 2016

Data Availability Statement: All relevant data are within the paper.

Funding: This work was funded by the Czech Ministry of Health, grant RVO-VFN64165/2015 (http://www.mzcr.cz/), the Charles University in Prague, grants SVV2665161/2015, GAUK No. 556912, and PRVOUK-P25/LF1/2 (http://www.cuni.cz/), and the Czech Science Foundation, grant P206/11/0836 (http://www.gacr.cz/). This work was also supported in part by the Czech Ministry of Education, grant KONTAKT LH15097 (http://www.msmt.cz/). The funders had no role in study design, data collection

Abstract

Although phototherapy was introduced as early as 1950's, the potential biological effects of bilirubin photoisomers (PI) generated during phototherapy remain unclear. The aim of our study was to isolate bilirubin PI in their pure forms and to assess their biological effects *in vitro*. The three major bilirubin PI (ZE- and EZ-bilirubin and Z-lumirubin) were prepared by photo-irradiation of unconjugated bilirubin. The individual photoproducts were chromatographically separated (TLC, HPLC), and their identities verified by mass spectrometry. The role of Z-lumirubin (the principle bilirubin PI) on the dissociation of bilirubin from albumin was tested by several methods: peroxidase, fluorescence quenching, and circular dichroism. The biological effects of major bilirubin PI (cell viability, expression of selected genes, cell cycle progression) were tested on the SH-SY5Y human neuroblastoma cell line. Lumirubin was found to have a binding site on human serum albumin, in the subdomain IB (or at a close distance to it); and thus, different from that of bilirubin. Its binding constant to albumin was much lower when compared with bilirubin, and lumirubin did not affect the level of unbound bilirubin (Bf). Compared to unconjugated bilirubin, bilirubin PI did not have any effect on either SH-SY5Y cell viability, the expression of genes involved in bilirubin metabolism or cell cycle progression, nor in modulation of the cell cycle phase. The principle bilirubin PI do not interfere with bilirubin albumin binding, and do not exert any toxic effect on human neuroblastoma cells.

Introduction

Phototherapy as a treatment option for neonatal hyperbilirubinemia was first used by Cremer and co-workers in the 1950's [1]. This technique is based on the fact that blue-green light converts bilirubin into more polar derivatives. Configurational and structural photoisomers (PI),

and analysis, decision to publish, or preparation of the manuscript.

Competing Interests: The authors have declared that no competing interests exist.

ZE- and EZ-bilirubins, lumirubin (also called cyclobilirubin) (Fig 1) [2–4], as well as propentdyopents and other oxidation products [5,6], can be relatively easily excreted from the body.

Although phototherapy for neonatal hyperbilirubinemia is accepted as the 'gold standard' of treatment, it may be accompanied with side effects such as impairment of thermoregulation,

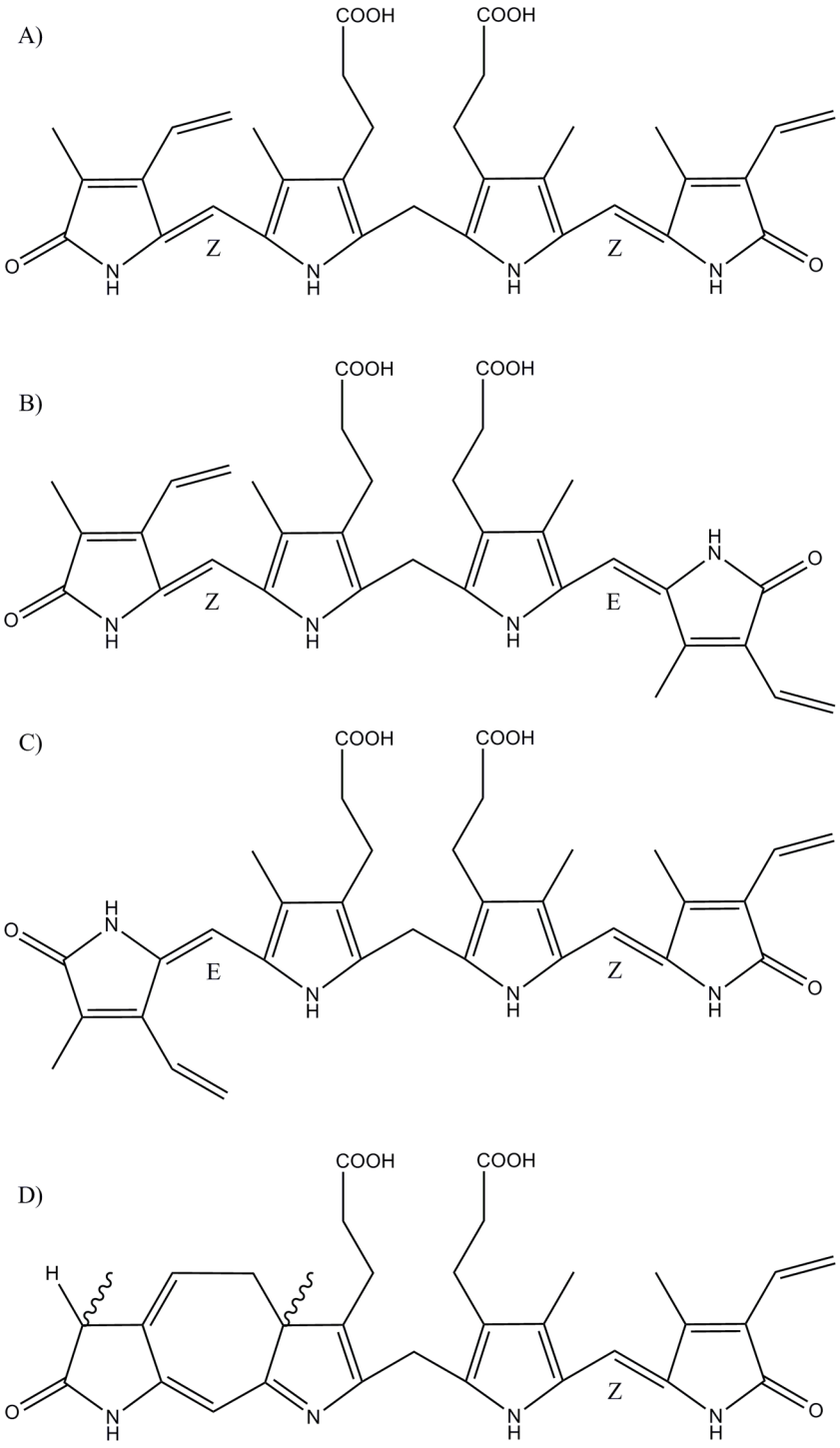

Fig 1. Bilirubin and its photoderivatives. (A) Z,Z-Bilirubin IXα. (B) Z,E-Bilirubin IXα. (C) E,Z-Bilirubin IXα. (D) Z-Lumirubin IXα.

doi:10.1371/journal.pone.0148126.g001

mineral dysbalance [7], and direct genotoxic effects on lymphocyte DNA [8]. This might also be one of the reasons for the increased prevalence of allergic conditions reported in these newborns [9]. In addition, intensive phototherapy in very low birth-weight newborns has been associated with increased risk of ileus [10]; also surprisingly by increased mortality, as demonstrated in the Collaborative Phototherapy Trial, as well as the NICHD Neonatal Network Trial [11,12].

The neurotoxicity of bilirubin is directly associated with the concentration of the fraction unbound to albumin (or other solubilizing substances), which is called Bf (bilirubin free) [13,14]. Bf is critically dependent on the presence of compounds that are potentially competing with bilirubin in binding to albumin [15]. Nothing is known about whether bilirubin PI may affect the bilirubin-albumin interaction. Previous studies on the biological effects of bilirubin photoproducts [16–23] suffered from a major limitation (insufficient purity of the bilirubin photoproducts), as well as inconsistent study designs. Thus, there is still uncertainty on the potential toxicity of bilirubin breakdown products not only for the central nervous system, but also other organs.

Therefore, the aim of the current study was to isolate and characterize pure forms of bilirubin PI; and then to assess their potential effects on bilirubin-albumin binding, as well as their possible biological effects *in vitro* using the neuroblastoma cell line SH-SY5Y.

Materials and Methods

Chemicals

The bilirubin (AppliChem, Darmstadt, Germany) was purified before use, according to McDonagh and Assissi [24]. The chloroform and di-n-octylamine were purchased from Sigma (MO, USA). The methanol was from Merck (Darmstadt, Germany), and ammonia from Penta (Czech Republic).

Because of light-sensitivity of bilirubin and bilirubin PI, all procedures were carried out under dim light in aluminium wrapped flasks. Evaporation was performed under vacuum and stream of nitrogen.

Preparation of PI

The pure bilirubin photoderivatives were prepared as previously described [25–27] with a slight modification of the original protocol. Briefly, bilirubin (100 mg) was dissolved in slightly basified methanol (1% NH_3 solution in methanol); the solution underwent 90 minutes of photo-irradiation using a Lilly phototherapeutical device (TSE, Czech Republic), composed of a field of LEDs emitting light (wavelength range = 430–500 nm with a broad peak between 445 and 474 nm (width at half max) with a maximal spectral irradiance of 100 $\mu W/cm^2/nm$ corresponding to the total irradiance of 3.1 mW/cm^2. The sample was then evaporated under vacuum, dissolved in pure methanol, decanted from the residual bilirubin, and re-evaporated. The residue of bilirubin PI was protected from light, and stored at -20°C until use.

Thin layer chromatography

The residue after photo-irradiation was dissolved in a small amount of methanol:chloroform (1:1, v/v), and separated by thin layer chromatography (200 x 200 x 0.25 mm Kieselgel 60 TLC plates [Merck, Darmstadt, Germany]; the mobile phase = chloroform:methanol:water, 40:9:1, v/v/v). During the first chromatography, the mixture of bilirubin derivatives was separated into 8 major bands, which were extracted using the mobile phase, evaporated to dryness, and then re-chromatographed using the same conditions. The individual separated compounds were re-

extracted, the solvent evaporated, and the isolated compounds were stored at -20°C until used. The isolated compounds 1 and 7, corresponding to ZE/EZ-bilirubins and lumirubin, as verified by HPLC [28,29] (Figs 2 and 3, also see Results), in a 1:1 ratio, were used for functional and biological studies as being representative of the principle bilirubin PI.

High-performance liquid chromatography analyses

The HPLC analyses were performed using an Agilent 1200 system (CA, USA) with a diode-array detector. The method was a modification of that by McDonagh *et al.* [28,29]. The mobile phase consisted of 0.1 M di-n-octylamine acetate in methanol and water; the stationary phase was represented by a Poroshell 120, SB-C18 column (4.6 x 100 mm, 2.7 μm; Agilent, CA, USA). Samples were prepared by mixing 20 μl of bilirubin solution with 180 μl of ice-cold 0.1 M di-n-octylamine acetate in methanol, then vortexed and centrifuged to eliminate proteins. Twenty μl of the prepared sample was injected onto the column.

Spectrophotometry

The absorption spectra of pure bilirubin PI were measured using a Lambda 25 spectrophotometer (Perkin Elmer, USA) in the spectral range from 200 to 900 nm. Samples for analyses were diluted in pure methanol, and measured against methanol as the blank.

Mass Spectrometry

Mass spectra were measured by using an Escuire 3000 mass spectrometer (Bruker Daltonics, Germany) coupled with electrospray ionization. All samples for MS analysis, dissolved in methanol, were injected directly on MS and measured in a negative mode. The masses were scanned in the range between 50 and 800 m/z. The capillary exit was set at -106.7 V.

Estimation of binding constant by fluorescence quenching

A fluorescence quenching method was used for measurement of either lumirubin-albumin or bilirubin-albumin interactions, as well as their binding constants [30]. The determination is based on the fact that bile pigments do not emit any fluorescence; on the other hand, human serum albumin (HSA) contains a tryptophan residue (Trp-214) in the subdomain IIA, which is responsible for its fluorescence. Thus, the binding constant for bilirubin and lumirubin to HSA was determined by quenching of the intrinsic Trp fluorescence.

For the *Ka* determination, formula (1) was used:

$$Ka = \frac{F_0 - F}{F\left(C_L - n\frac{F_0 - F}{F_0}C_p\right)} \quad (1)$$

- where F_0 was the fluorescence of HSA without a quencher, F the fluorescence of HSA with a quencher, C_L was the quencher concentration, and C_P was the concentration of HSA.

The effect of cooperative binding of lumirubin and bilirubin was also studied, and the results were compared to the *Ka* obtained in the systems with biliverdin and gossypol, which served as a displacing agent of bilirubin from HSA [31,32].

Characterization of the bile pigment albumin binding sites by circular dichroism (CD) spectroscopy

Unbound pigments were dissolved in 0.1 mol/L NaOH and mixed with the HSA solution in PBS (pH 7.4) at the molar ratio [pigment]/[HSA] = 1/1, the concentration of the pigment was

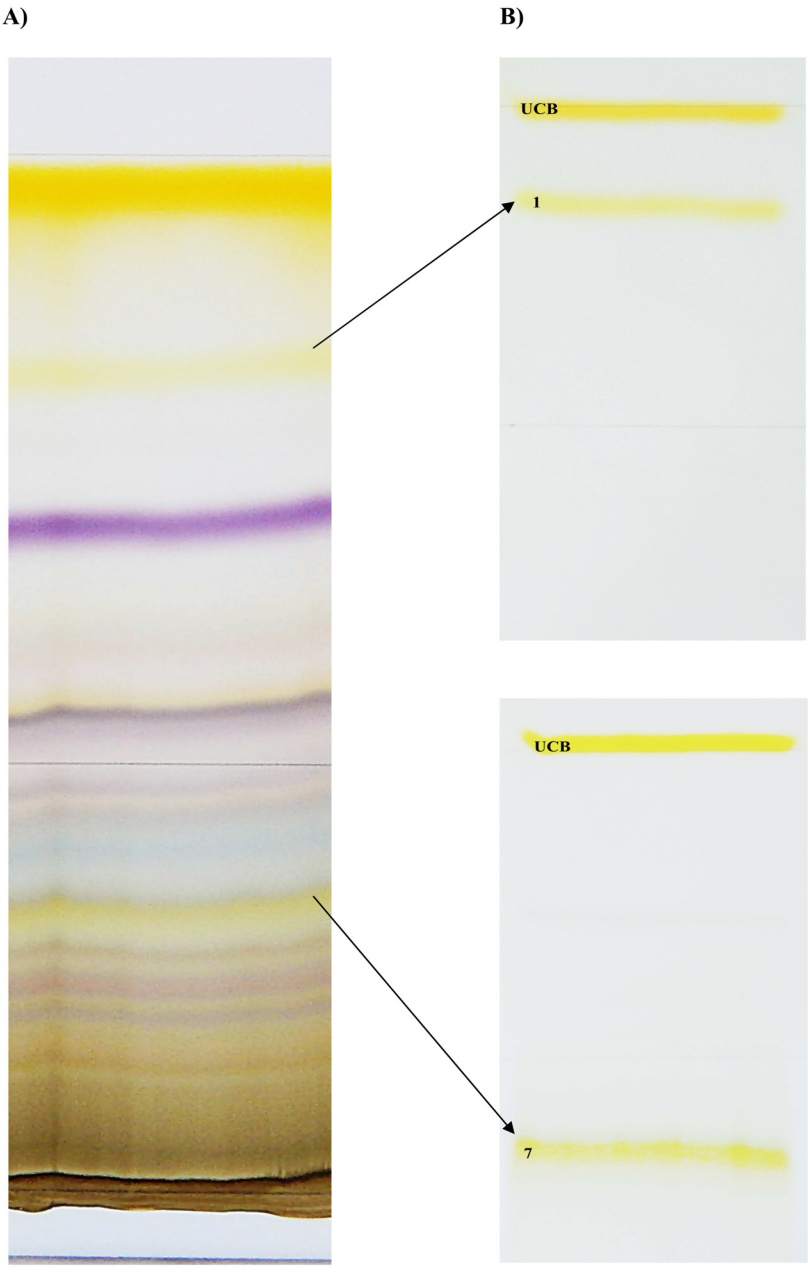

Fig 2. Compounds produced by bilirubin phototherapy. (A) TLC plate after first chromatography. (B) Most important compounds 1 and 7 were separated by re-chromatography from the 1st (upper panel), and 7th zone (lower panel). UCB, unconjugated bilirubin.

doi:10.1371/journal.pone.0148126.g002

1.5×10^{-5} mol/L. Bilirubin did not undergo aggregation, as verified by spectrophotometry [33]. CD spectra were obtained using a J-810 spectropolarimeter (Jasco, Japan) and analyzed as described elsewhere [34]. The method is based on the fact that the unbound pigment does not give any CD signal, and monitoring of their CD intensity provides information about their co-binding or displacement and localization in the albumin subdomains. For determination of the subdomain for lumirubin binding two compounds were used, hemin and bilirubin, as marker ligands for subdomain IB and IIA, respectively [31,35].

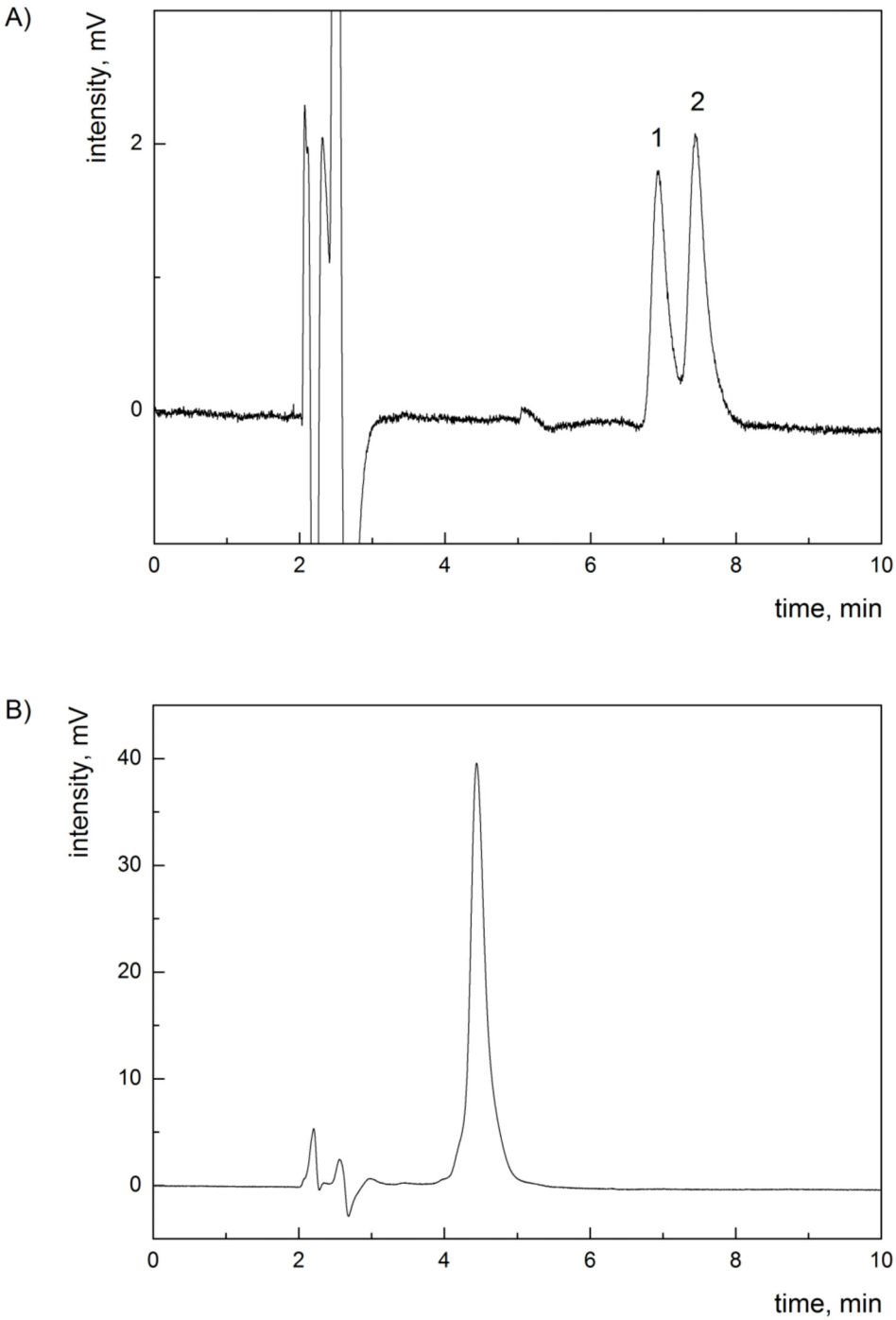

Fig 3. HPLC chromatograms of isolated bilirubin PI. (A) HPLC chromatogram of band 1 from TLC—mixture of ZE/EZ-bilirubins; peak 1 = EZ-bilirubin, peak 2 ZE-bilirubin. (B) HPLC chromatogram of band 7 from TLC—Z-lumirubin.

doi:10.1371/journal.pone.0148126.g003

Determination of Bf

The effect of bilirubin PI on Bf levels was studied by a peroxidase method [36]. Briefly, the standard stock solution of horseradish peroxidase (HRP) was made (1 mg/ml), which was

diluted by PBS to different concentrations ranging from 1:2 to 1:100. For each enzyme dilution the K_p value (oxidation constant of bilirubin) was determined. For enzyme standardization (K_p constant determination, also see below), the solution of bilirubin in PBS without albumin was used (bilirubin concentrations were between 1 and 3 μM). Bilirubin absorbance was measured at 440 nm (Beckman Coulter DU-730 spectrophotometer, CA, USA). Afterwards, 5 μl of H_2O_2 and 10 μl of HRP were added, the solution was slightly mixed, and the decrease of absorbance at 440 nm in 60 s was measured. The K_p constant was counted according to K_p calculation formula (2):

$$K_p = \frac{V_0}{[Bf] \cdot [HRP]} \quad (2)$$

- where K_p = constant for oxidation of bilirubin, and V_0 = the initial oxidation velocity (expressed as ΔAbs/min).

The measurements of Bf in PBS-containing albumin or in complete culture medium was performed with enzymes whose K_p values were similar (in our experimental setup, enzyme dilutions of 1:2, 1:3, and 1:4 were used). We first determined the bilirubin concentration corresponding (under the conditions used) to 140 nM (approximately 24 μM bilirubin). Then, we studied whether Bf is affected by the addition of increasing concentrations of bilirubin PI (15% and 30% of total bilirubin concentrations, respectively, based on the fact that as much as 30% decrease of total serum/plasma bilirubin concentrations can be achieved during phototherapy of neonatal jaundice [37]). A mixture of ZE/EZ-bilirubins and Z-lumirubin was used for these studies. To assess the possible effect of solvent on Bf concentration, DMSO was used in the same concentration as for dissolving of bilirubin PI. To check the stability of bilirubin PI, concentrations of bilirubin IXα, and EZ/ZE-bilirubins as well as Z-lumirubin after 1 and 24 hrs in the incubation medium were analysed by HPLC method (see above). Whereas all studied pigments did not change their concentrations after 1 hr and bilirubin IXα, and EZ/ZE-bilirubins were stable also after 24 hrs under conditions used, concentrations of Z-lumirubin decreased to 31% after 24 hrs.

Cell culture studies

The SH-SY5Y human neuroblastoma cell line was used for the *in vitro* studies (ATCC, Manassas, VA, USA). Authentication of the cell line was confirmed by independent laboratory (Generi Biotech, Czech Republic). The cells were tested for Mycoplasma contamination using the MycoAlert luminescence test (Lonza, Switzerland). Cells were cultured in a mixture of MEM Eagle and Ham's F12 media (1:1, v/v), containing 15% of fetal bovine serum, in 75 cm^2 culture flasks, at 37°C, in a 5% CO_2 atmosphere. For functional tests, cells were seeded at a concentration of 50,000 cells per 1 cm^2.

Cell viability analyses

The effect of bilirubin (24 μM), pure bilirubin PI (5%, 15%, and 30% of bilirubin PI in complete culture media), and the combination of bilirubin with bilirubin PI on cell viability was analyzed by both MTT (Sigma, Germany) as well as by luminescent CellTiter-Glo (Promega, USA) tests, using a Sunrise Microplate Reader (Tecan, Austria) and Synergy 2 Multi-mode Microplate Reader (BioTek, USA), respectively.

Gene expression studies

The effect of bilirubin and bilirubin PI (24 μM bilirubin (corresponding to 140 nM Bf), 15% bilirubin PI, and a mixture of bilirubin and 15% PI) on the expression of genes involved in

Table 1. List of genes used for gene expression analyses.

Gene	Accession Number	Forward	Reverse	Ampl Lenght	Efficiency
CFTR/MRP (ABCC1)	NM_004996.3	tgatggaggctgacaagg	gcggacacatggttacac	127	99.20
MDR/TAP (ABCB1)	NM_000927	tgctcagacaggatgtgagttg	aattacagcaagcctggaacc	122	92.90
HMOX1	NM_002133.2	atgccccaggatttgtca	cccttctgaaagttcctcat	95	95.00
HMOX2	NM_001127204.1	tgagtataacatgcagatattca	ccatcctccaaggtctct	75	92.40
BLVRA	NM_000712	cgttcctgaacctgattg	aaagagcatcctccaaag	87	96.00
CyclinD1	XM_006718653.1	acagatgtgaagttcatt	tagtaggacaggaagttg	110	96.50
CyclinE1	NM_001238.2	agcccttgggacaataatg	cggtcatcatcttctttg	76	94.50
GAPDH	NM_002046	tcagccgcatcttcttttg	gcaacaatatccactttaccag	146	103.00
HPRT1	NM_000194	acatctggagtcctattgacatcg	ccgcccaaagggaactgatag	193	105.00

HPRT1 and GAPDH were used as house-keeping genes.

doi:10.1371/journal.pone.0148126.t001

heme catabolism and in the regulation of the cell cycle (Table 1) was investigated in SH-SY5Y cells exposed to pigments for 1 and 24 hrs, respectively. Briefly, total RNA was isolated in TriReagent (Sigma-Aldrich, St Louis, MO, USA) according to the manufacture's protocol and stored at -80°C until analysis. RNA quantity and purity were evaluated spectrophotometrically at 260 nm, and RNA integrity was evaluated by agarose gel electrophoresis. Retrotranscription of total RNA (1 μg) was performed with an iScript cDNA Synthesis Kit (Bio-Rad Laboratories, Hercules, CA, USA) according to the manufacturer's instructions. The final cDNA was conserved at -20°C until used. The primers for the targeted genes and the two housekeeping genes [hypoxanthine-guanine phosphoribosyltransferase (Hprt1) and glyceraldehydes 3-phosphate dehydrogenase (Gapdh)] were designed using Beacon Designer 2.0 software (PREMIER Biosoft International, Palo Alto, CA, USA). The quantitative analysis of gene expression was performed by real-time PCR. The reaction was performed on 25 ng of cDNA, with the corresponding gene-specific sense and anti-sense primers (250 nM, all genes) with iQ SYBER Green Supermix in an I-Cycler iQ thermocycler (Bio-Rad Laboratories, Hercules, CA, USA). The thermal cycler conditions consisted of 3 min at 95°C; plus 40 cycles each at 95°C for 20 s, 60°C for 20 s, and 72°C for 30 s. A melting curve analysis was performed to assess product specificity. The relative quantification was made using iCycler iQ software, version 3.1 (Bio-Rad Laboratories, Hercules, CA, USA), by the ΔΔCt method, taking into account the efficiencies of the individual's genes, and normalizing the results to the two housekeeping genes [38,39]. The levels of mRNA were expressed relative to a reference sample. The results are expressed as the mean ± SD.

Heme oxygenase activity determination

The activity of heme oxygenase (HMOX) was measured as described previously [40]. In brief, culture media harvested from SH-SY5Y batches were added to CO-free, septum-sealed vials. CO released into the vial headspace was quantified using gas chromatography with a reduction gas analyzer (Peak Laboratories, Mountain View, CA, USA).

Flow cytometry

Cells for flow cytometry analyses were treated with bilirubin (24 μM corresponding to 140 nM Bf), bilirubin PI (15%), and a combination of bilirubin and PI for 1 and 24 hrs. At the end of the treatment the medium was aspired, the cells were washed twice with PBS, then fixed by adding 5 ml of cold (-20°C) 80% ethanol drop-wise under constant gentle vortexing. After

centrifugation (310 x g; RT; 6 min), the sediments were re-suspended in 1 ml of staining solution in PBS containing 0.1% v/v Triton X-100, 20 μg/ml propidium iodide (PI), and 0.2 mg/ml DNAse free RNaseA. Samples were incubated in the dark for 30 min at RT, and subjected to FACS analysis (cytometer BD FACSCalibur TM; and CellQuest software, BD Biosciences, San Jose, CA). Data were collected for 10,000 events per sample.

Statistical analyses

Data are presented as the median and 25–75% range. Differences between variables were evaluated by the Mann-Whitney Rank Sum test. Differences were considered statistically significant when p-values were less than 0.05. Statistical analyses were performed using Prism 6 software (GraphPad, CA, USA).

Results

The isolation of bilirubin PI

Photo-exposure of unconjugated bilirubin, under the conditions defined above, lead to the generation of 18 different PI (Fig 2). These compounds were further characterized by HPLC, UV/VIS spectrophotometry, and mass spectrometry to check for their purity and identity.

Out of these 18 individual substances, several were clearly identified (unconjugated bilirubin, biliverdin, ZE/EZ-bilirubin, and lumirubin); the others are likely to represent unstable, oxidized, and as yet undefined intermediates. Pigments 1 and 7 (Fig 2), identified as ZE/EZ-bilirubins and lumirubin (the principal bilirubin PI), were used for further functional studies. (Figs 2 and 3).

Effect of bilirubin PI on the bilirubin-albumin binding

To investigate whether bilirubin PI might affect Bf levels, we directly analyzed this effect by measuring Bf using a peroxidase method. The addition of 3.6 and 7.2 μM of bilirubin PI (corresponding to 15% and 30% of total bilirubin concentration, respectively) had no effect on the Bf concentration (Fig 4).

To a solution with 140 nM Bf concentration (approximately 24 μM bilirubin), bilirubin PI were added in increasing concentrations (15% and 30%); the resultant bar was constructed from the difference between the decrease of absorbance after addition of bilirubin PI or DMSO to the bilirubin solution. n = 6 for each group.

These data were further confirmed by the study of lumirubin-albumin binding (Table 2), where a fluorescence quenching method was used for the estimation of the albumin binding constant (*Ka*) for bilirubin and lumirubin. Lumirubin had a significantly lower *Ka* compared to bilirubin (Table 2). Its effect was comparable with that of biliverdin, which does not affect bilirubin binding to serum albumin because their high-affinity binding sites are located in two different subdomains (IB for biliverdin, and IIA for bilirubin). In line with this conclusion, the bilirubin-albumin binding constant was notably affected by gossypol, a displacer of bilirubin from HSA [31,32]. Therefore, lumirubin only moderately affected bilirubin binding to HSA (Table 2).

The results of the CD analyses further supported this conclusion. Bilirubin was found to be bound to a high-affinity site inducing the CD positive couplet [460(+)/410(-) nm] that is characteristic for the bound P-conformer of bilirubin (see Fig 5, *left panel*). In the complexes with HSA, bilirubin shows an absorption maximum at 475 nm, which is shifted closer to the red spectrum compared to the unbound pigment in solution (440 nm; as can be seen on Fig 5, *left panel*). In contrast, CD spectrometric analysis of the lumirubin-albumin complex revealed that

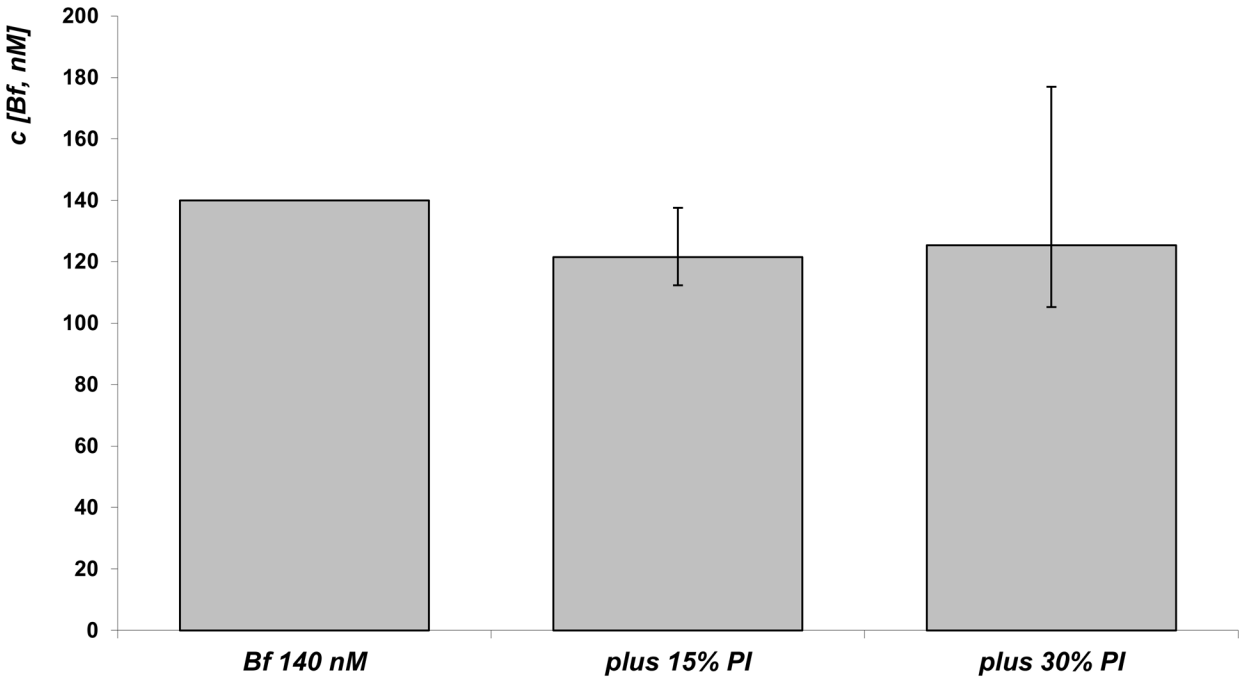

Fig 4. Effect of bilirubin PI on Bf concentrations.

doi:10.1371/journal.pone.0148126.g004

lumirubin has one binding site on HSA with right-helical conformation (it is also a P-conformer) of the bound pigment [weak positive couplet 445(+)/407(-) nm; Fig 5, *left panel*]. The obtained lumirubin-HSA complex had also a slight red-shifted absorption band with the maximum at 445 nm, compared to unbound lumirubin that absorbed at 430 nm.

To clarify the albumin domain that binds lumirubin, three different complexes of HSA and the marker ligand were used (Fig 5, *right panel*). The HSA-bilirubin system (green line, Fig 5A) was first compared with that of HSA-lumirubin (blue line). The resulted signal (black line) of the lumirubin-(HSA-bilirubin) complex is not the sum of lumirubin-HSA and bilirubin, and has indicating that the bilirubin and lumirubin binding sites are not independent. Lumirubin is bound close to the bilirubin high-affinity binding site, and it is able to affect bilirubin binding to HSA. In the HSA-hemin system (CD spectrum in green, Fig 5B), the addition of lumirubin did not induce the positive couplet characteristic for lumirubin bound to HSA (Fig 5B). It confirms that lumirubin and hemin bind to the same binding site. The binding site of lumirubin is localized in the subdomain IB [35] (or at a close distance to it), so the hemin presented there hindered the lumirubin binding. However, in the case where both bilirubin and hemin were bound to HSA (green spectrum in Fig 5C), the addition of lumirubin led to a moderate decrease of the bilirubin signal. This strongly suggests that the binding of lumirubin moderately affects bilirubin binding to HSA, and that the lumirubin binding site is localized close to the hemin and bilirubin binding sites.

Table 2. The binding constant for the ligand-HSA complexes.

	bilirubin-HSA	lumirubin-HSA	bilirubin-(HSA-biliverdin)	bilirubin-(HSA- gossypol)	bilirubin-(HSA-lumirubin)
***Ka* [M^{-1}]**	$(1.8\pm0.3)\cdot10^{8}$	$(9.3\pm0.8)\cdot10^{5}$	$(1.1\pm0.4)\cdot10^{8}$	$(1.4\pm0.2)\cdot10^{5}$	$(8.7\pm1.3)\cdot10^{7}$

HSA, human serum albumin; *Ka*, the binding constant

doi:10.1371/journal.pone.0148126.t002

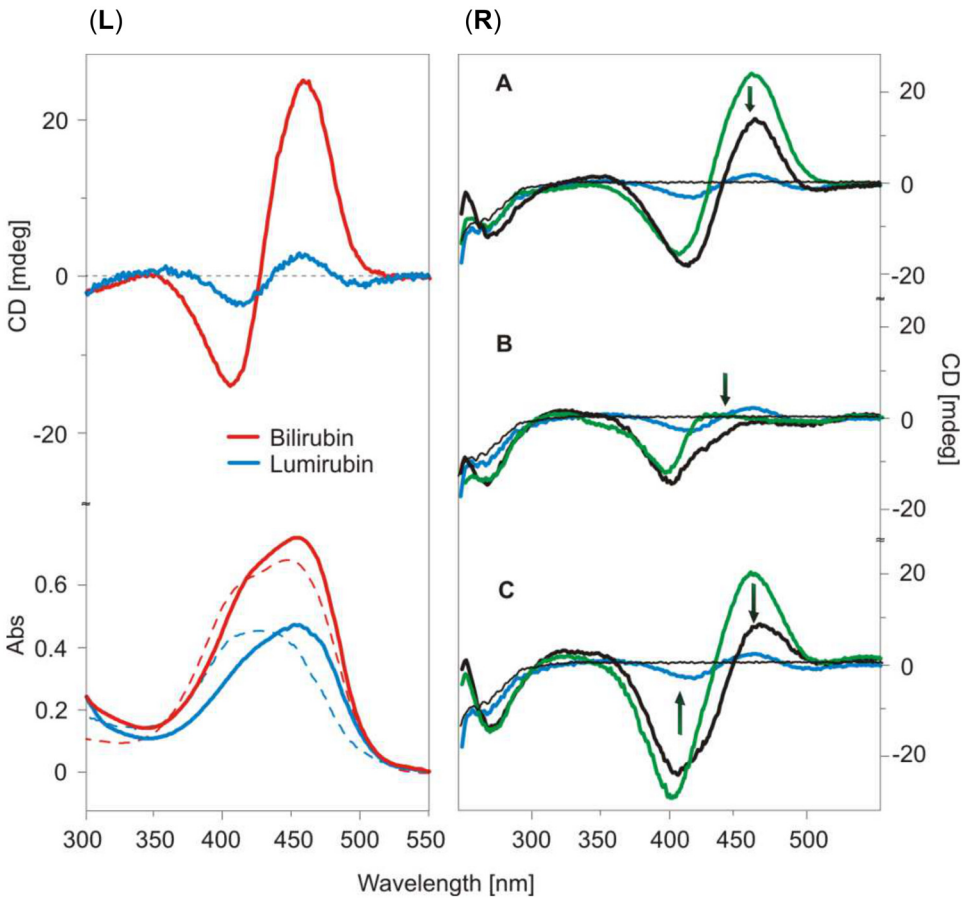

Fig 5. (*Left panel*) CD and UV/Vis absorption spectra of unbound (broken line), lumirubin (blue), bilirubin (red), and their complexes with HSA (full line). Pigment/HSA molar ratio = 1/1; c (pigment) = 1.5 x 10^{-5} mol/L. Bilirubin was dissolved in 0.1 mol/L NaOH and mixed with the HSA solution in PBS (pH 7.4) at the molar ratio [pigment]/[HSA] = 1/1, the concentration of the pigment was 1.5 x 10^{-5} mol/L. **(*Right panel*) Effect of lumirubin on HSA binding with different marker ligands: bilirubin (A), hemin (B), and with both bilirubin and hemin (C)**. CD spectra of HSA-marker ligand are shown in green, lumirubin-HSA complex and lumirubin bound to the complex HSA-marker ligand are shown as blue and black full lines, respectively. Black arrows show the changes in signals after formation of lumirubin-(marker ligand-HSA) complexes. Lumirubin/HSA/marker molar ratio = 1/1/1.

doi:10.1371/journal.pone.0148126.g005

Collectively, our data indicate that lumirubin only negligibly influences bilirubin binding to albumin. Although lumirubin binds to albumin, its binding has a much lower affinity and occurs at a different binding site. Nevertheless, the binding sites for bilirubin and lumirubin are at a close distance to one another, and these binding sites are not independent.

The effect of bilirubin PI on SH-SY5Y cell viability

The short-term exposure (60 min) of bilirubin or its PI did not have any effect on cell viability (data not shown). However, cell viability was significantly reduced after the 24 or 48 hr cell treatments with bilirubin, and this effect further increased after 48 hours of exposure (Fig 6A and 6B, respectively). In contrast, bilirubin PI did not affect cell viability, even after 48 hr exposure and a high concentration used (30%) (Fig 6A and 6B).

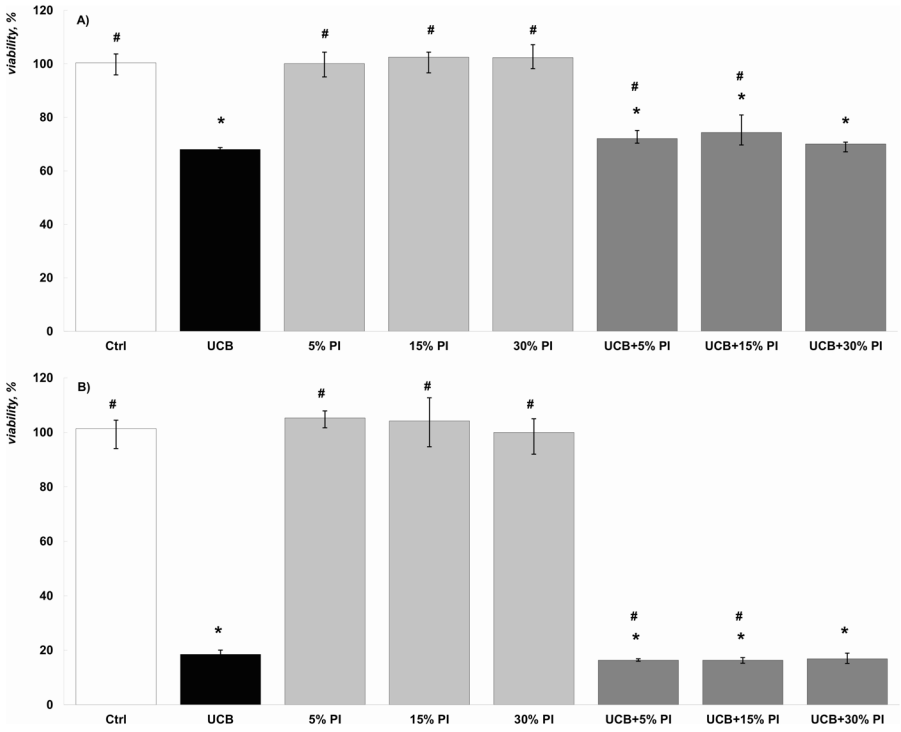

Fig 6. The effect of bilirubin and bilirubin PI on the cell viability in our *in vitro* model. (A) 24 hr exposure; n = 7. (B) 48 hr exposure; n = 4. * $p < 0.05$ vs. control; # $p < 0.05$ vs. bilirubin. Cell viability tested by CellTiter-Glo test; exactly the same results were obtained with MTT test. UCB, unconjugated bilirubin.

doi:10.1371/journal.pone.0148126.g006

The effect of bilirubin and bilirubin PI on expression of genes involved in the heme catabolic pathway and cell cycle progression

Bilirubin is the final product of the heme catabolic pathway, and its formation is under the control of both HMOX and biliverdin reductase (BLVRA). Since these enzymes are protective tools of the organism against increased oxidative stress [41,42] (as well as responsible for bilirubin production), we investigated the effects of PI on the expression of these genes.

The expressions of both *HMOX1* and *HMOX2* were significantly increased after 1 hr of exposure to toxic concentrations of bilirubin, and the same trend was observed also for *BLVRA* (Table 3). These changes in mRNA expressions were, however, not translated onto increase of

Table 3. The effect of bilirubin and bilirubin PI on expression of selected genes.

	Bilirubin	15% PI	Bilirubin+15% PI
HMOX1	232.2 (197–240)*	105.6 (93–109)	277.1 (175–358)*
HMOX2	130.3 (129–166)*	84.8 (74–88)	100.3 (91–151)
BLVRA	142.9 (109–179)	86.3 (53–122)	158.4 (94–180)
MRP1	76.3 (71–90)	84.9 (51–100)	76.7 (61–89)
MDR1	54.9 (35–84)	86.3 (35–113)	87.3 (33–99)
Cyclin D1	71.8 (64–157)	64.5 (52–81)*	175.3 (137–232)*
Cyclin E	78.9 (50–126)	76.4 (59–84)	84.3 (77–106)

data are expressed as % of control (median and IQ range), n = 5 for each measurement. PI, bilirubin photoisomers

* $p < 0.05$ vs. control

doi:10.1371/journal.pone.0148126.t003

HMOX activity (data not shown). Interestingly, exposure to bilirubin PI did not lead to the changes in mRNA expression profiles seen after exposure to bilirubin.

Additionally, no difference was found in the expressions of either *MRP1* or *MDR1*—genes coding transporting proteins responsible for export of multiple compounds also possibly including bilirubin [43,44]. Expressions of genes encoding cyclins D1 and E involved in regulating the G_0 to S phase, and G_1 to S phase transition, respectively [45,46] tended to be down-regulated upon exposure to bilirubin and bilirubin PI (Table 3). Nevertheless, these mRNA expression changes were not functionally translated, as evidenced by flow cytometry analysis of the cell cycle phase of the SH-SY5Y cells exposed to bilirubin, bilirubin PI, or their mixture. This analysis revealed that compared to control cells, treatments with studied pigments had no effect on the cell cycle progression after either short or long exposure (data not shown).

Discussion

Phototherapy is a non-invasive and effective treatment for neonatal hyperbilirubinemia, as well as one which facilitates the disposal of toxic bilirubin and avoids brain injury. Since its development in the 1950's, it has become a standard and widely available treatment for this condition.

Phototherapy can reduce serum bilirubin by its conversion into its structural photoisomers and photooxidation products, which are excreted from the human body without the need of further biotransformation in the liver. It is generally believed that bilirubin photoisomers are non-toxic; however, no clear evidence for this viewpoint exists, and insufficient data about bilirubin PI's biological effects have thus far been provided. [16–23]. Of note is the fact that in none of these studies were the pure forms of the bilirubin photoderivatives used, most likely because of their complicated isolation and handling. To the contrary, short-term as well as long-term side effects of phototherapy have been repeatedly reported [7–12]; the mechanisms of which are unclear and might theoretically be accounted for by the biological activities of bilirubin PI.

In our experiments, we were able to successfully separate 18 different bilirubin photoderivatives generated during photo-irradiation of bilirubin solution. Out of these, we identified and isolated the major bilirubin photoderivatives (ZE/EZ-bilirubin and lumirubin) in sufficient purity and quantity for biological studies.

We were able to demonstrate that these bilirubin PI do not increase Bf levels, and thus do not increase bilirubin toxicity *per se*. Lumirubin was found to have only one binding site on HSA, and this binding site was the same as for hemin (i.e. in the subdomain IB or close to it). Nevertheless, the bilirubin and lumirubin binding sites on albumin are not totally independent, because the lumirubin binding site is close to the bilirubin high-affinity binding site; to a certain extent it is also able to lower bilirubin's ability to bind to HSA. However, this effect is probably not clinically relevant. In support of this data, we confirmed that lumirubin-HSA's binding constant is much lower, compared to bilirubin. These data collectively demonstrate that although lumirubin binds to albumin, the binding has no biological relevance in terms of any possible influence on bilirubin-albumin binding.

The experiments, focused on the potential cytotoxicity of major bilirubin PI, revealed no apparent effects on cell viability in our *in vitro* model, even after prolonged exposure. This was in striking contrast with the known toxic effects of bilirubin. This indicates that only unconjugated bilirubin is toxic, and that the conformational changes induced by irradiation almost completely abolishes the noxious effects of the pigment on the cell.

Neither bilirubin, nor bilirubin PI had any functional effect on two key enzymes (HMOX and BLVRA) important in heme degradation and bilirubin production. The lack of any effect

of bilirubin PI on *BLVRA* mRNA expression was not expected, since biliverdin to some extent is also produced during phototherapy [6]. Similar negative results of bilirubin/bilirubin PI exposure were also found for *MRP1* and *MDR1* mRNA gene expression, indicating that these transporters are not inducible, at least in our cell system, by either bilirubin or their PI.

Our study has several limitations. First, we only assessed the biological effects of three major bilirubin PI, ZE/EZ-bilirubins and Z-lumirubin, and thus we cannot exclude that other photoproducts or bilirubin oxidation products formed during phototherapy, especially those short-lived and not detected in our study, might be toxic. Thus, it is still needed to be carefully assessed, whether minor oxidation products produced from bilirubin during phototherapy can exert any biological action. In addition, our studies were only performed on one cell line, representing a neuronal *in vitro* model. However, other brain cells, such as astrocytes, microglia, or even endothelial cells should also be tested; ideally in an organotypic brain slice *ex vivo* model to bring conclusive evidence.

In conclusion, our data indicate that the major bilirubin PI, ZE/EZ-bilirubin and lumirubin, seem to be biologically inert, and do not exert any negative biological effects. The side effects of phototherapy, theoretically attributable to bilirubin PI, are most likely due to other mechanisms.

Author Contributions

Conceived and designed the experiments: LV CT MU MC. Performed the experiments: JJ MDB EV SG IG MS KV. Analyzed the data: JJ MDB EV SG IG MS KV LV CT MU MC. Contributed reagents/materials/analysis tools: JJ MDB EV SG IG MS KV. Wrote the paper: JJ MDB EV SG IG MS KV LV CT MU MC.

References

1. Cremer RJ, Perryman PW, Richards DH. Influence of light on the hyperbilirubinaemia of infants. Lancet. 1958; 1: 1094–1097. PMID: 13550936
2. Onishi S, Isobe K, Itoh S, Kawade N, Sugiyama S. Demonstration of a geometric isomer of bilirubin-IX alpha in the serum of a hyperbilirubinaemic newborn infant and the mechanism of jaundice phototherapy. Biochem J. 1980; 190: 533–536. PMID: 7470068
3. Onishi S, Miura I, Isobe K, Itoh S, Ogino T, Yokoyama T, et al. Structure and thermal interconversion of cyclobilirubin IX alpha. Biochem J. 1984; 218: 667–676. PMID: 6721828
4. McDonagh AF, Palma LA. Phototherapy for neonatal jaundice. Stereospecific and regioselective photoisomerization of bilirubin bound to human serum albumin and NMR characterization of intramolecularly cyclized photoproducts. J Am Chem Soc. 1982; 104: 6867–6869.
5. Lightner DA, McDonagh AF. Molecular mechanisms of phototherapy for neonatal jaundice. Acc Chem Res. 1984; 17: 417–424.
6. Knobloch E, Mandys F, Hodr R, Hujer R, Mader R. Study of the mechanism of the photoisomerization and photooxidation of bilirubin using a model for the phototherapy of hyperbilirubinemia. J Chromatogr. 1991; 566: 89–99. PMID: 1885724
7. Xiong T, Qu Y, Cambier S, Mu D. The side effects of phototherapy for neonatal jaundice: what do we know? What should we do? Eur J Pediatr. 2011; 170: 1247–1255. doi: 10.1007/s00431-011-1454-1 PMID: 21455834
8. Tatli MM, Minnet C, Kocyigit A, Karadag A. Phototherapy increases DNA damage in lymphocytes of hyperbilirubinemic neonates. Mutat Res. 2008; 654: 93–95. doi: 10.1016/j.mrgentox.2007.06.013 PMID: 18534897
9. Beken S, Aydin B, Zencirogglu A, Dilli D, Ozkan E, Dursun A, et al. The effects of phototherapy on eosinophil and eosinophilic cationic protein in newborns with hyperbilirubinemia. Fetal Pediatr Pathol. 2014; 33: 151–156. doi: 10.3109/15513815.2014.883456 PMID: 24527832
10. Raghavan K, Thomas E, Patole S, Muller R. Is phototherapy a risk factor for ileus in high-risk neonates? J Matern Fetal Neonatal Med. 2005; 18: 129–131. PMID: 16203599
11. Arnold C, Pedroza C, Tyson JE. Phototherapy in ELBW newborns: Does it work? Is it safe? The evidence from randomized clinical trials. Semin Perinatol. 2014; 38: 452–464. doi: 10.1053/j.semperi.2014.08.008 PMID: 25308614

12. Tyson JE, Pedroza C, Langer J, Green C, Morris B, Stevenson D, et al. Does aggressive phototherapy increase mortality while decreasing profound impairment among the smallest and sickest newborns? J Perinatol. 2012; 32: 677–684. doi: 10.1038/jp.2012.64 PMID: 22652561
13. Ostrow JD, Pascolo L, Shapiro SM, Tiribelli C. New concepts in bilirubin encephalopathy. Eur J Clin Invest. 2003; 33: 988–997. PMID: 14636303
14. Calligaris SD, Bellarosa C, Giraudi P, Wennberg RP, Ostrow JD, Tiribelli C. Cytotoxicity is predicted by unbound and not total bilirubin concentration. Pediatr Res. 2007; 62: 576–580. PMID: 18049372
15. Ahlfors CE, Wennberg RP. Bilirubin-albumin binding and neonatal jaundice. Semin Perinatol. 2004; 28: 334–339. PMID: 15686264
16. Roll EB. Bilirubin-induced cell death during continuous and intermittent phototherapy and in the dark. Acta Paediatr. 2005; 94: 1437–1442. PMID: 16263630
17. Roll EB, Christensen T. Formation of photoproducts and cytotoxicity of bilirubin irradiated with turquoise and blue phototherapy light. Acta Paediatr. 2005; 94: 1448–1454. PMID: 16263632
18. Roll EB, Christensen T, Gederaas OA. Effects of bilirubin and phototherapy on osmotic fragility and haematoporphyrin-induced photohaemolysis of normal erythrocytes and spherocytes. Acta Paediatr. 2005; 94: 1443–1447. PMID: 16263631
19. Christensen T, Roll EB, Jaworska A, Kinn G. Bilirubin- and light induced cell death in a murine lymphoma cell line. J Photochem Photobiol B. 2000; 58: 170–174. PMID: 11233646
20. Christensen T, Kinn G, Granli T, Amundsen I. Cells, bilirubin and light: formation of bilirubin photoproducts and cellular damage at defined wavelengths. Acta Paediatr. 1994; 83: 7–12. PMID: 8193477
21. Christensen T, Reitan JB, Kinn G. Single-strand breaks in the DNA of human cells exposed to visible light from phototherapy lamps in the presence and absence of bilirubin. J Photochem Photobiol B. 1990; 7: 337–346. PMID: 2128329
22. Silberberg D, Johnson L, Schutta H, Ritter L. Photodegradation products of bilirubin studied in myelinating cerebellum cultures. Birth Defects Orig Artic Ser. 1970; 6: 119–123. PMID: 4941648
23. Silberberg DH, Johnson L, Schutta H, Ritter L. Effects of photodegradation products of bilirubin on myelinating cerebellum cultures. J Pediatr 1970; 77: 613–618. PMID: 5454708
24. McDonagh AF, Assisi F. The ready isomerization of bilirubin IX-a in aqueous solution. Biochem J. 1972; 129: 797–800. PMID: 4659001
25. Stoll MS, Zenone EA, Ostrow JD, Zarembo JE. Preparation and properties of bilirubin photoisomers. Biochem J. 1979; 183: 139–146. PMID: 534477
26. Stoll MS, Vicker N, Gray CH, Bonnett R. Concerning the structure of photobilirubin II. Biochem J. 1982; 201: 179–188. PMID: 7082282
27. Bonnett R, Buckley DG, Hamzetash D, Hawkes GE, Ioannou S, Stoll MS. Photobilirubin II. Biochem J. 1984; 219: 1053–1056. PMID: 6743241
28. McDonagh AF, Agati G, Fusi F, Pratesi R. Quantum yields for laser photocyclization of bilirubin in the presence of human serum albumin. Dependence of quantum yield on excitation wavelength. Photochem Photobiol. 1989; 50: 305–319. PMID: 2780821
29. McDonagh AF, Palma LA, Trull FR, Lightner DA. Phototherapy for neonatal jaundice. Configurational isomers of bilirubin. J Am Chem Soc. 1982; 104: 6865–6869.
30. Lakowicz JR (2006) Principles of fluorescence spectroscopy. New York: Springer. xxvi, 954 p. p.
31. Goncharova I, Orlov S, Urbanova M. The location of the high- and low-affinity bilirubin-binding sites on serum albumin: ligand-competition analysis investigated by circular dichroism. Biophys Chem. 2013; 180–181: 55–65. doi: 10.1016/j.bpc.2013.06.004 PMID: 23838624
32. Royer RE, Vander Jagt DL. Gossypol binds to a high-affinity binding site on human serum albumin. FEBS Lett. 1983; 157: 28–30. PMID: 6862017
33. Brodersen R. Binding of bilirubin to albumin. CRC Crit Rev Clin Lab Sci. 1980; 11: 305–399. PMID: 6985857
34. Goncharova I, Urbanova M. Stereoselective bile pigment binding to polypeptides and albumins: a circular dichroism study. Anal Bioanal Chem. 2008; 392: 1355–1365. doi: 10.1007/s00216-008-2427-8 PMID: 18946665
35. Zsila F. Subdomain IB is the third major drug binding region of human serum albumin: toward the three-sites model. Mol Pharm. 2013; 10: 1668–1682. doi: 10.1021/mp400027q PMID: 23473402
36. Ahlfors CE. Measurement of plasma unbound unconjugated bilirubin. Anal Biochem. 2000; 279: 130–135. PMID: 10706781
37. Mreihil K, McDonagh AF, Nakstad B, Hansen TW. Early isomerization of bilirubin in phototherapy of neonatal jaundice. Ped Res. 2010; 67: 656–659.

38. Vandesompele J, De Preter K, Pattyn F, Poppe B, Van Roy N, De Paepe A, et al. Accurate normalization of real-time quantitative RT-PCR data by geometric averaging of multiple internal control genes. Genome Biol. 2002; 3: RESEARCH0034. PMID: 12184808

39. Bustin SA, Benes V, Garson JA, Hellemans J, Huggett J, Kubista M, et al. The MIQE guidelines: minimum information for publication of quantitative real-time PCR experiments. Clin Chem. 2009; 55: 611–622. doi: 10.1373/clinchem.2008.112797 PMID: 19246619

40. Vreman HJ, Wong RJ, Kadotani T, Stevenson DK. Determination of carbon monoxide (CO) in rodent tissue: effect of heme administration and environmental CO exposure. Anal Biochem. 2005; 341: 280–289. PMID: 15907874

41. Vitek L, Schwertner HA. The heme catabolic pathway and its protective effects on oxidative stress-mediated diseases. Adv Clin Chem. 2007; 43: 1–57. PMID: 17249379

42. Abraham NG, Kappas A. Pharmacological and clinical aspects of heme oxygenase. Pharmacol Rev. 2008; 60: 79–127. doi: 10.1124/pr.107.07104 PMID: 18323402

43. Gazzin S, Berengeno AL, Strazielle N, Fazzari F, Raseni A, Ostrow JD, et al. Modulation of Mrp1 (ABCc1) and Pgp (ABCb1) by bilirubin at the blood-CSF and blood-brain barriers in the Gunn rat. PLoS One. 2011; 6: e16165. doi: 10.1371/journal.pone.0016165 PMID: 21297965

44. Rigato I, Pascolo L, Fernetti C, Ostrow JD, Tiribelli C. The human multidrug-resistance-associated protein MRP1 mediates ATP-dependent transport of unconjugated bilirubin. Biochem J. 2004; 383: 335–341. PMID: 15245331

45. Pestell RG. New roles of cyclin D1. Am J Pathol. 2013; 183: 3–9. doi: 10.1016/j.ajpath.2013.03.001 PMID: 23790801

46. Moroy T, Geisen C. Cyclin E. Int J Biochem Cell Biol. 2004; 36: 1424–1439. PMID: 15147722

PUBLIKACE VI

Ubiquinone-binding site mutagenesis reveals the role of mitochondrial complex II in cell death initiation

Kluckova, K.; Sticha, M.; Cerny, J.; et al.

CELL DEATH & DISEASE Volume: 6 Article Number: e1749 2015

OPEN

Citation: Cell Death and Disease (2015) 6, e1749; doi:10.1038/cddis.2015.110

www.nature.com/cddis

Ubiquinone-binding site mutagenesis reveals the role of mitochondrial complex II in cell death initiation

K Kluckova[1], M Sticha[2], J Cerny[1], T Mracek[3], L Dong[4], Z Drahota[3], E Gottlieb[5], J Neuzil*[,1,4] and J Rohlena*[,1]

Respiratory complex II (CII, succinate dehydrogenase, SDH) inhibition can induce cell death, but the mechanistic details need clarification. To elucidate the role of reactive oxygen species (ROS) formation upon the ubiquinone-binding (Q_p) site blockade, we substituted CII subunit C (SDHC) residues lining the Q_p site by site-directed mutagenesis. Cell lines carrying these mutations were characterized on the bases of CII activity and exposed to Q_p site inhibitors MitoVES, thenoyltrifluoroacetone (TTFA) and Atpenin A5. We found that I56F and S68A SDHC variants, which support succinate-mediated respiration and maintain low intracellular succinate, were less efficiently inhibited by MitoVES than the wild-type (WT) variant. Importantly, associated ROS generation and cell death induction was also impaired, and cell death in the WT cells was malonate and catalase sensitive. In contrast, the S68A variant was much more susceptible to TTFA inhibition than the I56F variant or the WT CII, which was again reflected by enhanced ROS formation and increased malonate- and catalase-sensitive cell death induction. The R72C variant that accumulates intracellular succinate due to compromised CII activity was resistant to MitoVES and TTFA treatment and did not increase ROS, even though TTFA efficiently generated ROS at low succinate in mitochondria isolated from R72C cells. Similarly, the high-affinity Q_p site inhibitor Atpenin A5 rapidly increased intracellular succinate in WT cells but did not induce ROS or cell death, unlike MitoVES and TTFA that upregulated succinate only moderately. These results demonstrate that cell death initiation upon CII inhibition depends on ROS and that the extent of cell death correlates with the potency of inhibition at the Q_p site unless intracellular succinate is high. In addition, this validates the Q_p site of CII as a target for cell death induction with relevance to cancer therapy.

Cell Death and Disease (2015) **6,** e1749; doi:10.1038/cddis.2015.110; published online 7 May 2015

Mitochondrial respiratory complex II (CII), aka succinate dehydrogenase (SDH), directly links the tricarboxylic acid (TCA) cycle to the electron transport chain (ETC) by mediating electron transfer from the TCA cycle metabolite succinate to ubiquinone (UbQ).[1] For this reason, CII is subjected to a high electron flux between the succinate-binding dicarboxylate site in the matrix-exposed subunit A and the proximal UbQ-binding (Q_p) site, formed by the subunits C (SDHC) and D embedded in the mitochondrial inner membrane (Figure 1b).[2–5] Disruption of electron transfer to UbQ, for example by Q_p site inhibition, leads to reactive oxygen species (ROS) generation from CII due to the leakage of 'stalled' electrons to molecular oxygen at the reduced flavin adenine dinucleotide (FAD) prosthetic group. However, ROS production from reduced FAD is only possible when the adjacent dicarboxylate site is neither occupied by its substrate succinate, typically at low succinate conditions, nor inhibited by other dicarboxylates, for example by malonate.[6–10]

Beyond bioenergetics, CII has emerged as an important factor in cell death induction.[11,12] On one hand, it has been proposed that increased ROS production from CII, resulting from changes in matrix pH and calcium status, amplifies cell death signals originating at other sites.[12–15] On the other hand, the inhibition of CII may also directly initiate cell death, as suggested by our previous results with vitamin E (VE) analogs such as the mitochondrially targeted VE succinate (MitoVES). This compound inhibits CII activity leading to ROS generation and cell death induction in cancer cells, as evidenced by the suppression of tumor growth in experimental animal models.[16–20] The efficacy of MitoVES is greatly reduced in the absence of functional CII, and computer modeling along with other corroborative evidence suggests that MitoVES binds to the Q_p site of CII.[16] However, this is only circumstantial evidence with respect to cell death induction, as cells lacking electron flux within CII due to a structural defect should not be able to produce CII-derived

[1]Institute of Biotechnology, Academy of Sciences of the Czech Republic, Prague, Czech Republic; [2]Faculty of Sciences, Charles University, Prague, Czech Republic; [3]Institute of Physiology, Academy of Sciences of the Czech Republic, Prague, Czech Republic; [4]School of Medical Science, Griffith University, Southport, Queensland, Australia and [5]The Beatson Institute for Cancer Research, Glasgow, UK

*Corresponding author: J Neuzil, Mitochondria, Apoptosis and Cancer Research Group, School of Medical Science and Griffith Health Institute, Griffith University, Southport, Queensland 4222, Australia. E-mail: j.neuzil@griffith.edu.au

or J Rohlena, Molecular Therapy Group, Institute of Biotechnology, Academy of Sciences of the Czech Republic, Videnska 1083, Prague 4 142 20, Czech Republic. E-mail: jakub.rohlena@ibt.cas.cz

Abbreviations: α-TOS, alpha tocopheryl succinate; CII, respiratory complex II; SDH, succinate dehydrogenase; CCCP, carbonyl cyanide 3-chlorophenylhydrazone; ETC, electron transport chain; FAD, flavin adenine dinucleotide; FCCP, carbonyl cyanide 4-(trifluoromethoxy)phenylhydrazone; GFP, green fluorescence protein; GPD2, mitochondrial glycerophosphate dehydrogenase; MitoVES, mitochondrially targeted vitamine E succinate; Q_p site, proximal ubiquinone binding site; ROS, reactive oxygen species; SDHC, CII subunit C; SQR, succinate-ubiquinone reductase; TCA, tricarboxylic acid; TTFA, thenoyltrifluoroacetone; TMRM, tetramethylrhodamine methyl ester; UbQ, ubiquinone; VE, vitamin E

Received 12.9.14; revised 22.1.15; accepted 19.2.15; Edited by A Finazzi-Agrò

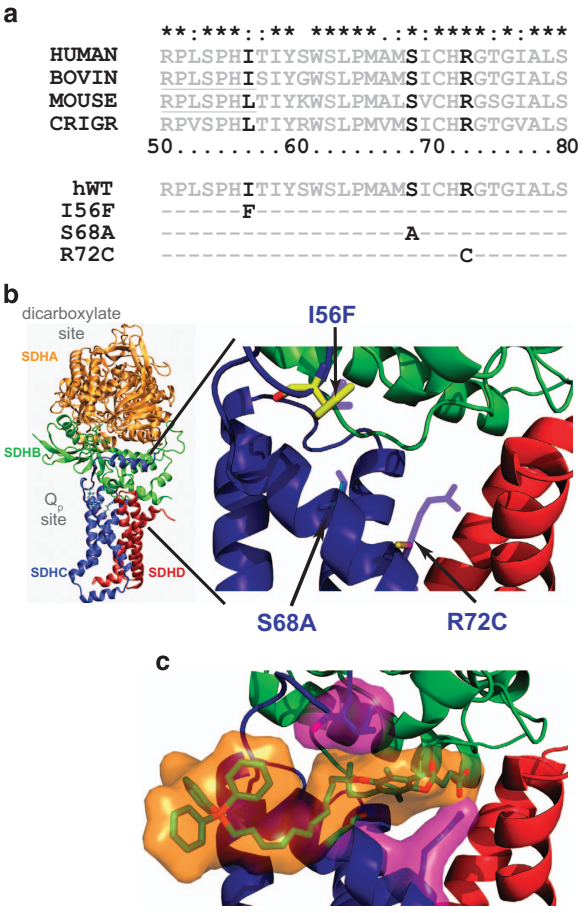

Figure 1 Amino-acid substitutions in the Q_p site of CII. (**a**) Multiple species alignment of the SDHC region bordering the Q_p site shows a high level of conservation. Amino-acid substitutions prepared for this study are indicated in human SDHC. (**b**) Three dimensional representation of CII and the topology of the Q_p site. SDHC residues mutated in this study are indicated by arrows. Displayed is the humanized crystal structure of porcine CII.[3] (**c**) A snapshot from molecular dynamics simulation of MitoVES interaction with the Q_p site of CII in the presence of phospholipid bilayer.[16] One of the possible conformations of MitoVES is shown in orange, substituted SDHC residues are depicted in magenta

ROS. Accordingly, not only the direct cell death initiation upon CII inhibition will be compromised in this situation, but also the indirect signal amplification mentioned above will be affected.

In the present study, we combined site-directed mutagenesis of Q_p site amino-acid residues with the use of Q_p site inhibitors MitoVES, thenoyltrifluoroacetone (TTFA) and Atpenin A5 to assess the link between Q_p site inhibition and cell death initiation. We show that for MitoVES and TTFA, the potency of Q_p site inhibition correlates with the extent of ROS production and cell death induction in respiration-competent CII variants, and that the induced cell death is dependent on CII-derived ROS.

Atpenin, however, did not induce cell death, possibly due to the rapid accumulation of succinate in intact cells, incompatible with ROS generation from CII. These results provide evidence for the role of CII in cell death initiation and establish the Q_p site as a target for cell death induction.

Results

CII Q_p site mutagenesis and the experimental model. To explore the role of CII in cell death induction, we performed site-directed mutagenesis within SDHC, a CII subunit that contributes to Q_p site formation.[3] We concentrated on SDHC residues predicted to be in close contact with bound MitoVES. Serine 68 was mutated to alanine, arginine 72 was replaced by cysteine, and isoleucine 56 was substituted by phenylalanine (Figure 1). Recent data indicate reduced cell death induction by MitoVES in the S68A variant,[16] but the functional consequences of this mutation for CII activity have not been studied. Nevertheless, substitutions of S68 as well as of R72 are expected to compromise CII activity, based on analogy with *E.coli* and *S. cerevisiae* SDH.[21–24] The I56 residue is further away from the Q_p site and its role in CII function is unknown. To evaluate these substitutions, we utilized a mammalian model of SDHC deficiency, the Chinese hamster lung fibroblast cell line B9.[25] These cells lack the functional CII due to a nonsense mutation in the SDHC subunit and fail to assemble CII. In consequence they do not respire on succinate and are completely devoid of CII enzymatic activity. Stable transfectants of human wild-type (WT) and variant SDHC cDNA were prepared in B9 cells, and the clones with similar level of SDHC were selected. These cells were further transformed by H-Ras fused to green fluorescence protein (GFP), making them plausible models to study the effect of MitoVES and other Q_p site inhibitors on transformed cells (Supplementary Figure S1). Transformants with similar level of H-Ras were selected to control for H-Ras level.

Q_p site mutations differentially affect CII assembly and enzymatic function. The selected clones did not significantly differ in their mitochondrial content, as evidenced by similar citrate synthase activity and mitochondrial protein levels (Figures 2a and b). Mitochondrial morphology and membrane potential were also similar for all the tested cell lines (Figures 2c and d). To verify CII assembly, mitochondrial fractions were subjected to blue native gel electrophoresis and western blotting using an anti-SDHA antibody. As expected, parental B9 cells did not assemble CII. In contrast, CII was fully assembled in WT and most of the SDHC variant cells (Figure 2e), with a minor assembly defect found for R72C variant. These results were confirmed using an in-gel SDH activity assay (Figure 2e), which documented assembled CII with functional dicarboxylate site in all variants except for B9 cells. To assess the condition of the Q_p site and its functional coupling to the dicarboxylate site, succinate-UbQ reductase (SQR) activity in the mitochondrial fraction was determined. Whereas no SQR activity was measurable in B9 cells (Figure 2f), it was high in WT and I56F clones. For S68A and R72C variants the SQR activity was significantly reduced yet remained above the level of parental B9 cells. This suggests that although CII assembles properly in all tested variants, there is a defect in electron transfer to UbQ in the S68A and R72C variants.

Q_p site mutations differentially affect basal CII-driven respiration under native conditions. As the CII activity

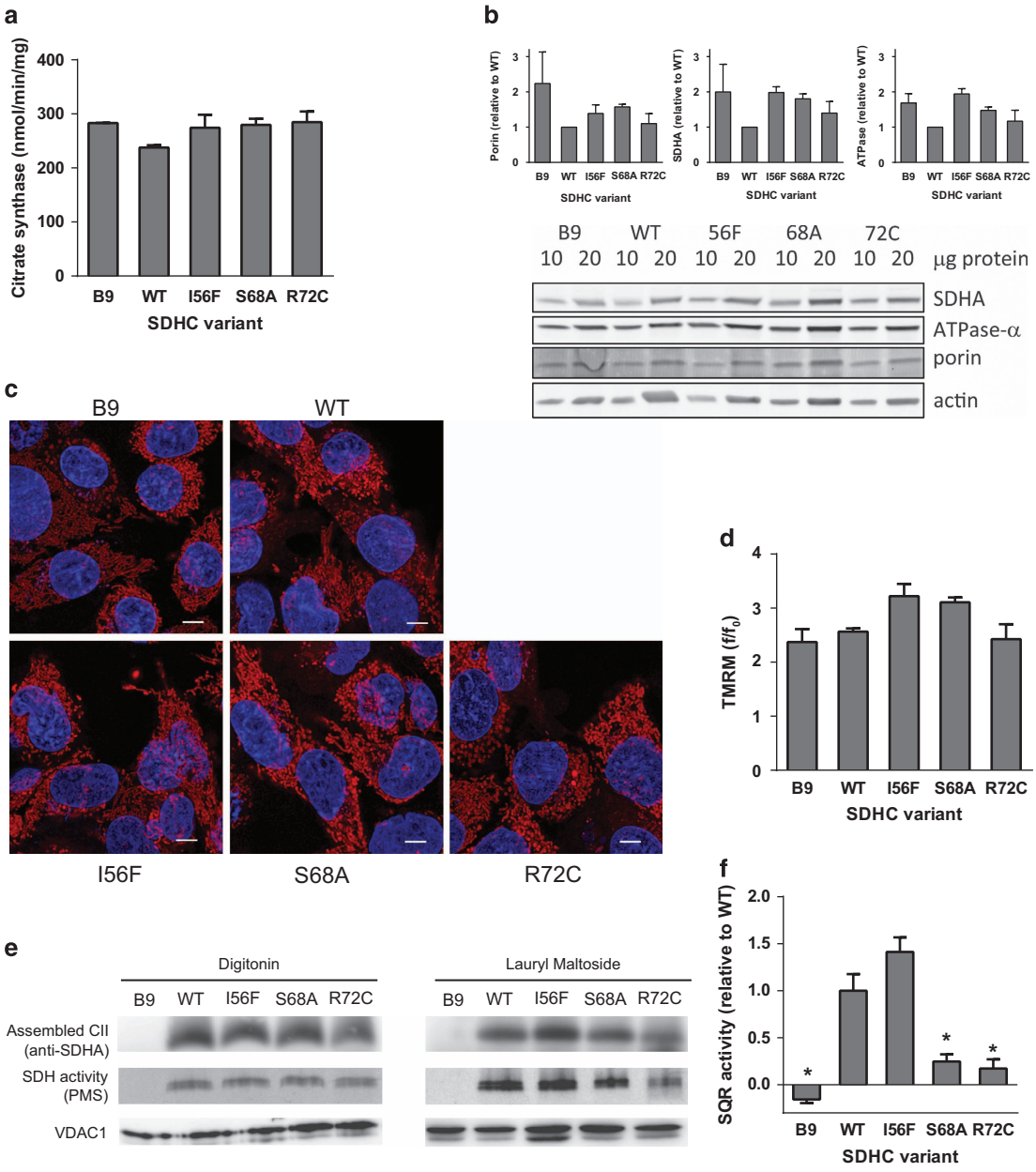

Figure 2 Q_p site substitutions do not decrease mitochondrial content, membrane potential or CII assembly, but can compromise CII activity in the presence of detergents. (**a**) Citrate synthase was measured in the whole-cell lysates and corrected to the protein content. (**b**) Selected mitochondrial proteins were analyzed by western blotting using 10 and 20 μg of whole-cell protein. A representative blot is shown along with quantifications based on three independent experiments (**c**) Mitochondria were visualized by live confocal microscopy using TMRM, the nuclei were counterstained by Hoechst 33342. Scale bar, 5 μm. (**d**) Mitochondrial membrane potential was determined as a ratio of TMRM loading in the presence and absence of FCCP, $n = 3$, mean $\pm$ S.E.M. (**e**) Native blue gel electrophoresis of either digitonin- or lauryl maltoside-solubilized mitochondrial fraction isolated from CII variant cell lines. Assembled CII was detected by anti-SDHA antibody, or by in-gel SDH activity assay using PMS (phenazine methosulfate). Representative experiments are shown (**f**) SQR activity measurement in isolated mitochondrial fraction in the presence of 0.1% Triton X-100 indicates activity impairment for amino-acid substitutions in position S68 and R72. Data represent mean values $\pm$ S.E.M. of three independent experiments. The symbol * indicates values significantly different from WT

assays described above were done on solubilized enzyme, we also examined the effect of Q_p site mutations on CII-mediated respiration in a more natural environment of permeabilized cells. In this set-up respiratory substrates can reach mitochondria, but the mitochondrial outer and inner membranes remain intact in their 'native', undisturbed condition.[26] In the presence of the CII substrate succinate, WT, S68A and, in particular, I56F cells efficiently consumed oxygen. In contrast, R72C and parental B9 cells showed little or no respiration (Figure 3a). The uncoupler carbonyl cyanide 4-(trifluoromethoxy)phenylhydrazone (FCCP) significantly increased oxygen consumption in WT and I56F, but not in S68A, R72C or B9 cells (Figure 3a). Hence, the S68A mutation only affects the reserve capacity of this mutant and may not be limiting in intact cells. In contrast, a severe defect in R72C CII substantially compromises its ability to support

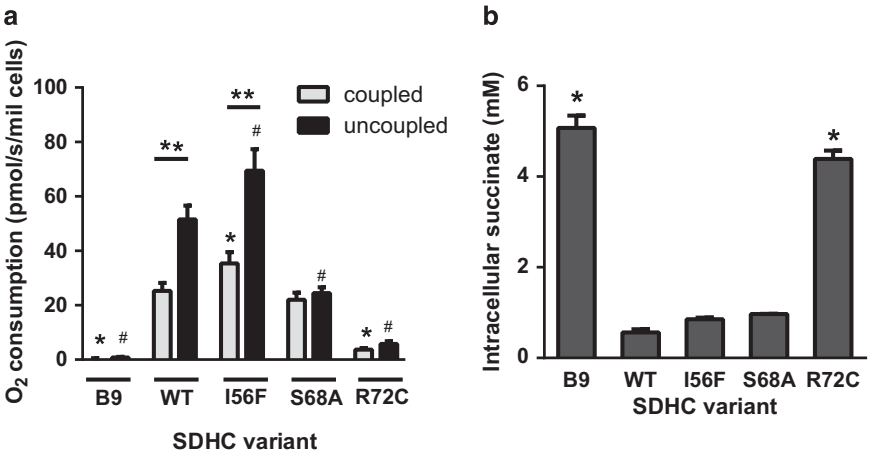

Figure 3 Substitutions in the Q_p site affect CII activity less severely in the native environment. (**a**) Oxygen consumption of digitonin-permeabilized cells respiring on 10 mM succinate in the presence of rotenone and ADP (coupled) and the maximal rate after addition of FCCP (uncoupled). While I56F and S68A variants support the respiration on succinate, B9 and R72C cells are deficient. The S68A defect is apparent only upon uncoupling. Mean ± S.E.M. of 3–4 independent experiments. The symbol * indicates values significantly different from WT in the coupled state (oneway ANOVA), the symbol # values significantly different from WT in the uncoupled state (oneway ANOVA) and the symbol ** values significantly increased after FCCP addition (*t*-test). (**b**) Intracellular succinate measured by mass spectroscopy in extracts from an equal number of cells indicates functional CII in the WT, I56F and S68A. Mean ± S.E.M. of two independent experiments, the symbol * indicates values significantly different from WT

respiration. To confirm these findings in intact cells, we determined the steady-state levels of intracellular succinate, a proxy for CII activity.[27] As shown in Figure 3b, succinate concentration in WT, I56F and S68A cells was low, consistent with fully functional CII. On the other hand, in B9 and R72C cells the succinate levels were considerably increased. These data demonstrate that whereas B9 and R72C cells cannot utilize succinate for respiration due to the absent or dysfunctional CII, WT, I56F and S68A cells maintain CII respiration under coupled conditions expected to occur in a physiological situation.

Q_p site mutations compromise the efficacy of cell death induction by MitoVES. Should cell death induction by the VE analog MitoVES be dependent on its binding to the Q_p site of CII as our previous work suggested,[16] then the efficacy of this agent would be compromised in Q_p site mutants. Hence, the variant cell lines were exposed to MitoVES, a compound previously described to induce apoptosis,[17] and the percentage of annexin V-positive cells quantified. The induced cell death displayed signs typical for apoptosis (Supplementary Figures S2A and B), and was significantly reduced in all tested variant cell lines compared with WT cells (Figure 4a). In fact, all substitutions in the Q_p site reduced MitoVES-induced cell death nearly to the level observed in parental B9 cells. Given the absence of assembled CII in B9 cells, this basal level of cell death must be CII independent and possibly related to the direct effect of MitoVES on cytochrome c.[28]

As ROS generation is the pivotal, early event in the cell death-initiating cascade induced by MitoVES,[16,17] we assessed ROS production in cultured cells upon MitoVES treatment with dihydroethidium, a fluorescent probe responsive to superoxide. Compared with WT, all Q_p site variant cells showed reduced ROS formation, which remained at the level similar to that of parental B9 cells (Figure 4b). In addition, catalase overexpression and co-treatment with the dicarboxylate site inhibitor malonate reduced cell death and ROS production in WT cells to the level found in the mutants (Figures 4c–e). These data indicate that the Q_p site mutations decrease the efficacy of MitoVES-induced ROS generation and that the induced cell death depends on CII-derived ROS.

Mitochondrial glycerophosphate dehydrogenase (GPD2) feeds electrons into the mitochondrial UbQ pool similarly to CII and can also produce ROS. It has recently been shown that alpha tocopheryl succinate (*α*-TOS), an untargeted analog of MitoVES, inhibits GPD2 activity in brown adipose tissue (BAT).[29] However, it is unlikely that GPD2 is responsible for the observed ROS and cell death induction upon MitoVES treatment in our experimental model, as the GPD2 levels are much lower than in BAT (Supplementary Figure S2D). In addition, GPD2 inhibition by *α*-TOS decreases, rather than increases, GPD2-derived ROS[29], and MitoVES accumulation at the inner mitochondrial membrane/matrix interface[16] owing to the mitochondria-targeting triphenyl phosphonium group will keep it physically separated from the intermembrane space-localized GPD2. The role of the reverse electron flow from GPD2 to FAD[6] in CII and subsequent ROS generation from that site can also be discounted, as this would be inhibited, not stimulated, by MitoVES bound to the Q_p site. Therefore, CII functioning in the forward manner is the likely source of ROS observed upon MitoVES treatment of the intact cells.

Sensitivity to Q_p site inhibition correlates with the efficacy of cell death induction unless succinate is rapidly accumulated. If the attenuated ROS and cell death induction described above resulted from the reduced displacement of UbQ by MitoVES at the Q_p site of variant CII, then these variants should display resistance to inhibition by MitoVES. For this reason, we assessed the effect of increasing concentrations of MitoVES on CII-driven

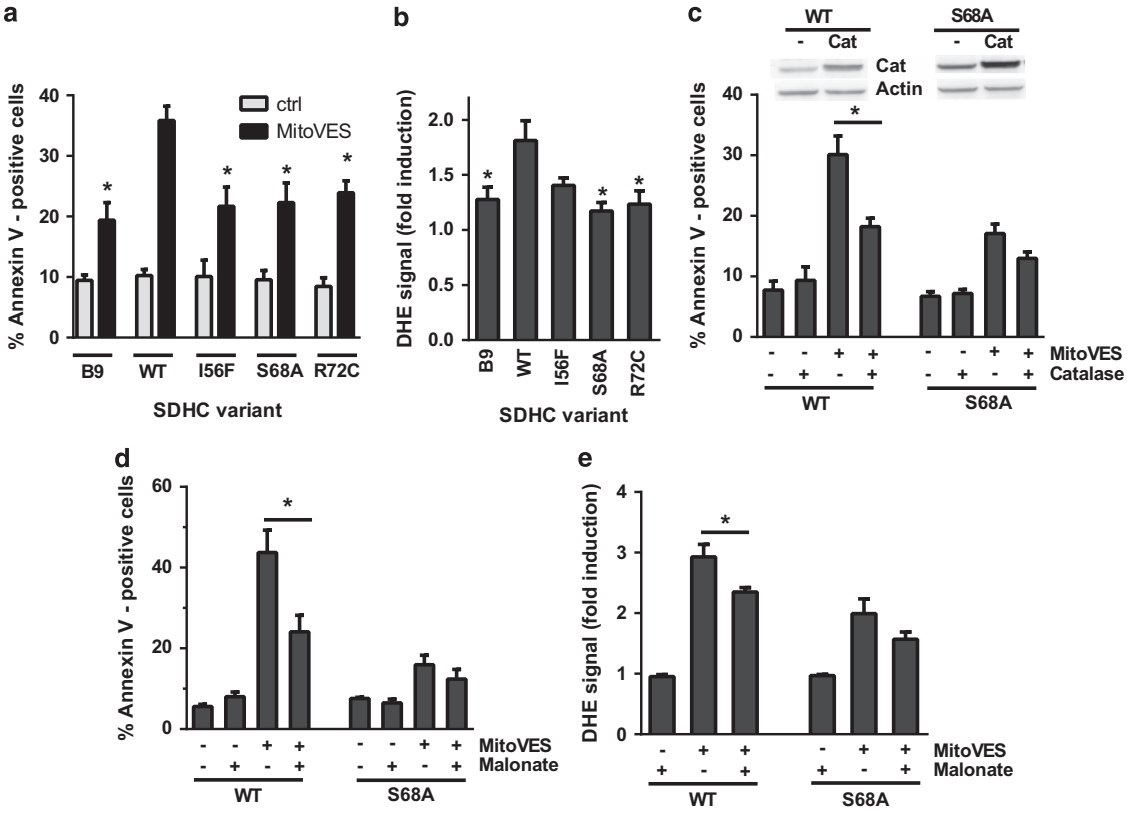

Figure 4 Q_p site substitutions lead to reduced cell death induction and ROS generation in response to MitoVES, and the induced cell death is dependent on CII-derived ROS. (**a**) Variant cell lines were exposed to 20 μM MitoVES for 24 h and the percentage of annexin V-positive cells was determined by flow cytometry. $n \geq 5$, mean $\pm$ S.E.M., * values significantly different from WT. (**b**) Variant cell lines were exposed to 2 μM MitoVES for 30 min and the level of ROS was determined by dihydroethidium (DHE) staining and flow cytometry. $n \geq 5$, mean $\pm$ S.E.M., * values significantly different from WT. (**c**) Cells were transfected with catalase-coding or control vector, exposed to 20 μM MitoVES for 20 h and the percentage of annexin V-positive cells was determined by flow cytometry. $n \geq 4$, mean $\pm$ S.E.M., * values significantly different between catalase and mock-transfected cells. Inset, catalase overexpression verified by western blot. (**d**) Cells were exposed to 30 μM MitoVES for 12 h in the presence or absence of 20 mM malonate (30 min pretreatment). The percentage of annexin V-positive cells was determined by flow cytometry. $n \geq 3$, mean $\pm$ S.E.M., * values significantly different in the presence and absence of malonate. (**e**) Cells were exposed to 5 μM MitoVES for 30 min in the presence or absence of 50 mM malonate (30 min pretreatment) and the level of ROS was determined by DHE staining and flow cytometry. $n = 5$, mean $\pm$ S.E.M., * values significantly different in the presence and absence of malonate

respiration at high succinate (10 mM). Only respiration-competent variants, that is WT, I56F and S68A lines, were used in this experiment. As shown in Figure 5a, the efficacy of respiration inhibition was reduced for I56F and S68A variants compared with the WT cells, in direct correlation with the observed decrease in ROS levels and cell death induction (see, for example, Figures 4a and b). In contrast to MitoVES, malonate suppressed oxygen consumption similarly for all the CII variants tested (Figure 5b), confirming that the mutations introduced do not substantially affect the dicarboxylate site.

To better understand this phenomenon, we performed *in silico* molecular docking simulation of MitoVES and UbQ with the Q_p site of WT and variant CII. These simulations support the assumption that steric hindrance and differences in affinity can explain the less efficient inhibition by MitoVES in S68A and I56F CII (Supplementary Figures S3B and C). Since MitoVES is a relatively large molecule (Supplementary Figure S3A), we also examined the much smaller Q_p site inhibitor TTFA using the same methodology. Surprisingly, the highest TTFA-binding affinity was calculated for the Q_p site of the S68A variant (Supplementary Figure S3C). We therefore evaluated oxygen consumption in the presence of increasing concentrations of this smaller Q_p site inhibitor (Figure 5c) and found that while for the I56F variant the inhibition by TTFA was similar to WT cells, the S68A variant was inhibited much more efficiently. For this reason we speculated that the S68A mutation could also lead to enhanced cell death induction by TTFA, which is known to induce apoptosis.[14] Indeed, while ROS and cell death were significantly increased in S68A cells, only limited ROS and cell death induction were observed in B9, I56F, R72C and WT cells upon TTFA treatment (Figures 5d and e). Features typical of apoptotic cell death were observed (Supplementary Figures S2A and C), and catalase over-expression or malonate treatment reduced cell death and ROS in S68A cells more than in WT cells (Figures 5f–h). These results suggest a direct correlation between the potency of Q_p site inhibition, CII-mediated ROS production and the extent of ensuing cell death for MitoVES as well as TTFA.

Surprisingly, the CII Q_p site inhibitor Atpenin A5,[24,30] despite efficient suppression of respiration in WT and I56F cells (Figure 5i), did not induce cell death or ROS production

(Figures 5j and k). In contrast to MitoVES and TTFA, Atpenin caused rapid increase of intracellular succinate in intact cells (Figure 5l), which is incompatible with ROS generation from CII. Hence, CII inhibition results in cell death only when succinate accumulation is not too rapid and ROS can efficiently be produced.

ROS generation in isolated mitochondria correlates with effective Q_p site inhibition at low succinate levels. To establish the link between ROS production and CII inhibition, we assessed these two parameters simultaneously in isolated mitochondria by combining the Amplex Red method of ROS detection with oxygen consumption measurements.

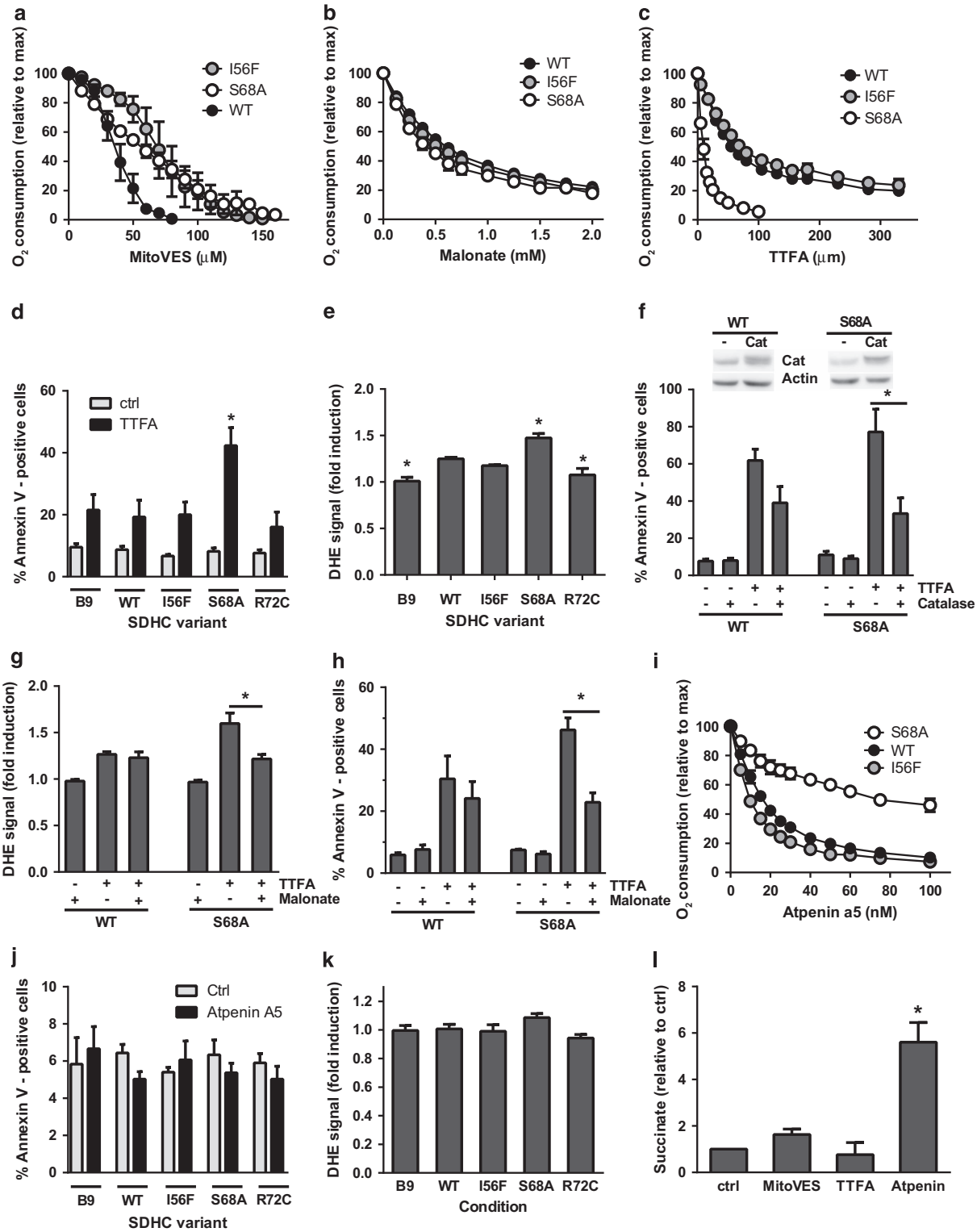

We used 0.5 mM succinate, because this concentration closely reflects its non-pathological intracellular levels (see Figure 3b) and favors direct ROS production from CII.[6,7] Exposure of WT cell mitochondria to increasing concentrations of MitoVES resulted in considerable stimulation of ROS production. In contrast, ROS generation was limited in S68A and I56F mitochondria (Figure 6a). A modest level of ROS production was also observed in R72C mitochondria, indicating that the low respiration rate of this mutant can still support ROS generation in response to its inhibition. As expected, no ROS increase upon MitoVES treatment was detected in mitochondria from parental B9 cells, which do not assemble CII (Figure 6b). In addition, the induction of ROS by MitoVES was malonate sensitive, confirming the involvement of CII (Figure 6c). Evaluation of oxygen consumption revealed reduced sensitivity of CII variants to inhibition compared with WT mitochondria. This effect was visible at higher concentrations of the inhibitor (Figure 6d), which, importantly, is within the concentration range where ROS induction becomes apparent (see Figure 6a). Finally, no stimulation of ROS production by MitoVES could be detected at a high succinate concentration (10 mM) for any of the variants tested (Figure 6e), which was confirmed by their insensitivity to malonate (Figure 6f).

Compared with MitoVES, ROS induction by TTFA followed a different pattern. While for the I56F variant it was similar to WT, much more ROS were generated by S68A cell mitochondria (Figure 7a). This is in agreement with the very high sensitivity of this mutant to the inhibition by TTFA (Figure 5c). Surprisingly, induction of ROS in R72C mitochondria was also increased, which is supported by computer modeling and is expected to occur only at low succinate levels not encountered in intact R72C cells (see Discussion for details; see Figures 3b and 5e, Supplementary Figure S3C). In contrast, no ROS production was induced in B9 cell mitochondria (Figure 7b). Similarly to MitoVES, TTFA-induced ROS generation was suppressed by malonate (Figure 7c), directly implicating CII.

With non-saturating concentrations of succinate, the build-up of oxaloacetate may lead to CII inhibition at the dicarboxylate site,[6,7,31] complicating the interpretation of results. Oxaloacetate accumulation is prevented in the presence of CI inhibitor rotenone, which at the same time limits reverse electron transfer to CI.[8,32] The inclusion of rotenone in experiments did not substantially alter the response to either MitoVES (Supplementary Figure S4) or TTFA (Supplementary Figure S5), excluding these additional factors. In summary, these results demonstrate that MitoVES and TTFA induce ROS from CII in direct proportion to their ability to achieve Q_p site inhibition at low, physiological succinate, which in turn correlates with the efficacy of cell death induction.

Discussion

In the last decade it has become clear that various complexes of the mitochondrial ETC have a multifaceted role in the execution of cell death.[33–35] CII has received particular attention as a target of experimental anticancer agents, and the inhibition of the Q_p site of CII was shown to induce cell death in cancer cells *in vitro* and *in vivo*.[16,36,37] Clear evidence was missing, however, because the potential function of CII as an amplifier of pro-death signals originating elsewhere should also be considered.[13,14] In principle, it cannot be excluded that a given compound, anticipated to engage the Q_p site of CII, triggers a pro-death signal further upstream, followed by indirect amplification of this signal at CII. It is impossible to distinguish between these two scenarios using cellular models where CII is not assembled or is inhibited at the dicarboxylate site. Hence, to demonstrate the autonomous role of CII in cell death induction, functional CII is required.

The CII Q_p site variants I56F and S68A employed in this report respire on succinate similarly to WT under native conditions, yet display alterations in cell death induction upon Q_p site ligation with MitoVES and TTFA. The level of cell death induction directly correlates with the efficacy of inhibition of succinate-driven respiration by these agents. Accordingly, both I56F and S68A variants were relatively resistant to the inhibition by MitoVES and to cell death induced by this agent, whereas the S68A variant, which is more efficiently inhibited by TTFA, underwent proportionally higher level of cell death upon TTFA treatment. This likely stems from the altered ability of the two inhibitors to displace UbQ at the Q_p site of the individual variant proteins. Indeed, experimental data could be explained by different binding affinities and various degrees of steric hindrance computationally predicted for variant Q_p sites (Supplementary Figure S3). These observations are consistent with the direct, autonomous role of CII in cell death

Figure 5 Suppression of CII-driven respiration correlates with cell death for Q_p site inhibitors that do not rapidly increase the succinate level. (**a**) Digitonin-permeabilized respiration-competent variant cell lines respiring on 10 mM succinate in the presence of 0.5 μM rotenone and FCCP were exposed to increasing concentrations of MitoVES. The variants show reduced inhibition compared with WT. (**b**) Inhibition by the dicarboxylate-binding site inhibitor malonate in the same experimental set-up shows similar efficiency for all Q_p site substitutions. (**c**) Similar to **a** and **b**, but the Q_p site inhibitor TTFA was used. (**a**–**c**) The data represent the mean ± S.E.M. of 3–4 independent experiments. (**d**) Variant cell lines were exposed to 0.5 mM TTFA for 24 h and the percentage of annexin V-positive cells was determined by flow cytometry. $n = 5$, mean ± S.E.M., * values significantly different from WT. (**e**) Cells were exposed to 250 μM TTFA for 30 min and the level of ROS was determined by dihydroethidium (DHE) staining and flow cytometry. $n = 5$, mean ± S.E.M., * values significantly different from WT. (**f**) Cells were transfected with catalase-coding or control vector, exposed to 2 mM TTFA for 20 h, and the percentage of annexin V-positive cells was determined by flow cytometry. $n = 4$, mean ± S.E.M., * values significantly different between catalase and mock-transfected cells. Inset, catalase overexpression verified by western blot. (**g**) Cells were exposed to 250 μM TTFA for 30 min in the presence or absence of 50 mM malonate (30 min pretreatment), and the level of ROS was determined by DHE staining and flow cytometry. $n = 4$, mean ± S.E.M., * values significantly different in the presence and absence of malonate. (**h**) Cells were exposed to 1.5 mM TTFA for 12 h in the presence or absence of 20 mM malonate (30 min pretreatment). The percentage of annexin V-positive cells was determined by flow cytometry. $n = 4$, mean ± S.E.M., * values significantly different in the presence and absence of malonate. (**i**) Atpenin A5-induced inhibition of respiration of permeabilized cells as described in **a**. $n \geq 3$, mean ± S.E.M. (**j**) Cells were exposed to 1 μM Atpenin A5 for 24 h and the percentage of annexin V-positive cells was determined by flow cytometry. $n = 3$, mean ± S.E.M. (**k**) Cells were exposed to 0.5 μM Atpenin A5 for 30 min and the level of ROS was determined by DHE staining and flow cytometry. $n = 5$, mean ± S.E.M. (**l**) Succinate levels were determined in WT cells exposed to 20 μM MitoVES, 1 mM TTFA or 1 μM Atpenin A5 for 30 min. $n = 3$, mean ± S.E.M., * values significantly different from control

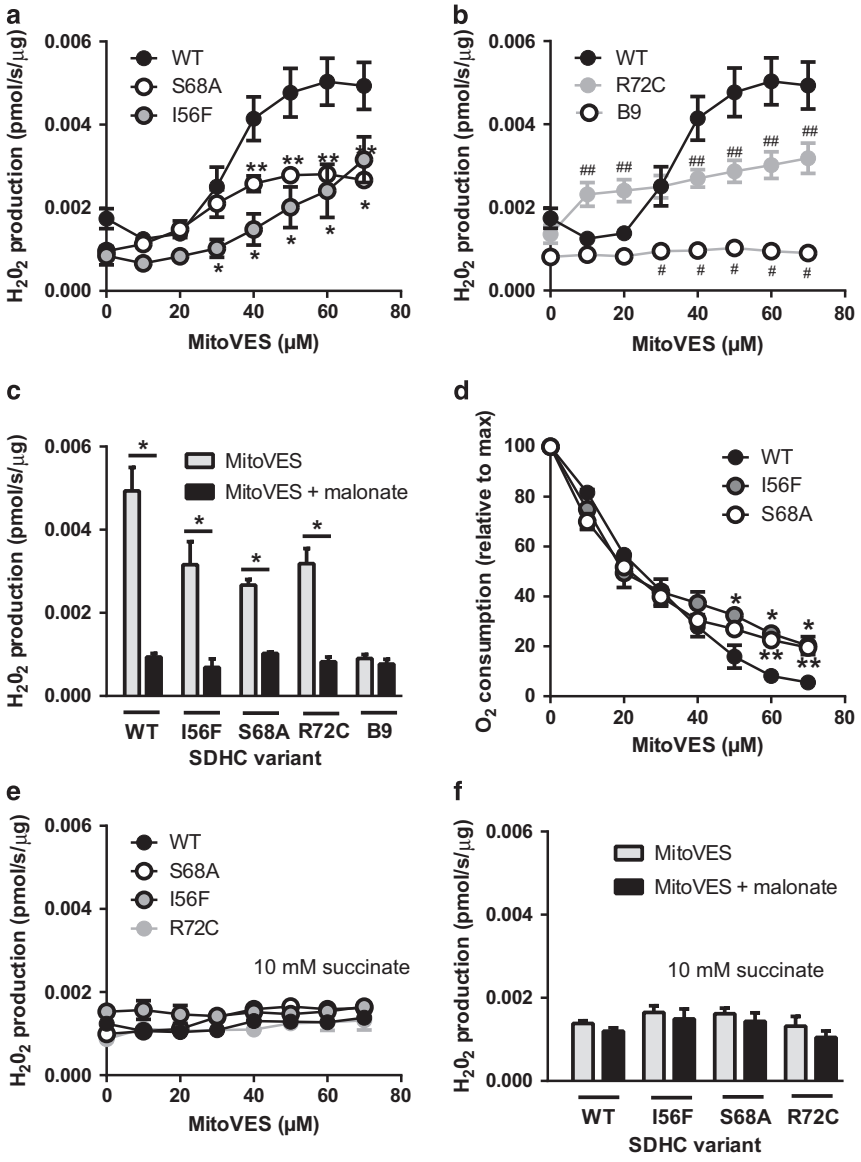

Figure 6 ROS induction by MitoVES correlates with CII inhibition in isolated mitochondria at low succinate. (**a** and **b**) Mitochondria isolated from variant cells respiring on 500 μM succinate in an oxygraph chamber were exposed to increasing concentrations of MitoVES, and ROS production was followed in real time in the presence of Amplex Ultra Red and peroxidase. (**a**) Shows reduced ROS production for I56F and S68A variants compared with WT, (**b**) shows the same for R72C and B9 cells. The same WT data are used in **a, b**, the panels are separated for clarity only. (**c**) Under the same conditions, 5 mM malonate inhibits ROS generation by 70 μM MitoVES in all cell lines except for B9 cells. (**d**) Respiratory data extracted from the experiments shown in **a** reveal that the respiration of WT cells is inhibited by MitoVES most efficiently. (**e**) ROS were measured as in **a**, **b**, but at 10 mM succinate. No increase in ROS generation was detected. (**f**) At 10 mM succinate there is no effect of 5 mM malonate on ROS at 70 μM MitoVES. Data represent the mean ± S.E.M. of 3–5 independent experiments. Significant differences from WT: *I56F, **S68A, $^{\#}$B9, $^{\#\#}$R72C. Panel c: * denotes a significant decrease after the addition of malonate

initiation by these agents, and cannot be reconciled with the role of CII as a mere amplifier of upstream effects originating at other sites. The engagement of cell death induction pathways unrelated to CII can be also discounted. In the latter scenarios, all variants retaining CII activity would behave similarly, which is clearly not the case. Compared with WT cells, the variant cell lines show lower response to MitoVES but higher (or similar) level of cell death upon TTFA treatment. This indicates that the mutations are not associated with nonspecific defects in cell death induction in our system, and excludes CII-unrelated ROS sources such as GPD2. Accordingly, this study establishes, for the first time, a direct connection between CII inhibition at the Q_p site and initiation of cell death.

In sub-mitochondrial particles, it has been previously established that CII can produce ROS upon Q_p site inhibition only when FAD is reduced and the dicarboxylate site is unoccupied.[7,38] In intact cells, this introduces an additional level of complexity, because the lack of enzymatically active CII will result in the accumulation of its substrate succinate due to the poor membrane permeability of this metabolite.[27] Succinate then might block the dicarboxylate site and restrict oxygen access to FAD, attenuating ROS production.[6] Indeed,

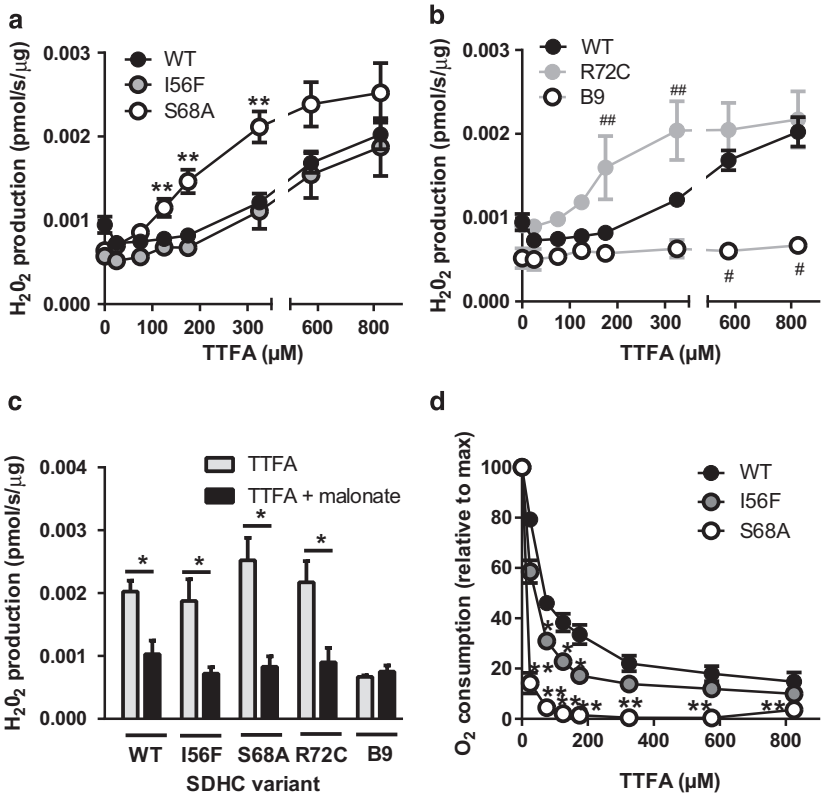

Figure 7 ROS induction by TTFA also correlates with CII inhibition in isolated mitochondria at low succinate levels. (**a** and **b**) Mitochondria isolated from variant cells respiring on 500 μM succinate in an oxygraph chamber were exposed to increasing concentrations of TTFA, and ROS production was followed in real time in the presence of Amplex Ultra Red and peroxidase. (**a**) Shows increased ROS production for S68A variant compared with WT, (**b**) shows the higher ROS for R72C and no ROS for B9 cells. The same WT data are used in **a** and **b**, the panels are separated for clarity only. (**c**) Under the same conditions, 5 mM malonate inhibits ROS generation by 825 μM TTFA in all cell lines except for B9 cells. (**d**) Respiratory data extracted from the experiments shown in **a** reveal that the respiration of S68A cells is inhibited by TTFA most efficiently. Data represent mean ± S.E.M. of 4–5 independent experiments. Significant differences from WT: *I56F, **S68A, $^{\#}$B9, $^{\#\#}$R72C. **c**: * denotes a significant decrease after the addition of malonate

the R72C mutation associated with low residual enzymatic activity of CII did not reduce the TTFA-dependent induction of ROS in isolated mitochondria where succinate is low (Figure 7b, Supplementary Figure S5B), but suppressed TTFA-induced ROS and cell death in intact cells where succinate is high (Figure 3b, Figures 5d and e). Similarly, Atpenin A5, a high-affinity Q_p site inhibitor,[24,30] did not induce ROS and cell death in intact cells (Figures 5j and k) in this and an unrelated[39] study, even though it had been previously shown to efficiently generate ROS from CII in sub-mitochondrial particles, where succinate cannot accumulate.[7] We propose that in intact cells the blockade of the dicarboxylate site of Atpenin-inhibited CII, possibly by oxaloacetate as reported[6] or by the rapidly accumulated succinate (Figure 5l), is the likely reason for this discrepancy. This is consistent with the known behavior of CII and suggests that CII is the bona fide source of ROS in intact cells upon Q_p site inhibition. Furthermore, co-treatment with dicarboxylate site inhibitor malonate suppressed ROS generation and cell death upon MitoVES and TTFA administration in responsive cell lines, and MitoVES/TTFA-induced cell death was catalase sensitive (Figures 4c–e, Figures 5f–h). We therefore propose that cell death will be induced only when the Q_p site is inhibited in a manner that allows ROS to be generated (Figure 8). Accordingly, Q_p site inhibition that is too efficient or rapid, such as with Atpenin, will suppress all CII activity and reduce FAD, but at the same time block the dicarboxylate site by succinate (or other dicarboxylate), quenching ROS formation. Slower, less efficient inhibition, such as with MitoVES or TTFA, will leave some CII molecules unoccupied, slowing down succinate accumulation such that the Q_p site-blocked CII molecules can produce ROS and induce cell death. Reduction of Q_p site inhibition by mutations that do not reduce CII activity will then leave insufficient number of Q_p site-blocked CII molecules to generate ROS, whereas mutations that compromise CII activity will upregulate succinate, limiting the ROS production from FAD.

In conclusion, the data presented in this study provide support for the direct role of CII in cell death initiation by demonstrating a clear correlation between the efficacy of inhibition at the Q_p site of CII and the magnitude of cell death in respiration-proficient CII variants for Q_p site inhibitors that do not excessively upregulate succinate. Despite being focused on CII, our results may also be relevant for other ETC complexes, as many ETC inhibitors reported to promote cell death also modulate cell death pathways independent of the ETC. For example, the CI inhibitor rotenone destabilizes microtubules,[40,41] and the CII inhibitor α-TOS as well as the complex III inhibitor antimycin act as BH3 mimetics.[42,43] To our knowledge, it has never been unequivocally shown for any of

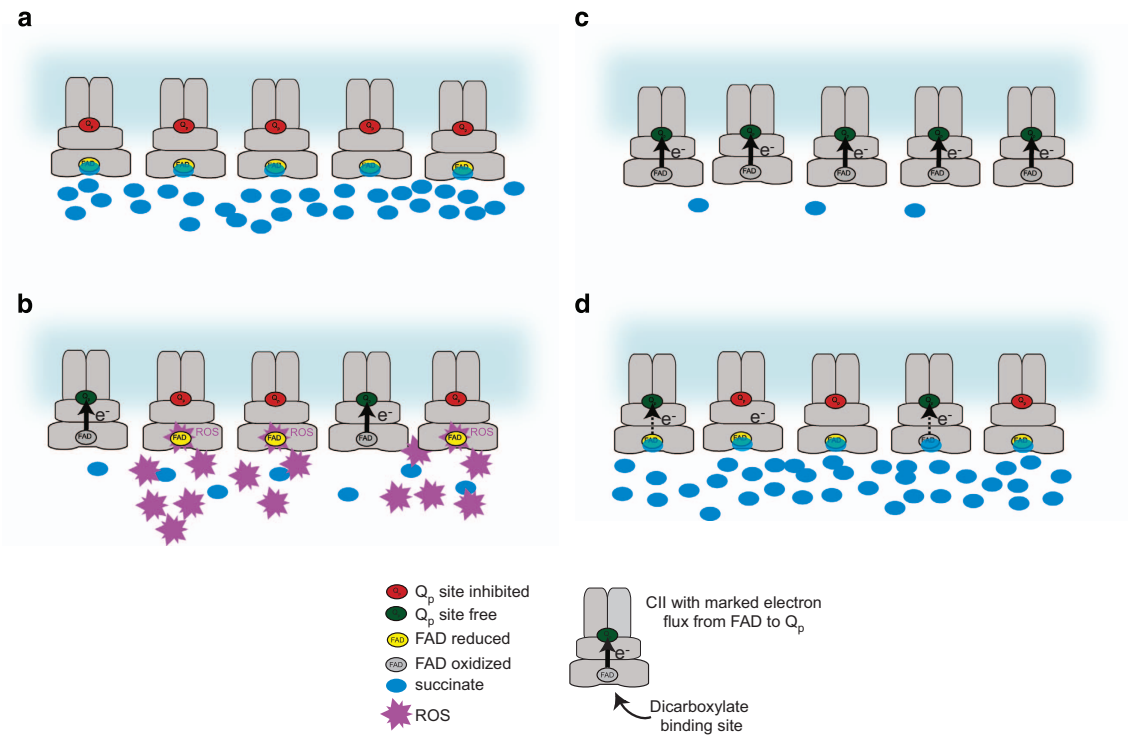

Figure 8 A proposed model of cell death initiation at CII explaining the regulation of ROS production from reduced FAD group in intact cells. (**a**) High-affinity Q_p site inhibitors, such as Atpenin A5, will immediately block most of the available Q_p sites in a cell and rapidly upregulate intracellular succinate. CII will be inhibited and FAD reduced, but no ROS will be produced, because succinate in the dicarboxylate site will block oxygen access. (**b**) Medium affinity inhibition such as with MitoVES or TTFA will not immediately block all the available Q_p sites, and some free CII will be left to keep succinate levels from rising rapidly. Because of the free dicarboxylate site, the reduced FAD in Q_p-inhibited CII molecules will be able to produce cell death-inducing ROS. (**c**) Mutations in the Q_p site that do not affect CII activity will lower the ability of an inhibitor such as MitoVES to displace ubiquinone, and despite low intracellular succinate FAD will not be reduced and therefore unable to produce ROS. (**d**) Q_p site mutations that affect CII activity will upregulate succinate, blocking dicarboxylate site and preventing ROS generation from FAD. Additional Q_p site inhibition will not generate ROS under these conditions

these compounds that ETC inhibition is instrumental in cell death induction by correlating ETC inhibitory efficacy of a single compound at any of the ETC complexes with the extent of cell death. Hence, this report defines the Q_p site of CII as a suitable target for cytotoxic agents and demonstrates that ETC targeting may present a potential clinically relevant approach to cancer treatment.[44]

Materials and Methods

Chemicals and reagents. All chemicals and reagents were from Sigma (St. Louis, MO, USA), unless otherwise stated. MitoVES was synthesized in-house as described earlier.[16] Atpenin A5 was from Enzo Life Sciences (Farmingdale, NY, USA).

Cell culture. Parental cells and variant cell lines were cultured in high-glucose (4.5 g/l) DMEM medium (Lonza, Basel, Switzerland) supplemented with 10% FCS, non-essential amino acids (both Life Technologies, Carlsbad, CA, USA) and antibiotics at 37 °C and 5% CO_2. Eahy926 cells were cultured as described in Rohlena *et al.*[18]

Q_p site mutagenesis and the generation of variant cell lines. Generation of the S68A variant was described earlier.[16] For other variants, site-directed mutagenesis of human wt SDHC cDNA was performed in the pEF-IRES-PURO expression vector using the QuickChange Lightening mutagenesis kit (Stratagene, La Jolla, CA, USA) and the following mutagenesis primers: I56F, 5′-gtc ctctgtctccccactttactatctacagttgg-3′ (forward), 5′-ccaactgtagatagtaaagtggggagac agaggac-3′ (reverse), R72C, 5′-gatgtccatctgccactgtggcactggtattgc-3′ (forward), 5′-gcaataccagtgccacagtggcagatggacatc-3′ (reverse). The sequences were confirmed by DNA sequencing and used to transfect the SDHC-deficient B9 fibroblasts using the Attractene reagent (Qiagen, Hilden, Germany), followed by incubation with 2–4 μg/ml puromycin for 2 weeks. Clones were analyzed for the expression of human SDHC by RT-PCR and those selected were stably transfected with pEGFP-C3-H-Ras as described with the exception of using Attractene for transfections,[36] after which transfectants with similar level of GFP-H-Ras expression were selected. Total RNA was collected, and the presence of the variant transcript was verified by cDNA sequencing.

Quantitative Real time-PCR. Was performed essentially as described.[16] Primers for human SDHC detection were 5′-cacttccgtccagaccggaac-3′ (forward) and 5′-atgctgggagcctcctttcttca-3′ (reverse).

Western blotting. Cells were lysed in RIPA buffer (150 mM NaCl, 1.0% Nonidet NP-40, 1% sodium deoxycholate, 0.1% SDS, 50 mM Tris, pH 8.0) supplemented with protease and phosphatase inhbibitors for 30 min with shaking on ice. Protein content was determined by the BCA assay (Pierce, Rockford, IL, USA). Samples were boiled for 5 min in reducing loading buffer before separation on SDS-PAGE gels. Wet blotting was used to transfer the separated samples to nitrocellulose membranes (Whatman-GE, Little Chalfont, UK). Immunoblotting was done in TBS/tween supplemented with 5% non-fat dried milk overnight at 4 °C. Following antibodies were used: anti-H-Ras (Santa Cruz, Dallas, TX, USA, sc-520), anti-actin HRP labeled (Cell Signaling, Danvers, MA, USA, 5125), unlabeled actin (Millipore, Darmstadt, Germany, MAB1501, used for Figure 2b), anti-cleaved caspase 3 (Cell Signaling, 9664), anti-catalase (Abcam, Cambridge, UK, Ab1877), Anti-Vdac1/porin (Abcam, ab15895), anti-SDHA (Abcam, ab14715), anti-ATPase alpha subunit (Abcam, ab14748). Rabbit polyclonal antibody to GPD2 was custom prepared.[45] HRP-conjugated secondary antibodies were used in TBS/tween with 5% non-fat dried milk for 1 h at room temperature. WB signals were quantified using the Aida 3.21 Image Analyzer software (Raytest, Straubenhardt, Germany).

Mitochondria isolation. Mitochondrial isolation was performed according to a recently described method, with some adaptations.[46] Cells were released by

trypsin, washed in PBS, and 40–50 × 10^6 cells were transferred to 5 ml of mitochondria isolation buffer (200 mM sucrose, 1 mM EGTA, 10 mM Tris/Mops pH 7.4). The cell suspension was homogenized by three passes through a cell homogenizer (Isobiotec, Heidelberg, Germany) set to 10 μm clearance using 5 ml syringe (SGE, 5MDF-LL-GT) at 0.5 ml/min flow at 4 °C. The homogenate was centrifuged (at 4 °C) at 800 × *g* for 8 min, the supernatant was collected and pre-cleared at 3000 × *g* for 5 min. The final collection of mitochondrial pellet was done at 10 000 × *g* for 15 min. Protein content was determined by the BCA assay. The mitochondria were undamaged, viable and well coupled, as determined by respirometry (see below) from their reaction to the addition of ADP (about 5x increase in respiration), FCCP (substantial increase of respiration) and cytochrome c (no or very little increase in respiration).

Blue native electrophoresis. Isolated mitochondria were solubilized in the extraction buffer (1.5 M aminocaproic acid, 50 mM Bis-Tris, 0.5M EDTA and pH 7) containing 1.3% lauryl maltoside or 8 g digitonin / g protein. Samples comprising 20–30 μg of protein were then mixed with the sample buffer (0.75 M aminocaproic acid, 50 mM Bis-Tris, 0.5M EDTA, pH 7, 5% Serva-Blue G-250 and 12% glycerol) and loaded on the precast NativePAGE Novex 4–16% Bis-Tris gels (Life Technologies) and run overnight at a constant voltage of 25 V. Separated protein complexes were then transferred to the PVDF membrane (Millipore), using the Trans-Blot Turbo transfer system (Biorad, Hercules, CA, USA). CII was detected with the anti-SDHA (2E3) antibody (Abcam, AB14715-200).

In-gel SDH activity. Lauryl maltoside (20–30 μg) or digitonine solubilized mitochondria (see above) were mixed with sample buffer containing 50% glycerol with 0.1% Ponceau dye and run on the precast NativePAGE Novex 4–16% Bis-Tris gel at constant voltage of 100 V, which was raised to 500 V after the samples entered the separation gel. Deoxycholate (0.05%) and lauryl maltoside (0.01%) were added to the cathode buffer for higher resolution as described.[47] Gels with separated protein complexes were incubated for 30 min in assay buffer containing 20 mM sodium succinate, 0.2 mM phenazine methosulfate and 0.25% nitrotetrazolium blue in 5 mM Tris/HCl, pH 7.4. The reaction was stopped using solution of 50% methanol and 10% acetic acid and gels were immediately photographed.

SQR activity measurement. Mitochondria (25 μg) were incubated in 200 μl of 25 mM phosphate potassium buffer (pH 7.4) containing 0.1% Triton X-100, 20 mM succinate, 2 μM antimycine, 5 μM rotenone, 10 mM sodium azide, 50 μM decylubiquinone for 3–5 min in a 96-well plate. After 30 s recording of the measurement at 600 nm, 10 μl of 2,6-dichlorphenol indophenol (0.015% w/v) was added and the reaction was recorded for another 2–3 min. Identical measurements were performed in the presence of 20 mM malonate and the net SQR activity was obtained by subtracting malonate-insensitive rates.

Mitochondrial membrane potential measurements. Cells were seeded in 12-well plates a day before the experiment. On the day of experiment, one well was used to determine the total cellular protein by BCA. The rest of the cells were collected by trypsin, washed with PBS, and resuspended in Mir05 medium (see below) at 0.5 mg/ml concentration with 10 mM succinate, 2 mM malate, 10 mM glutamate, 3 mM ADP and 20 nM tetramethylrhodamine methyl ester (TMRM). Next, 60 μl of this cell suspension was permeabilized with 0.1 μg digitonin per μg protein for 5 min at room temperature, and immediately measured on LSR-II flow cytometer (Becton Dickinson, Franklin Lakes, NJ, USA) for the TMRM fluorescence signal. Finally, 0.2 μ*l* of 1 mM carbonyl cyanide 3-chlorophenylhydrazone (CCCP) was added and the TMRM signal after uncoupling was assessed. The relative mitochondrial membrane potential was determined as the ratio of TMRM signal before and after the addition of CCCP (f/f_0).

Confocal microscopy. Live confocal images were obtained basically as described[48] with minor modifications. The cells in complete medium in microscopy glass-bottom dishes were incubated with 250 ng/ml Hoechst 33342 nuclear stain and 10 nM TMRM for 15 min and imaged with x63 oil immersion lens at the heated stage of an SP5 confocal microscope (Leica Microsystems, Wetzlar, Germany). 2-μm-thick stacks were obtained, deconvoluted with the Huygens Professional software (SVI, Hilversum, The Netherlands) and presented as maximal intensity projections.

Determination of intracellular succinate. Cells were cultured for 24 h, washed with PBS, scrapped and extracted in 96% ethanol in a cold methanol bath. Extracts corresponding to equal number of cells were used in further analysis (10^6 cells per 1.6 ml). After the addition of the internal standard the extracts were dried under argon stream. Afterwards, 50 μ*l* of benzyl alcohol and 30 μl of TMS-chloride were added to the dried samples, and the closed Eppendorf tubes were placed in the ultrasonic bath (room temperature, 45 min) and in an oven (80 °C, 45 min). A final volume of 500 μl was adjusted by adding acetonitrile. Quantification of the derivatized acids was performed with an LC–ESI/MS system (Bruker Esquire 3000, Billerica, MA, USA), in positive ionization mode. The mass spectrometer was connected to a liquid chromatography system of the 1100/1200 series from Agilent Technologies (Santa Clara, CA, USA). Reversed-phase separation of the derivatives was performed on a Supelcosil 150 × 4.6 mm column with a silica-based C-18 stationary phase (5-μm particle diameter). The mobile Phase A was acetonitrile and Phase B was H_2O, 0.1% formic acid. Agilent ChemStation for LC 3D systems B01.03 was used to control the instruments and for data processing. The gradient program was 0 min 50% B, from 0 to 8 min to 5% B and at 20 min back to the initial conditions of 50% B. The injection volume was 10 μl. The LC separation and the ESI settings of the Esquire instrument were optimized utilizing a dibenzyl oxalate as an internal standard. Intracellular succinate concentration was calculated using an average cell diameter of 14 μm.

Measurement of CII respiration in permeabilized cells. Cells were collected by trypsinization, washed in PBS, resuspended in Mir05 medium (0.5 mM EGTA, 3 mM $MgCl_2$, 60 mM K-lactobionate, 20 mM taurine, 10 mM KH_2PO_4, 110 mM sucrose, 1 g/l essentially fatty acid-free BSA, 20 mM Hepes, pH 7.1 at 30 °C) and transferred to the chamber of the Oroboros Oxygraph-2k (Oroboros Instruments, Innsbruck, Austria) for respiration measurements at 37 °C. The chamber was closed when the oxygen signal became stable, and after recording the routine respiration on intracellular substrates the plasma membrane was permeabilized by 10 μg digitonin per million cells. The CII respiration was determined in the presence of 0.5 μM rotenone, 10 mM succinate, 3 mM ADP and 10 μM cytochrome c. The maximal respiration in the uncoupled state was then achieved by FCCP titration in 0.5 μM steps. Antimycin A (2.5 μM) was added at the end to inhibit ETC and the residual oxygen consumption after antimycin addition was subtracted from all the results to obtain the mitochondria-specific rates.

Inhibition of CII respiration. Cells were permeabilized as above and the effect of CII inhibitors was assessed in the presence of 10 mM succinate, 3 mM ADP, 0.5 μM rotenone, 10 μM cytochrome c and FCCP. The inhibitors (MitoVES, TTFA, Atpenin A5 or malonate) were titrated to the chamber in regular intervals (5 min) and the rate of oxygen consumption was assessed after each addition.[49] Solvent only was titrated into control chambers in parallel to check for nonspecific effects and cell deterioration, but the respiration rates remained virtually unaffected ($<$10% decrease at the end of the experiment). Respiration rates after 2.5 μM antimycin A addition were subtracted to obtain the mitochondria-specific rates.

Simultaneous measurements of ROS production and oxygen consumption in isolated mitochondria. The chambers of the Oroboros Oxygraph instrument equipped with the O2k-Fluorescence LED2-Module (Oroboros Instruments) were calibrated at 37 °C with the Budapest-modified respiration medium (120 mM KCl, 20 mM HEPES, 10 mM KH_2PO_4, 2.86 mM $MgCl_2$, 0.2 mM EGTA, 0.025% BSA, pH 7). After closing the chambers, Amplex Ultra Red (Life Technologies) and peroxidase were injected (at final concentrations 5 μM and 1 U/ml, respectively), followed by the addition of 200 μg of isolated mitochondria, 0.5 μM rotenone (where indicated), 0.5 or 10 mM succinate and 3 mM ADP. The tested inhibitors were titrated as above, and the amount of hydrogen peroxide generated was determined based on the conversion of Amplex Ultra Red to the highly fluorescent product resorufin[50] using excitation LED 525 nm equipped with the Amplex red filter set. Oxygen consumption was recorded simultaneously in the same chamber. Malonate (5 mM) was added at the end of the titration experiment to confirm that the signal is succinate dependent. After this, hydrogen peroxide of known concentration was titrated to the chamber in several steps to calibrate the fluorescence signal. Finally, 2.5 μM antimycin A was added to subtract the nonspecific respiration rates.

ROS measurement in intact cells. The cells were seeded in 12-well culture plates and grown for 24 h. To start the experiment, tested compounds were added to the culture medium and after 15 min, dihydroethidium was added to the final concentration of 20 μM. After another 15 min, the cells were harvested by trypsin and oxidized ethidium fluorescence was measured on a LSR-II flow cytometer (Becton Dickinson) and expressed as a mean fluorescence intensity.

Cell death measurements. Cells were seeded in 12-well culture plates and grown for 24 h. After that, the tested compounds were added as indicated. The medium was collected after the required incubation time, the adherent cells were washed by PBS and harvested by trypsin. All these fractions were combined, washed by PBS and incubated with PE- or Dy647-labeled annexin V (Becton Dickinson and Apronex, Vestec, Czech Republic) in the supplied binding buffer for at least 10 min. Hoechst 33258 was added to mark the cells with ruptured cell membrane. Annexin V-positive fraction was measured by flow cytometry. The results were expressed as the percentage of annexin V-positive cells. For the catalase experiments, cells were transfected two days before the experiment with a control or catalase-containing vector (a kind gift of Dr. S Lortz)[51] using the Fugene transfection reagent (Promega, Fitchburg, WI, USA) according to manufacturer's instruction.

Computer modeling. The structure of WT human mitochondrial complex II was obtained as a homology model based on the highly homologous template of the porcine CII[3] (pdb id 1zoy, sequence identity 95, 96, 92, and 88% for SDHA to SDHD) using the Modeller suite of programs.[52] The single point SDHC mutations (I56F, S68A, R72C) were then introduced using the FoldX program,[53] which was also used to optimize the side chain rotamers within the WT as well as mutated structures. All the structures were further subjected to a short (10 ns, implicit solvation) molecular dynamics (MDs) run in order to relax the potentially non-equilibrium structures. The MD was prepared and performed using the GPU version of the GROMACS suite of programs[54] as implemented in the OpenMM Zephyr package.[55] Average structures from second half of the simulations were further used for the docking study. The docking study of the MitoVES, TTFA and ubiquinone ligands/inhibitors to a series of mutated mitochondrial complex II structures was performed using the autodock suite of programs.[56] The ligands were docked into the homology model of human CII and its single point mutants using Python Molecular Viewer version 1.5.6rc3.[57] Each ligand was allowed to sample docking poses in a box ($70 \times 70 \times 70$ grid points with 0.375 Å spacing) centered at the level of the ubiquinone binding site (based on the crystal structure). The side chains of residues surrounding the binding site were considered flexible. A series of four separate "local search" runs of 50 cycles each was performed and the results were combined to find the most stable poses.

Statistical analysis. Statistical analysis was performed using GraphPad Prism 6 software (GraphPad Software, La Jolla, CA, USA). Statistical significance was determined by oneway ANOVA followed by Dunnett's post test. For pair-wise comparisons (Figures 3a and 4c–e, Figures 5f–h, Figures 6c and 7c,Supplementary Figures S4C and S5C), we used unpaired *t*-test. $P \leq 0.05$ was considered statistically significant. The value of *n* indicates the number of independent experiments.

Conflict of Interest

The authors declare no conflict of interest.

Acknowledgements. We are grateful to Dr Christian Frezza (MRC, Cambridge, UK) for critically reading the manusript, to Dr Stephan Lortz (Hannover Medical School, Hannover, Germany) for the gift of the catalase overexpression vector and to Dr Lydie Plecita-Hlavata for consultations. This work was supported by the Czech Science Foundation grant no. P301-12-1851 and EMBO travel fellowship to JR, the National and Health Medical Research Council of Australia and the Australian Research Council to JN and LD, the Czech Science Foundation grant 14-36804G to TM as well as by the BIOCEV European Regional Development Fund CZ.1.05/1.1.00/02.0109.

1. Cecchini G. Function and structure of complex II of the respiratory chain. *Annu Rev Biochem* 2003; **72**: 77–109.
2. Maklashina E, Cecchini G. The quinone-binding and catalytic site of complex II. *Biochim Biophys Acta* 2010; **1797**: 1877–1882.
3. Sun F, Huo X, Zhai Y, Wang A, Xu J, Su D *et al.* Crystal structure of mitochondrial respiratory membrane protein complex II. *Cell* 2005; **121**: 1043–1057.
4. Iverson TM. Catalytic mechanisms of complex II enzymes: a structural perspective. *Biochim Biophys Acta* 2013; **1827**: 648–657.
5. Huang LS, Sun G, Cobessi D, Wang AC, Shen JT, Tung EY *et al.* 3-nitropropionic acid is a suicide inhibitor of mitochondrial respiration that, upon oxidation by complex II, forms a covalent adduct with a catalytic base arginine in the active site of the enzyme. *J Biol Chem* 2006; **281**: 5965–5972.
6. Quinlan CL, Orr AL, Perevoshchikova IV, Treberg JR, Ackrell BA, Brand MD. Mitochondrial complex II can generate reactive oxygen species at high rates in both the forward and reverse reactions. *J Biol Chem* 2012; **287**: 27255–27264.
7. Siebels I, Drose S. Q-site inhibitor induced ROS production of mitochondrial complex II is attenuated by TCA cycle dicarboxylates. *Biochim Biophys Acta* 2013; **1827**: 1156–1164.
8. Moreno-Sanchez R, Hernandez-Esquivel L, Rivero-Segura NA, Marin-Hernandez A, Neuzil J, Ralph SJ *et al.* Reactive oxygen species are generated by the respiratory complex II–evidence for lack of contribution of the reverse electron flow in complex I. *FEBS J* 2013; **280**: 927–938.
9. Messner KR, Imlay JA. Mechanism of superoxide and hydrogen peroxide formation by fumarate reductase, succinate dehydrogenase, and aspartate oxidase. *J Biol Chem* 2002; **277**: 42563–42571.
10. Zhang L, Yu L, Yu CA. Generation of superoxide anion by succinate-cytochrome c reductase from bovine heart mitochondria. *J Biol Chem* 1998; **273**: 33972–33976.
11. Kluckova K, Bezawork-Geleta A, Rohlena J, Dong L, Neuzil J. Mitochondrial complex II, a novel target for anti-cancer agents. *Biochim Biophys Acta* 2013; **1827**: 552–564.
12. Grimm S. Respiratory chain complex II as general sensor for apoptosis. *Biochim Biophys Acta* 2013; **1827**: 565–572.
13. Hwang MS, Schwall CT, Pazarentzos E, Datler C, Alder NN, Grimm S. Mitochondrial Ca influx targets cardiolipin to disintegrate respiratory chain complex II for cell death induction. *Cell Death Differ* 2014; **21**: 1733–1745.
14. Lemarie A, Huc L, Pazarentzos E, Mahul-Mellier AL, Grimm S. Specific disintegration of complex II succinate:ubiquinone oxidoreductase links pH changes to oxidative stress for apoptosis induction. *Cell Death Differ* 2011; **18**: 338–349.
15. Hwang MS, Rohlena J, Dong LF, Neuzil J, Grimm S. Powerhouse down: complex II dissociation in the respiratory chain. *Mitochondrion* 2014; **19**(Pt A): 20–28.
16. Dong LF, Jameson VJ, Tilly D, Cerny J, Mahdavian E, Marin-Hernandez A *et al.* Mitochondrial targeting of vitamin E succinate enhances its pro-apoptotic and anti-cancer activity via mitochondrial complex II. *J Biol Chem* 2011; **286**: 3717–3728.
17. Dong LF, Jameson VJ, Tilly D, Prochazka L, Rohlena J, Valis K *et al.* Mitochondrial targeting of alpha-tocopheryl succinate enhances its pro-apoptotic efficacy: a new paradigm for effective cancer therapy. *Free Radic Biol Med* 2011; **50**: 1546–1555.
18. Rohlena J, Dong LF, Kluckova K, Zobalova R, Goodwin J, Tilly D *et al.* Mitochondrially targeted alpha-tocopheryl succinate is antiangiogenic: potential benefit against tumor angiogenesis but caution against wound healing. *Antioxid Redox Signal* 2011; **15**: 2923–2935.
19. Rodriguez-Enriquez S, Hernandez-Esquivel L, Marin-Hernandez A, Dong LF, Akporiaye ET, Neuzil J *et al.* Molecular mechanism for the selective impairment of cancer mitochondrial function by a mitochondrially targeted vitamin E analogue. *Biochim Biophys Acta* 2012; **1817**: 1597–1607.
20. Neuzil J, Dong LF, Rohlena J, Truksa J, Ralph SJ. Classification of mitocans, anti-cancer drugs acting on mitochondria. *Mitochondrion* 2013; **13**: 199–208.
21. Szeto SS, Reinke SN, Sykes BD, Lemire BD. Ubiquinone-binding site mutations in the *Saccharomyces cerevisiae* succinate dehydrogenase generate superoxide and lead to the accumulation of succinate. *J Biol Chem* 2007; **282**: 27518–27526.
22. Tran QM, Rothery RA, Maklashina E, Cecchini G, Weiner JH. The quinone binding site in *Escherichia coli* succinate dehydrogenase is required for electron transfer to the heme b. *J Biol Chem* 2006; **281**: 32310–32317.
23. Yang X, Yu L, He D, Yu CA. The Quinone-binding Site in Succinate-ubiquinone Reductase fromEscherichia coli: quinone-binding domain and amino acid residues involved in quinone binding. *J Biol Chem 1998* 1998; **273**: 31916–31923.
24. Horsefield R, Yankovskaya V, Sexton G, Whittingham W, Shiomi K, Omura S *et al.* Structural and computational analysis of the quinone-binding site of complex II (succinate-ubiquinone oxidoreductase): a mechanism of electron transfer and proton conduction during ubiquinone reduction. *J Biol Chem* 2006; **281**: 7309–7316.
25. Oostveen FG, Au HC, Meijer PJ, Scheffler IE. A Chinese hamster mutant cell line with a defect in the integral membrane protein CII-3 of complex II of the mitochondrial electron transport chain. *J Biol Chem* 1995; **270**: 26104–26108.
26. Pesta D, Gnaiger E. High-resolution respirometry: OXPHOS protocols for human cells and permeabilized fibers from small biopsies of human muscle. *Methods Mol Biol* 2012; **810**: 25–58.
27. Selak MA, Armour SM, MacKenzie ED, Boulahbel H, Watson DG, Mansfield KD *et al.* Succinate links TCA cycle dysfunction to oncogenesis by inhibiting HIF-alpha prolyl hydroxylase. *Cancer Cell* 2005; **7**: 77–85.
28. Yanamala N, Kapralov AA, Djukic M, Peterson J, Mao G, Klein-Seetharaman J *et al.* Structural re-arrangement and peroxidase activation of cytochrome c by anionic analogues of vitamin E, tocopherol succinate and tocopherol phosphate. *J Biol Chem* 2014; **289**: 32488–32498.
29. Rauchova H, Vokurkova M, Drahota Z. Inhibition of mitochondrial glycerol-3-phosphate dehydrogenase by alpha-tocopheryl succinate. *Int J Biochem Cell Biol* 2014; **53**: 409–413.
30. Miyadera H, Shiomi K, Ui H, Yamaguchi Y, Masuma R, Tomoda H *et al.* Atpenins, potent and specific inhibitors of mitochondrial complex II (succinate-ubiquinone oxidoreductase). *Proc Natl Acad Sci U S A* 2003; **100**: 473–477.
31. Kearney EB, Ackrell BA, Mayr M. Tightly bound oxalacetate and the activation of succinate dehydrogenase. *Biochem Biophys Res Commun* 1972; **49**: 1115–1121.

32. Muller FL, Liu Y, Abdul-Ghani MA, Lustgarten MS, Bhattacharya A, Jang YC *et al.* High rates of superoxide production in skeletal-muscle mitochondria respiring on both complex I- and complex II-linked substrates. *Biochem J* 2008; **409**: 491–499.
33. Lemarie A, Grimm S. Mitochondrial respiratory chain complexes: apoptosis sensors mutated in cancer? *Oncogene* 2011; **30**: 3985–4003.
34. Ricci JE, Gottlieb RA, Green DR. Caspase-mediated loss of mitochondrial function and generation of reactive oxygen species during apoptosis. *J Cell Biol* 2003; **160**: 65–75.
35. Kwong JQ, Henning MS, Starkov AA, Manfredi G. The mitochondrial respiratory chain is a modulator of apoptosis. *J Cell Biol* 2007; **179**: 1163–1177.
36. Dong LF, Freeman R, Liu J, Zobalova R, Marin-Hernandez A, Stantic M *et al.* Suppression of tumor growth *in vivo* by the mitocan alpha-tocopheryl succinate requires respiratory complex II. *Clin Cancer Res* 2009; **15**: 1593–1600.
37. Dong LF, Low P, Dyason JC, Wang XF, Prochazka L, Witting PK *et al.* Alpha-tocopheryl succinate induces apoptosis by targeting ubiquinone-binding sites in mitochondrial respiratory complex II. *Oncogene* 2008; **27**: 4324–4335.
38. Drose S. Differential effects of complex II on mitochondrial ROS production and their relation to cardioprotective pre- and postconditioning. *Biochim Biophys Acta* 2013; **1827**: 578–587.
39. Mbaya E, Oules B, Caspersen C, Tacine R, Massinet H, Pennuto M *et al.* Calcium signalling-dependent mitochondrial dysfunction and bioenergetics regulation in respiratory chain Complex II deficiency. *Cell Death Differ* 2010; **17**: 1855–1866.
40. Choi WS, Palmiter RD, Xia Z. Loss of mitochondrial complex I activity potentiates dopamine neuron death induced by microtubule dysfunction in a Parkinson's disease model. *J Cell Biol* 2011; **192**: 873–882.
41. Ren Y, Feng J. Rotenone selectively kills serotonergic neurons through a microtubule-dependent mechanism. *J Neurochem* 2007; **103**: 303–311.
42. Tzung SP, Kim KM, Basanez G, Giedt CD, Simon J, Zimmerberg J *et al.* Antimycin A mimics a cell-death-inducing Bcl-2 homology domain 3. *Nat Cell Biol* 2001; **3**: 183–191.
43. Shiau CW, Huang JW, Wang DS, Weng JR, Yang CC, Lin CH *et al.* alpha-Tocopheryl succinate induces apoptosis in prostate cancer cells in part through inhibition of Bcl-xL/Bcl-2 function. *J Biol Chem* 2006; **281**: 11819–11825.
44. Rohlena J, Dong LF, Ralph SJ, Neuzil J. Anticancer drugs targeting the mitochondrial electron transport chain. *Antioxid Redox Signal* 2011; **15**: 2951–2974.
45. Mracek T, Jesina P, Krivakova P, Bolehovska R, Cervinkova Z, Drahota Z *et al.* Time-course of hormonal induction of mitochondrial glycerophosphate dehydrogenase biogenesis in rat liver. *Biochim Biophys Acta* 2005; **1726**: 217–223.
46. Schmitt S, Saathoff F, Meissner L, Schropp EM, Lichtmannegger J, Schulz S *et al.* A semi-automated method for isolating functionally intact mitochondria from cultured cells and tissue biopsies. *Anal Biochem* 2013; **443**: 66–74.
47. Wittig I, Karas M, Schagger H. High resolution clear native electrophoresis for in-gel functional assays and fluorescence studies of membrane protein complexes. *Mol Cell Proteomics* 2007; **6**: 1215–1225.
48. Truksa J, Dong LF, Rohlena J, Stursa J, Vondrusova M, Goodwin J *et al.* Mitochondrially targeted vitamin E succinate modulates expression of mitochondrial DNA transcripts and mitochondrial biogenesis. *Antioxid Redox Signal* 2015; **22**: 883–900.
49. Hroudova J, Fisar Z. *In vitro* inhibition of mitochondrial respiratory rate by antidepressants. *Toxicol Lett* 2012; **213**: 345–352.
50. Zhou M, Diwu Z, Panchuk-Voloshina N, Haugland RP. A stable nonfluorescent derivative of resorufin for the fluorometric determination of trace hydrogen peroxide: applications in detecting the activity of phagocyte NADPH oxidase and other oxidases. *Anal Biochem* 1997; **253**: 162–168.
51. Lortz S, Gurgul-Convey E, Naujok O, Lenzen S. Overexpression of the antioxidant enzyme catalase does not interfere with the glucose responsiveness of insulin-secreting INS-1E cells and rat islets. *Diabetologia* 2013; **56**: 774–782.
52. Webb B, Sali A. Protein Structure Modeling with MODELLER. *Protein Structure Prediction, 3rd Edition* 2014; **1137**: 1–15.
53. Schymkowitz J, Borg J, Stricher F, Nys R, Rousseau F, Serrano L. The FoldX web server: an online force field. *Nucleic Acids Res* 2005; **33**: W382–W388.
54. Hess B, Kutzner C, van der Spoel D, Lindahl E. GROMACS 4: Algorithms for highly efficient, load-balanced, and scalable molecular simulation. *J Chem Theory Comput* 2008; **4**: 435–447.
55. Eastman P, Friedrichs MS, Chodera JD, Radmer RJ, Bruns CM, Ku JP *et al.* OpenMM 4: A Reusable, Extensible, Hardware Independent Library for High Performance Molecular Simulation. *J Chem Theory Comput* 2013; **9**: 461–469.
56. Morris GM, Huey R, Lindstrom W, Sanner MF, Belew RK, Goodsell DS *et al.* AutoDock4 and AutoDockTools4: automated docking with selective receptor flexibility. *J Comput Chem* 2009; **30**: 2785–2791.
57. Sanner MF. Python: a programming language for software integration and development. *J Mol Graph Model* 1999; **17**: 57–61.

Supplementary Information accompanies this paper on Cell Death and Disease website (http://www.nature.com/cddis)

5.Analýza vybraných léčiv a jejich metabolitů v tělních tekutinách

5.1.Význam stanovení koncentrace léčiva pro klinickou praxi

V klinické praxi se lékaři setkávají s pacienty, u kterých léčba nevede k požadovanému terapeutickému účinku. Jednou z příčin tohoto jevu jsou velké interindividuální rozdíly ve vstřebávání, metabolizmu a ve vylučování léku. Studiem genetických příčin různorodosti genetické odpovědi se zabývá farmakogenetika [1, 2].

Častou příčinou variability farmakokinetických vlastností léčiv jsou mutace přítomné na typických místech genů jaterních enzymů. Tyto mutace se nazývají polymorfismy.

Existují dva způsoby, jak určit aktivitu enzymů podílejících se na biotransformaci léčiv – určení *fenotypu* a *genotypu*. Při stanovování fenotypu je podána jedna dávka modelového léčiva, které je metabolizováno enzymem, jehož aktivitu stanovujeme. Jako parametr aktivity enzymu potom používáme metabolický poměr (koncentrace metabolitu/koncentrace mateřské látky). Jeho hodnota udává rychlost přeměny mateřské látky na metabolit a lze podle ní odlišit pomalé a rychlé metabolizátory. [1].

V případě, že je podáváno profarmakum, snížená aktivita enzymu způsobí, že mateřská látka není dostatečně transformována na aktivní metabolit, není dosaženo terapeutické koncentrace a očekávaný účinek se nedostaví. Kdyby tedy bylo u pacienta před vlastním zahájením terapie známo, do jaké skupiny metabolizátorů patří, bylo by možné na základě individuálních potřeb upravit dávkování, případně zvolit alternativní léčebný postup v situaci, kdy by měla být léčba neúčinná, nebo toxická. Jednou z možností je stanovení genotypu. Vliv genotypu však není u mnoha farmak zatím dostatečně prostudován [3].

5.2.Vývoj rychlé metody LC–MS/MS pro kvantifikaci rilmenidinu v lidském séru: objasnění fragmentačních cest pomocí HRMS (publikace VII)

5.2.1. Teoretický úvod

Rilmenidin je látka využívaná k léčbě vysokého krevního tlaku a působí zejména na imidazolové receptory. Je vhodný zejména pro léčbu pacientů s mírnou až středně těžkou hypertenzí [4,5]. Rilmenidin je slabá báze s p*K*a 9.0 nejčastěji se používá ve formě fosfátu, kdy je velmi dobře rozpustný ve vodě. Po podání 1 mg rilmenidinu dosáhne koncentrace v séru zdravého dobrovolníka maximální hodnoty mezi 3,25 až 3,97 ng/ml asi po 1,33 až

1,94 h[6-8]. Pro preklinické a klinické farmakologické studie bylo nutné vyvinout selektivní, vysoce citlivou a robustní analytickou metodu. Doposud existuje je několik metod stanovení rilmenidin v biologických matricích využívající převážně GC-MS a LC-MS [9-13]. Cílem této práce bylo vyvinout a validovat citlivou a široce použitelnou metodu stanovení rilmenidinu ve vzorcích lidského séra. Součástí práce bylo srovnání selektivity, extrakční účinnosti, citlivosti a přesnosti dvou separačních technik založených na principu extrakce kapalinou LLE (liquid-liquid extraction) a extrakcí na pevné fázi SPE (solid-phase extraction). Navržený fragmentační mechanismus rilmenidinu při měření MS/MS spekter byl potvrzen za pomocí přístroje s vysokou rozlišovací schopností (HRMS). Schéma hmotnostního spektrometru s trojitým kvadrupólem (QqQ) pracujícího v režimu SRM je na obrázku 5.1 [14].

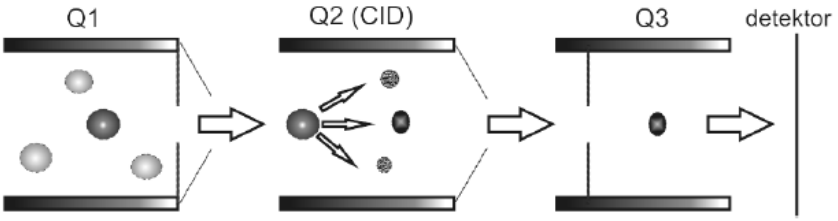

Obr.5.1 Schéma hmotnostního spektrometru typu trojitý kvadrupól pracujícího v režimu monitorování vybraných reakcí

5.2.2. Výsledky a diskuse – doplňkový komentář k publikaci

Úplné separace rilmenidinu a interního standardu trimipraminu-d_3(IS) bylo dosaženo isokratickou elucí na koloně C18 směsí acetonitrilu a 5 mM mravenčanu amonného. Jak se ukázalo, zvyšování obsahu acetonitrilu v mobilní fázi vedlo ke snižování separační účinnosti kolony, zatím co zvyšování poměrného zastoupení pufru výrazně prodlužovalo retenční čas. Jako optimální byl zvolen poměr 50:50 (v/v), se kterým bylo dosaženo nejlepší separace píků a zároveň dobré odezvy MS detektoru. Dále bylo zjištěno, že optimální průtoková rychlost mobilní fáze je 1,15 ml/min a že změna teploty v intervalu 20-50°C separační proces výraznějším způsobem neovlivňuje. Podmínky pro MS detektor, který pracoval v režimu monitorování vybraných reakcí ("selected reaction monitoring", SRM), byly optimalizovány s ohledem na nejintenzivnější odezvu produktových iontů. Pro rilmenidin byly sledovány dva iontové přechody m/z 181,1 → 95,1 a 67,1 a pro interní standard byl vybrán přechod m/z 298,2 → 103,1, tento přechod analogicky odpovídá vzniku iontu m/z 101,1 pro izotopicky neznačený trimipramin.

Fragmentace protonovaného rilmenidinu byla studována s pomocí HRMS. Bylo zjištěno, že nejintenzivnější fragment m/z 95,1 odpovídá iontu $C_7H_{11}^+$, který vzniká eliminací neutrální molekuly heterocyklického aminu $C_3H_6N_2O$. Další ion m/z 93,1 odpovídá složení $C_7H_9^+$ a vzniká ztrátou $C_3H_8N_2O$. Druhý nejintenzivnější signál m/z 67,1 přísluší iontu $C_5H_7^+$ vznikajícího pravděpodobně z iontu $C_7H_{11}^+$ eliminací etylenu. Ztráta C_3H_6 ze stejného iontu poskytuje C_4H_7+m/z 55,1. Méně intenzivní ion obsahující heterocyklickou část m/z 99,1 odpovídá složení $C_3H_7N_2O^+$. Navržené fragmentační schéma rilmenidinu je zachyceno na obrázku 5.2.

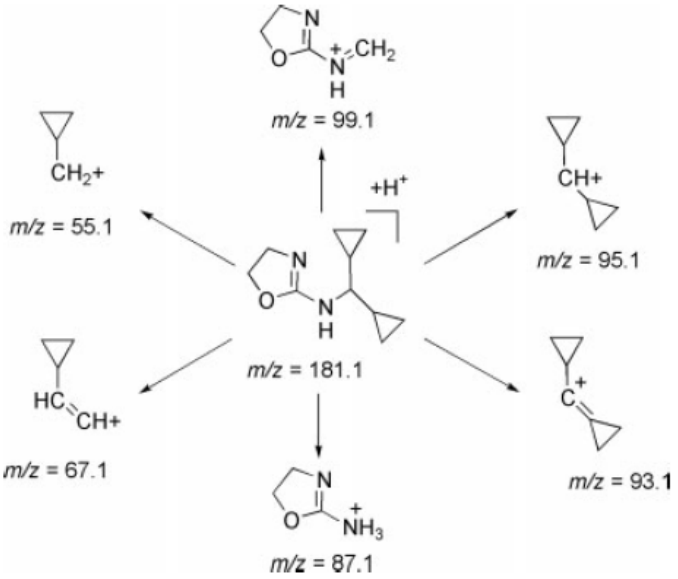

Obr.5.2 Navržené fragmentační cesty rilmenidinu

5.3. Stanovení enantiomerů tramadolu a O-desmethyltramadolu v lidské moči pomocí GC-MS (publikace VIII)

5.3.1. Teoretický úvod

Tramadol (1RS, 2 RS)-2-[(Dimethylamino)methyl]-1-(3-methoxyphenyl)cyclohexanol hydrochlorid je syntetické centrálně působící analgetikum patřící mezi slabé opinoidy. V lékových formách se vyskytuje jako racemická směs dvou enantiomerů lišících se afinitou k různým receptorům CNS. [15]. Struktura tramadolu a jeho hlavního metabolitu je na obrázku 5.3. Metabolismu tramadolu je neobyčejně komplikovaný a poskytuje nejméně 11 nekonjugovaných a 12 konjugovaných metabolitů. Za nejaktivnější metabolit zodpovědný za analgetický účinek je považován O-desmethyltramadol (ODT) [16].

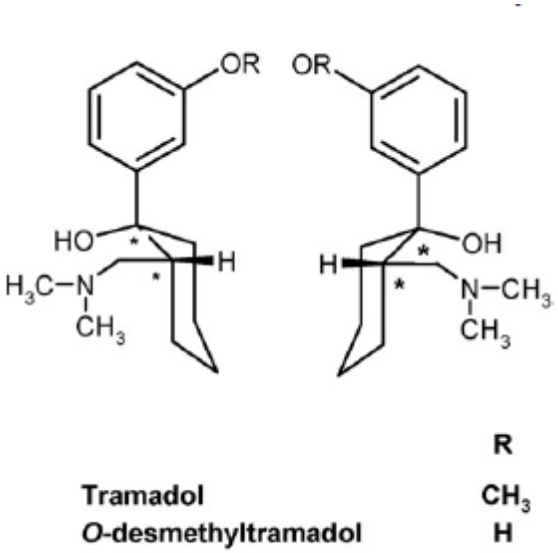

Obr.5.3 Sruktura tramadolu a O-desmetyl tramadolu

Tramadol byl díky svému metabolismu, který je závislý na aktivitě CYP2D6, navržen pro snadnou a bezpečnou fenotypizaci aktivity jaterních enzymů ve farmakogenetických studiích [17]. Právě v těchto případech je nezbytné stereoselektivní stanovení uvažovaných analytů v lidské moči. Mnoho nestereospecifických analytických metod stanovení využívajících GC-MS bylo vypracováno již dříve [18-25], ale jak již bylo dříve zmíněno, vzhledem k odlišnému farmakodynamickému chování jednotlivých enantiomerů je vyžadována chirální analýza. Pro stereoselektivní stanovení tramadolu a DOT byly dosud popsány metody CZE [26-28] a HPLC [29-34]. Alternativní metoda využívající plynovou chromatografii s hmotnostní detekcí doposud nebyla popsána.

5.3.2. Výsledky a diskuse – doplňkový komentář k publikaci

Byla vypracována metoda stereoselektivního stanovení tramadolu a jeho hlavního metabolitu pomocí GC-MS bez nutnosti derivatizace. Metoda zahrnuje jednoduchou a rychlou SPE extrakci analytu z biologické matrice, kterou bylo možno připravit vzorky pro přímé dávkování do GC. Enantiomery byly za optimalizovaných chromatografických podmínek dobře rozděleny a byla naměřena všechna potřebná data pro validaci metody. Úspěšná chromatografická separace je zachycena na obrázku 5.4 (a). Na obrázku 5.4 (b) je záznam analýzy reálného vzorku moči dobrovolníka 2 hodiny po podání standardní dávky tramadolu 0,7mg/kg.

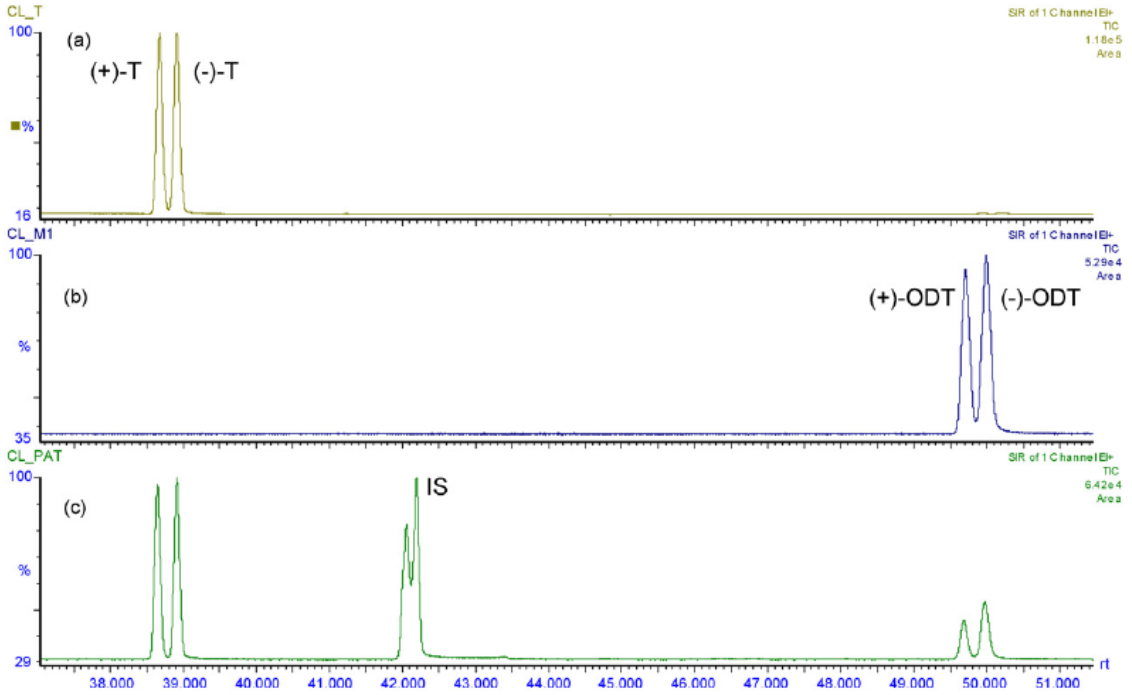

Obr.5.4 SIM chromatogram moči po SPE s přídavkem 3 µg/mL enantiomerů T (a), ODT (b) a moči zdravého dobrovolníka 2 h po podání standardní orální dávky tramadolu 0,7 mg/kg.

Bylo ověřeno, že metoda je použitelná pro CYP2D6 fenotypické testování a plně validovaná metoda může být doporučena pro farmakokinetické studie.

5.4. Stanovení nabumetonu a kyseliny 6-methoxy-2-naftyloctové v plasmě pomocí HPLC s UV a MS detekcí (publikace IX)

5.4.1. Teoretický úvod

Nabumeton (4-(6-methoxy-2-naftyl)-butan-2-on) je léčivo, které patří mezi nesteroidní protizánětlivé látky vykazující preferenční inhibici cyklooxygenázy [35]. Je používán u zánětlivých a degenerativních revmatoidních onemocnění (revmatoidní artritida, osteoartritida), u revmatismu měkkých tkání a u bolestivých poúrazových a pooperačních stavů [36,37]. Nabumeton sám o sobě je proléčivo, které nevykazuje farmakologický účinek. Po orálním podání je dobře absorbován z trávícího traktu a následně v játrech podléhá rozsáhlé biotransformaci za vzniku řady metabolitů. Hlavní metabolit, 6-methoxy-2-naftyloctová kyselina (6-MNA) vzniká oxidačním štěpením postranního řetězce a má farmakodynamické účinky antipyretické, antiflogistické a analgetické, které jsou způsobeny tlumením syntézy prostaglandinů a dalších mediátorů zánětu [38].

Přestože jsou klinické účinky nabumetonu dobře popsány, farmakokinetika nabumetonu dosud podrobněji popsána nebyla kvůli příliš nízkým koncentracím mateřské látky v krvi. Dobře je naopak popsána farmakokinetika 6-MNA díky dostupnosti dostatečně citlivých analytických technik [39-42]. Maxima plasmatické koncentrace 6-MNA je dosaženo průměrně 4–12 h po podání nabumetonu [43]. Cílem práce bylo vyvinout a validovat analytickou metodu, která by umožnila současně stanovit nízké koncentrace nabumetonu a 6-MNA po jednorázovém podání terapeutické dávky léčiva.

5.4.2. Výsledky a diskuse – doplňkový komentář k publikaci

HPLC separace byla prováděna na reverzní C18 koloně. Jako mobilní fáze byly testovány mobilní fáze ze směsi acetonitril/voda a acetonitril/0,1% TFA v izokratickém módu. Byla použita duální UV absorpční (λ = 230 nm) a MS detekce v módu SIM s použitím měkkých ionizačních technik APCI a ESI, obecně vhodných pro polární analyty snadno podléhající protonaci či deprotonaci. Modelový vzorek obsahoval směs 6-MNA, naproxenu (IS) a nabumetonu o koncentraci složek 2.10^{-5} mol.dm^{-3}. Dávkovaný objem vzorku do kolony činil 30 μl. Pro předúpravu vzorků byla zvolena technika extrakce na tuhou fázi (SPE). Vzhledem k povaze studovaných látek byly testovány tři nepolární sorbenty – silikagel modifikovaný C8, C18 a Ph, které byly dále porovnávány. Ionizace elektrosprejem patří stejně jako APCI a APPI mezi měkké ionizační techniky z hlediska maximálního výtěžku

extrakce. V případě 6-MNA a naproxenu s volnou karboxylovou skupinou snadno odštěpující proton byly obě látky dobře ionizovatelné elektrosprejem v negativním módu. Naopak struktura nabumetonu obsahuje karbonyl, který je přístupný protonaci, poskytovala signál v pozitivním módu. Při použití chemické ionizace za atmosférického tlaku všechny tři sledované látky poskytovaly signál pouze spektra kladných iontů.

Celkový přehled všech významných iontů sledovaných látek je uveden v tabulce 5.1

Tab. 5.1 Přehled významných iontů 6-MNA, naproxenu a nabumetonu

	ESI+		ESI–		APCI+	
sloučenina	iont	m/z	iont	m/z	iont	m/z
6-MNA			2M–2H+Na	453	M+H	217
			M–60	156	M–45	171
					M–29	187
6-MNA (TFA)					M+H	217
					M–45	171
naproxen			2M–2H+Na	481	M+H	231
			M–61	169	M–45	185
naproxen (TFA)					M+H	231
					M–45	185
nabumeton	M+Na	251			M+H	229
	M–57	171			M–57	171
					M–17	211
nabumeton (TFA)	M+Na	251			M+H	229
	M–57	171			M–57	171
					M–17	211

Vysvětlivky: 2M-2H+Na ... ion tvořený dvěma molekulami analytu se ztrátou dvou atomů vodíku a připojením jednoho atomu sodíku; M+H ... ion odpovídající protonované molekule analytu; M-H ... ion odpovídající deprotonované molekule analytu; M-60 ... fragmentový ion odpovídající molekule se ztrátou 60 u, obdobně ostatní fragmentové ionty.

Závěrem je možno konstatovat, že se podařilo nalézt optimální podmínky pro stanovení nabumetonu a jeho metabolitu (6-MNA) v krevní plasmě metodou SPE–HPLC/UV/MS. Vypracovaná metoda je spolehlivá, přesná a byla úspěšně validována. Následně byly tímto postupem zpracovány a analyzovány reálné vzorky z klinické studie.

5.5. Literatura VII –IX

1. Slanař, O.:*Farmakoterapie* 3, 296 (2005).
2. Bultas J. *Současná klinická praxe* 3, 6 (2004).
3. Nebert, D. W.: *Am. J. Hum. Genet.* 60, 265 (1997)
4. K. Weerasuriya, E. Shaw, P. Turner: *Eur. J. Clin. Pharmacol.* 1984, *27*, 281.
5. J. P. Fillastre, B. Letac, F. Galinier, G. Le Bihan, J. Schwartz:.*Am. J. Cardiol.* 1988, *61*, 81D.
6. M. Aparicio, M. Dratwa, N. el Esper, J. P. Fillastre, B. Levaltier,R. Lins, A. Meyrier, F. Mignon, J. P. Ryckelynck, J. Sennesael: *Am. J. Cardiol.* 1994, *74*, 43A.
7. J. L. Reid, V. Panfilov, G. MacPhee,H. L. Elliott: *Ann. N. Y. Acad. Sci.* 1995, *763*, 673.
8. J. L. Reid: *Am. J. Hypertens.* 2001, *14*, 322S.
9. R. L. Lins, R. Daelemans, M. Dratwa, D. Verbeelen, J. Sennesael, B. Brisgand, N. Lameire: Am. J.Med. 1989, 87, 41S.
10. C. T. Dollery,D. S. Davies, J. Duchier, B. Pannier,M. E. Safar: Am. J. Cardiol. 1988, 61, 60D.
11. J. D. Ehrhardt: Biomed. Mass Spectrom. 1985, 12, 593.
12. H. L. Ung, J. Girault, M. A. Lefebvre, A. Mignot, J. B. Fourtillan: Biomed. Environ. Mass Spectrom. 1987, 14, 289.
13. S. Murray, D. Watson,D. S. Davies: Biomed.Mass Spectrom. 1985, 12, 230.
14. J. Faktor, I. Struhárová, A. Fučíková, M. Hubálek, B. Vojtěšek, P. Bouchal: Chemické Listy 105, 846-850 (2011)
15. P. Dayer, J. Desmeules, L. Collart, Drugs 53 (Suppl. 2) (1997) 18.
16. W.N.Wu, L.A. McKown, S. Liao, Xenobiotica 32 (2002) 411.
17. R.S. Pedersen, P. Damkier, K. Brosen, Clin. Pharmacol. Ther. 77 (2005) 458.
18. Y.F. Sha, S. Shen, G.L. Duan, J. Pharm. Biomed. Anal. 37 (2005) 143.
19. K.A. Hadidi, J.K. Almasad, T. Al-Nsour, S. Abu-Ragheib, Forensic Sci. Int. 135 (2003) 129.
20. H.J. Leis, G. Fauler,W.Windischhofer, J. Chromatogr. B: Analyt. Technol. Biomed. Life Sci. 804 (2004) 369.
21. C. Moore, S. Rana, C. Coulter, J. Chromatogr. B: Analyt. Technol. Biomed. Life Sci. 850 (2007) 370.

22. M. Merslavic, L. Zupancic-Kralj, J. Chromatogr. B: Biomed. Sci. Appl. 693 (1997) 222.
23. W. Lintz, H. Uragg, J. Chromatogr. 341 (1985) 65.
24. V. Gambaro, C. Benvenuti, L. De Ferrari, L. Dell'Acqua, F. Fare, Farmaco 58 (2003) 947.
25. Y.X. Xu, Y.Q. Xu, C.J. Zhang, L. Shen, Yao Xue Xue Bao 28 (1993) 379.
26. S. Rudaz, J.L. Veuthey, C. Desiderio, S. Fanali, J. Chromatogr. A 846 (1999) 227.
27. S. Rudaz, S. Cherkaoui, P. Dayer, S. Fanali, J.L. Veuthey, J. Chromatogr. A 868 (2000) 295.
28. L. Hui-Chen, Y. Yang, W. Na, D. Ming, L. Jian-Fang, X. Hong-Yuan, Chirality 16 (2004) 112.
29. A.Ceccato, P. Chiap, P. Hubert, J. Crommen, J. Chromatogr. B: Biomed. Sci. Appl. 698 (1997) 161.
30. R. Mehvar, K. Elliott, R. Parasrampuria, O. Eradiri, J. Chromatogr. B: Analyt. Technol. Biomed. Life Sci. 852 (2007) 152.
31. M.A. Campanero, E. Garcia-Quetglas, B. Sadaba, J.R. Azanza, J. Chromatogr. A 1031 (2004) 219.
32. A.Ceccato, F. Vanderbist, J.Y. Pabst, B. Streel, J. Chromatogr. B: Biomed. Sci. Appl. 748 (2000) 65.
33. Y.H. Ardakani, R. Mehvar, A. Foroumadi, M.R. Rouini, J. Chromatogr. B: Analyt. Technol. Biomed. Life Sci. 864 (2008) 109.
34. F. Musshoff, B. Madea, F. Stuber, U.M. Stamer,
35. Boyle E.A., Freeman P.C., Mangan F.R., Thomson M.J.: J Pharm Pharmacol. 1982; 562-569.
36. Battisti W.P., Katz N.P., Weaver A.L., Matsumoto A.K., Kivitz A.J., Polis A.B., Geba G.P.: J Pain. 2004; 511-520.
37. Hedner T., Samulesson O., Wahrborg P., Wadenvik H., Ung K.A., Ekbom A.: Drugs. 2004; 2315-2343; discussion 2344-2315.
38. *Pharmindex kompendium.* Praha, MediMedia Information 2001.
39. Kendall M.J., Chellingsworth M.C., Jubb R., Thawley A.R., Undre N.A., Kill D.C.: Eur. J. Clin. Pharmacol. 1989; 299-305.
40. Davies N.M.: Clin. Pharmacokinet. 1997; 404-416.
41. Patel B.N., Sharma N., Sanyal M., Prasad A., Shrivastav P.S.:. Biomed.

Chromatogr. 2008; 1213-1224.
42. Srinivas N.R.: Biomed. Chromatogr. 2009; 674-675.
43. Hedner, T.; Samuelsson, O.; Währborg, P.; Wadenvik, H.; Ung, K.; Ekbom, A.: *Drugs* 64, 2315 (2004).

PUBLIKACE VII

Development of a fast LC–MS/MS method for quantification of rilmenidine in human serum: elucidation of fragmentation pathways by HRMS

Chytil, L.; Cvačka, J.; Marešová, V.; Štrauch, B.; Widimský Jr, J.;
Štícha, M.; Slanař, O.

Journal of Mass Spectrometry. 45 (2010) 1179-1185.

Research Article

Journal of MASS SPECTROMETRY

Received: 28 June 10 Accepted: 12 August 10 Published online in Wiley Online Library:

(wileyonlinelibrary.com) DOI 10.1002/jms.1809

Development of a fast LC–MS/MS method for quantification of rilmenidine in human serum: elucidation of fragmentation pathways by HRMS

Lukáš Chytil,[a,b]* Josef Cvačka,[c] Věra Marešová,[a] Branislav Štrauch,[d] Jiří Widimský Jr,[d] Martin Štícha[e] and Ondřej Slanař[b]

Rilmenidine is an alpha 2 adrenoreceptor agonist used in the treatment of mild and moderate hypertension. In this study, a fast and accurate liquid chromatographic method with tandem mass spectrometric detection has been validated in order to assure quantification of rilmenidine in human serum. The fragmentation pathway of protonated rilmenidine was studied using high-resolution mass spectrometry (HRMS). This study compared selectivity, linearity, accuracy, precision, extraction efficiency, matrix effect and sensitivity using common liquid–liquid extraction (LLE) and solid-phase extraction (SPE) procedures. The limit of quantitation for both extraction techniques was 0.1 ng/ml. Several differences between the LLE and SPE have been observed in terms of linearity, accuracy, precision and matrix effect. Additionally, the advantages of SPE included less manual work load and increased recovery of rilmenidine in human serum to approximately 80% (LLE, 57%). The developed method involving SPE was found to be accurate (relative error (RE) <5%), reproducible (relative standard deviation, RSD <7%), robust and suitable for quantitative analysis of rilmenidine in serum samples obtained from patients under antihypertensive treatment.

Keywords: rilmenidine; LC–MS/MS; serum; quantification; HRMS

Introduction

Primary or essential hypertension relates to high blood pressure with no identifiable origin. It represents a major modifiable risk factor for the development of cardiovascular disease. If lifestyle and diet modifications are not satisfactory, medical treatment with antihypertensive drugs is required. Rilmenidine [(*N*-dicyclopropylmethyl)amino-2-oxazoline] is an alpha 2 adrenoreceptor agonist[1] effective after oral administration in the treatment of mild-to-moderate hypertension.[2,3] The hypotensive action of rilmenidine is mediated through a reduction in peripheral sympathetic tone, resulting from a central and possibly also a peripheral action. Rilmenidine also decreases catecholamine release from the adrenal medulla, which might contribute to the antihypertensive effect.

Rilmenidine is a weak base with pK_a of approximately 9.0. At physiological pH (7.4), 97% of the substance is ionized.[4] However, it is a mildly lipid-soluble compound with a true partition coefficient between octanol and water of about 20.[5] Rilmenidine is mainly used as a phosphate salt, which is freely soluble in water. Absorption of rilmenidine (1 mg) in healthy volunteers is rapid, with t_{max} ranging between 1.33 and 1.94 h[6–9] and maximal plasma concentration (c_{max}) between 3.25 and 3.97 ng/ml.[6,7,9]

To meet the requirements for preclinical, biopharmaceutical and clinical pharmacology studies, a rapid, selective, sensitive and robust analytical method is highly desirable. Very few analytical procedures, applied mainly to pharmacokinetic studies, have been reported for the determination of rilmenidine, which include gas chromatography–mass spectrometry (GC–MS)[10–14] and liquid chromatography–tandem mass spectrometry (LC–MS/MS).[9] Other methods such as LC coupled with ultraviolet or fluorescence (LC–UV/FL) detection have not been described to date. GC–MS analysis was performed using a negative chemical ionization and two-step extraction and derivatization[12–14] with the lower limit of quantification (LLOQ) of 0.1[14] and 0.2 ng/ml.[13] These methods, however, do not meet modern bioanalytical needs with respect to a simple extraction procedure or short analytical run time, as they require a prior derivatization procedure. Nowadays, LC–MS/MS is a preferred tool for quantitative bioanalysis because of its speed, selectivity and sensitivity. The LC–MS/MS method[9] was used for

* *Correspondence to: Lukáš Chytil, Institute of Forensic Medicine and Toxicology, 1st Faculty of Medicine, Charles University in Prague, Ke Karlovu 2, 120 00 Praha 2, Czech Republic. E-mail: lukas.chytil@lf1.cuni.cz*

a *Institute of Forensic Medicine and Toxicology, 1st Faculty of Medicine, Charles University in Prague, 121 08 Prague 2, Czech Republic*

b *Institute of Pharmacology, 1st Faculty of Medicine, Charles University in Prague, 121 08 Prague 2, Czech Republic*

c *Institute of Organic Chemistry and Biochemistry Academy of Sciences of the Czech Republic, v.v.i., Flemingovo nám. 2, 166 10 Prague 6, Czech Republic*

d *Third Department of Internal Medicine, 1st Faculty of Medicine, Charles University in Prague, 121 08 Prague 2, Czech Republic*

e *Department of Organic Chemistry, Faculty of Science, Charles University in Prague, 128 43 Prague 2, Czech Republic*

quantification of rilmenidine in plasma samples obtained from volunteers as a background for a bioequivalence study of two rilmenidine formulations. The aim of this published work was to demonstrate pharmacokinetics data obtained after ingestion of rilmenidine, while a detailed description of the analytical method development was not provided. However, it was reported, that the LLOQ was 0.212 ng/ml and other validation parameters were within acceptable criteria.

The objective of this study was to develop and validate a robust, sensitive and high throughput LC–MS/MS method for routine determination of rilmenidine in human serum samples. In the presented work, we have compared two extraction techniques based on a liquid–liquid extraction (LLE) and a solid-phase extraction (SPE). In both extraction procedures, all main validation parameters such a selectivity, extraction efficiency, matrix effect, linearity, sensitivity and an accuracy were investigated. We used high-resolution MS (HRMS) for the identification of product ions of rilmenidine, which are formed from protonated rilmenidine during MS/MS analysis. The LC–MS/MS assay will be useful in a rilmenidine serum concentration measurement in clinical trials as well as for therapeutic drug monitoring.

Experimental

Chemicals and reagents

Standard of pure rilmenidine phosphate (>99.0%) was kindly supplied by Farmak (Olomouc, Czech Republic). Trimipramine-d_3 (99.0%), which was used as internal standard (IS), was obtained from Alltech (Prague, Czech Republic). Formic acid (p.a.), ammonium formate (p.a.) and acetonitrile (HPLC grade) were purchased from Sigma Aldrich (Steinheim, Germany) and *tert*-butyl methyl ether (TBME) (pure) was obtained form Merck (Darmstad, Germany). Deionized water (DI) was produced in-house using a Milli-Q system from Millipore (Bedford, MA, USA). Bond Elut Certify 50 SPE column was purchased from Varian (Palo Alto, CA, USA).

Sample preparation

Liquid–liquid extraction

Serum samples (1 ml) were diluted with 1 ml of borate buffer (pH 9.5). After addition of 10 µl of a methanolic solution of the IS containing 2 µg/ml of trimipramine-d_3 and an appropriate amount of rilmenidine methanolic solution, the samples were mixed for 10 s on a rotary shaker and consequently extracted with 4 ml of TBME. After centrifugation (4000 *g* for 8 min), the organic phase was separated, acidified with 100 µl 1% HCl in methanol (v/v) and evaporated to dryness under a stream of nitrogen at 40 °C. The residue was dissolved in 100 µl of LC mobile phase, and a 5-µl aliquot was injected into the chromatographic system.

Solid-phase extraction

The Bond Elut Certify column was conditioned with 1 ml of methanol, followed by 1 ml of DI water. A mixture of 1 ml of centrifuged serum (4000 *g* for 8 min), 1 ml of 0.1 M phosphate buffer (pH 6.0), and 10 µl of IS working solution (2 µg/ml) was applied to the column. The sample was forced through the bed at a low flow rate by vacuum. The column was subsequently washed with 1 ml of water, 0.5 ml of 0.1 M HCl, 1 ml of methanol/water solution (50 : 50, v/v) and dried for 5 min under vacuum. Analytes were eluted by 2 ml of mixture containing isopropanol, dichloromethane and ammonium hydroxide (80 : 20 : 2, v/v/v). The extract was evaporated to dryness under a stream of nitrogen at 40 °C after addition of 100 µl 1% HCl in methanol (v/v). The residue was redissolved in 100 µl of mobile phase and 5 µL was injected into the chromatographic system.

Liquid chromatography–mass spectrometry

Apparatus

Apparatus. The chromatographic separation was performed on a 1200 rapid resolution LC (RRLC) Agilent (Waldbronn, Germany), consisting of a degasser, binary pump, autosampler and thermostatted column compartment. The MS/MS analysis was performed using a 3200 Q trap triple quadrupole/linear ion trap mass spectrometer with a TurbolonSpray source (MDS Sciex, Ontario Canada). For data analysis was used Analyst software version 1.5.1.

LC conditions

Chromatographic separation was achieved with an Agilent Zorbax Eclipse XBD–C18 column (1.8 µm, 50 × 4.6 mm I.D.), protected by a C18 security guard cartridge (4 × 2 mm I.D.). Isocratic elution occurred with (A) 5 mM ammonium formate with 0.02% formic acid and (B) 0.02% formic acid in acetonitrile (50 : 50, v/v) at a flow rate of 1.15 ml/min. The mobile phase was thermostatted at 30 ± 0.5 °C.

MS/MS conditions

The mass spectrometer was operated in the positive TurbolonSpray mode and selected reaction monitoring (SRM) was used for data acquisition of rilmenidine and IS. The following transitions were monitored: *m/z* 181.1 → 95.1 and 67.1 for rilmenidine and *m/z* 298.2 → 103.1 for IS. The more abundant product ion (*m/z* 95.1) was used for quantification. The MS parameters for the analysis were as follows: ion source temperature 550 °C; ion-spray voltage 2000 V; nebulizer gas 40 psi; auxiliary gas 40 psi; curtain gas 30 psi and medium collision gas. Conditions of mass spectrometric detection were optimized by direct infusion of standard solutions into the MS. The compound-dependent parameter settings are listed in Table 1.

Table 1. Parameters of MS detection for rilmenidine and trimipramine-d_3

	SRM transitions	Dwell time (ms)	Declustering potential (V)	Entrance potential (V)	Collision energy (V)	Collision entrance potential (V)	Cell exit potential (V)	Ion ratio, SRM2/SRM1
Rilmenidine	181.1 → 95.1	75	23	6	19	15	3	0.58
	181.1 → 67.1	75	23	6.5	28	15	3	–
Trimipramine-d_3	298.2 → 103.1	75	40	5	25	15	2.8	–

Journal of MASS SPECTROMETRY

High-resolution mass spectrometry

High-resolution exact mass MS/MS spectra were obtained with an LTQ Orbitrap XL hybrid mass spectrometer (Thermo Fisher Scientific, Waltham, MA, USA) equipped with an electrospray ion (ESI) source. The spectrometer was operated in the positive ion mode with a mass resolving power of 100 000. The MS/MS experiments were performed in CID and HCD mode with normalized collision energy of 30 and 40%, respectively. Nitrogen was used as sheath/auxiliary gas (35 a.u./5 a.u.) and helium served as the collision gas. The mobile phase was delivered using a Rheos Allegro UHPLC pump (Flux Instruments AG, Switzerland) and consisted of methanol/water (1 : 1), at a flow rate of 50 µl/min. The sample was diluted with the mobile phase and injected using a 2-µl loop. Spray voltage, capillary voltage, tube lens voltage and capillary temperature were 4.3 kV, 40 V, 155 V and 275 °C, respectively. The mass spectra were internally calibrated using sodium adduct of dibutyl pthalate (*m/z* 301.14103) to provide high-accuracy mass measurements within 2.0 ppm.

Assay validation for quantification of rilmenidine in human serum

The following parameters were evaluated for the validation of the LC–MS/MS method for the determination of rilmenidine in human serum: selectivity, sensitivity (limits of detection and quantification), linearity, precision, accuracy, extraction recovery, matrix effect and stability.

Standard working solutions

Standard solutions (200 µg/ml) of rilmenidine or IS were prepared in methanol. Working solutions at rilmenidine concentrations of 2, 0.2 and 0.02 µg/ml were prepared by diluting with mixture of methanol and water (50 : 50, v/v). The IS working solution was prepared by diluting with methanol at the final concentration of 2 µg/ml.

Calibration samples and quality control samples

Blood samples obtained from drug-free volunteers were centrifuged (4000 *g* for 5 min) and the serum was stored at −20 °C prior to analysis. Appropriate amounts of working solutions were added to 1 ml of drug-free human serum to create calibration samples at final concentrations of 0.1, 0.5, 1.5, 3, 6 and 12 ng/ml of rilmenidine (free base). Quality control (QC) samples at concentrations of 0.4 (QC1), 4 (QC2) and 8 (QC3) ng/ml of rilmenidine were prepared daily.

Selectivity

The method selectivity was assessed by analyzing six different lots of pooled blank human serum and by comparing them with spiked serum samples at concentration near to the lowest point of calibration curve. A zero sample (blank sample with IS) was analyzed to check for the absence of ions of the IS in the respective peaks to rilmenidine. Additionally, serum samples from patients receiving other medications frequently used for therapy of cardiovascular diseases (amlodipine, betaxolol, bisoprolol, hydrochlorothiazide, losartan, metoprolol, perindopril, ramipril and telmisartan) were tested to exclude possible interferences.

Linearity

The peak-area ratio of rilmenidine/IS was measured and plotted against the theoretical concentration of the spiked standards. A six-point calibration curve was constructed over the whole concentration range (0.1–12 ng/ml) with a weighting factor of $1/x$. Least square linear regression analysis was performed to determine slopes, intercepts and correlation coefficients (R^2 required to be $\geq$0.99). Replicates ($n = 6$) at each concentration level were prepared by both extraction techniques as described above and the obtained results were compared. The calibration range was defined considering the normal therapeutic concentrations obtained from previously published works.[5,6,9] The working range was extended in comparison to the methods applied in studies with healthy volunteers since overdosed patients are likely to be monitored in real clinical settings.

Accuracy and precision

Accuracy, intra- and interday precision for rilmenidine were evaluated according to the requirements of FDA guidelines on bioanalytical method validation.[15] However, the QC1 level was greater than 3 × LLOQ, which was more suitable for the application of this method in clinical settings with drug levels expected to be higher than in samples from single-dose bioavailability studies. Intraday variation was assessed by six replicate determinations of three concentrations (QC1, QC2, and QC3) over the tested range. Intraday accuracies were expressed as the mean of assays relative to the exact value. The intraday precision of the method was calculated as the relative standard deviation (RSD) of the assay made for intraday accuracy. Interday variation was determined by analyzing replicates of QC samples with the same concentrations for 3 days. Accuracies were calculated as the mean of the assays relative to the nominal value. The interday precision of this method was expresses as the RSD of the assays made for interday accuracy.

Extraction efficiency and matrix effect

Peak areas obtained from QC serum samples and those found by direct injection of mobile phase solutions at the same concentration levels were compared to the calculated extraction efficiency of analyzed compounds. The matrix effect was calculated according to the method by Matuszewski *et al.*[16] as peak areas of the samples spiked after extraction procedure divided by the corresponding areas of the standard solutions dissolved in serum before extraction. Recovery and matrix effect experiments were performed for five different lots of human serum at three concentration levels (QC) of rilmenidine and at one concentration level of IS. Obtained values were converted to a percentage and subtracted from 100 to represent the amount of signal suppressed or enhanced by the presence of matrix.

Limits

The LLOQ refers to the lowest concentration of each compound in human serum, that can be analyzed quantitatively by the LC–MS/MS method with precision less than or equal to 20% and accuracy within 80–120% ($n = 6$). The limit of detection (LOD) is the lowest concentration with a signal to noise ratio higher than 3 : 1. Both parameters were empirically evaluated by analyzing samples with low concentrations of analytes.

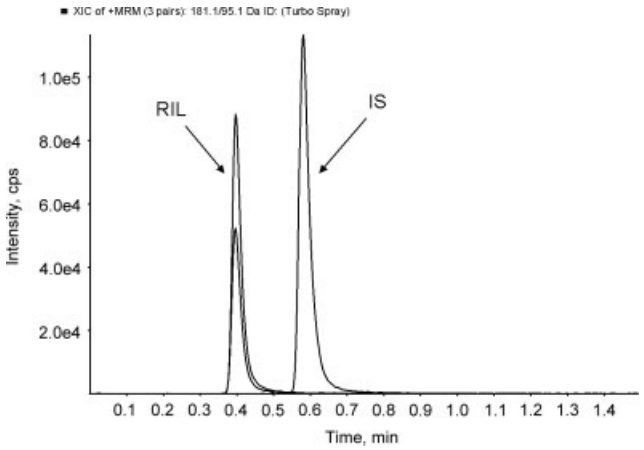

Figure 1. SRM chromatograms obtained after SPE of serum samples collected in a period of 2 h after an oral dose of rilmenidine in dose of 1 mg (3.51 ng/ml).

Stability

Stability was evaluated with human serum fortified with rilmenidine at the three QC concentrations ($n = 6$). Short-term temperature stability was tested during the whole working day at room temperature, at 4 °C for 10 days and at −20 °C for 1 month. QC samples were kept at these storage conditions and calculated concentrations of stability specimens were compared to QC samples prepared freshly on the day of analysis.

Results and Discussion

LC–MS method development

Separation of rilmenidine and IS was performed under acidic conditions. Chromatographic behavior of both analytes on an octadecyl reversed phase packing material was suitable. No extensive tailing was observed during the chromatographic method development. Different ratios of acetonitrile and solution A, temperature and flow rate were tested for obtaining good chromatographic separation. A higher content of acetonitrile (≥90%) resulted in insufficient analytes separation and stability of retention times. Additionally, a high content of acetonitrile gave rise to insufficient response of the analytical system, while a higher content of solution A (≥70%) induced a significantly longer chromatographic run. Finally, using a mobile phase with 50% fraction of acetonitrile provided the best separation and a good response of MS detector was obtained. The optimal flow rate of mobile phase was found to be 1.15 ml/min. The tested column oven temperature changes (20–50 °C) did not substantially affect the time of analysis or response of the MS detector, while the best peak sharpness was observed using 30 °C. Stability of the chromatographic method was evaluated by calculating retention time variability. RSD for retention times was lower than 0.17% for both analytes over 20 consecutive injections. Analyte and IS were eluted within 0.7 min with a total chromatographic run time of 1.5 min (Fig. 1).

The conditions of MS detection were optimized for maximum product ion formation by direct infusion of the single compound of interest. Product spectra of protonated molecule $[M + H]^+$ of rilmenidine and IS are displayed in Fig. 2. For rilmenidine two SRMs were set up, one for quantification and one as a qualifier using one precursor ion and two product ions per compound as shown in Table 1. The ratios of signal intensities of SRM1 and SRM2 and retention time deviations were used for analyte identification in analyzed unknown samples. The RSD of SRM ratios were lower than 2.82% over the whole working range. The transition m/z 298.2 → 103.1 was used for the SRM analysis of trimipramine-d_3. Formation of the most abundant fragment ion m/z 103.1 was analogical to the formation of m/z 101.1 in unlabelled trimipramine.[17,18]

Accurate mass measurement of the product ions of rilmenidine

The fragmentation of protonated rilmenidine was studied using HRMS. The most intense fragment at m/z 95.1 was found to be $C_7H_{11}^+$ (95.08549, −0.4 ppm) and formally explained by elimination of neutral molecule of heterocyclic amine $C_3H_6N_2O$. The ion at m/z 93.1 is $C_7H_9^+$ (93.06985, −0.3 ppm) was formed by loss of $C_3H_8N_2O$. The second most intense signal observed at m/z 67.1 was $C_5H_7^+$ (67.05417, −0.8 ppm) probably originated from $C_7H_{11}^+$ after elimination of ethylene. The loss of C_3H_6 from the same ion gives m/z 55.1 ($C_4H_7^+$; 55.05411, −2.1 ppm). The less abundant ions contain heterocyclic moiety; m/z 99.1 corresponding to $C_4H_7N_2O^+$ (99.05525, −0.4 ppm), m/z 87.1 representing $C_3H_7N_2O^+$ (87.05529, 0.1 ppm). The chemical structure and fragmentation pathway of rilmenidine are displayed in Fig. 3.

Sample preparation

The determination of extraction efficiencies and matrix effects is a major part of bioanalytical LC–MS/MS method validation procedure. For analysis of medications in biological matrices, sample clean up is used to reduce possible ion enhancement or suppression. Serum concentration of rilmenidine is very low, which can lead to trouble during routine clinical analysis. To avoid potential problems with sensitivity it was necessary to find a very effective extraction technique.

Different buffers for alkalization of serum samples and different solvents were tested during optimization of LLE for rilmenidine. The most common buffers used for the extraction of basic drugs are Sörensen's buffer,[19] TRIS buffer[20] and borate buffer[21] and the most frequent organic solvents used for the LLE of drugs are TBME,[22] butyl acetate[23] and dichloromethane.[24] In the initial experiment, rilmenidine (1 ng/ml) was extracted from human serum, using nine different combinations of solvents and buffers. LLE using borate buffer and TBME showed the best results and, therefore, this method was chosen for further comparison of LLE and SPE. Chromatograms obtained by analyzing serum samples extracts from various pHs are displayed in Fig. 4. Similar to the optimization of LLE, different buffers for pH adjustment and various compositions of elution solvents were examined during SPE method development. The best extraction efficiency was observed using the phosphate buffer (pH 6.0), which was also recommended by the column manufacturer. In solvent testing, comparable results were obtained using a mixture of isopropanol, dichloromethane, ammonium hydroxide (80 : 20 : 2, v/v/v) and ethyl acetate, ammonium hydroxide (98 : 2, v/v) for elution of rilmenidine and IS. However, reproducible recoveries were obtained using isopropanolic solution only.

Assay validation

Selectivity

The selectivity of the method was tested by comparing the chromatograms of six different lots of blank human serum. All

Journal of MASS SPECTROMETRY

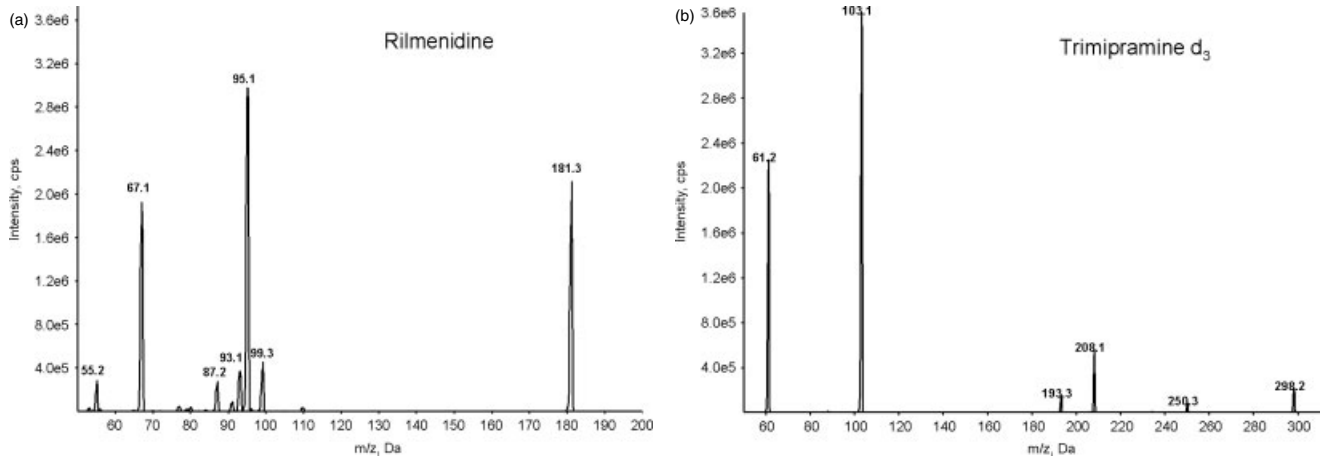

Figure 2. Product ion spectra of $[M + H]^+$ of (a) rilmenidine and (b) trimipramine-d_3, the internal standard.

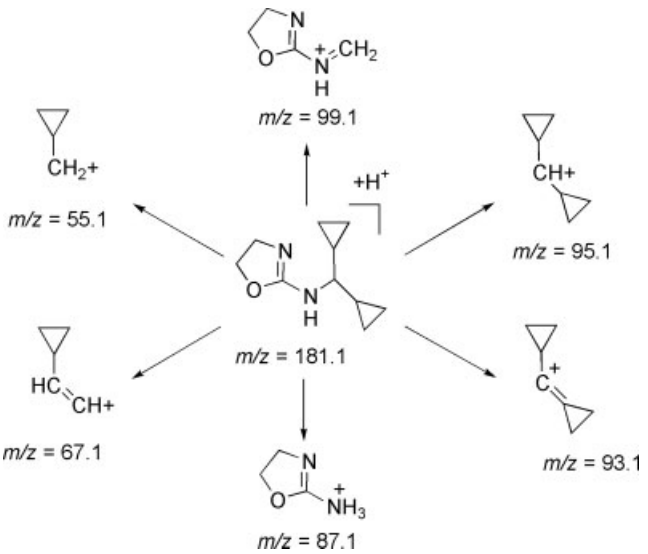

Figure 3. Chemical structure and fragmentation pathways proposed for rilmenidine.

blank serum samples, prepared by both extraction techniques, were found to be free of interferences with respect to both SRM transitions. Analysis of zero samples (blank plus IS) gave no indication of possible interferences from IS. Additionally, no interfering peaks to rilmenidine and IS were found with potentially interfering compounds.

Linearity

Replicates ($n = 6$) of matrix calibrator at six different concentrations from 0.1 to 12 ng/ml were extracted using both described method and consequently analyzed. The back-calculated concentrations of all calibrators were compared with their respective nominal values. If the LLE was used for extraction, it was necessary to exclude some calibrators, whose back-calculated concentrations deviated more than ±15% (±20 LLOQ). Back calculations of the calibrators extracted using SPE were more accurate and the deviation did not exceed 9.8%. The parameters of the calibration curve equations obtained after analysis and computations of calibrators extracted through both methods are listed in Table 2.

Table 2. Comparison of slopes, intercepts and correlations coefficients of calibrations curves obtained after LC–MS/MS analysis of calibrators prepared by two different extraction methods

	a	*b*	R^2	*a*	*b*	R^2
$n = 6$		SPE			LLE	
Mean	1.267	−0.0038	0.9992	0.848	0.0065	0.9972
SD	0.026	0.0011	0.0002	0.077	0.0063	0.002
RSD (%)	2.07	–	–	9.08	–	–

a, slope; *b*, intercept; R^2, correlation coefficient; SD, standard deviation; RSD, relative standard deviation.

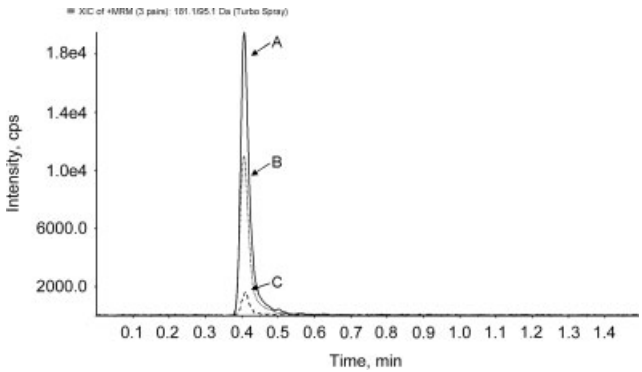

Figure 4. SRM chromatograms of rilmenidine extracted from spiked human serum (1 ng/ml) using liquid–liquid extraction with *tert*-butyl methyl ether. Alkalinization was performed by adding 1 ml of Sörensen's buffer (pH 7.2; A), 1 ml of TRIS buffer (pH 8.1; B) and 1 ml of borate buffer (pH 9.5; C).

Accuracy and precision

QC samples at low (QC1), medium (QC2) and high (QC3) concentration levels were analyzed and calculated on the basis of a freshly prepared calibration curve. QCs and calibrators were prepared using both extraction procedures. The results are summarized in Table 3. The criteria for precision (≤15%) were fulfilled for both tested extraction techniques at each concentration level. However, in the case of LLE, the deviations were significantly higher than for SPE. The data for accuracy were within the

Table 3. Inter- and intraday variation data from the determination of rilmenidine in human serum

	QC1		QC2		QC3	
	Accuracy (%)	Precision (%)	Accuracy (%)	Precision (%)	Accuracy (%)	Precision (%)
Intraday variation						
LLE	102.4	7.5	105.4	6.5	106.6	3.9
SPE	104.4	2.5	97.0	5.8	97.7	1.3
Interday variation						
LLE	92.8	9.9	108.7	6.7	117.9	7.0
SPE	96.6	2.9	97.3	6.9	99.3	2.4

QC, quality control; LLE, liquid–liquid extraction; SPE, solid-phase extraction.

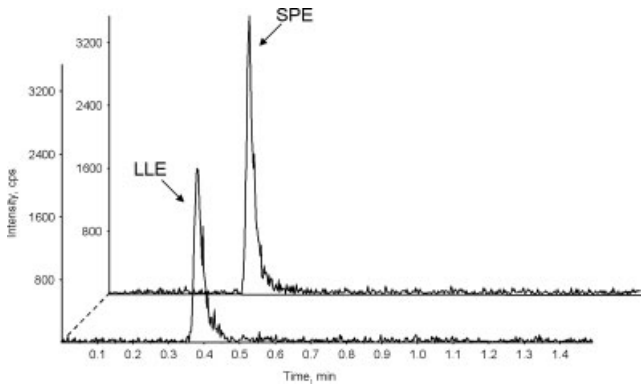

Figure 5. SRM mass chromatograms obtained after analysis of a spiked serum sample containing 0.1 ng/ml (LLOQ) of rilmenidine (*m/z* 181.1 → 95.1).

acceptance limit (±15% of the nominal value), with the exceptions of LLE at the high concentration level. Better results obtained after SPE extraction are probably due to the smaller amount of organic solvent that must be evaporated during preparation.

Extraction efficiency and matrix effect

Generally, solvent selection and evaporation are crucial steps in LLE. LLE requires a large volume of organic solvents that must be evaporated with caution because of suspect volatility of small molecules as rilmenidine. In order to prevent rilmenidine volatility, hydrochloric acid was added to form rilmenidine salt prior to evaporation. The detailed description of LLE optimization is summarized above. SPE simplified specimen preparation and reduced extraction time and solvent consumption compared to LLE. Mean extraction efficiency of rilmenidine at three QC concentrations was higher than 57.1 and 76.0% for LLE and SPE, respectively. The recovery of IS at one concentration level (20 ng/ml) reached 81.0 and 71.1% for LLE and SPE, respectively. The matrix effect was observed regardless of applied extraction technique. The ion enhancement less than 34.8% (<13% RSD) was calculated for LLE, while a level of the ion suppression for SPE of rilmenidine was better than 19.9% (<8% RSD). The ion suppression for IS was better than 17.2% (10% RSD) and 13.4% (5% RSD) for LLE and SPE, respectively. Pretreatment of serum samples by SPE seems to be more functional to minimize the matrix effect and increase extraction efficiency of rilmenidine (Table 4).

Table 4. Comparison of recovery and matrix effect for rilmenidine extracted from human serum using LLE and SPE

	Recovery (%, $n = 5$)			Matrix effect (%, $n = 5$, RSD)		
	QC1	QC2	QC3	QC1 (%)	QC2 (%)	QC3 (%)
LLE	66.1	57.1	71.9	113.2 (13)	134.8 (11)	118.2 (9)
SPE	80.3	76.0	88.4	84.9 (5)	80.1 (5)	94.0 (8)

RSD, relative standard deviation; LLE, liquid–liquid extraction; SPE, solid-phase extraction.

Limits

Computations of LLOQ and LOD were conducted for both extraction techniques. Criteria for LLOQ were fulfilled by the lowest point of the calibration curves, while the empirical determination of LOD with decreasing concentrations of analyte resulted in LOD values of 0.02 and 0.04 ng/ml for SPE and LLE, respectively. Chromatograms of spiked serum sample containing 0.1 ng/ml of rilmenidine obtained after LLE and SPE are presented in Fig. 5.

Stability

Rilmenidine was found to be relatively stable under different storage conditions. The variations in concentrations were within ±9.6% of values obtained from the freshly prepared samples. Thus, storage of serum samples under above-mentioned laboratory conditions was not critical for this method.

Application of the method

The developed assay has been successfully applied to serum samples obtained from five patients under treatment with rilmenidine (1 mg once a day ($n = 3$) and twice daily ($n = 2$)). All the patients were using co-medication of diuretics, statins and/or ACE inhibitors. The blood samples were taken between 2 and 3 h post-dose and at 12 h post-dose in patients using rilmenidine in once a day regime. The samples were transferred into venous blood collection tubes (4 ml, BD Vacutainer, Heidelberg, Germany) containing no additives or gels for serum separations. The concentrations at time near to c_{max} were 3.51 and 3.59 ng/ml in patients using 1 mg per day while ranging between 6.70 and 7.20 ng/ml in patients using 1 mg of rilmenidine twice daily. These values correspond to previously reported c_{max} levels in healthy volunteers[6,7,9] and also demonstrate a linear, dose-dependent increase of drug concentration in the serum. The drug

concentrations of the two patients at 12 h post-dose were 0.33 and 0.39 ng/ml, respectively. The representative chromatogram obtained after analysis of serum samples is displayed in Fig. 1.

Conclusion

A novel analytical procedure based on LC–MS/MS is a suitable and valid method for the determination of rilmenidine in serum samples obtained from patients under a treatment with the drug. This LC–MS/MS method, which is described for the first time, is fast, accurate, sensitive and applicable in clinical practice. It was shown to be selective without interferences from the endogenous compounds and co-administered drugs. Matrix effect in terms of ion enhancement or suppression was investigated in this work and seems to be insignificant. Interpretation of the product ion spectra and their correctly structural assignment was performed using HRMS. Application of the method in real samples showed rilmenidine concentrations in line with known pharmacokinetic characteristics of the drug and also demonstrated the ability to determine rilmenidine dose-dependent increase of c_{max} levels.

Acknowledgements

The authors thank Dr Přemysl Indrák (Farmak Olomouc, Czech Republic) for his kind donation of analytical standard of rilmenidine. The authors gratefully acknowledge the technical assistance of Mrs Alena Kopecká. This work was supported by the Academy of Sciences of the Czech Republic (Project No Z4 055 0506) and Czech Ministry of Education (VZ MSMT No 0021620849).

References

[1] P. A. Van Zwieten. Pharmacology of the alpha 2-adrenoceptor agonist rilmenidine. *Am. J. Cardiol.* **1988**, *61*, 6D.
[2] K. Weerasuriya, E. Shaw, P. Turner. Preliminary clinical pharmacological studies of s3341, a new hypotensive agent, and comparison with clonidine in normal males. *Eur. J. Clin. Pharmacol.* **1984**, *27*, 281.
[3] J. P. Fillastre, B. Letac, F. Galinier, G. Le Bihan, J. Schwartz. A multicenter double-blind comparative study of rilmenidine and clonidine in 333 hypertensive patients. *Am. J. Cardiol.* **1988**, *61*, 81D.
[4] M. Remko, M. Swart, F. M. Bickelhaupt. Theoretical study of structure, pka, lipophilicity, solubility, absorption, and polar surface area of some centrally acting antihypertensives. *Bioorg. Med. Chem.* **2006**, *14*, 1715.
[5] P. Genissel, N. Bromet. Pharmacokinetics of rilmenidine. *Am. J. Med.* **1989**, *87*, 18S.
[6] M. Aparicio, M. Dratwa, N. el Esper, J. P. Fillastre, B. Levaltier, R. Lins, A. Meyrier, F. Mignon, J. P. Ryckelynck, J. Sennesael. Pharmacokinetics of rilmenidine in patients with chronic renal insufficiency and in hemodialysis patients. *Am. J. Cardiol.* **1994**, *74*, 43A.
[7] J. L. Reid, V. Panfilov, G. MacPhee, H. L. Elliott. Clinical pharmacology of drugs acting on imidazoline and adrenergic receptors. Studies with clonidine, moxonidine, rilmenidine, and atenolol. *Ann. N. Y. Acad. Sci.* **1995**, *763*, 673.
[8] J. L. Reid. Update on rilmenidine: clinical benefits. *Am. J. Hypertens.* **2001**, *14*, 322S.
[9] G. Groenewoud, L. Potgieter, B. Meyer. Bioequivalence evaluation of rilmenidine in healthy volunteers. *Arzneimittelforschung* **2009**, *59*, 233.
[10] R. L. Lins, R. Daelemans, M. Dratwa, D. Verbeelen, J. Sennesael, B. Brisgand, N. Lameire. Acceptability of rilmenidine and long-term surveillance of plasma concentrations in hypertensive patients with renal insufficiency. *Am. J. Med.* **1989**, *87*, 41S.
[11] C. T. Dollery, D. S. Davies, J. Duchier, B. Pannier, M. E. Safar. Dose and concentration-effect relations for rilmenidine. *Am. J. Cardiol.* **1988**, *61*, 60D.
[12] J. D. Ehrhardt. Gas chromatographic negative ion mass spectrometric assay of 2-dicyclopropylmethylamino-2-oxazoline (s-3341), a new antihypertensive drug. *Biomed. Mass Spectrom.* **1985**, *12*, 593.
[13] H. L. Ung, J. Girault, M. A. Lefebvre, A. Mignot, J. B. Fourtillan. Quantitative analysis of s3341 in human plasma and urine by combined gas chromatography-negative ion chemical ionization mass spectrometry: 15 month inter-day precision and accuracy validation. *Biomed. Environ. Mass Spectrom.* **1987**, *14*, 289.
[14] S. Murray, D. Watson, D. S. Davies. Bistrifluoromethylaryl derivatives for drug analysis by gas chromatography electron capture negative ion chemical ionization mass spectrometry. Application to the measurement of (n-dicyclopropylmethyl)amino-2-oxazoline in plasma. *Biomed. Mass Spectrom.* **1985**, *12*, 230.
[15.] Food and Drug Administration. *FDA Guidance for Industry: Bioanalytical Method Validation. US Department of Health and Human Services*, Food and Drug Administration, Center for Drug Evaluation and Research: **2001**.
[16] B. K. Matuszewski, M. L. Constanzer, C. M. Chavez-Eng. Strategies for the assessment of matrix effect in quantitative bioanalytical methods based on HPLC-MS/MS. *Anal. Chem.* **2003**, *75*, 3019.
[17] S. McClean, E. J. O'Kane, W. F. Smyth. Electrospray ionisation-mass spectrometric characterisation of selected anti-psychotic drugs and their detection and determination in human hair samples by liquid chromatography-tandem mass spectrometry. *J. Chromatogr. B. Biomed. Sci. Appl.* **2000**, *740*, 141.
[18] B. Doherty, V. Rodriguez, J. C. Leslie, S. McClean, W. F. Smyth. An electrospray ionisation tandem mass spectrometric investigation of selected psychoactive pharmaceuticals and its application in drug and metabolite profiling by liquid chromatography/electrospray ionisation tandem mass spectrometry. *Rapid Commun. Mass Spectrom.* **2007**, *21*, 2031.
[19] S. St-Hilaire, P. M. Belanger. Simultaneous determinations of tolbutamide and its hydroxy and carboxy metabolites in serum and urine: application to pharmacokinetic studies of tolbutamide in the rat. *J. Pharm. Sci.* **1989**, *78*, 863.
[20] E. Saar, D. Gerostamoulos, O. H. Drummer, J. Beyer. Comparison of extraction efficiencies and LC-MS-MS matrix effects using LLE and SPE methods for 19 antipsychotics in human blood. *Anal. Bioanal. Chem.* **2009**, *393*, 727.
[21] S. Wenzel, R. Aderjan, R. Mattern, I. Pedal, G. Skopp. Tissue distribution of mirtazapine and desmethylmirtazapine in a case of mirtazapine poisoning. *Forensic Sci. Int.* **2006**, *156*, 229.
[22] M. Polinko, K. Riffel, H. Song, M. W. Lo. Simultaneous determination of losartan and exp3174 in human plasma and urine utilizing liquid chromatography/tandem mass spectrometry. *J. Pharm. Biomed. Anal.* **2003**, *33*, 73.
[23] S. S. Johansen, J. L. Jensen. Liquid chromatography-tandem mass spectrometry determination of LSD, iso-LSD, and the main metabolite 2-oxo-3-hydroxy-LSD in forensic samples and application in a forensic case. *J. Chromatogr. B. Analyt. Technol. Biomed. Life Sci.* **2005**, *825*, 21.
[24] S. Mennickent, R. Fierro, M. Vega, M. de Diego, C. G. Godoy. Instrumental planar chromatographic method for determination of carbamazepine in human serum. *J. Sep. Sci.* **2009**, *32*, 1454.

PUBLIKACE VIII

Enantiomeric determination of tramadol and O-desmethyltramadol in human urine by gass chromatography–mass spectrometry

Chytil, L.; Štícha, M.; Matoušková, O.; Perlík, F.; Slanař, O.

Journal of Chromatography B.: 877 (2009) 1937-1942.

Journal of Chromatography B, 877 (2009) 1937–1942

Contents lists available at ScienceDirect

Journal of Chromatography B

journal homepage: www.elsevier.com/locate/chromb

Short communication

Enatiomeric determination of tramadol and *O*-desmethyltramadol in human urine by gas chromatography–mass spectrometry

Lukáš Chytil[a,b,*], Martin Štícha[c], Olga Matoušková[b], František Perlík[b], Ondřej Slanař[b]

[a] *Institute of Forensic Medicine and Toxicology, 1st Faculty of Medicine, Charles University in Prague, 121 08 Prague 2, Czech Republic*
[b] *Institute of Pharmacology, 1st Faculty of Medicine, Charles University in Prague, 121 08 Prague 2, Czech Republic*
[c] *Department of Organic Chemistry, Faculty of Science, Charles University in Prague, 12843 Prague 2, Czech Republic*

ARTICLE INFO

Article history:
Received 24 November 2008
Accepted 27 April 2009
Available online 3 May 2009

Keywords:
Tramadol
O-Desmethyltramadol
Enantiomeric separation
Metabolic phenotype
Urine
Excretion
Probe drug
Cytochrome P450 2D6

ABSTRACT

A GC–MS assay for stereoselective determination of tramadol and its pharmacologically active phase I metabolite *O*-desmethyltramadol in human urine was developed. Nefopam was used as internal standard. The method involves a simple solid phase extraction with chiral analysis by gas chromatography–electron ionization mass spectrometry using *m*/*z* 263; 58, 249; 58, and 179; 58 for the determination of concentration of tramadol, *O*-desmethyltramadol and internal standard, respectively. Chromatography was performed on a Rt-βDEXcst column containing alkylated beta-cyclodextrins as a chiral selector. The calibration curves were linear in the concentration range 0.1–20 μg/mL ($R^2 \geq 0.998$). Intra-day accuracies ranged between 97.2–104.9%, 96.1–103.2%, and 97.3–102.8% at the lower, intermediate, and high concentration for all analytes, respectively. Inter-day accuracies ranged between 95.2–105.7%, 99.1–105.2%, and 96.5–101.2% at the lower, intermediate, and high concentration for all analytes, respectively. This method was successfully used to determine the concentration of enantiomers of T and ODT in a pharmacogenetic study.

1. Introduction

Tramadol hydrochloride (T) (1RS, 2RS)-2-[(dimethylamine) methyl-1-(methoxyphenyl)-cyclohexanol HCl] (Fig. 1) is a centrally acting analgetic drug with analgesic efficacy and potency that ranges between weak opioids and morphine. T is used as the racemate for therapy. Each enantiomer displays different binding properties for various receptors. (+)-T preferentially inhibits serotonin reuptake while (−)-T mainly inhibits noradrenalin reuptake [1,2]. (+)-T is 10-times more potent than (−)-T [3].

The metabolic fate of tramadol is unusually complex having at least 11 unconjugated metabolites and 12 conjugated compounds [4]. There are three major metabolic pathways via three distinct cytochrome P450 enzymes CYP2D6, CYP3A, and CYP2B6 forming *O*- and *N*-demethylated metabolites. Major active metabolite *O*-desmethyltramadol (ODT), which is considered to be the main agent responsible for the drug-induced opioid analgesia, is, however, formed in the liver [2,4] predominantly via CYP2D6 enzyme. (−)-ODT also possesses potent monoamine reuptake inhibitory activity and, moreover, has been reported to potentiate the antinociceptive effects of (+)-ODT in rats [5]. Studies using the cloned human μ-opioid receptor have also established that (+)-ODT has approximately 200-times the affinity of the parent (±)-T [6]. Moreover, (+)-ODT had the greatest intrinsic efficacy in an in vitro screen [6].

Cytochrome P450 2D6 is a highly polymorphic gene locus with more than 70 variant alleles. Its single nucleotide polymorphisms can greatly affect the phenotype leading to complete enzyme deficiency in poor metabolizers, incomplete deficiency in intermediate metabolizers in comparison to extensive metabolizers. The pharmacokinetics of T and ODT is greatly affected by CYP2D6 deficency [7] and the metabolism catalyzed through CYP2D6 is stereoselective for (+)-ODT formation in vivo [8–10]. The genetic enzyme deficiency predispose poor metabolizers to have no or extremely low levels of (+)-ODT in blood, while ultrarapid metabolizers were shown to have unusually high (+)-ODT levels in blood [11]. Although there is no convincing evidence that the genotype-dependent pharmacokinetics differences relate to analgesic action of the drug in clinical practise, pharmacodynamic action of the drug is modified by CYP2D6 polymorphism [7,11–13]. Due to the metabolic fate of tramadol that is depedent on the activity of CYP2D6, the drug has been proposed to be used as a probe drug for easy and safe phenotyping of the liver enzyme activity in human pharmacogenetic studies [14]. For this purpose, a stereoselective determination from human urine needs to be applied.

Achiral determinations of T or ODT in biological matrices are still routinely used in bioequivalence studies. Number of achiral

* Corresponding author at: Institute of Forensic Medicine and Toxicology, 1st Faculty of Medicine, Charles University in Prague, Ke Karlovu 2, 120 00 Praha 2, Czech Republic. Tel.: +420 224967196; fax: +420 224911267.
E-mail address: lukas.chytil@lf1.cuni.cz (L. Chytil).

1570-0232/$ – see front matter © 2009 Elsevier B.V. All rights reserved.
doi:10.1016/j.jchromb.2009.04.042

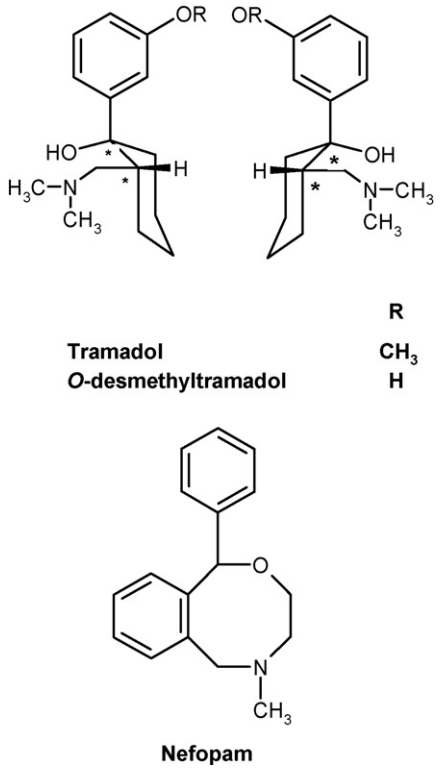

Fig. 1. Structures of tramadol, *O*-desmethyltramadol and nefopam.

methods have been developed previously using TLC [15], GC with nitrogen–phosphorous detection [16], GC with flame ionization detection [17], GC–MS [18–25], and HPLC [26–32]. Chiral analysis of T and ODT is important in clinical studies due to the different pharmacodynamic action of individual enantiomers. As the drug undergoes a stereoselective metabolism, which is dependent on the activity of liver cytochrome P450 2D6, enantiomeric determination of T and ODT in urine may be reliably used as a simple noninvasive phenotyping test for the evaluation of CYP2D6 activity in vivo. Stereoselective determinations of T and ODT have been described using CE [33–35] or HPLC [36–42], but no GC method was described so far.

The aim of this work was to develop a simple method for simultaneous enantiomeric determination of T and ODT in urine as an analytical method for CYP2D6 phenotyping in vivo. T, ODT and IS. were analysed by gas chromatography with mass spectrometric detection, which is more available than CE and can be used as alternative method to generally more costly HPLC technique. This method is easy to provide and is aplicable for routine enantiomeric determination of T and ODT in a single sample of human urine as a basis for CYP2D6 phenotype determination in vivo. Described procedure involves a simple SPE extraction for obtaining clear extract, which is prepared for injecting onto GC/MS system without derivatization step.

2. Experimental

2.1. Materials

BondElut Certify 130 SPE column and Vac Elut 20 vacuum manifold were purchased from Varian (Palo Alto, CA, USA). Automatic pipettes were obtained by Eppendorf (Hamburg, Germany). Glass vials were obtained from Jaytee Biosciences (Whitstable, UK). Heating block was purchased from Barkey (Bielefeld, Germany).

2.2. Chemicals and reagents

Standards of pure T and ODT enantiomers and racemic compounds were kindly supplied by Grünenthal (Stolberg, Germany). Internal standard nefopam hydrochloride was purchased from MP Biomedicals (Illkirch, France). Ammonium hydroxide (28%), methanol, 2-propanol and dichloromethane (gradient grade) were purchased from Merck (Darmstadt, Germany). TRIS buffer was purchased from Sigma–Aldrich (Prague, Czech Republic). Natrium acetate for the preparation of acetate buffer pH 4 was supplied by Penta Chemicals (Prague, Czech Republic). Ultra/high quality water was obtained using a Milli-Q apparatus Millipore (Bedford, MA, USA). Helium (purity 6.0) and nitrogen (purity 5.0) were purchased from Linde Gas (Prague, Czech Republic). All chemicals were obtained in p.a. grade unless specified otherwise.

2.3. Gas chromatography–mass spectrometry

A GC Fisons Instruments 8000 series chromatograph with autosampler CTC-2005, CTC Analytics (Zwingen, Switzerland) coupled to a mass spectrometer Fisons Instruments MD 800 was used. Chromatographic separation was achieved by Rt-βDEXcst capillary column (30 m × 0.25 mm ID, 0.25 μm film thickness) from Restek (Bellefonte, PA, USA).

The oven temperature initially set at 120 °C was increased at a rate of 2.5 °C/min to 230 °C and then held for 10 min. The injector temperature was 230 °C. Pressure of carrier gas (helium) was 70 kPa. Injection was performed in splitless mode (60 s delay before opening the splitter).

The MS detector parameters were GC–MS transfer line temperature 230 °C, electron energy 70 eV. Selected ion monitoring mode for quantitative analysis from 35 to 55 min was used, *m*/*z*: 58; 263 for T, 58; 249 for ODT and 58; 179 for IS (*m*/*z* 58 was used for the quantification of both analytes and IS).

2.4. Stock and standard working solutions

Separate stock solutions of racemic T and ODT (200 μg/mL) in methanol were stored at +4 °C. Standards were prepared from stock solutions at final concentrations of 5, 25, 100, 250, 500, and 1000 μg/mL. The IS working solution was prepared at the final concentration of 1 mg/mL.

2.5. Standard samples and quality control samples

Aliquotes of blank urine obtained during a 24-h urine collection from a healthy volunteer were stored at −70 °C and used to prepare spiked urine samples. Standard working solutions of T and ODT were added to 1 mL of drug free human urine creating final concentrations from 0.1 to 20 μg/mL. Quality control samples of T and ODT at concentrations of 0.5, 5 and 10 μg/mL were prepared daily.

2.6. Sample preparation

All standard, quality control and biological samples were processed by identical method. Bond Elut Certify column was conditioned with 2 mL of methanol, followed by 2 mL of water. A mixture of 1 mL of centrifuged urine, 2 mL of TRIS buffer and 10 μL of IS working solution was applied to the column. Sample was forced through the bed at a low-flow rate by vacuum. The column was subsequently washed with 4 mL of water, 1 mL of acetate buffer pH 4 and 2 mL of methanol and dried for 5 min under 250 mmHg vacuum. Analytes were eluted by 3 mL of mixture containing isopropanol, dichloromethane and ammonium hydroxide (80:20:2, v/v/v). The extract was evaporated to dryness under a stream of nitrogen at 45 °C in a heating block. The residue was redissolved in 150 μL of methanol and 2 μL was injected into the GC/MS system.

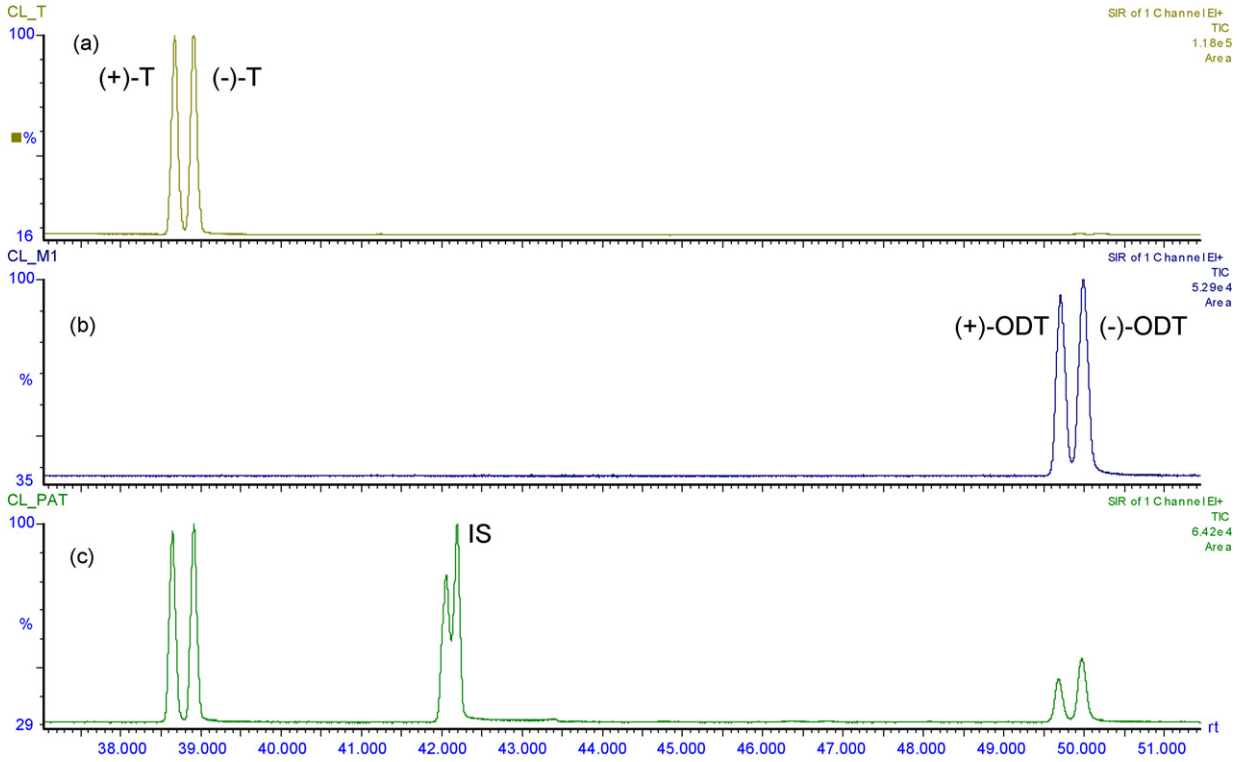

Fig. 2. SIM chromatograms obtained after SPE of a blank urine spiked with 3 μg/mL of each enantiomers of T (a), ODT (b) and a healthy volunteer urine sample (c) collected in a period of 2 h after an oral dose of tramadol drops in standardized dose of 0.7 mg/kg (1.93 μg/mL (+)-T, 1.97 μg/mL (−)-T, 0.73 μg/mL (+)-ODT and 1.08 μg/mL (−)-ODT).

2.7. Calibration

Six-point calibration curves were constructed over the whole concentration range (0.1–20 μg/mL). Normalized peak area ratio of T and ODT enantiomers/IS was measured and plotted against the theoretical concentration of the spiked standards. Least-square linear regression analysis was performed to determine correlation coefficients, slopes and intercepts. Mean accuracy was evaluated on back-calculated concentrations at each calibration level.

2.8. Precision, accuracy and recovery

Accuracy, intra- and inter-day precisions for all analytes were evaluated according to the requirements of FDA guideline on bioanalytical method validation. Intra-day variation was assessed by six replicate determinations of three concentrations over the tested range (0.5, 5 and 10 μg/mL). Intra-day accuracy was expressed as the mean of the assays relative to the theoretical value. The intra-day precision of the method was calculated as the relative standard deviation (RSD) of the assays made for intra-day accuracy. Inter-day variation was assessed by analysing replicates of standards with the same concentrations on three days. Accuracy was computed as the mean of the assays relative to the nominal concentration. The inter-day precision of this method was expressed as the RSD of the assays made for inter-day accuracy.

Recoveries of T and ODT over entire concentration range were determined by comparing peak areas obtained from processed quality control urine samples with those achieved after direct injections of methanolic standard solutions at the same concentrations.

2.9. Peak purity and selectivity

Ten different blank urine samples were analysed for peaks interfering with the detection of the analytes and the IS. The noise data from the assay of blank urine were used in the LOD and LOQ experiment.

2.10. Application of the method

To apply the newly developed method for CYP2D6 phenotyping from a single urinary sample we analysed samples from six healthy, young adult volunteers who received a single oral dose of tramadol drops in standardized dose of 0.7 mg/kg. The volunteers were selected according to their genotype of *CYP2D6* that was determined by polymerase chain reaction–restriction fragment length polymorphism (PCR–RFLP) analysis revealing the presence of *CYP2D6*3*, **4*, **5*, **6* alleles and gene duplication/multiplication according to the previously published method [43]. Two subjects who carried no variant allele in their *CYP2D6* gene were classified as extensive metabolizers (EM), two intermediate metabolizers (IM) had one variant and one wild-type allele of *CYP2D6* and two poor metabolizers (PM) were homozygous carriers of variant *CYP2D6*4* allele. The study drug was administered with 150 mL of water at 8 a.m. after a 10 h overnight fast. Urine samples were collected 2 h after dosing and stored at −70 °C until analysis.

3. Results

3.1. Chromatography

Peaks of enantiomers of both analytes were well resolved. Further, no interfering peaks to T, ODT and IS were found in the urine.

Fig. 2 shows *m/z* 58 SIM chromatograms of blank urine samples spiked with 3 μg/mL of each enantiomers of T (a), blank urine sample spiked with 3 μg/mL of each enantiomers of ODT (b) and result (c) of the analysis of urine sample obtained at 2 h from a volunteer who received tramadol drops.

3.2. Extraction

Mean recovery values ± RSD for T and ODT were 86 ± 8.1% and 84 ± 9.1%, respectively. The recovery for IS was 78 ± 7.2% in concentration of 10 μg/mL.

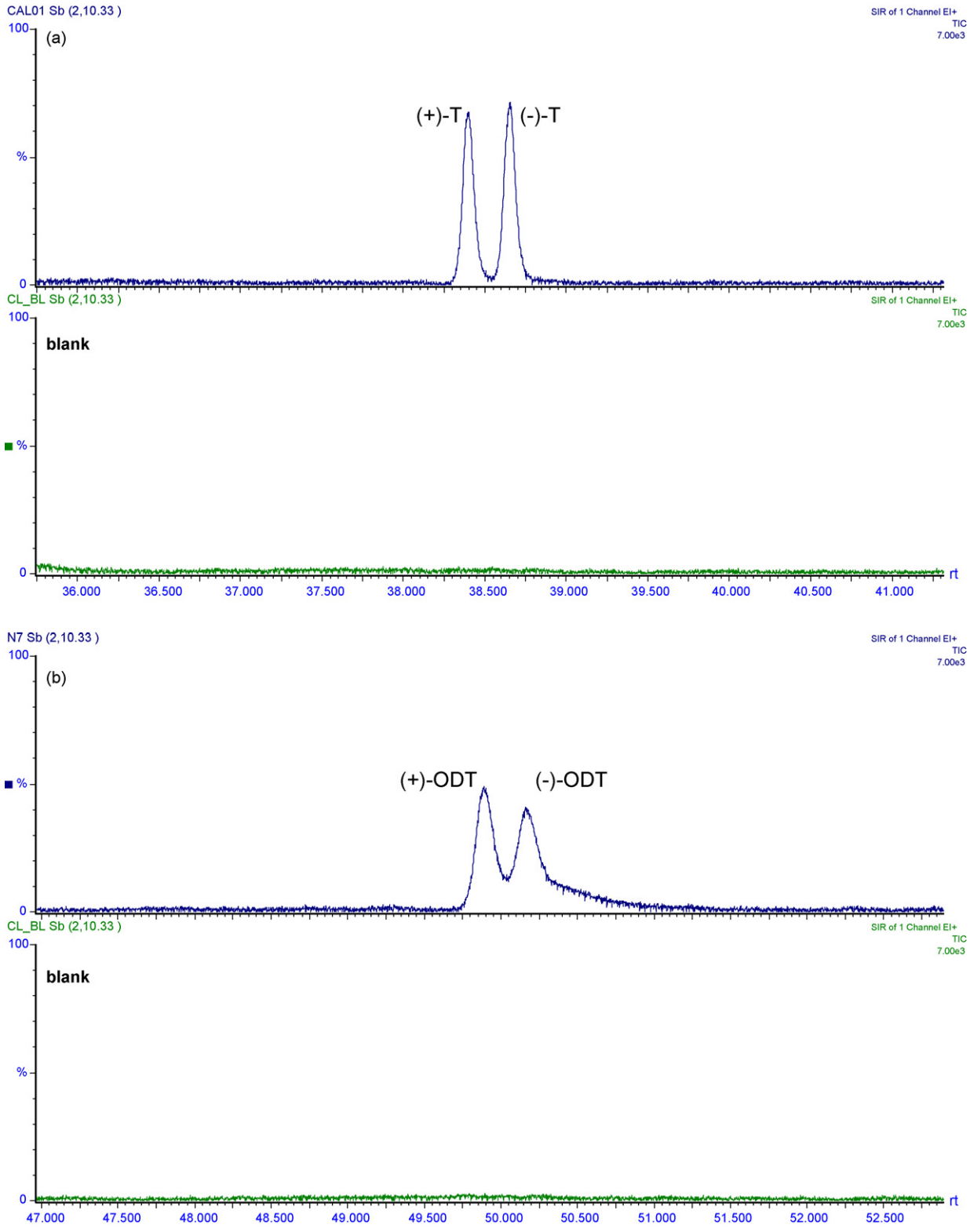

Fig. 3. SIM mass chromatograms obtained after analysis of spiked urine sample containing 0.1 μg/mL (LOQ) of each enantiomers of T (a) and ODT (b).

3.3. Limits of detection and quantification

The limit of detection (LOD, signal-to-noise greater than 3:1) for enantiomers of T and ODT were found to be 0.01 μg/mL for T and 0.03 μg/mL for ODT and the criteria for the limit of quantification (LOQ, signal-to-noise greater than 10:1) were fulfilled by the lowest point of the calibration curve (0.1 μg/mL for both enantiomers of T and ODT). Chromatograms of spiked urine sample containig 0.1 μg/mL of each enantiomers of T and ODT are presented in Fig. 3.

3.4. Calibration

Calibration curves of T and ODT were linear over the range 0.1–20 μg/mL. Mean parameters of equatations are described in

Table 1
Parameters of calibration curves.

	a	*b*	R^2	*a*	*b*	R^2
	(+)-T			(−)-T		
n	6	6	6	6	6	6
Mean	0.5068	−0.0126	0.9988	0.5022	−0.0144	0.9981
SD	0.0315	0.0351	0.0011	0.0292	0.0255	0.0007
RSD (%)	6.22			5.81		
	(+)-ODT			(−)-ODT		
n	6	6	6	6	6	6
Mean	0.3007	−0.0169	0.9992	0.3031	−0.0167	0.9992
SD	0.0241	0.0405	0.0005	0.0187	0.0283	0.0004
RSD (%)	8.01			6.17		

a: slope; *b*: intercept; R^2: correlation coefficient.

Table 2
Inter- and intra-day variation data from the chiral determination of T and ODT.

	0.5 μg/mL		5.0 μg/mL		10 μg/mL	
	Accuracy (%)	Precision (%)	Accuracy (%)	Precision (%)	Accuracy (%)	Precision (%)
Intra-day variation						
(+)-T	104.9	4.7	103.2	5.6	97.3	5.4
(−)-T	102.3	5.5	100.6	3.6	96.9	6.7
(+)-ODT	97.2	7.2	98.8	5.1	100.7	5.3
(−)-ODT	98.6	6.6	96.1	7.9	102.8	5.3
Inter-day variation						
(+)-T	105.7	5.2	105.2	2.3	96.5	2.3
(−)-T	103.2	5.3	102.6	3.8	99.8	3.1
(+)-ODT	96.4	7.5	99.1	4.2	101.2	2.3
(−)-ODT	95.2	8.0	101.2	4.6	100.5	3.7

Table 1. Correlation coefficients were higher than 0.998 and RSD values of concentrations, which were back calculated from the equation of the regresion curves, for each level of calibration curve, ranged from 98.1% to 104.3% for both enantiomers of T and ODT.

3.5. Precision and accuracy

The results obtained from the inter- and intra-day precision and accuracy studies are listed in Table 2.

Intra-day accuracies ranged between 97.2–104.9%, 96.1–103.2%, and 97.3–102.8% at the lower, intermediate, and high concentration for all analytes, respectively.

Inter-day accuracies ranged between 95.2–105.7%, 99.1–105.2%, and 96.5–101.2% at the lower, intermediate, and high concentration for all analytes, respectively.

Precision was 8.0% or less in all analyses.

3.6. CYP2D6 phenotype determination

Metabolic ratios of ODT/T concentrations for enantiomers and total analyte levels in urinary samples are shown in Table 3. The metabolic ratio based on (+)-ODT/(+)-T was clearly the most sensitive for phenotyping of CYP2D6 based on known genotype of the volunteers. The urinary levels of (+)-ODT were below the limit of detection in both poor metabolizers at 2 h post-dose and the excretion of (+)-ODT in intermediate metabolizers was lower than in the extensive metabolizers. Excretion of (−)-ODT was not specific for subjects with an active CYP2D6 enzyme. These findings are fully consistent with previously reported stereoselective production of (+)-ODT by liver CYP2D6.

Table 3
Mean (±SD) urinary metabolic ratios (enatiomer-specific and racemic) in extensive (EM), intermediate (IM) and poor (PM) metabolizers of CYP2D6.

	(+)-ODT/(+)-T	(−)-ODT/(−)-T	(±)-ODT/(±)-T
EM (*n* = 2)	0.63 (0.12)	0.51 (0.49)	0.57 (0.07)
IM (*n* = 2)	0.38 (0.01)	0.30 (0.02)	0.34 (0.02)
PM (*n* = 2)	0.00 (0.00)	0.51 (0.02)	0.26 (0.18)

4. Conclusions

A simple, accurate and precise method based on GC/MS has been developed for the simultaneous enantioselective determination of T and ODT in human urine. The method was verified for use in a CYP2D6 phenotyping test and may be fully recommended in clinical pharmacogenetic studies.

Acknowledgements

This work was supported by a grant IGA MZ CR No. 1A8632-5. The authors wish to thank Grünenthal, GmbH for their kind donation of T and ODT enantiomers. We would like to thank Prof. Jeffrey R. Idle (Charles University, Prague) for technical development of the laboratory and help in obtaining the analytical standards for this study. OS would also like to acknowledge US Smokeless Tobacco Company for a laboratory refurbishment grant.

References

[1] P. Dayer, J. Desmeules, L. Collart, Drugs 53 (Suppl. 2) (1997) 18.
[2] W.D. Paar, P. Frankus, H.J. Dengler, Clin. Investig. 70 (1992) 708.
[3] E. Frankus, E. Friderichs, S.M. Kim, G. Osterloh, Arzneimittelforschung 28 (1978) 114.
[4] W.N. Wu, L.A. McKown, S. Liao, Xenobiotica 32 (2002) 411.
[5] M.J. Garrido, M. Valle, M.A. Campanero, R. Calvo, I.F. Troconiz, J. Pharmacol. Exp. Ther. 295 (2000) 352.
[6] C. Gillen, M. Haurand, D.J. Kobelt, S. Wnendt, Naunyn Schmiedebergs Arch. Pharmacol. 362 (2000) 116.
[7] O. Slanar, M. Nobilis, J. Kvetina, R. Mikoviny, T. Zima, J.R. Idle, F. Perlik, Physiol. Res. 56 (2007) 129.
[8] L. Poulsen, L. Arendt-Nielsen, K. Brosen, S.H. Sindrup, Clin. Pharmacol. Ther. 60 (1996) 636.
[9] R.S. Pedersen, P. Damkier, K. Brosen, Eur. J. Clin. Pharmacol. 62 (2006) 513.
[10] J. Halling, P. Weihe, K. Brosen, Ther. Drug Monit. 30 (2008) 271.

[11] J. Kirchheiner, J.T. Keulen, S. Bauer, I. Roots, J. Brockmoller, J. Clin. Psychopharmacol. 28 (2008) 78.
[12] U.M. Stamer, F. Stuber, T. Muders, F. Musshoff, Anesth. Analg. 107 (2008) 926.
[13] U.M. Stamer, F. Stuber, Anaesthesia 62 (2007) 1294.
[14] R.S. Pedersen, P. Damkier, K. Brosen, Clin. Pharmacol. Ther. 77 (2005) 458.
[15] B. Ahrens, D. Blankenhorn, B. Spangenberg, J. Chromatogr. B: Analyt. Technol. Biomed. Life Sci. 772 (2002) 11.
[16] Q. Tao, D.J. Stone Jr., M.R. Borenstein, V. Jean-Bart, E.E. Codd, T.P. Coogan, D. Desai-Krieger, S. Liao, R.B. Raffa, J. Chromatogr. B: Biomed. Sci. Appl. 763 (2001) 165.
[17] S.T. Ho, J.J. Wang, W.J. Liaw, C.M. Ho, J.H. Li, J. Chromatogr. B: Analyt. Technol. Biomed. Life Sci. 736 (1999) 89.
[18] Y.F. Sha, S. Shen, G.L. Duan, J. Pharm. Biomed. Anal. 37 (2005) 143.
[19] K.A. Hadidi, J.K. Almasad, T. Al-Nsour, S. Abu-Ragheib, Forensic Sci. Int. 135 (2003) 129.
[20] H.J. Leis, G. Fauler, W. Windischhofer, J. Chromatogr. B: Analyt. Technol. Biomed. Life Sci. 804 (2004) 369.
[21] C. Moore, S. Rana, C. Coulter, J. Chromatogr. B: Analyt. Technol. Biomed. Life Sci. 850 (2007) 370.
[22] M. Merslavic, L. Zupancic-Kralj, J. Chromatogr. B: Biomed. Sci. Appl. 693 (1997) 222.
[23] W. Lintz, H. Uragg, J. Chromatogr. 341 (1985) 65.
[24] V. Gambaro, C. Benvenuti, L. De Ferrari, L. Dell'Acqua, F. Fare, Farmaco 58 (2003) 947.
[25] Y.X. Xu, Y.Q. Xu, C.J. Zhang, L. Shen, Yao Xue Xue Bao 28 (1993) 379.
[26] Y.H. Ardakani, M.R. Rouini, J. Pharm. Biomed. Anal. 44 (2007) 1168.
[27] M.R. Rouini, Y.H. Ardakani, F. Soltani, H.Y. Aboul-Enein, A. Foroumadi, J. Chromatogr. B: Analyt. Technol. Biomed. Life Sci. 830 (2006) 207.
[28] Y. Gu, J.P. Fawcett, J. Chromatogr. B: Analyt. Technol. Biomed. Life Sci. 821 (2005) 240.
[29] A. Kucuk, Y. Kadioglu, F. Celebi, J. Chromatogr. B: Analyt. Technol. Biomed. Life Sci. 816 (2005) 203.
[30] S.H. Gan, R. Ismail, W.A. Wan Adnan, Z. Wan, J. Chromatogr. B: Analyt. Technol. Biomed. Life Sci. 772 (2002) 123.
[31] M. Nobilis, J. Kopecky, J. Kvetina, J. Chladek, Z. Svoboda, V. Vorisek, F. Perlik, M. Pour, J. Kunes, J. Chromatogr. A 949 (2002) 11.
[32] M. Nobilis, J. Pastera, P. Anzenbacher, D. Svoboda, J. Kopecky, F. Perlik, J. Chromatogr. B: Biomed. Appl. 681 (1996) 177.
[33] S. Rudaz, J.L. Veuthey, C. Desiderio, S. Fanali, J. Chromatogr. A 846 (1999) 227.
[34] S. Rudaz, S. Cherkaoui, P. Dayer, S. Fanali, J.L. Veuthey, J. Chromatogr. A 868 (2000) 295.
[35] L. Hui-Chen, Y. Yang, W. Na, D. Ming, L. Jian-Fang, X. Hong-Yuan, Chirality 16 (2004) 112.
[36] A. Ceccato, P. Chiap, P. Hubert, J. Crommen, J. Chromatogr. B: Biomed. Sci. Appl. 698 (1997) 161.
[37] R. Mehvar, K. Elliott, R. Parasrampuria, O. Eradiri, J. Chromatogr. B: Analyt. Technol. Biomed. Life Sci. 852 (2007) 152.
[38] M.A. Campanero, E. Garcia-Quetglas, B. Sadaba, J.R. Azanza, J. Chromatogr. A 1031 (2004) 219.
[39] A. Ceccato, F. Vanderbist, J.Y. Pabst, B. Streel, J. Chromatogr. B: Biomed. Sci. Appl. 748 (2000) 65.
[40] Y.H. Ardakani, R. Mehvar, A. Foroumadi, M.R. Rouini, J. Chromatogr. B: Analyt. Technol. Biomed. Life Sci. 864 (2008) 109.
[41] F. Musshoff, B. Madea, F. Stuber, U.M. Stamer, J. Anal. Toxicol. 30 (2006) 463.
[42] B. Elsing, G. Blaschke, J. Chromatogr. 612 (1993) 223.
[43] H. Buzkova, K. Pechandova, O. Slanar, F. Perlik, Cell Biochem. Funct. 26 (2008) 76.

PUBLIKACE IX

Stanovení nabumetonu a kyseliny 6-methoxy-2-naftyloctové v plazmě pomocí HPLC s UV a MS detekcí

Nespěšná, L.; Štícha, M.; Matoušková, O.; Perlík, F.; Slanař, O.

Česká s slovenská farmacie. 60 (2011) 17-24.

Stanovení nabumetonu a kyseliny 6-methoxy-2-naftyloctové v plazmě pomocí HPLC s UV a MS detekcí

LENKA NESPĚŠNÁ[1, 2], MARTIN ŠTÍCHA[1], OLGA MATOUŠKOVÁ[2], FRANTIŠEK PERLÍK[2], ONDŘEJ SLANAŘ[2]
[1]Univerzita Karlova v Praze, Katedra organické a jaderné chemie, Přírodovědecká fakulta
[2]Univerzita Karlova v Praze, Farmakologický ústav 1. lékařské fakulty

Došlo 26. listopadu 2010 / Přijato 20. prosince 2010

SOUHRN

Stanovení nabumetonu a kyseliny 6-methoxy-2-naftyloctové v plazmě pomocí HPLC s UV a MS detekcí

Cílem práce bylo zavést a validovat analytickou metodu, která by umožnila detekovat koncentrace nabumetonu a kyseliny 6-methoxy-2-naftyloctové (6-MNA) po jednorázovém podání terapeutické dávky léčiva. Byly porovnány dvě metody stanovení pomocí HPLC s UV a hmotnostní detekcí. Při úpravě vzorku bylo optimálních výsledků dosaženo pomocí extrakce na pevné fázi (SPE). Výtěžnost se pohybovala okolo 84 % pro nabumeton a 86–90 % pro 6-MNA. HPLC separace analytů byla prováděna na reverzní C18 koloně. Limit UV detekce pro 6-MNA byl 50 nM, pro nabumeton 0,1 μM. Limit MS detekce pro 6-MNA činil 1 μM, pro nabumeton 0,5 μM. Přesnost metody pro stanovení nabumetonu se pohybovala v rozmezí 4,2–14,4 % při UV detekci a 4,6–8,5 % při MS detekci. Přesnost metody pro 6-MNA byla 2,4–12,5% při UV detekci a 2,1–9,4 % při MS detekci. Správnost metody pro stanovení nabumetonu se pohybovala v rozmezí 93,4–109,6 % při UV detekci a 86,2–107,9 % při MS detekci. Správnost metody pro 6-MNA byla 87,8–107,4 % při UV detekci a 86,3–106,4 % při MS detekci. Vhodnost metody byla ověřená na vzorcích pro stanovení farmakokinetiky léčiva u 24 zdravých dobrovolníků.

Klíčová slova: nabumeton – farmakokinetika – kyselina 6-methoxy-2-naftyloctová – HPLC – LC/MS

Čes. slov. Farm. 2011; 60, 17–24

SUMMARY

Determination of nabumetone and 6-methoxy-2-naphthylacetic acid in plasma using HPLC with UV and MS detection

The study aimed to establish and validate an analytical method for the determination of nabumetone and 6-methoxy-2-naphthylacetic acid (6-MNA) in human plasma after a single therapeutic dose of the drug. Two methods based on HPLC with UV and MS detection were compared. Optimal results in sample preparation were achieved using solid phase extraction. The recovery reached approximately 84% and 86–90% for nabumetone and 6-MNA, respectively. A reverse C18 column was used for HPLC separation of the analytes. The limit of UV detection was 50 nM and 0.1 μM for 6-MNA and nabumetone, respectively. The limit of MS detection was 1 μM and 0.5 μM for 6-MNA and nabumetone, respectively. Precision ranged between 4.2–14.4% and 4.6–8.5% using UV and MS detection for nabumetone, respectively. The respective values for 6-MNA were 2.4–12.5% and 2.1–9.4%. Accuracy ranged between 93.4–109.6% in UV detection and 86.2–107.9% using UV and MS detection for nabumetone, respectively. The respective values for 6-MNA were 87.8–107.4% and 86.3–106.4%. The method was subsequently applied to determine the pharmacokinetic parameters of nabumetone and 6-MNA in a group of 24 healthy volunteers.

Key words: nabumetone – pharmacokinetics – 6-methoxy-2-naphthylacetic acid – HPLC – LC/MS

Čes. slov. Farm. 2011; 60, 17–24 *Má*

Adresa pro korespondenci:
doc. MUDr. Ondřej Slanař, Ph.D.
Farmakologický ústav 1. LF UK
Albertov 4, 128 00 Praha 2
e-mail: oslan@lf1.cuni.cz

Úvod

Nabumeton (4-(6-methoxy-2-naftyl)-butan-2-on) patří mezi nesteroidní protizánětlivé látky vykazující preferenční inhibici cyklooxygenázy 2 [1]. Je používán v léčbě akutních i chronických symptomů revmatoidní artritidy a osteoartrózy [2, 3]. Nabumeton je proléčivo, které nevykazuje protizánětlivou aktivitu, zatímco jeho hlavní metabolit kyselina 6-methoxy-2-naftyloctová (6-MNA) vykazuje farmakodynamické účinky antiflogistické, antipyretické a analgetické.

Přestože jsou klinické účinky nabumetonu dobře popsány, farmakokinetika nabumetonu dosud podrobněji popsána nebyla kvůli příliš nízkým koncentracím mateřské látky v krvi po podání terapeutických dávek. Z důvodu nízkých hladin nabumetonu v krvi je dosud publikována jen jedna metoda HPLC s fluorimetrickou detekcí nabumetonu pro použití v klinických studiích [4]. Dobře je naopak popsána farmakokinetika 6-MNA díky dostupnosti dostatečně citlivých analytických technik [5–9].

Cílem naší práce bylo zavést a validovat analytickou metodu, která by umožnila detekovat koncentrace nabumetonu a 6-MNA po jednorázovém podání terapeutické dávky léčiva.

POKUSNÁ ČÁST

Chemikálie

Nabumeton p.a. (Sigma-Aldrich), 6-MNA p.a. (MP Biomedicals), naproxen 98% (Sigma-Aldrich), methanol pro HPLC (Lach-Ner), aceton p.a. (Merck), propan-2-ol p.a. (Lach-Ner) kyselina *o*-fosforečná 85% (Merck), fosforečnan sodný terciární čistý (Lachema), acetonitril pro HPLC (Lach-Ner), kyselina trifluorooctová 99% (Sigma-Aldrich), deionizovaná voda (Millipore), dusík 4.6 (Linde Gas), helium 4.6 (Linde Gas).

Příprava vzorků

Vzorky krve jsme odebírali do zkumavek Vacutainer s přídavkem heparinu. Ihned po odebrání krve jsme oddělili plasmu centrifugací při 3000 g. Plasma byla poté uložena do -70 °C až do doby analýzy.

Pro předúpravu vzorků jsme zvolili techniku extrakce na tuhou fázi (SPE). K 0,5 ml vzorku jsme přidali 50 µl roztoku vnitřního standardu o koncentraci 0,1 mmol/l. Vzorek jsme naředili 0,5 ml fosfátového pufru pH 2 (10 mM), okyselili 50 µl 10% kyseliny fosforečné a řádně promíchali.

Takto připravený vzorek jsme aplikovali na kolonku *Discovery® DSC-18 (1 ml, 100 mg)*, Supelco, USA předem promytou 2 ml methanolu a 2 ml fosfátového pufru pH 2 (10 mM). Všechny roztoky protekly rychlostí 1 ml.min^{-1}.

Následně jsme kolonku prosávali vzduchem po dobu 5 minut. Zachycené látky byly vymyty 2 ml methanolu. Získaný extrakt jsme odpařili dosucha při 45 °C pod mírným proudem dusíku. Reziduum jsme poté rozpustili ve 250 µl mobilní fáze a 30 µl nastříkli do HPLC.

HPLC/UV/MS analýza

Pro analýzu extraktu jsme použili kapalinový chromatograf *HP 1100* s UV DAD, Hewlett Packard, USA. Jako hmotnostní detektor jsme použili přístroj Esquire 3000, Bruker Daltonics, Německo.

Separace probíhala na koloně *Supelcosil LC-18* 15 cm × 4,6 mm 5 µm, Supelco, USA a jako mobilní fázi jsme použili směs acetonitrilu a 0,1% TFA v poměru 50 : 50 (*v/v*) o průtokové rychlosti 0,3 ml.min^{-1}.

UV detekce proběhla při vlnové délce absorpčního maxima sledovaných látek λ = 230 nm. Současně jsme sledovali i hmotnostní detekci s chemickou ionizací za atmosférického tlaku v pozitivním módu. Podmínky APCI detekce byly následující: rozsah skenu 50–800 u, teplota sušícího plynu 250 °C, teplota iontového zdroje 400 °C, tlak plynu v zamlžovači 30 psi, průtok sušícího plynu (N2) 5 l. min^{-1}, napětí na kapiláře 4 kV.

Vyhodnocení jsme provedli podle chromatogramu náležejícího nejintenzivnějšímu iontu ve spektru příslušné látky. Pro 6-MNA a nabumeton to byl ion m/z 171 a pro vnitřní standard – naproxen ion m/z 185.

Validace metody

Validaci metody jsme provedli na základě požadavků pro validaci bioanalytických metod [10]. V souladu s těmito požadavky jsme stanovili mez stanovitelnosti (LLOQ), správnost, přesnost, výtěžnost, linearitu a selektivitu detekce.

Pro nabumeton i 6-MNA byly sestrojeny kalibrační křivky. Vzorky o známé koncentraci s přídavkem vnitřního standardu byly zpracovány SPE a dále analyzovány pomocí HPLC s UV a MS detekcí. Pro 6-MNA byly připraveny roztoky o těchto koncentracích: 0,2; 0,5; 1; 2; 5; 10; 20; 50 a 100 µmol/l pro nabumeton 0,2; 0,5; 1; 2; 5; 10 a 20 µmol/l.

Mez stanovitelnosti jsme určili jako nejnižší bod kalibrační křivky, kde pík analytu je indentifikovatelný, oddělený a reprodukovatelný s přesností 20 % a správností 80–120 %.

Součástí validace metody bylo také studium stability zásobních roztoků a vzorků. V případě zásobních roztoků analytů a vnitřního standardu jsme měřili koncentrace látek přítomných ve vzorku v závislosti na čase u skladovaných roztoků po nástřiku 5 µl zásobního roztoku. Detekční podmínky byly shodné s podmínkymi při měření extraktů z plazmy. První měření proběhlo ihned po jejich přípravě.

Dále jsme sledovali vliv zmrazení a roztátí vzorků v několika cyklech na koncentraci analytů ve vzorku. Vzorky o vysoké a nízké koncentraci analytů (množství dostatečné pro tři analýzy na koncentraci, pro 6-MNA 1 a 50 µM; pro nabumeton 0,5 a 10 µM) jsme skladovali při teplotě -70 °C po dobu 24 hodin. Poté roztály při laboratorní teplotě a následně byly znovu zmraženy. Tento postup jsme opakovali a po čtvrtém cyklu roztátí vzorků jsme provedli analýzu.

Pro studium krátkodobé teplotní stability jsme připravili vzorky o vysoké a nízké koncentraci (pro 6-MNA 1 a 50 μM; pro nabumeton 0,5 a 10 μM, tři alikvoty od každé). Vzorky byly ponechány při laboratorní teplotě 6 hodin a následně zpracovány.

Pro stanovení dlouhodobé teplotní stability vzorků jsme připravili vzorky o vysoké a nízké koncentraci analytů (pro 6-MNA 1 a 50 μM; pro nabumeton 0,5 a 10 μM). Vzorky jsme uchovávali při teplotě -70 °C a v časových intervalech je analyzovali ve třech stanoveních v každé koncentraci.

Reprodukovatelnost metody jsme zhodnotili na základě výsledků analýz kontrolních vzorků, které jsme provedli v průběhu pěti týdnů. Celkem jsme analyzovali deset sérií po třech koncentracích (nízké, střední a vysoké) pro oba analyty. 6-MNA byla sledována na koncentračních úrovních 1; 10 a 50 μM, nabumeton pak v koncentracích 0,5; 2 a 10 μM.

Aplikace metody

Metodu jsme následně použili na stanovení farmakokinetických parametrů nabumetonu a 6-MNA u 24 zdravých dobrovolníků po podání 500 mg nabumetonu (Relifex, MEDA AB Švédsko). Zdraví dobrovolníci byli po vstupním fyzikálním, biochemickém a hematologickém vyšetření krátkodobě hospitalizováni na našem oddělení. Během hospitalizace dostal každý dobrovolník jednorázovou dávku přípravku Relifex s 250 ml vody na zapití. Podání léčiva probíhalo vždy v ranních hodinách pod dohledem zdravotní sestry. Po dobu studie měli dobrovolníci volný přístup k pitné vodě ad libitum. První lehké standardizované jídlo bylo podáváno za 4 hodiny od podání nabumetonu. Odběry jsme prováděli v čase před podáním léčiva a 1, 2, 3, 4, 6, 8, 10, 12, 24, 48, 72 a 96 hodin po podání léku. Tato studie byla schválena Etickou komisí VFN a všichni dobrovolníci podepsali informovaný souhlas před zařazením do studie.

VÝSLEDKY A DISKUZE

Optimalizace metody

HPLC separace analytů proběhla na reverzní C18 koloně. Testovali jsme mobilní fáze o složení acetonitril/voda a acetonitril/0,1% TFA. Chromatografická separace byla ve všech případech provedena isokratickou eluční technikou.

Jako výchozí bod jsme zvolili mobilní fázi acetonitril : voda 50 : 50 (v/v), kdy jsme pozorovali dobrou separaci analytů a vnitřního standardu. Zjistili jsme, že rostoucí průtoková rychlost měla negativní vliv na symetrii píků a odezva MS detekce (výška píku) při překročení průtoku 0,3 ml.min^{-1} klesala.

Při použití mobilní fáze acetonitril: 0,1% TFA v poměru 50 : 50 (v/v) došlo k očekávanému vylepšení symetrie píků a k navýšení signálu MS, nicméně při překročení průtokové rychlosti 0,3 ml.min^{-1} i za těchto podmínek účinnost ionizace MS klesala.

Vyšší obsah acetonitrilu vedl ke snížení retence a zhoršení symetrie píků. Odezva MS při obsahu acetonitrilu 50 % a více setrvávala na přibližně konstantní úrovni. Pro další práci jsme zvolili poměr acetonitril : 0,1% TFA 50 : 50 (*v/v*).

MS detekce

Současné požadavky na validaci bioanalytických metod vyžadují průkaz nepřítomnosti matričních efektů. V naší práci jsme tento průkaz nezjišťovali, protože jsme použili metodu chemické ionizace za atmosferického tlaku (APCI), která je podstatně robustnější vzhledem ke složení matrice a riziko matričních efektů je významně nižší ve srovnání s metodou elektrosprejové ionizace (ESI). Pro použití v rámci TDM, ke kterému jsme naší

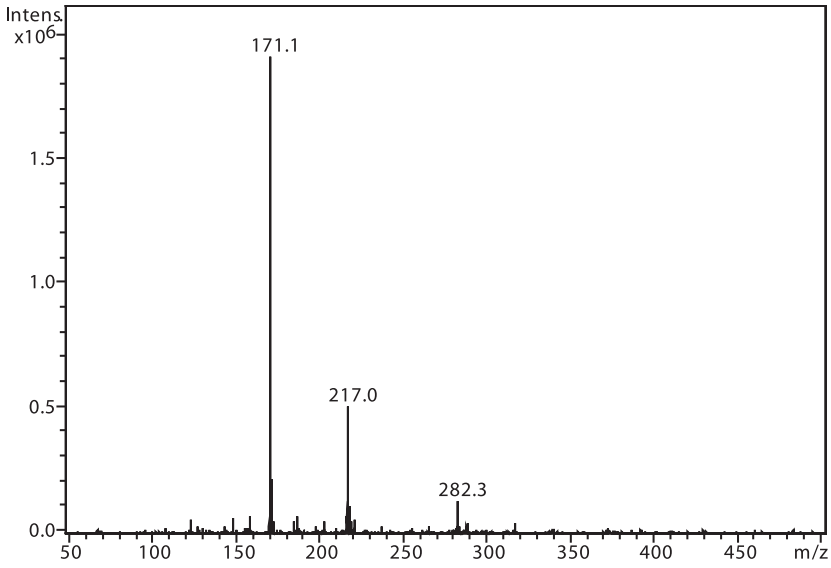

Obr. 1. Hmotnostní APCI spektrum 6-MNA, pozitivní mód (50 μM roztok, ACN : 0,1% TFA 50 : 50 (v/v))

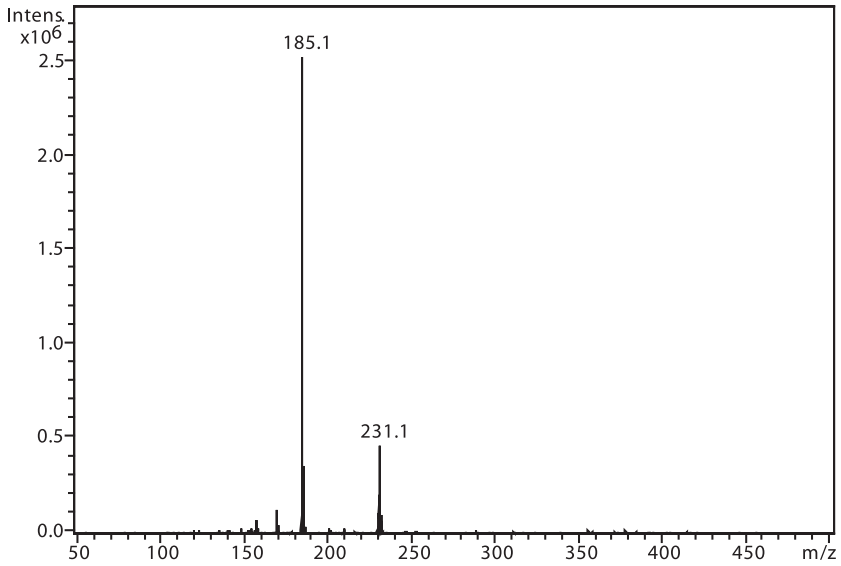

Obr. 2. Hmotnostní APCI spektrum naproxenu, pozitivní mód (50 μM roztok, ACN : 0,1% TFA 50 : 50 (v/v))

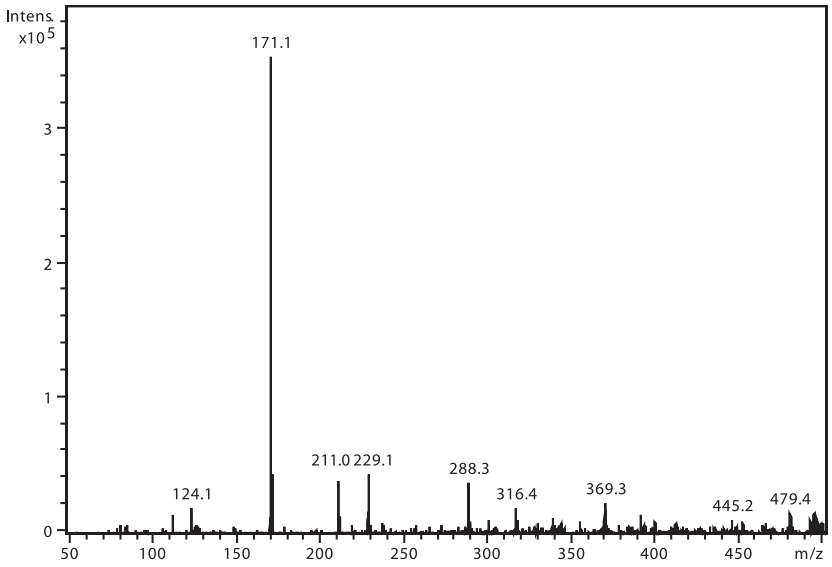

Obr. 3. Hmotnostní APCI spektrum nabumetonu, pozitivní mód (50 μM roztok, ACN : 0,1% TFA 50 : 50 (v/v))

metodu vyvinuli, lze proto popisovanou metodu považovat za dostatečně robustní s ohledem na matriční efekty.

Při použití chemické ionizace za atmosferického tlaku všechny tři sledované látky poskytovaly signál pouze při záznamu kladných iontů.

Na obrázku 1 je zobrazeno spektrum 6-MNA, kde lze vidět ion m/z 217, který je tvořen protonovanou molekulou $(M+H)^+$ a fragmentový ion m/z 171, vzniklý dekarboxylací molekuly. Ion m/z 282 nepatří sledované látce, jedná se o ion z pozadí. Na obrázku 2 je APCI spektrum naproxenu. Opět je zde pozorovatelná protonovaná molekula $(M+H)^+$ o hmotě m/z 231 a intenzivní fragmentový ion m/z 185 vzniklý dekarboxylací.

Na obrázku 3 je zobrazeno spektrum nabumetonu. Ion m/z 229 patří protonované molekule $(M+H)^+$ a intenzivní m/z 171 je fragment vzniklý odštěpením části postranního řetězce $(M–CH_3COCH_2)^+$. Ion m/z 211 pak odpovídá ztrátě 17 u. Ostatní přítomné ionty patří k signálu pozadí.

Validace

Metoda stanovení 6-MNA a nabumetonu splňuje požadavky na přesnost a správnost. Selektivita metody byla testována analýzou deseti „slepých“ vzorků, přičemž jsme nepozorovali žádné interference.

Zároveň jsme určili detekční limity pro obě stanovované látky. Limit UV detekce pro 6-MNA byl 50 nM, pro nabumeton 0,1 μM. Limit MS detekce pro 6-MNA činil 1 μM, pro nabumeton 0,5 μM.

V přítomnosti naproxenu jako vnitřního standardu (10 μM) byla v koncentračním rozmezí 0,2–200 μM na

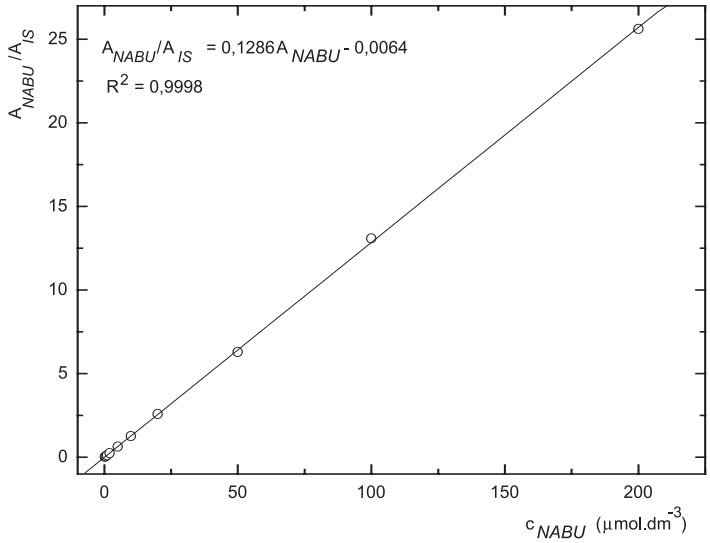

Obr. 4. Závislost odezvy standardních roztoků 6-MNA na koncentraci (kolona Supelcosil LC-18 15 cm × 4,6 mm 5 µm; ACN : 0,1% TFA 50 : 50 0,3 ml.min^{-1}; nástřik 30 µl, UV 230 nm)

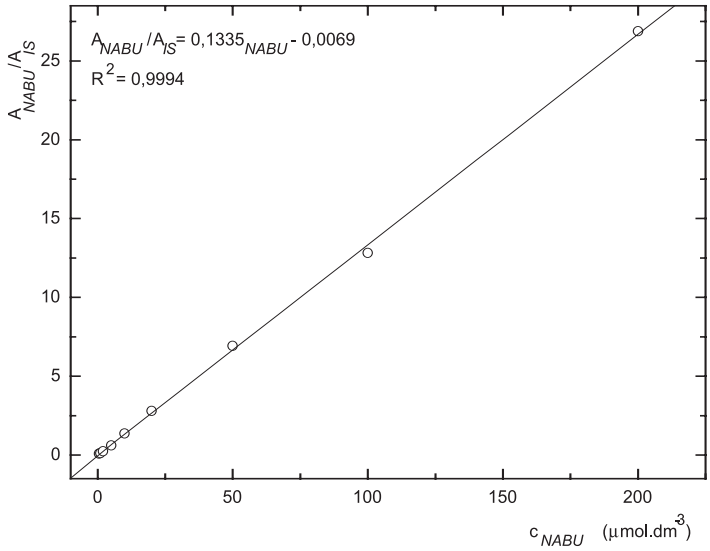

Obr. 5. Závislost odezvy standardních roztoků 6-MNA na koncentraci (kolona Supelcosil LC-18 15 cm × 4,6 mm 5 µm; ACN : 0,1% TFA 50 : 50 0,3 ml.min^{-1}; nástřik 30 µl, MS m/z 171, m/z 185)

deseti koncentračních úrovních proměřena odezva standardních roztoků 6-MNA a nabumetonu s využitím UV detekce. Rozmezí pro MS detekci bylo 0,5–200 µM, devět koncentračních úrovní.

Odezva byla pro oba analyty v uváděném rozsahu lineární při použití UV i MS detekce (obr. 4 až 7).

Validace byla provedena pro UV a pro MS detekci zvlášť. Parametry validace pro stanovení 6-MNA jsou uvedeny v tabulce 1. Validace metody stanovení nabumetonu je shrnuta v tabulce 2. Výtěžnost se pohybovala okolo 84 % pro nabumeton a 86–90 % pro 6-MNA (tab. 3).

Stabilita zásobních roztoků

Stabilitu zásobních roztoků jsme sledovali v intervalech 14, 30, 60 a 120 dní. V žádném z intervalů se plochy píku pro 6-MNA, nabumeton nebo vnitřní standard neodchylovaly o více než 2 % od bazálních hodnot.

Stabilita vzorků krevní plazmy

Čtyři cykly zmrazení a opětovného roztátí nevedly k významnému poklesu obsahu analytů ve vzorku.

Krátkodobou teplotní stabilitu jsme sledovali u vzorků krevní plazmy, kdy jsme roztoky ponechali při laboratorní teplotě po dobu 6 hodin. Po této době opět nedošlo k významnému poklesu obsahu analytů ve vzorku podobně jako při testech dlouhodobé stability po 60 a 120 dnech skladování při -70 °C. Všechny výsledky stabilit testů krevní plazmy jsou sumarizovány v tabulce 4.

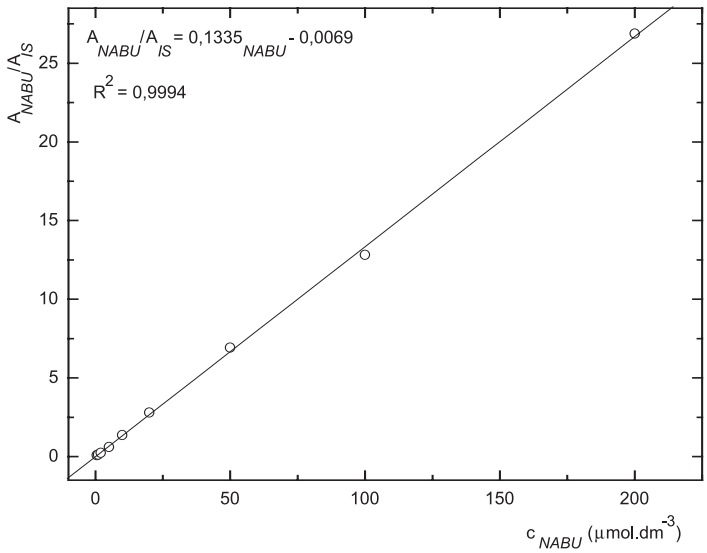

Obr. 6. Závislost odezvy standardních roztoků nabumetonu na koncentraci (kolona Supelcosil LC-18 15cm × 4,6 mm 5 µm; ACN : 0,1% TFA 50 : 50 0,3 ml.min^{-1}; nástřik 30 µl, MS m/z 171, m/z 185)

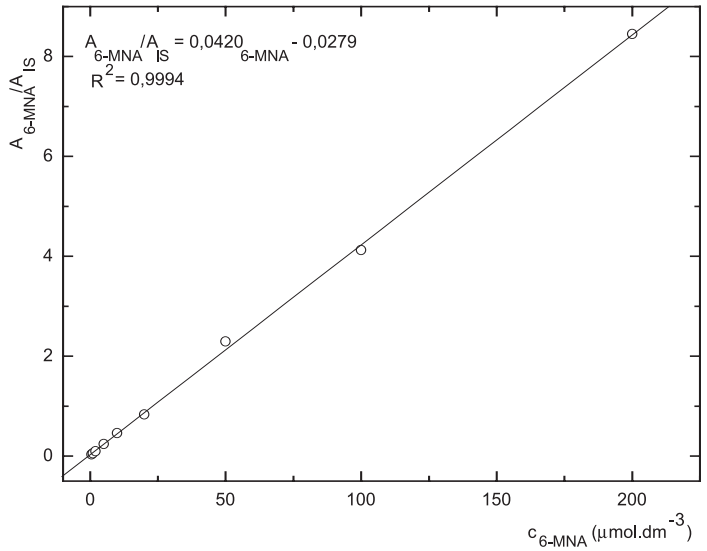

Obr. 7. Závislost odezvy standardních roztoků 6-MNA na koncentraci (kolona Supelcosil LC-18 15cm × 4,6 mm 5 µm; ACN : 0,1% TFA 50 : 50 0,3 ml.min^{-1}; nástřik 30 µl, MS m/z 171, m/z 185)

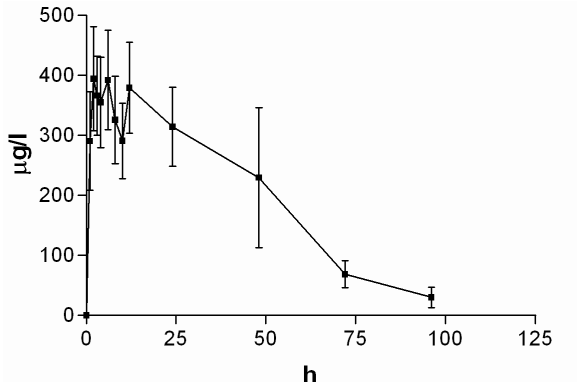

Obr. 8. Průběh průměrných koncentrací nabumetonu v čase (± 95%CI)

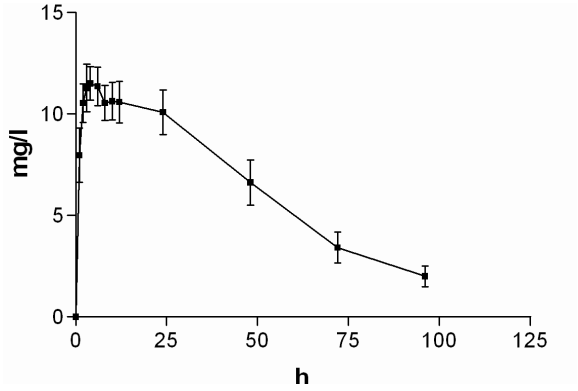

Obr. 9. Průběh průměrných koncentrací 6-MNA v čase (± 95%CI)

Tab. 1. Validace metody stanovení 6-MNA

Detekce	UV	MS
rovnice regrese	y = 98284x + 0,0073	y = 49262x – 0,0884
R^2	0,9993	0,9989
LLOQ (μM)	0,5	2
ULOQ (μM)	100	100
počet kalibračních bodů	8	6
přesnost (%)	2,4–12,5	2,1–9,4
správnost (%)	87,8–107,4	86,3–106,4

Tab. 2. Validace metody stanovení nabumetonu

Detekce	UV	MS
rovnice regrese	y = 90991x – 0,0006	y = 107776x – 0,0479
R^2	0,9990	0,9977
LLOQ (μM)	0,2	2
ULOQ (μM)	20	20
počet kalibračních bodů	6	6
přesnost (%)	4,2–14,4	4,6–8,5
správnost (%)	93,4–109,6	86,2–107,9

Tab. 3. Výtěžnost metody pro 6-MNA a nabumeton (UV detekce)

Koncentrace (μM)		Výtěžnost (%)			Medián
6-MNA	1	86	89	91	86
	10	85	92	87	87
	50	90	91	90	90
nabumeton	0,5	79	80	84	84
	2	84	82	88	84
	10	85	86	84	85

Reprodukovatelnost metody

Relativní směrodatná odchylka stanovení 6-MNA v kontrolních vzorcích na třech různých koncentračních hladinách se pohybovala v rozmezí 2,9–6,1 %. Obdobně nabývala i v případě nabumetonu relativní směrodatná odchylka hodnot 1,6–3,6 %.

Aplikace metody

Průměrné hladiny (95% CI) nabumetonu a 6-MNA získané UV detekcí jsou uvedeny na obrázcích 8 a 9. Základní farmakokinetické parametry nabumetonu a 6-MNA jsou uvedeny v tabulce 5.

Tab. 4. Krátkodobá a dlouhodobá stabilita vzorků krevní plasmy a stabilita po čtyřech cyklech zmrazení a roztátí. Medián ze 3 měření (UV detekce)

	6-MNA		Nabumeton	
Koncentrace vzorku (μM)	1	50	0,5	10
Medián nalezené koncentrace čtyř cyklů zmrazení a roztátí (μM)	1,07	48,4	0,48	9,87
s	0,04	1,30	0,016	0,34
s_r (%)	4,5	2,7	3,4	3,5
Medián nalezené koncentrace krátkodobé stability (mol.dm^{-3})	0,98	47,6	0,50	9,56
s	0,054	0,59	0,007	0,08
s_r (%)	5,5	1,2	1,5	0,9
Medián nalezené koncentrace po 60 dnech (mol . dm^{-3})	0,97	48,1	0,48	9,75
s	0,01	1,06	0,02	0,08
s_r (%)	1,2	2,2	4,4	0,9
Medián nalezené koncentrace po 120 dnech (mol.dm^{-3})	1,04	49,2	0,51	10,1
s	0,059	0,77	0,01	0,58
s_r (%)	5,7	1,6	2,0	5,8

Tab. 5. Průměrné (SD) hodnoty základních farmakokinetických parametrů ve skupině 24 dobrovolníků

FK parametr	Nabumeton	6-MNA
C_{max} (mg/l)	0,56 (0,19)	12,75 (1,40)
AUC $_{0\text{-}96}$ (h.mg/l)	18,07 (7,05)	633,25 (174,05)
AUC$_{0\text{-}\infty}$ (h.mg/l)	18,22 (6,87)	721,50 (237,78)
$T_{1/2}$ (h)	20,91	27,26*

***medián**

ZÁVĚR

Při srovnání obou detekčních technik, lze říci, že UV detekce, jak dokládají směrnice z rovnic kalibračních přímek, je stejně citlivá pro 6-MNA i pro nabumeton. Pokud stejným způsobem zhodnotíme hmotnostní detekci, je citlivější pro nabumeton (směrnice kalibrační přímky nabumetonu je přibližně 2× než směrnice kalibrační

přímky 6-MNA). Při použití UV detekce jsme u obou analytů dosáhli nižší meze stanovitelnosti než v případě detekce hmotnostní. Lze předpokládat, že použitím techniky SIM u kvadrupólového hmotnostního spektrometru, případně techniky MRM u tandemových přístrojů by bylo možné zvýšit citlivost o několik řádů a dostat se minimálně na úroveň UV detekce. Tyto módy detekce však námi použité přístrojové vybavení neumožnilo.

Zavedené metody UV i hmotnostní detekce umožňují stanovit koncentrace nabumetonu a 6-MNA po jednorázovém podání terapeutické dávky léčiva.

Práce vznikla za podpory grantu GA UK 52707.

LITERATURA

1. **Boyle, E. A., Freeman, P. C., Mangan, F. R., Thomson, M. J.:** Nabumetone (BRL 14777, 4-[6-methoxy-2-naphthyl]-butan-2-one): a new anti-inflammatory agent. J Pharm Pharmacol. 1982; 34, 562–569.
2. **Battisti, W. P., Katz, N. P., Weaver, A. L., Matsumoto, A. K., Kivitz, A. J., Polis, A. B., Geba, G. P.:** Pain management in osteoarthritis: a focus on onset of efficacy – a comparison of rofecoxib, celecoxib, acetaminophen, and nabumetone across four clinical trials. J Pain. 2004; 5, 511–520.
3. **Hedner, T., Samulesson, O., Wahrborg, P., Wadenvik, H., Ung K. A., Ekbom, A.:** Nabumetone: therapeutic use and safety profile in the management of osteoarthritis and rheumatoid arthritis. Drugs. 2004; 64, 2315–2343; discussion 2344–2315.
4. **Kobylinska, K., Barlinska, M., Kobylinska, M.:** Analysis of nabumetone in human plasma by HPLC. Application to single dose pharmacokinetic studies. J Pharm Biomed Anal. 2003; 32, 323–328.
5. **Starek, M., Krzek, J.:** A review of analytical techniques for determination of oxicams, nimesulide and nabumetone. Talanta. 2009; 77, 925–942.
6. **Kendall, M. J., Chellingsworth, M. C., Jubb, R., Thawley, A. R., Undre, N. A., Kill, D. C.:** A pharmacokinetic study of the active metabolite of nabumetone in young healthy subjects and older arthritis patients. Eur J Clin Pharmacol. 1989; 36, 299–305.
7. **Davies, N. M.:** Clinical pharmacokinetics of nabumetone. The dawn of selective cyclo-oxygenase-2 inhibition? Clin Pharmacokinet. 1997; 33, 404–416.
8. **Patel, B. N., Sharma, N., Sanyal, M., Prasad, A., Shrivastav, P. S.:** High-throughput LC-MS/MS assay for 6-methoxy-2-naphthylacetic acid, an active metabolite of nabumetone in human plasma and its application to bioequivalence study. Biomed Chromatogr. 2008; 22, 1213–1224.
9. **Srinivas N. R.:** Applicability of LC/MS/MS assay for 6-methoxy-2-napthylacetic acid to support the bioequivalence study of nabumetone-comments on the research work of Patel et al. (2008). Biomed Chromatogr. 2009; 23, 674–675.
10. **Food and Drug Administration:** FDA Guidance for Industry: Bioanalytical Method Validation. 2001; http://www.fda.gov/cder/quidance (15. 11. 2010).

6. ZÁVĚR

Předkládaná dizertační práce je tvořena komentovaným souborem devíti publikací, které vyšly v mezinárodních impaktovaných časopisech. V práci jsou uvedeny a diskutovány možnosti využití hmotnostní spektrometrie pro analýzu biologicky významných látek ze skupiny organokovových komplexů, biologických markerů a vybraných léčiv. Využití hmotnostní spektrometrie pro analýzu komplexů, umožněné především vývojem měkkých iontových zdrojů, patří ještě stále mezi méně běžné aplikace této metody. Na základě série experimentů s komplexy rhenia a komplexy ferrocenu je možno konstatovat, že hmotnostní spektrometrie přináší v oblasti strukturní charakterizace a kvantifikace těchto látek cenná data, významně doplňující informace ostatních metod strukturní charakterizace. Hmotnostní spektra nízkého rozlišení, zvláště pokud jsou kombinována s rozborem izotopického profilu (isotopic pattern), poskytují věrohodnou informaci o struktuře molekulárního iontu. Volbou konkrétního typu a podmínek měkké ionizace je možno ovlivnit rozsah fragmentace molekulárního iontu, spektrum a intenzita fragmentových iontů poskytují další cenná data o struktuře komplexu i jeho stabilitě za daných specifických podmínek ionizace (redoxní stabilita v podmínkách ESI, fotochemická stabilita při APPI, výměna ligandů v APCI aj.) Věrohodnost strukturní charakterizace mohou významně zvýšit měření $(MS)^n$. Při analýze komplexů rhenia byla potvrzena možnost strukturní charakterizace komplexů ve směsi. ESI/MS s přímým vstupem vzorku byla použita pro charakterizaci vznikajících komplexů přímo v reakční směsi a poskytla cenné údaje o kinetice vzniku a dalších chemických reakcích těchto látek a to i ve velmi nízkých koncentracích, kde ostatní techniky strukturní charakterizace neposkytly měřitelná data. Pozitivní charakteristiky hmotnostní spektrometrie byly prokázány i při strukturní charakterizaci ferrocenových komplexů s navázanou mědí, stříbrem a zlatem. Současnou přítomnost dvojice kovových iontů s charakteristickými izotopy bylo možno věrohodně prokázat na základě rozboru izotopického profilu v molekulárním a fragmentových iontech.

S pomocí hmotnostní spektrometrie bylo možno získat podklady pro identifikaci a kvantifikaci významných biomarkerů. V případě analýzy billirubinu a jeho derivátů prokázala hmotnostní spektrometrie jako jedna z mála analytických technik schopnost práce s takto chemicky labilními látkami bez nežádoucí degradace během analýzy.

V souvislosti s analýzou billirubinu a jeho derivátů je nutno zmínit obecně známou negativní vlastnost hmotnostní spektrometrie, neschopnost rozlišit strukturně blízké izomery. V rámci studie fotoizomerů billirubinu nebylo možno jednotlivé typy na základě hmotnostních spekter rozlišit. Tento problém je možno vyřešit například použitím vhodné separační metody jako vstupu do hmotnostního spektrometru. Příkladem tohoto přístupu je popsané stanovení enantiomerů tramadolu a O-desmethyltramadolu v lidské moči pomocí GC/MS s chirální chromatografickou kolonou. Dosažitelná vysoká citlivost stanovení s použitím hmotnostního spektrometru se ukázala být klíčovou při monitorování velmi nízkých intracelulárních koncentrací sukcinátu a farmakokinetických studiích léčiv rilmenidinu a nabumetonu LC-ESI/MS.

SEZNAM PUBLIKACÍ

1. Jasprova, Jana; Dal Ben, Matteo; Vianello, Eleonora ; Goncharova, Iryna; Urbanova, Marie; Vyroubalova, Karolina; Gazzin, Silvia; Tiribelli, Claudio; **Sticha, Martin**; Cerna, Marcela : *The Biological Effects of Bilirubin Photoisomers;* PLOS ONE 11 (2) Article Number: e0148126 2016

2. **Sticha, Martin;** Jelinek, Ivan; Polakova, Jana; et al.: *Characterization of Rhenium (V) Complexes with Phenols Using Mass Spectrometry with Selected Soft Ionization Techniques;* ANALYTICAL LETTERS, 48 (15): 2329-2342 2015

3. Kluckova, K.; **Sticha, M**.; Cerny, J.; et al.:*Ubiquinone-binding site mutagenesis reveals the role of mitochondrial complex II in cell death initiation;* CELL DEATH & DISEASE Volume: 6 Article Number: e1749 2015

4. Fernandes, TA ; Solarova, H; Cisarova, I; Uhlik, F; **Sticha, M** ; Stepnicka, P.: *Synthesis of phosphinoferrocene amides and thioamides from carbamoyl chlorides and the structural chemistry of Group 11 metal complexes with these mixed-donor ligands;* DALTON TRANSACTIONS, 44 (7): 3092-3108 2015

5. Konickova, R; Jiraskova, A; Zelenka, J ; Leseticky, L ; **Sticha, M** ; Vitek, L.: *Reduction of bilirubin ditaurate by the intestinal bacterium Clostridium perfringens;* ACTA BIOCHIMICA POLONICA 59 (2) : 289-291 2012

6. Nesmerak, K; **Sticha, M**; Cvancarova, M.: *HPLC/MS Analysis of Historical Pharmaceutical Preparations of Heroin and Cocaine*; ANALYTICAL LETTERS, 43 (16): 2572-2581 2010

7. Chytil, L; Cvacka,J; Maresova,V; Strauch,B; Widimsky,J; **Sticha, M**; Slanar, O.: *Development of a fast LC–MS/MS method for quantification of rilmenidine in human serum: elucidation of fragmentation pathways by HRMS;* JOURNAL OF MASS SPECTROMETRY, 45, 1179–1185 AUG 2010

8. Nesmerak, K; Dolezal, R; Hudska, V; Bartl, J; **Sticha, M**; Waisser, K: Quantitative *Structure-Electrochemistry Relationship of 1-Phenyl-5-benzyl-sulfanyltetrazoles and Their Electrooxidation as a Metabolic Model;* ELECTROANALYSIS, 22 (17-18): 2117-2122 SEP 2010

9. Dufkova, V; Cabala, R; Maradova, D; **Sticha, M**: *A fast derivatization procedure for gas chromatographic analysis of perfluorinated organic acids;* JOURNAL OF CHROMATOGRAPHY A, 1216 (49): 8659-8664 DEC 4 2009

10. Chytil, L; **Sticha, M**; Matouskova, O; Perlik, F; Slanar, O: Enatiomeric *determination of tramadol and O-desmethyltramadol in human urine by gas chromatography-mass spektrometry;* JOURNAL OF CHROMATOGRAPHY B-ANALYTICAL TECHNOLOGIES IN THE BIOMEDICAL AND LIFE SCIENCES, 877 (20-21): 1937-1942 JUL 1 2009

11. Hlavaty, J; **Sticha, M**.: Novel *carbonaceous coupling products containing sulphur;* POLYMER BULLETIN, 59 (6): 767-776 JAN 2008

12. Hlavaty, J; **Sticha, M.**: *Electrochemical oxidation of but-2-yne-1,4-diol;* COLLECTION OF CZECHOSLOVAK CHEMICAL COMMUNICATIONS, 71 (11-12): 1517-1524 2006

13. Kaderavek, J; Kozempel, J; **Sticha, M**; Petrasek, J; Jirsa, M; Taimr, P; Leseticky, L: Vitamin *derivatives labelled with I-131 potential agents for liver scintigraphy;* CZECHOSLOVAK JOURNAL OF PHYSICS, 56: D711-D717 Suppl. 4 DEC 2006

14. Nesmerak, K; Nernec, I; **Sticha, M**; Waisser, K; Palat, K: *Quantitative structure-property relationships of new benzoxazines and their electrooxidation as a model of metabolic degradation;* ELECTROCHIMICA ACTA, 50 (6): 1431-1437 JAN 30 2005

15. Kutnerova, B; Jelinek, I; **Sticha, M**; Nemcova, I.: *Identification and purity control of thioacridine derivatives by gas and capillary liquid chromatography with mass spectrometric detection;* ANALYTICAL LETTERS, 37 (2): 263-272 JAN 2004

16. Naus, P; Leseticky, L; Smrcek, S; Tislerova, I; **Sticha, M.**: *Copper-assisted arylation of 1-thiosugars: Efficient route to triazene substituted arylthioglycosides;* SYNLETT, (14): 2117-2122 NOV 2003

17. Hlavaty, J; Kubista, J; **Sticha, M**.: *Short communication - The preparation of stable protected 3-ethynylpyrrole suitable for electrochemical polymerization;*POLYMERS FOR ADVANCED TECHNOLOGIES, 14 (9): 658-661 SEP 2003

18. Leseticky, L; Barth, R; Nemec, I; **Sticha, M**; Tislerova, I.: *Synthesis and spectra of N-15 labelled phenylazides;* CZECHOSLOVAK JOURNAL OF PHYSICS, 53: A777-A782 Part 2 Suppl. A 2003

19. Stepnicka, P; Base, T; Cisarova, I; Kubista, J; Vyskocil, S; **Sticha, M**.: *Synthesis and catalytic activity of spaced ferrocene oxazolines;* COLLECTION OF CZECHOSLOVAK CHEMICAL COMMUNICATIONS, 68 (7): 1206-1232 2003

20. Weber, T; Dalen, H; Andera, L; Negre-Salvayre, A; Auge, N; **Sticha, M**; Lloret, A; Terman, A; Witting, PK; Higuchi, M; Plasilova, M; Zivny, J; Gellert, N; Weber, C; Neuzil,J.: *Mitochondria play a central role in apoptosis induced by alpha-tocopheryl succinate, an agent with antineoplastic activity:Comparison with receptor-mediated pro-apoptotic signaling;* BIOCHEMISTRY, 42 (14): 4277-4291 APR 15 2003

21. Nesmerak, K; Nemec, I; **Sticha, M**; Nemcova, I; Horka, V.: *Structure-property relationships of thioacridines; Their electrochemical oxidation as a model of metabolic degradation;* ANALYTICAL LETTERS, 35 (10): 1617-1629 2002

22. Neuzil, J; Zhao, M; Ostermann, G; **Sticha, M**; Gellert, N; Weber, C; Eaton, JW; Brunk, UT.: *Alpha-tocopheryl succinate, an agent with in vivo anti-tumour activity, induces apoptosis by causing lysosomal instability;* BIOCHEMICAL JOURNAL, 362: 709-715 Part 3 MAR 15 2002

23. Hlavaty, J; Kavan, L; **Sticha, M**.: *New synthesis of alpha,omega-diiodoalkynes and capped iodobutadiynes;* JOURNAL OF THE CHEMICAL SOCIETY-PERKIN TRANSACTIONS 1, (6): 705-706 2002

24. Neuzil, J; Weber, T; Schroder, A; Lu, M; Ostermann, G; Gellert, N; Mayne, GC; Olejnicka, B; Negre-Salvayre, A; **Sticha, M**; Coffey, RJ; Weber, C.: *Induction of cancer cell apoptosis by alpha-tocopheryl succinate: molecular pathways and structural requirements;* FASEB JOURNAL, 15 (2): 403-415 FEB 2001

25. Nesmarak, K; Nemec, I; **Sticha, M**; Gabriel, J; Mirceski, V.: *Electrochemical oxidation of probucol in anhydrous acetonitrile;* COLLECTION OF CZECHOSLOVAK CHEMICAL COMMUNICATIONS, 64 (7): 1100-1110 JUL 1999

26. Vyskocil, S; Jaracz, S; Smrcina, M; **Sticha, M**; Hanus, V; Polasek, M; Kocovsky, P.: *Synthesis of N-alkylated and N-arylated derivatives of 2-amino-2 '-hydroxy-1,1 '-binaphthyl (NOBIN) and 2,2;'-diamino-1,1 '-binaphthyl and their application in the enantioselective addition of diethylzinc to aromatic aldehydes;* JOURNAL OF ORGANIC CHEMISTRY, 63 (22): 7727-7737 OCT 30 1998

27. Vyskocil, S; Jaracz, S; Smrcina, M; **Sticha, M**; Hanus, V; Polasek, M; Kocovsky, P.*: N-alkylated derivatives of 2-amino-2 '-hydroxy-1,1 '-binaphthyl (NOBIN) and their application in the enantioselective addition of diethylzinc to aromatic aldehydes;* ABSTRACTS OF PAPERS OF THE AMERICAN CHEMICAL SOCIETY, 216: 537-ORGN Part 2 AUG 23 1998

28. Sedlacek, J; Vohlidal, J; Cabioch, S; Lavastre, O; Dixneuf, P; Balcar, H; **Sticha, M**; Pfleger, J; Blechta, V.: *Polymerization of p-nitrophenylacetylene with metathesis catalysts. Photoelectrical properties of phenylacetylene/pnitrophenylacetylene copolymer;* MACROMOLECULAR CHEMISTRY AND PHYSICS, 199 (1): 155-161 JAN 1998

29. Klinotova, E; Krecek, V; Klinot, J; Endova, M; Eisenreichova, J; Budesinsky, M; **Sticha, M.**: *Glycosylation of triterpene alcohols and acids of the lupane and A-secolupane series - Part CVII;* COLLECTION OF CZECHOSLOVAK CHEMICAL COMMUNICATIONS, 62 (11): 1776-1798 NOV 1997

30. WEBER, J; KAVAN, L; **STICHA, M.***: ELECTRODES MODIFIED BY PERFLUORO ION-EXCHANGE POLYMERIC FILMS PREPARED FROM AQUEOUSSOLUTIONS OF NAFION AND TOSFLEX;* JOURNAL OF ELECTROANALYTICAL CHEMISTRY, 303 (1-2): 237-244 MAR 25 1991

SEZNAM PLAKÁTOVÝCH SDĚLENÍ

M. Chochkova, P. Petrova, B. Stoykova, N. Gyoshkova, G. Ivanova, **M. Štícha**, T. Milkova, *Synthesis and biological activity of cinnamic acid esters-P08*. 7th Bulgarian Peptide Symposium, Blagoevgrad, Bulgaria, 10.-12.6.2016

B. Stoykova1, M. Chochkova1, L. Georgiev, G. Ivanova, L. Mukova, N. Nikolova, L. Nikolaeva-Glomb, T. Milkova1, **M. Štícha**, *Amino acids amides of anti-influenza drugs: synthesis and biological activities-P09*; 7th Bulgarian Peptide Symposium, Blagoevgrad, Bulgaria, 10.-12.6.2016

Štícha M., Kaliba D., Jelínek I., Dian J.: *Spectroelectrochemistry of rhenium-catechol complex;* 16. ročník Pracovního setkání fyzikálních chemiků a elektrochemiků; Brno, 6.-9.6.2016

Kaliba D., Jelínek I., **Štícha M.,** Vaňátková P.: *Characterization of rhenium (V) complexes with phenols using mass spektrometry with soft ionization techniques and stability investigation for complex with 1,2,3-trihydroxybenzene ligand;* 18th edition of EuroAnalysis, Bordeaux, France, 6. – 10.9,2015

B. Stoykova, M. Chochkova, G. Ivanova, L. Mukova, N. Nikolova, L. Nikolaeva-Glomb, P. Vojtíšek, T. Milkova, **M. Štícha**, D. Havlíček: *Synthesis of fluorinated hydroxycinnamoyl derivatives of anti-influenza drugs and their biological aktivity*. 6th International Conference of FMNS, Blagoevgrad, Bulgaria 10.-14.6.2015

Vaníková J, Gončarová I, Urbanová M, Vyroubalová K, Vianello E, Dal Ben M, Gazzin S, Tiribelli C, **Štícha M,** Černá M, Vítek L: *BILIRUBIN PHOTOISOMERS DO NOT AFFECT BILIRUBIN BINDING TO ALBUMIN;* 8th International Conference on Heme Oxygenases, BioIron & Oxidative Stress; Sydney, Australia, 8. -11.10. 2014

Smrcek S., Habartova V., Psondrova S., **Sticha M.**: *Phytoremendiation and pharmaceuticals in the environment;* International Conference on Environmental Pollution and Clean Bio/Phytoremediation, Pisa, Itálie 16.-19.6.2010

Smrček S., Břichnáčová V., Pšondrová Š., **Štícha M**.: *Pharmaceuticals in the environment – occurence and perspectives for thein phytoextraction.* Phytotechnologies to Promote Sustainable Land Use and Improve Food Safety, , Ascona Švýcarsko. 12.-15.10.2009

Smrček S., Břichnáčová V., Pšondrová Š., **Štícha M.:** *Pharmaceuticals in the environment. and detoxification* . Szeged Maďarsko 16-19 duben 2009

Chytil L., **Sticha M**., Slanar O. : *Enantiomeric determination of tramadol and O-desmethyltramadol by GC/MS in urine;* 46th meeting of the International Association of Forensic Toxicologists; Martinique, 2. - 8.6.2008

Smrček S., Břichnáčová V., Pšondrová Š., **Štícha M.:** *Removal of Pharmaceuticals from Aquatic Media.* Genes and proteins involved in steps of phytoextraction and degradation of pollutants., Verona, Itálie, 4.-7.6. 2008

Smrček S., Habartová V., **Štícha M.,** Pšondrová Š.: *Plants as useful tool for the removal of pharmaceuticals and musk compounds from water;* Phytotechnologies to promote sustainable land use and improve food safety, Vilnius, Litva, 30. 5 - 1. 6. 2007